Hawassa University
Institute of Technology

Land Degradation Dynamics Under Land Use Land Cover and Climate Change Projection Towards the Appraisal of Potential Soil and Water Conservation Practices in the Gidabo Watershed, Ethiopian Rift Valley Lakes Basin

PhD Dissertation

By

Rediet Girma Legesse

A Dissertation Submitted to the School of Graduate Studies in Partial Fulfillment of the Requirements for Degree of Doctor of Philosophy in Civil Engineering (Water Resources Engineering)

Hawassa, Ethiopia
May, 2024

Land Degradation Dynamics Under Land Use Land Cover and Climate Change Projection Towards the Appraisal of Potential Soil and Water Conservation Practices in the Gidabo Watershed, Ethiopian Rift Valley Lakes Basin

PhD Dissertation

By

Rediet Girma Legesse

Supervisors:

Christine Fürst (Prof. Dr. habil.), Martin Luther University Halle-Wittenberg, Germany
Awdenegest Moges (Asso. Prof), Institute of Technology, Hawassa University

A Dissertation Submitted to the School of Graduate Studies in Partial Fulfillment of the Requirements for Degree of Doctor of Philosophy in Civil Engineering (Water Resources Engineering)

Hawassa, Ethiopia

May, 2024

ADVISORS' APPROVAL SHEET

SCHOOL OF GRADUATE STUDIES

HAWASSA UNIVERSITY ADVISORS' APPROVAL SHEET

This is to certify that the dissertation entitled "Land Degradation Dynamics Under Land Use Land Cover and Climate Change Projection Towards the Appraisal of Potential Soil and Water Conservation Practices in the Gidabo Watershed, Ethiopian Rift Valley Lakes Basin" submitted in partial fulfillment of the requirements for the degree of Doctor of Philosophy (PhD) with specialization in Water Resources Engineering, the Graduate Program of the Department of Civil Engineering, and has been carried out by Rediet Girma Legesse ID. No. PhDCiEnR/0001/12, under our supervision. Therefore, we recommend that the student has fulfilled the requirements and hence hereby can submit the dissertation to the department.

Prof. Christine Fürst	________________	May 27, 2024
Name of major supervisor	Signature	Date
Dr. Awdenegest Moges	________________	May 28, 2024
Name of co-supervisor	Signature	Date

EXAMINER'S APPROVAL SHEET

SCHOOL OF GRADUATE STUDIES

HAWASSA UNIVERSITY EXAMINERS' APPROVAL SHEET

We, the undersigned, members of the Board of Examiners of the final open defense by Rediet Girma Legesse have read and evaluated his dissertation entitled "Land Degradation Dynamics Under Land Use Land Cover and Climate Change Projection Towards the Appraisal of Potential Soil and Water Conservation Practices in the Gidabo Watershed, Ethiopian Rift Valley Lakes Basin", and examined the candidate. This is, therefore, to certify that the dissertation has been accepted in partial fulfillment of the requirements for the Doctor of Philosophy degree (PhD).

Prof. Christine Fürst	________________	27/05/2024
Name of major supervisor	Signature	Date
Dr. Brook Abate	________________	29/05/2024
Name of Examiner-I	Signature	Date
Dr. Ing Adane Abebe	________________	30/05/2024
Name of Examiner-II	Signature	Date
Dr. Abiot Ketema	________________	____________
Name of Chairperson	Signature	Date
____________________	________________	____________
SGS Approval	Signature	Date

Final approval and acceptance of the thesis/dissertation is contingent upon the submission of the final copy of the dissertation to the School of Graduate Studies (SGS) through the Department/School Graduate Committee (DGC/SGC) of the candidate's department.

Stamp of SGS **Date:** ____________

Declaration

I hereby declare that this PhD dissertation is my original work and has not been presented for a degree in any other university, and all sources of material used for this dissertation have been duly acknowledged.

Name: Rediet Girma Legesse
Signature: _______________
Date: May 27, 2024

Table of Contents

Acknowledgments

I accomplished this significant chapter of my academic journey by the help of the almighty God and the support from different organizations/institutions and many individuals who have played a pivotal role in making this dissertation a reality. First and foremost, I thank the almighty God for the faith and source of strength that have sustained me through the challenges and uncertainties. It is through divine providence that I have been able to embark on this scholarly endeavor.

I extend my sincerest gratitude to my esteemed supervisors, namely Prof. Christine Fürst and Dr. Awdenegest Moges. Their unwavering support, profound insights, constant encouragement, and constructive feedback have been wind beneath my wings, propelling me toward the successful completion of my PhD. Furthermore, their presence extended beyond the academic realm, providing me with invaluable life lessons and skills that I will carry with me throughout my career, and I am truly honored to have had the privilege of working under their supervision. Dear Prof. Christine Fürst and Dr. Awdenegest Moges, your contributions will forever be etched in the pages of my life and my dissertation. I am excited to embrace the challenges and opportunities that lie ahead, knowing that your influence will continue to guide and inspire me in my future endeavors.

I am deeply thankful for the Hawassa University of Ethiopia and German Academic Exchange Service (DAAD), who funded this PhD research project under the Engineering Capacity Building Program. I am also sincerely grateful to the Norwegian Agency for Development Cooperation (NORAD) at Hawassa University for additional funding. Moreover, I want to express my gratitude to the faculty of Biosystems and Water Resources Engineering of Hawassa University, particularly Biosystems Engineering department, for granting me study leave and facility support while I am in Ethiopia.

I would like to express my sincere gratitude to the extraordinary support of the working group at the department of Sustainable Landscape Development, Martin Luther University (MLU), Germany. The collaborative environment and diverse perspectives have significantly broadened my horizons, contributed to the development and execution of my research. Furthermore, I would like to extend my heartfelt appreciation to MLU for the generous support in covering the article publication charge (APC) for the article published in Land.

I would like to reiterate my profound appreciation for those their name is not listed for being an integral part of this remarkable journey. As I embark on the next phase of my academic and professional career, I am committed to upholding the values of diligence, curiosity, and collaboration that you have instilled in me. With your unwavering support and the grace of the almighty God, I look forward to making meaningful contributions to my field of study, the society and the country as a whole.

Lastly, I am also indebted to my family and friends who have been my pillars of strength throughout this journey. To my parents, brothers and sisters, your boundless love, steadfast support and sacrifices have been a cornerstone of my success and did not go unnoticed. Special thanks are to my kind wife, Aster Worku; her persistent support, patience, and understanding have been my anchor during the turbulence of this demanding endeavor. Your presence has been a source of solace and inspiration. I could not have achieved this without you. To my friends and colleagues, who have offered camaraderie, moral support, and shared in the highs and lows of this academic voyage, I am profoundly grateful.

List of Abbreviations and Acronyms

1OAO	One-Out, All-Out
ASTER	Advanced Spaceborne Thermal Emission and Reflection Radiometer
AVHRR	Advanced Very-High-Resolution Radiometer
BAU	business-as-usual
CA	Cellular Automata
CA-MC	Cellular Automata-Markov chain
CN	curve number
CORDEX	Coordinated Regional Climate Downscaling Experiment
CRMSE	centered root mean squared error
CV	coefficient of variation
DEM	digital elevation model
ERVLB	Ethiopian Rift Valley Lakes Basin
ESGF	Earth System Grid Federation
FAO	Food and Agriculture Organization
GCM	Global Climate Model
GIMMS	Global Inventory Modeling and Mapping Studies
GIS	Geographic Information Systems
GPG	Good Practice Guidance
GPS	Global Positioning System
GTD	Ground truth data
GW	Gidabo Watershed
HRUs	hydrologic response units
LC	land cover
LCM	Land Change Modeler
LDN	Land Degradation Neutrality
LP	land productivity
LULC	Land use land cover
MC	Markov Chain
MCMC	Markov Chain Monte Carlo
MK	Mann-Kendall
MLC	Maximum likelihood classifier
MLP	Multi-Layer Perceptron
MODIS	Moderate Resolution Imaging Spectroradiometer

MoWE	Ministry of Water and Energy
MUSLE	Modified Universal Soil Loss Equation
NDVI	normalized difference vegetation index
NMA	National Meteorology Agency
NSE	Nash–Sutcliffe efficiency
OA	Overall accuracy
PA	producer accuracy
PBIAS	percent of bias
r	Pearson's correlation coefficient
RCM	regional climate models
RCP	representative concentration pathways
RMSE	Root Means Square Error
RR^2	revised R-squared
RS	remote sensing
SAI	standardized anomaly index
SCS-CN	soil conservation service curve number
SDG	Sustainable Development Goal
SOC	soil organic carbon
SRA	Standardized rainfall anomaly
SRC	sediment rating curve
SWAT	Soil and Water Assessment Tool
TSS	Taylor Skill Score
UA	user accuracy
UNCCD	United Nations Convention to Combat Desertification
WUE	Water Use Efficiency

List of Figures

List of Tables

Abstract

The intricate relationship between land use, climate dynamics, and land degradation profoundly impacts the sustainability of ecosystems and human well-being in Ethiopia. This study, conducted in the Gidabo Watershed (GW) within the Ethiopian Rift Valley Lakes Basin (ERVLB), aimed to assess the long-term land use land cover (LULC), evaluate regional climate models (RCMs), assess land degradation indicators, and propose management alternatives. To address these objectives, multidisciplinary approach integrating, remote sensing, geospatial analysis, statistical metrics and hydrological modeling were used. The study identified nine major LULC classes i.e., water body, grass land, forest, agriculture, bare/barren land, built-up, agroforestry, shrub and marsh land. The watershed experienced significant LULC changes between 1985 and 2021, predominantly driven by agricultural expansion at the expense of forest, shrub, and grasslands. Future (2035 and 2050) projections using a hybrid Multi-Layer Perceptron (MLP) and Cellular Automata-Markov chain (CA-MC) model indicated further agricultural expansion, accompanied by declines in forest and grasslands. Furthermore, the study evaluated 11 CORDEX-Africa RCMs and their mean ensemble performance, revealing varied accuracies in reproducing rainfall and temperature patterns over GW from 1991 to 2005. The observed climate trends indicated a significant declining rainfall (-13.38 mm/year) and warming temperatures, with future projections (RCP4.5 and RCP8.5) showing consistent temperature increases. Additionally, the study investigated the impact of LULC and climate change on surface runoff and sediment yield using SWAT model. The results revealed notable increases in surface runoff and sediment yield attributed to LULC changes. Whereas, climate change alone exhibited a diverse influence, with both increases and decreases in surface runoff and sediment yield. Similarly, the combined effects of LULC and climate change demonstrated that certain scenarios led to the increases in surface runoff and sediment yield, while others reduced these processes. This might be attributed to the offset of runoff and sediment reduction by climate change. Soil erosion rates were found to be high, particularly most of the southern and eastern parts of the watershed will generate the highest amount of surface runoff and sediment yield in to the future. Addressing these concerns, soil/stone bund, terracing, contour farming, and reforestation practice can significantly reduce the annual sediment yield in the future. The land degradation neutrality (LDN) assessment from 1985–2003 to 2003–2021 revealed land productivity decline, land cover degradation, SOC loss, and the expansion of land degradation trajectories by 26%. Overall, the findings provide valuable information for stakeholders.

Keywords: climate change; land use; soil erosion; land degradation; soil conservation practice

1. General introduction

1.1. Background

Land is an essential resource and principal basis for human well-being and livelihood as it provides food, shelter, and multiple other ecosystem services (Mahata and Sharma, 2021; Prăvălie, 2021). The global population continues to grow, so does the demand for land, however, land is a finite resource and its availability is limited (Mueller et al., 2014). Therefore, the competition among these uses puts immense pressure on available land resources (UNCCD, 2019). Consequently, the lands' positive multidimensional role was heavily altered over the past decades, amid large-scale land degradation that has affected numerous ecosystems across the globe (Prăvălie, 2021).

Land degradation is a broader term encompassing any detrimental changes of the services provided by the land, primarily due to changes in its chemical, physical, and biological characteristics (Adnan, 2020; UNCCD, 2019). Land degradation is influenced by a combination of social (e.g., population pressure, land tenure system and cultural practices), economic (e.g., market demand and economic policies), ecological (e.g., climate change, loss of biodiversity and soil erosion), and physical (e.g., geomorphology, hydrology and natural disasters) drivers. These drivers can vary in significance depending on the region and context, but they often interact and exacerbate each other (Mahata and Sharma, 2021).

Soil, vegetation, and water resources degradation are interconnected environmental challenges (FAO, 2016). Soil degradation involves the deterioration of soil quality due to factors like erosion, compaction, and contamination, impacting its ability to support plant life and sustainable agriculture (FAO, 2016; UNCCD, 2019). Vegetation degradation, often a consequence of deforestation, overgrazing, or land conversion, disrupts ecosystems, diminishes carbon sequestration, and exacerbates soil erosion. These processes collectively contribute to water resources degradation, as soil erosion and vegetation loss can lead to sedimentation in water bodies, reduced water quality due to pollutants, and altered hydrological patterns, compromising the availability and quality of freshwater resources (FAO, 2016).

Soil erosion is one of the most important forms of land degradation (Prăvălie, 2021; Vanmaercke et al., 2021). Soil erosion results multitude of negative effects, such as reducing the water-holding capacity and infiltration rates, decreasing organic matter and nutrients, degrading soil structure and reducing soil depth (Poesen, 2018; Sartori et al., 2019) consequently reducing the land productivity. It is clear that soil erosion is a serious threat to food security, and has the potential to intensify socio-economic disruptions by decreasing agricultural yields (Sartori et al., 2019). Soil erosion is caused by several factors of either geomorphological (e.g., steep slopes), climatic (e.g., rainfall erosivity) or anthropogenic (deforestation, overgrazing or agricultural intensification) (Panagos et al., 2016; Poesen, 2018). In many cases, anthropogenic factors generally play more important role in the large-scale intensification of erosion (Keesstra et al., 2018; Prăvălie, 2021; Poesen, 2018).

Land use land cover (LULC) changes can significantly increase soil erosion by altering the natural landscape in ways that disrupt the delicate balance of hydrological and erosional processes (Borrelli et al., 2020; Novara et al., 2021). Natural vegetation, such as trees and grasses, plays a vital role in reducing raindrop kinetic energy by intercepting rainfall while allowing it to infiltrate (Li and Fang, 2016). Thus, the conversation of forests into agricultural fields or urban areas including roads and buildings, leaves the soil exposed and create impervious surfaces, leading to more runoff, making it further vulnerable to erosion. The eroded soil is then easily transported by the increased surface runoff into rivers and streams, exacerbating the sedimentation of water bodies (Nyatuame et al., 2020; Tan et al., 2022).

Climate change can lead to complex regional variations in soil erosion through mainly affecting the erosivity and amount of the rainfall. The specific effects depend on local climatic conditions, trends, and geographic characteristics (Eekhout and de Vente, 2022). In some regions, climate change has increased surface runoff and sediment yield through more frequent and intense rainfall events, potentially causing erosion (Lu et al., 2013). Additionally, shifts in rainfall patterns, such as increased rainfall variability or prolonged droughts, can make landscapes more susceptible to erosion when rains eventually return (Li and Fang, 2016). However, in other areas, climate change may lead to decreased surface runoff and sediment yield. For instance, erosion has showed a decreasing trend in regions experiencing climate warming and decreased rainfall (Ma et al., 2021). Ultimately, the impact of climate change on surface runoff and sediment yield as well as on soil erosion is highly location-specific. Quantifying the impact of LULC and climate change on soil erosion and land degradation dynamics is crucial for understanding the environmental challenges (Leta et al., 2023). Such assessment provides valuable insights into the drivers of land degradation, can identify hotspots and inform sustainable land management strategies (Kumar et al., 2022).

The nexus among land use, climate, and land degradation forms a complex interplay that profoundly influences the sustainability of ecosystems (IPCC, 2022). Human activities, such as deforestation, urbanization, and intensive agriculture, alter land use patterns, often leading to increased vulnerability to climate change impacts (Chu et al., 2022). Climate change can also influence land use patterns. As temperature rise and extreme weather events become more frequent, this can lead to shifts in land use in response to climate change (Sleeter et al., 2018). These changes, coupled with unsustainable land management practices, contribute to land degradation (IPCC, 2022). Conversely, land degradation can intensify LULC change (Hermans and McLeman, 2021) and exacerbate climate variability (Shukla et al., 2019).

Addressing the aforementioned impacts of climate and LULC changes require both mitigation and adaptation strategies that combines sustainable land management practices, policy interventions, and community engagement (Almagro et al., 2016; FAO, 2017). It is crucial to implement sustainable land management practices that enhance soil resilience and reduce vulnerability to erosion (Terefe et al., 2020). This involves, for example, promoting conservation tillage/agriculture, water harvesting techniques and water-efficient methods, agroforestry, cover cropping, and the use of organic amendments, which help to maintain ground cover, improve soil structure, water retention, and overall ecosystem health (Rahman et al., 2022). Additionally, afforestation and reforestation efforts can play a vital role in stabilizing slopes, preventing erosion, and mitigating the impacts of extreme weather events (Ivetić, 2021). By restoring and protecting natural vegetation, these measures contribute to carbon sequestration and enhance biodiversity, fostering a more resilient landscape (Waring et al., 2020). Effective policies that integrate land-use planning, conservation incentives, and erosion control regulations are essential for fostering a holistic approach to land management (FAO, 2017). Moreover, community involvement through education and capacity-building programs ensures the adoption of sustainable practices at the grassroots level (Mengistu and Assefa, 2021)

Ethiopia is one of the most highly soil erosion affected countries in the Sub-Saharan Africa (Fenta et al., 2021). Soil erosion is a significant environmental challenge in the country, and it has a range of negative impacts on agriculture, food security, and the overall environment (Berihun et al., 2019.; Kassawmar et al., 2018). It is caused by several interconnected factors and primarily attributed to (i) topography characterized by steep slopes, rugged mountainous terrain and highland areas, (ii) climate change-induced factors, including increased frequency and intensity of extreme weather events, such as heavy rainfall and droughts, (iii) uncontrolled deforestation often driven by population pressure, demand for agricultural land and fuelwood, (iv) inadequate land management practices, (v) overgrazing, and (vi) the expansion of agriculture onto marginal lands (Fenta et al., 2021; Hurni et al., 2015; Wassie, 2020).

The consequences of soil erosion in Ethiopia are far-reaching, impacting agricultural productivity, water quality, and the overall stability of ecosystems (Yesuph and Dagnew, 2019).

One of the major consequences of soil erosion in Ethiopia is the degradation of fertile topsoil, diminishing its capacity to support plant growth (Wassie, 2020). This, in turn, jeopardizes agricultural yields and places considerable strain on the livelihoods of the predominantly agrarian population (Haregeweyn et al., 2015). Furthermore, the downstream effects of soil erosion, such as increased siltation in dams and reservoirs, pose a threat to the country's water infrastructure, affecting water availability for both agricultural and domestic purposes (Adugna and Cherie, 2021).

Institutionalized soil and water conservation program were rooted in Ethiopia during 1970s to cope with land degradation (Belayneh et al., 2019; Haregeweyn et al., 2015). Since then, nationwide efforts have been undertaken, reviewed and restructured, and their focus over time has shifted from food relief to land conservation and then to livelihoods (Gashaw et al., 2021; Haregeweyn et al., 2015). Most recently, community-based participatory watershed management approach has been emerged to link land rehabilitation with income generating activities and livelihoods (Gashaw et al., 2021; Mengistu and Assefa, 2020). Integrated watershed management include measures that collectively contribute to mitigate soil erosion and ensure sustainable management in Ethiopia. However, its success remains a significant concern due to the complex interplay of environmental, social, and economic factors in the country (Mekuriaw et al., 2018; Negasa, 2020).

Estimation of soil erosion involves a diverse array of methodologies and tools (Borrelli et al., 2021). Field-based methods like sediment sampling and erosion plot studies provide more detailed and direct measurement (Hsieh, 2022). Empirical and process-based models consider factors such as climate, soil properties, slope and land cover to predict erosion rates (Borrelli et al., 2021). Furthermore, standardized indicators, such as Land Degradation Neutrality (LDN) framework, provide consistent approaches for quantifying land degradation at large scale (Cowie et al., 2018). Recently, machine learning and artificial neural networks have gained prominence enhancing our understanding of soil erosion and land degradation dynamics (Sahour et al., 2021). These diverse tools and models facilitate a comprehensive understanding of these environmental threats helping informed decisions to mitigate soil erosion and land degradation effectively (Borrelli et al., 2021).

Remote sensing and Geographic Information Systems (GIS) play a pivotal role in land degradation assessment, offering powerful tools to monitor and combat this critical environmental challenge (Van Lynden and Mantel, 2001). RS technologies, such as satellite images can identify changes in land cover, vegetation health, and soil organic carbon, which are essential indicators of land degradation (Zhu et al., 2022). GIS complements remote sensing by providing a platform for data integration, analysis, and visualization. In essence, the integration of RS and GIS empowers us to better comprehend, assess, and mitigate land degradation (Thakur et al., 2017).

The Gidabo Watershed (GW) (Figure 1) faces critical challenges related to land degradation, driven by LULC change and climate variability which pose significant environmental, economic, and social threats (Wolde et al., 2021). Previous studies in the GW have primarily focused on historic land use changes, neglecting future projections, and often relied on limited climate data sources without rigorous assessment of climate models (Adi et al., 2023; Alehu et al., 2021; Aragaw et al., 2021; Belihu et al., 2020; Dananto et al., 2022). Moreover, there is a lack of information on the extent and magnitude of land degradation, hindering the development of strategies to achieve LDN goals. This study aims to employ an integrated approach to assess LULC changes, evaluate climate models, and assess their impacts on land degradation trajectories and appraise potential management alternatives while considering future scenarios.

1.2. Study area

The GW is situated in the Abaya-Chamo sub-basin of ERVLB between $6^0$8'N to $6^0$57'N latitude and $37^0$0'E to $38^0$40′E longitude (Figure 1) covering an area of approximately 3549 square kilometers. The watershed exhibits a diverse topography, ranging from highlands with rugged terrain to lowlands with flat plains. The elevation varies from over 3197 meters in the highland areas to around 1133 meters above sea level (a.s.l) in the lowlands. The major physiographic units in the area include undulating plains, valleys, steep stream banks, and a significant escarpment located in the eastern part of the watershed (Dananto et al., 2022). At the heart of this watershed is the Gidabo river, one of the major contributors to lake Abaya and a lifeline that provides sustenance and resources to the surrounding communities. Particularly, the Gidabo dam provides water for irrigation and supports local farming communities by allowing for the cultivation of crops year-round, reducing the dependency on rainfall (Desta and Belayneh, 2021; Mana and Abebe, 2023). The river's course is characterized by both gentle and cascading sections, creating a dynamic landscape and extending approximately 120km before draining into lake Abaya in the southwestern (Aragaw et al., 2021; Mechal et al., 2015).

The GW is inhabited by diverse ethnic groups, including the Gedeo, Guji, and Sidama. Each group has its own unique cultural practices and languages (Alehu et al., 2021). The populations are settled more towards the eastern highland, and the population density decreases towards the lowlands (Wolde et al., 2021). The area is characterized by a mix of urban and rural populations where majority of the population in these areas is rural. This demographic composition indicates the importance of agriculture in the livelihoods of the local communities. The population in the GW has been growing alarmingly in the last three decades, and it is currently more than 1.5 million, leading to increased pressure on natural resources (Wolde et al., 2021). The upper part is more populated (>500 inhabitants per square kilometer), and this has an immense impact on potential nexus resources. Due to limited economic prospects, many young people have migrated to urban areas in search of better opportunities (Wolde et al., 2021).

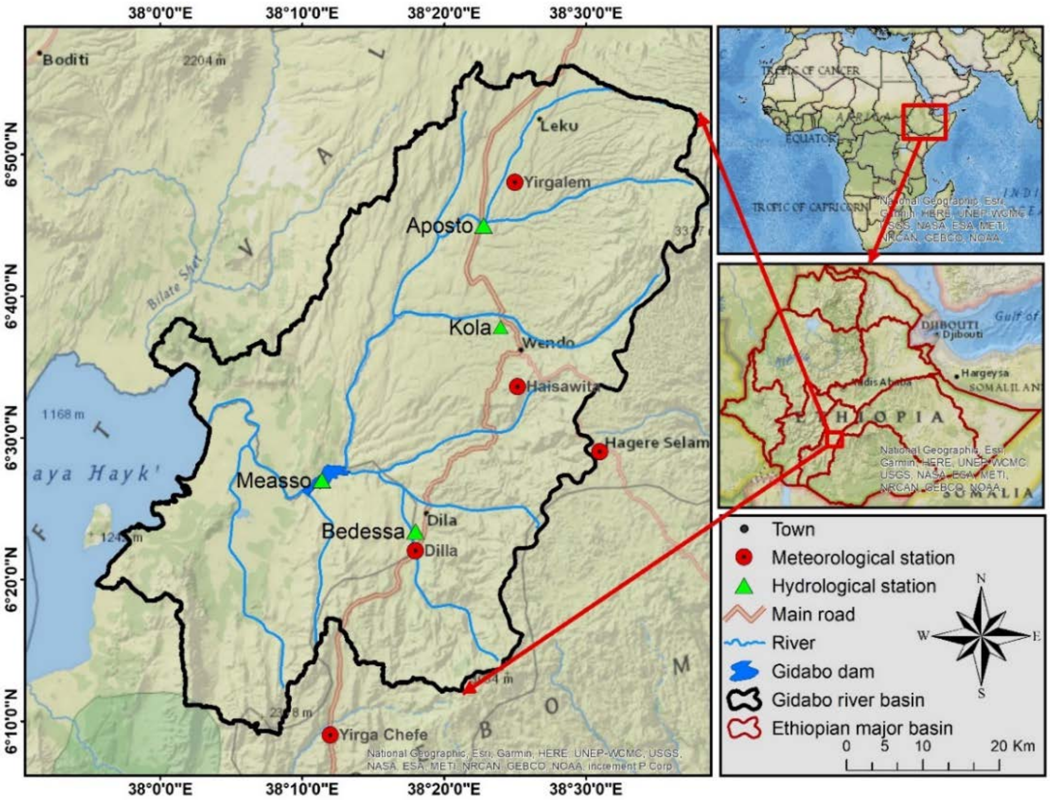

Figure 1. Location of the Gidabo watershed

The GW an average annual rainfall of 1315 mm with bimodal rainfall pattern from March to May and June to October with short transition, and monthly temperatures ranging from 11 to 25°C. The main dry season typically extends from November to February. The highest maximum average temperature is observed during February and March. This variability results in fluctuating water levels and flow rates within the Gidado River, with peak discharge during October. The spatial and temporal groundwater recharge variability is mainly controlled by the climate. Thus, the annual discharge is very sensitive to variations in precipitation and moderately sensitive to temperature changes. Moreover, sensitivity increases towards the rift floor across the watershed (Mechal et al., 2015). Based on the Ethiopian classification of agroecological zones, which uses altitude and rainfall as criteria, moist weyna dega and dry weyna dega are the two major agroecological zones, covering more than 73% of the watershed.

According to FAO’s soil classification, the catchment area has six soil groups, with Eutric Vertisols, Lithic Leptosols and Chromic Luvisols being the dominant type, covering a substantial area (70%). The geological composition in the region primarily consists of volcanic products, including pyroclastic fall deposits, alkali basalt, rhyolite, and volcanic centers compositionally acidic (Dananto et al., 2022). The soil units are also derived from volcanic materials. The land cover comprises a mix of intensively cultivated areas, agroforestry, shrubland, forests, grasslands, waterbodies, and marshlands, indicating the diverse ecological landscape. Agriculture and agroforestry are the predominant land uses and the primary source of income for the majority of residents in in this area. Crops such as maize, coffee, and beans are cultivated, while livestock rearing is also common. In recent years, there has been a shift towards commercial agriculture (Hassen, 2021; Wolde et al., 2020).

1.3. Problem statement

Despite its critical importance for local communities and the ecosystem, the GW faces a pressing issue of land degradation, characterized by accelerated soil erosion, loss of arable land, declining agricultural productivity, water deterioration that poses significant environmental, economic, and social challenges (Alehu et al., 2021; Belihu et al., 2018; Mana and Abebe, 2023; Mechal et al., 2015; Worako et al., 2022). Deforestation driven by various factors, including the expansion of farmland, logging for fuelwood and construction materials, and population growth continues to be the major concerns in the highland areas of the watershed (Belihu et al., 2020). The deforestation has adverse effects on the ecosystem, including increased surface runoff and decreased infiltration rates, which can exacerbate soil erosion (Belihu et al., 2020).

This not only affects soil fertility and crop production but also impacts downstream water resource infrastructures like the Gidabo dam due to excessive sedimentation and eutrophication, exacerbate water resources degradation (Desta and Belayneh, 2021; Guduru and Jilo, 2023). This is further aggravated by climate variability, particularly the decreasing rainfall as well as increasing temperature trends in the watershed (Alehu et al., 2021; Belihu et al., 2020, 2018; Mana and Abebe, 2023; Mechal et al., 2015). For example, Mana et al. (2023), reported that the water supply for irrigation drastically reduced due to the drop in reservoir’s water availability. As a result, the demand for more water to support agricultural activities might be a major challenge in future climatic conditions (Mana et al., 2023).

Despite the clear evidence of these problems, there is lack of comprehensive spatial and temporal information on the extent and magnitude of land degradation in the GW. This gap hinders the development of strategies to achieve LDN goals. Soil erosion and land degradation are complex processes influenced by climate and land use changes (Borrelli et al., 2020). Previous studies in the GW primarily focused on historic changes in land use while neglecting the critical aspect of future projections. Thus, a notable gap exists in predicting future trends for the GW. This omission is significant given the observed dramatic changes, particularly the LULC patterns. Additionally, previous studies in the GW often relied on limited climate data sources (e.g., either observed data or individual climate models) and did not rigorously assess the performance of different climate models, which are crucial for understanding the reliability and uncertainty of climate projections for impact modeling studies. The lack of future-focused studies hampers the development of effective land and water resource conservation strategies.

To address these gaps and challenges, this study aims to employ a comprehensive approach. It simulates LULC dynamics, evaluate the performance of multiple Regional Climate Models (RCMs), and use an integrated approach to assess the impacts of climate and land use change on runoff and sediment yield, and evaluate trends in land degradation. The study also seeks to identify erosion hotspots, and evaluate potential management alternatives to mitigate these challenges, providing valuable insights for policymakers, land-use planners, and other stakeholders to address soil erosion and land degradation in the GW while considering future scenarios.

While the chosen topic and methods employed may not be particularly innovative, one notable aspect of innovation in this work lies in synthesizing diverse perspectives, for example, the integration of soil erosion indicator with LDN indicators to enhance the land degradation assessment. The study assessed the pressing issue of land degradation in the GW by employing a comprehensive approach that integrates various datasets and methodologies. Notably, the study employed a forward-looking perspective by simulating future land use and assessing the performance of regional climate models to project potential impacts on soil erosion and land degradation. Overall, this study contributes significantly to the scientific understanding of the complex interactions between climate, land use, and soil degradation, offering actionable insights for stakeholders striving towards sustainable land and water management in similar watersheds.

1.4. Objectives and research questions

The general objective of this study was to explore soil erosion and land degradation neutrality in the context of climate and land use changes, and identify potential management alternatives to address these critical environmental challenges.

The specific objectives were:

- To assess the historic and future land use and land cover dynamics between 1985 and 2050
- To evaluate the performance of CORDEX-Africa climate models in reproducing the observed rainfall and temperature from 1991 to 2005
- To assess the impacts of climate and land use change on runoff and sediment yield between 1985 and 2060
- To evaluate land degradation dynamics between 1985 and 2021
- To appraise potential management alternatives for future scenarios

The research questions that were focused on are:

- What are the major LULC classes in the study area, and how evolved from 1985 to present and the future to 2050?
- What are the observed trends in climate variables and how different RCMs perform in simulating these variables?
- How climate change and LULC dynamics influence surface runoff and sediment yield?
- Where are critical sub-basins in terms of sediment yield and what are the common characteristics of these critical sub-basins?
- What are the trends in land degradation neutrality in the study area from 1985 to 2021?
- Can the implementation of soil conservation scenarios lead to a reduction in sediment yield?

1.5. Scope of the study

The overarching scope of this study was a multidisciplinary investigation of trends in soil degradation processes influenced by both climatic variables and changing land use patterns within the GW in the ERVLB. The study was structured around specific objectives, including the assessment of historical and future LULC dynamics spanning from 1985 to 2050, the evaluation of regional climate models' accuracy in simulating climate variables, and appraise the impacts of climate and land use changes on surface runoff and sediment yield from 1985 to 2060. Additionally, the studied identified critical sub-basins prone to soil degradation, analyzed trends in land degradation neutrality indicators from 1985 to 2021 and explored the potential effectiveness of soil conservation scenarios in reducing sediment yield. To achieve these objectives, spatiotemporal dataset and multidisciplinary approach was employed, integrating, remote sensing, geospatial analysis, statistical metrics and hydrological modeling.

1.6. Significance of the study

The study has significant importance in the realm of sustainable land and water management, especially in the context of the observed and projected changes in LULC and climate. Ultimately, supporting efforts to address environmental challenges and achieve land degradation neutrality goals in the Gidabo Watershed. The significance of this study lies in its comprehensive investigation ranging from assessing historical and future land use dynamics to evaluating the performance of regional climate models and understanding the impacts on soil and land degradation processes. The findings contribute to a holistic understanding of the complex interactions and environmental challenges faced by the watershed. The observed historical trends in land cover change, climate variables, and sediment yield provide crucial baseline information. The identification of erosion hotspots and critical sub-basins enhances the applicability of the findings for targeted land and water resource management. Additionally, the assessment of land degradation neutrality indicators over the study period revealed concerning trends, emphasizing the urgent need for sustainable land management practices. The study's evaluation of soil conservation scenarios and their effectiveness in reducing sediment yield not only adds practical value for local decision-makers but also aligns with national initiatives like LDN. Ultimately, this research contributes to the scientific understanding of the intricate dynamics between climate, land use, and soil degradation, offering actionable insights for policymakers, land managers, and researchers striving towards sustainable land and water management in similar watersheds.

1.7. The structure of the dissertation

In this dissertation, chapter 1 provides an overview of soil erosion and land degradation, encompassing their causes, consequences, and various factors involved. It also explores the impact of land use and climate change on soil erosion while emphasizing the significance of tools and models in assessing and combating these issues. Furthermore, this chapter outlines the study's aim, objectives and research questions. Chapter 2 aimed at exploring the LULC dynamics. It provides detailed picture of how the LULC has evolved over time (1985–2050). Chapter 3 explores the performance of regional climate models in replicating the observed climate variables (rainfall and temperature) at seasonal, annual and inter-annual time scale to select suitable models. Chapter 4 discusses the dynamics of land degradation indicators, identifies erosion hotspots and appraise potential management alternatives to mitigate soil erosion and land degradation. Finally, chapter 5 synthesizes key findings from previous chapters, offers concluding remarks from various perspectives, pinpoint the scientific contribution of the study. Likewise, the limitation of the study and an outlook for possible future works is also presented. Figure 2 represents the overall schematics of the study.

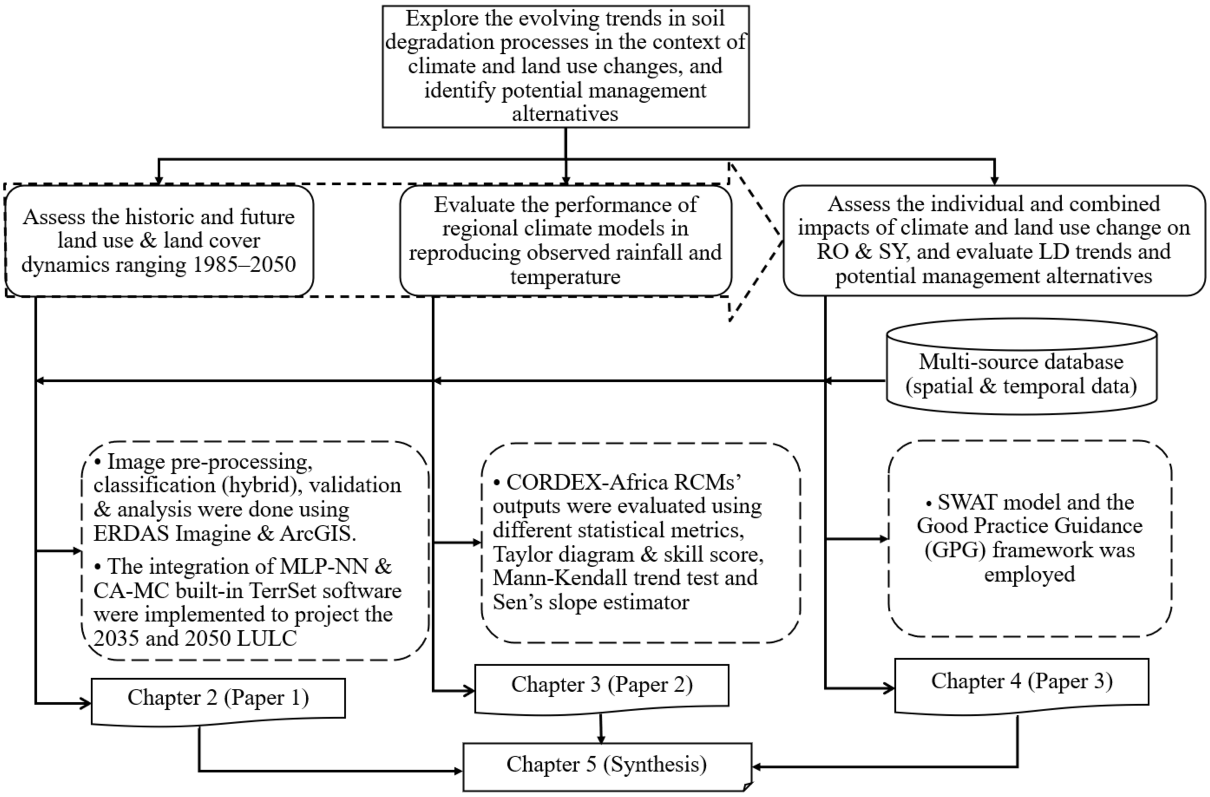

Figure 2. Schematic of the research (RO, SY and LD represents surface runoff, sediment yield and land degradation respectively)

2. Land use land cover change modeling by integrating Artificial Neural Network with Cellular Automata-Markov Chain model in the Gidabo watershed, Ethiopian Rift Valley Lakes Basin

Abstract

Modeling LULC change is crucial to understand its spatiotemporal trends to protect the land resources sustainably. The appraisal of this study was to model LULC change from 1985–2050 owing to the business-as-usual scenario (BAU). Different dependent and independent spatial datasets were used viz, 1985, 2003 and 2021 Landsat imagery; topography features, proximity variables, population density and evidence likelihood. Since the future projection requires the historical land use as a baseline, historical land use trends were detected using hybrid image classification procedure in ERDAS Imagine and nine major land cover classes were identified. Multi-Layer Perceptron Neural Network and Cellular Automata-Markov Chain model built-in TerrSet software were implemented to project the 2035 and 2050 LULC. The study depicts, GW experienced significant LULC dynamics and will also be extended for the coming several years. Agriculture land, settlement and water body showed significant gains at the expense of forest, shrub and grasslands loss. Unsustainable land use practices played a significant role in triggering land degradation. To minimize these adverse consequences of land use change, environmentally-friendly land use planning and management measures must be implemented. The outcome of this study will be helpful in providing the opportunity to develop adequate land and water resource conservation strategy plan for the future.

This chapter is originally published as:

Girma, R., Fürst, C., Moges, A., 2022. Land use land cover change modeling by integrating Artificial Neural Network with Cellular Automata-Markov Chain model in Gidabo river basin, main Ethiopian rift. Environmental Challenges, 6:100419. https://doi.org/10.1016/j.envc.2021.100419.

2.1. Introduction

Environmental changes and challenges to sustainable development can highly be linked to adverse human activities at the expense of demand for land (Lambin et al., 2003;Regasa et al., 2021). Worldwide, particularly in developing countries, extensive LULC changes are predominantly common in recent decades (Gebreslassie, 2014; Kafy et al., 2021; Yirsaw et al., 2017). Similarly, Ethiopia experienced pronounced LULC changes during the last decades with a considerable expansion of cultivated land at the expense of other LULC types (Bewket and Abebe, 2013; Kindu et al., 2013; WoldeYohannes et al., 2018). In the country, anthropogenic activities take the lion-sharing part adversely changing the landscape, which exerts unfavourable and adverse impacts on the environment and livelihood (Regasa et al., 2021). In the Ethiopian Rift, alarming trends in LULC change have been observed due to diverse driving factors. The ever-increasing human population and the subsequent demands on land resources were identified as the underlying major key drivers in the region (Ariti et al., 2015; Desta and Fetene, 2020; Garedew et al., 2009). Changing landscapes often influence the availability of ecosystem services, accelerate susceptibility to climate change (Salazar et al., 2015), and result in the increments of degraded land and eroded areas (Bekele, 2019; Wang et al., 2021).

Previous studies documented that modeling LULC change is crucial to understand its spatiotemporal trends to implement necessary measures and protect the land resources sustainably (Gebreslassie, 2014; Regasa et al., 2021). LULC change modeling is one of the innovative techniques for land resource inventory, monitoring and management (Anurag et al., 2018). Land use change modeling, especially if performed in an integrated, multi-scale, dynamism and spatially explicit manner, can be proved as an essential component for land use change detection and forecasting (Rozario et al., 2017). Modeling has the capability of representing a complex LULC system in an efficient way by incorporating multi-variates. Hence, accurate modeling enhances the understanding of LULC change processes, driving factors and also can project alternative land use scenarios which may lead to the goal of sustainability. Detecting past land-use change and predicting the future exhibit major modifications and has become of concern to conservation officers, environmentalists, and land use planners in promoting sustainable management and mitigating negative impacts (Halmy et al., 2015; Wang et al., 2021).

The integration of remote sensing (RS) and geographic information systems (GIS) made it possible to study the changes in LULC in less time, at a low cost, and with better accuracy (Hassan et al., 2016; Kafy et al., 2021; Rawat and Kumar, 2015; Roy et al., 2015). In the last few decades, the application of this combined approach has flourished significantly to assist in developing a model either to detect the historic or predict the future LULC change (Kafy et al., 2021). RS can cover large areas with both high spatial detail and temporal frequency, ensuring the spatial consistency of datasets (Kafy et al., 2021). This leads towards a fruitful way for sustainable development by providing a long-term view of LULC change dynamics with its future prediction (Gharaibeh et al., 2020; Kafy et al., 2021).

Several models and software packages are available to perform LULC change prediction including, but not limited to, CLUE-S, Cellular Automata (CA), Markov Chain model (MC), Cellular Automata-Markov Chain (CA-MC) model, Multi-Layer Perception Markov Chain, Artificial Neural Network (ANN), statistical, cellular and hybrid models, Binary Logistic Regression Algorithm, System dynamic simulation, Similarity weighted instance-based machine learning algorithm, spatiotemporal modeling, mathematical-equation-base, cellular and agent-based models or a hybrid of the two are some of the prediction models used to simulate the LULC change dynamics (Gharaibeh et al., 2020; Kafy et al., 2021). Most of these models are empirical approaches based on digital change detection algorithms using historic multi-temporal satellite imagery data (Burnicki et al., 2010; Mas et al., 2014; Rawat and Kumar, 2015). This helped to appraise the past land transformation and transition dynamics easily, which in combination with environmental variables can predict future land-use scenarios (Eastman, 2016a; Wang et al., 2021).

The hybrid Cellular Automata-Markov Chain (CA-MC) model is one of the commonly used most effective methods for modeling the spatiotemporal change in LULC (Dey et al., 2021; Hamad et al., 2018; Sang et al., 2011; Yirsaw et al., 2017). CA-MC is combined from the stochastic model (CA) and technique (Markov Chain) (Kafy et al., 2021) which models both temporal change and spatial distribution of land-uses respectively (Guan et al., 2011; Nouri et al., 2014). It is capable to simulate multi-directional LULC change analysis and provides ways for projecting different future scenarios (Halmy et al., 2015; Subedi et al., 2013). However, modeling LULC change needs to take into account the potential power of the explanatory variables such as socioeconomic and environmental data (Mas et al., 2014). In light of this, the integration of the CA-MC model with other models helped to improve its prediction capability (Aburas et al., 2017; Guan et al., 2011; Saputra and Lee, 2019).

Among many methodologies, Multi-Layer Perceptron (MLP) is an effective approach that introduces a better understating of land change process and more accurate results depending on artificial intelligence (Azari et al., 2016; Gharaibeh et al., 2020; H et al., 2017; Mohammady et al., 2014; Tayyebi et al., 2014). The MLP model consists of three layers including input, a few numbers of hidden layers, and output. The model predicts the geospatial changes with the aid of previous changes (Kafy et al., 2021, 2020). MLP has the highest capability to generalize the transition potential through backpropagation (BP) algorithm (Dey et al., 2021; Gharaibeh et al., 2020). Though CA-MC also determines the land transition area to predict the change dynamics (Shafizadeh-Moghadam et al., 2017), the integration of MLP and CA-MC (MLP-CA-MC) takes advantage of both models. MLP facilitates the automatic calibration of the CA-MC model and gives an outperform accurate future change scenario than CA-MC alone (Dey et al., 2021; Mishra et al., 2018).

In the Ethiopian context, few studies tried to model the future trends of LULC changes (Gashaw et al., 2017; Gidey et al., 2017; Hishe et al., 2019; Kura and Beyene, 2020; Leta et al., 2021; Mohamed and Worku, 2020; Tadese et al., 2021). Several studies conducted in the GW provided details of historic LULC change and effect analysis for the past decades while ignoring the expected future changes. These studies pointed out that human-induced LULC has been changed dramatically with a more serious bearing effect on the environment (Aragaw et al., 2021). The increment of encroachment aggravated soil erosion, surface runoff, and sediment inflow to Gidabo irrigation reservoir and drained to Lake Abaya, the biggest lake in the ERVLB (WoldeYohannes et al., 2018). The spatiotemporal variation in LULC is expected in the future, yet no study has attempted to simulate the future LULC dynamics and their effect on GW. Apparently, this study identified a lack of studies focused on predicting future trends of LULC in the watershed. The combined effects of land use and climate changes, for example on hydrology, are different from the separate impacts. In light of this, studies that only focused on projected climate were identified as a gap. Such gaps are then well-thought-out as a bottleneck and limit the opportunity to develop adequate land and water resource conservation strategy and irrigation management plan for the future. Therefore, the study employed the MLP-CA-MC modeling approach to simulate the 2035 and 2050 LULC change dynamics of GW. The findings insight into the deepened understanding of the LULC trends that can assist and guide hydrologists, land-use planners, and policymakers for future consideration.

2.2. Materials and methods

2.2.1. Data source and processing

Since the algorithm in the MLP-CA-MC model requires historical LULC data (dependent variables) to simulate the future dynamics, cloud-free multi-spectral satellite images (Table 1) dated 1985, 2003, and 2021 were collected from the United States Geological Survey Earth Resources Observation and Science (USGS EROS) Centre available at http://glovis.usgs.gov/. The acquisition years (1985, 2003 and 2021) were selected deliberately to coincide with a nationwide drought and famine, after regime change and subsequent policy shift of the country and following the Green Legacy Initiative, respectively. For the reason that the images are acquired for similar month, the acquisition period of imageries would have insignificant seasonal variation (Dey et al., 2021; Islam et al., 2018). MLP assists the incorporation of a variety of driver variables in the model (Mas et al., 2014). Hence, the following main drivers of land-use change were considered in this study viz; population density, elevation, slope, distance to roads, distance to stream and distance to urban. Advanced Spaceborne Thermal Emission and Reflection Radiometer digital elevation model (ASTER DEM 30x30m) version 3 is downloaded from https://search.earthdata.nasa.gov/. Population density and road-river network map of the study area were acquired from Water and Land Resources Centre at www.wlrc-eth.org and the OpenStreetMap (https://www.openstreetmap.org/).

Table 1. Information about the satellite data used in this study (http://glovis.usgs.gov/)

Satellite image	Sensor*	Path/Row	Resolution (m)	Date of acquisition
Landsat-5	TM	168/55	30	18/01/1985
	TM	168/56	30	18/01/1985
Landsat-7	ETM+	168/55	30	12/01/2003
	ETM+	168/56	30	12/01/2003
Sentinel-2	MSI	L1C_T37NDH_A029261	10	28/01/2021
	MSI	L1C_T37NCH_A029261	10	28/01/2021

*TM (Thematic Mapper); ETM+ (Enhanced Thematic Mapper Plus); MSI (Multi-Spectral Instrument)

These datasets were processed in QGIS 3.20 and ArcGIS 10.7 package such as projection to WGS 84 UTM Zone, 37N, data conversion, DEM masking, and separation of road network from other features (river) using Query tool. Euclidian distance function is employed to generate distance map to roads, river/stream, and urban using vector data of the features (Gharaibeh et al., 2020; Kafy et al., 2021). DEM was manipulated in ArcGIS spatial analyst tools to create elevation and slope maps. Ground truth data (GTD) was recorded using handheld Global Positioning System (GPS) receiver so that the controlling points can easily be identified, used in image classification and validation process (Kantakumar and Neelamsetti, 2015).

2.2.2. Working with historical image

Image pre-processing and classification

Image pre-processing, enhancement techniques, and classification were performed in ERDAS Imagine version 16 software. Layer stacking was carried out to convert multiple, usually single band, images into a single multi-band image layer (Islam et al., 2018). Since remotely sensed data are susceptible to distortions, pre-processing like haze and noise reduction was applied to remove such distortions due to acquisition systems and platform movements (Wang et al., 2021). The study boundary is overlaid in two different paths/rows (Table 1), therefore MosaicPro workstation was used to join the images and form a larger image. Image enhancement operations were performed using spatial enhancement tools such as Convolution function to improve the quality of the raster image. Statistics and pyramid layers were computed using the Image Commands tool dialog after removing the no data/null values. Masking and removing of extraneous data were performed using the Subset and Chip tool. To perform image classification the following bands were considered: band 1-5 and 7 were used in the case of Landsat 5 and 7 while band 2, 3, 4, and 8 were used for Sentinel-2.

Hybrid classification (unsupervised and supervised classification) approach, provides more accurate results for larger areas characterized by diverse biophysical composition (Gebreslassie, 2014; Kafy et al., 2021; Ma et al., 2017; Wang et al., 2021). In this regard, the study implemented the hybrid approach to attain more accurate land use classification scheme. Image pixel clustering (unsupervised classification) with similar spectral characteristics was performed using the Iterative Self-Organizing Data Analysis Technique Algorithm (ISODATA). Based on the analyst's experience/knowledge of the area and google earth observation, the clusters were differentiated into nine thematic classes (Table 2) i.e., water body, grass land, forest, agriculture, bare/barren land, built-up, agroforestry, shrub and marsh land. Training signatures (polygons) were drawn for each of the predefined classes (Chowdhury et al., 2020; Kafy et al., 2021). The resulting signature file was then used as input for Maximum likelihood classifier (MLC), it is a robust and popular supervised classification algorithm, to derive mapping rules for all other pixels into the class values (Chowdhury et al., 2020; Das et al., 2021; Islam et al., 2018; Killeen et al., 2015; Ma et al., 2017; Wang et al., 2021).

Validation of classified LULC maps

Prior to change detection and future prediction, assessment of classification accuracy is a prerequisite (Wang et al., 2021) to test the precision and accuracy of imagery. Image classification performance was evaluated using the accuracy assessment tool in ERDAS Imagine (Dey et al., 2021) through a stratified randomly sampled GTD. Overall accuracy (OA), user accuracy (UA), producer accuracy (PA), and kappa coefficient (Kappa) were calculated (Equation 1–4) based on the confusion matrix (Das et al., 2021; Gharaibeh et al., 2020; Kafy et al., 2021; Mi et al., 2019). Kappa values < 0 indicate no agreement, 0–0.2 a slight, 0.0–0.41 as poor, 0.41–0.60 as moderate, 0.60–0.80 as substantial, and 0.81–1.0 as almost perfect agreement (Wang et al., 2021). The validation process was supplemented by 270 reference points collected from Google Earth and 180 actual field level points, and visual interpretation of Landsat images in the respective years (Leisz et al., 2016).

$$OA = \frac{\sum_{i=1}^{r} D_{ii}}{N} \tag{1}$$

$$UA = \frac{\sum D_{ij}}{x_{+i}} \tag{2}$$

$$PA = \frac{\sum D_{ij}}{x_{i+}} \tag{3}$$

$$Kappa = \frac{N \sum_{i=1}^{r} x_{ii} - \sum_{i=1}^{r} (x_{i+} * x_{+i})}{N^2 - \sum_{i=1}^{r} (x_{i+} * x_{+i})} \tag{4}$$

where D_{ii} is number of correctly classified pixels, D_{ij} is number of correctly classified pixels in row i, D_{ij} - number of correctly classified pixels in column j, r is the number of rows in the matrix; x_{ii} is the number of pixels in row i and column i; x_{i+} and x_{+i} are the marginal totals of row i and column i, respectively; and N is the total number of pixels (observations).

Table 2. Major LULC types used and their descriptions (Hassan et al., 2016; Leta et al., 2021)

LULC Types	Description
Agriculture	Includes areas used for perennial and annual crop production, irrigated areas, commercial farms
Agroforestry	It includes a land use system in which woody perennials such trees, shrubs are grown together with perennial and annual crop agricultural crops on the same parcel of land
Barren land	Includes land areas of exposed soil, bare soil and barren area
Built-up Area	Includes commercial areas, urban, residential, and rural settlements, industrial areas
Forest	Areas covered with dense trees (deciduous forests, evergreen forests, mixed forests)
Grass Land	Areas covered by grasses are usually used for grazing and those remain for some months in a year
Marsh land	An area of land where water covers ground usually treeless and dominated by grasses and other herbaceous plants
Shrub land	Includes areas covered with small trees, bushes, and shrubs
Water Body	Areas covered by rivers, streams, canals and reservoir

LULC change detection analysis

The change detection was assessed using two software packages viz, ERDAS Imagine and TerrSet. Image difference algorithm in ERDAS Imagine software (Kafy et al., 2021) was employed to generate change maps between 1985–2003, and 2003–2021. The algorithm operates on continuous data by subtracting pixel values of the before theme from the after theme, and providing two outputs viz, image difference and highlight change image (Kafy et al., 2021). Since change detection calculates the change in brightness values over time, the image difference file reflects those changes using grayscale image composed of single band continuous data. The highlight changes file creates a thematic layer clustered into decreased, unchanged, and increased classes (Kafy et al., 2021). Graphical and statistical change detection was computed using the TerrSet change analysis panel. The panel provided three graphs of land cover change that tell the gains and losses, net change, and contributors to net change experienced by each category (Eastman, 2016a). The annual rate of change per each category was determined by using equations (5) and (6) (Leta et al., 2021).

$$Percent\ of\ change = \left(\frac{Later\ year - Intial\ year}{Intial\ year}\right) \times 100 \qquad (5)$$

$$Rate\ of\ change\ (ha/yr) = \left(\frac{Later\ year - Intial\ year}{Time\ interval}\right) \qquad (6)$$

2.2.3. LULC change simulation

Land Change Modeler (LCM) built in TerrSet software version 18.31 was used to simulate future LULC changes. It is an empirically driven stepwise process performing change analysis, transition potential modeling, and change prediction (Eastman, 2016a) based on the historical change from time 1 (T_1=1985) to time 2 (T_2=2003). The prediction task integrates MLP with CA-MC model. What follows, below, is the detail of executed methodologies to project the 2035 and 2050 LULC:

Change analysis module

The CA-MC analysis module, used to detect the landcover change between 1985 and 2003, is described by using equation 7 (Kafy et al., 2021; Wang et al., 2021):

$$S_{(t+1)} = P_{ij} \times S_{(t)} \qquad (7)$$

where $S_{(t)}$ and $S_{(t+1)}$ represent land use status at time t and $t + 1$ respectively; P_{ij} is the transition probability matrix, which is calculated by using equation 8 (Kumar et al., 2013; Wang et al., 2021):

$$P_{ij} = \begin{bmatrix} P_{11} & P_{12} & \cdots & P_{1n} \\ P_{21} & P_{22} & \cdots & P_{2n} \\ \vdots & \vdots & \vdots & \vdots \\ P_{n1} & P_{n2} & \cdots & P_{nn} \end{bmatrix}, \left(0 \leq P_{ij} \leq 1\right) \qquad (8)$$

where P is the Markov probability matrix, and P_{ij} stands for the probability of converting from current state i to another state j in next time period. Low and high transition will have a probability near to 0 and 1 respectively (Kumar et al., 2013; Wang et al., 2021). The changes were then identified as gains-and-losses to each LULC category, and transitions from one land cover state to another was used to generalize the spatial changing pattern (Dey et al., 2021; Leta et al., 2021). The evidence likelihood transformation panel is a very effective means of incorporating categorical variables into the analysis (Eastman, 2016b). Evidence likelihood[1] was created by determining the relative frequency with which different land cover categories, in this case agriculture land, occurred with in the areas that transitioned from 1985 to 2003.

Driver variables

LULC change simulation needs to take into account the potential power of the independent variables (Gharaibeh et al., 2020). The main driver variables (Var.), listed in Figure 3, were considered in this study. River proximity provides convenience to residents to access resources while changing the land use (Leta et al., 2021). Distance from road, determinant of accessibility, is one of the major drivers in attracting more urban uses and expansion (Gharaibeh et al., 2020; Kim et al., 2020). Distance from urban can be a very strong driver of change where the closer the land to urban centres the easier it is for land to change to urban uses (Gharaibeh et al., 2020). Population density is the most prominent anthropogenic factor in land use change where the higher the density more frequent land use change. Anthropogenic disturbance has a strong association with the land cover type (Chowdhury et al., 2020). Elevation is recognized as the imperative topographic factors affecting LULC change (Leta et al., 2021). Since the annual rate of agricultural expansion was significant, it is logical to create Evidence likelihood, quantitative variable that expresses the likelihood of finding change between agricultural land and all other land classes at the pixel in question (Eastman, 2016b; Leta et al., 2021). Slope affects the spatial trends of land cover change suppose that the gentler a land slope is, the easier it is to have land use changes (Gharaibeh et al., 2020; Zhang et al., 2018). The gain of urban land is highly concentrated on relatively flat slopes and deforestation decreases with the increase of slope gradient (Wang et al., 2017).

[1] Evidence likelihood was used for the determination of the relative frequency of pixels of different LULC types within the areas of change. It is recommended in cases where there are low Cramer’s V values (Leta et al., 2021).

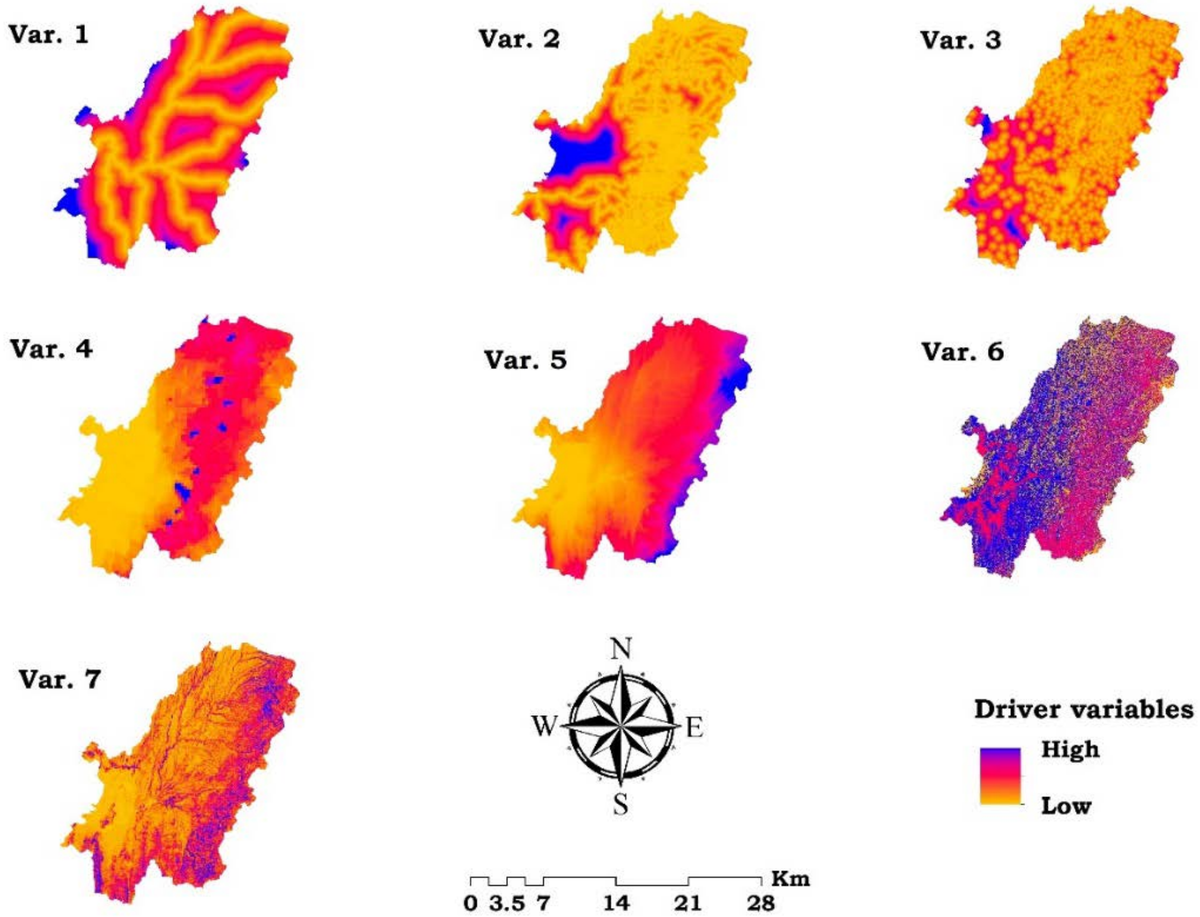

Figure 3. Input layer nodes: Var. 1–River proximity; Var. 2–Distance from road; Var. 3–distance from urban; Var. 4–Population density; Var. 5–Elevation; Var. 6–Evidence likelihood; Var. 7–Slope.

Sensitivity analysis and MLP performance evaluation

MLP involves BP learning algorithm whereby the forward and backward passes continue until the network has learned the characteristics of all the classes (Mandrekar, 2010). Since the selection of appropriate variables will affect the model learning accuracy (Gharaibeh et al., 2020), model sensitivity evaluation is fundamental prior to any LULC change simulation. Parameters and model performance was tested using the MLP classifier built-in TerrSet image processing toolset. Procedurally, the model was trained using all the explanatory variables (Figure 3) and 1985 LULC, then the system repeats the skill tests for the relative power of explanatory variables by selectively holding the inputs from selected variables constant (Eastman, 2016b). The difference in skill thus provides information on the power of that variable. Three different parameter sensitivity analyses were run to measure the skill, S (Equation 9) by forcing a single independent variable to be constant; forcing all independent variables except one to be constant; and backwards stepwise constant forcing mechanism. The skill statistic ranges between -1 and 1 where skill of 1 indicates perfect forecasting, while a skill of -1 means worse than chance and a skill of 0 indicates random chance (Gharaibeh et al., 2020). The acceptable range of model accuracy should be 80% and above to accept the training result (Eastman, 2016b; Gharaibeh et al., 2020; Silva et al., 2020).

$$S = \frac{(A - E(A))}{(1 - E(A))} \quad (9)$$

where *A* is measured accuracy, and *E(A)* is expected accuracy which is determined by using the number of transitions in the sub-model and the number of persistence classes.

The performance and prediction efficiency of the MLP was also assessed by using RMSE (Equation 10) (Elçiçek et al., 2014). RMSE is a benchmark of the deviation of predicated values about the observed values. The lower the value, more accurate is the prediction (Elçiçek et al., 2014).

$$RMSE = \sqrt{\frac{\sum_{i=1}^{N}(\hat{u}_i - u)^2}{N}} \quad (10)$$

Where $\hat{u}_i$ is the modelled for sample i, u_i is the observed data for sample i and N is the total number of samples.

Transition potential modeling and LULC change projection

Skill tested driver variables were imported to the LCM's transition sub-model and MLP was run to create the potential transition maps using the dependent variables (T_1 and T_2 imagery). At this stage, the transition potential images well-captured the effect of the driver variables (Gharaibeh et al., 2020) to provide the suitability of cell transformation for a particular land cover (Balogun and Ishola, 2017; Kafy et al., 2021). Next, hard and soft prediction for the year 2021 LULC change (T'_3) was created following the procedure illustrated in Figure 4 and used as a comparison image in the MLP-CA-MC model validation.

Validation of MLP-CA-MC model output

The validation process was executed to measure the existing agreement and disagreement between the actual satellite driven (T3) and simulated (T'3) LULC map of 2021 to ensure the reliability and acceptance of the MLP-CA-MC model in predicting the future 2035 and 2050 (Dey et al., 2021; Kafy et al., 2021). In this study, two different validations were performed using both the hard and soft predictions. For this purpose, VALIDATE and ROC modules in TerrSet were applied. ROC calculates the area under the receiver operating characteristic curve (AUC) called ROC statistics using the T'3 soft prediction as a comparison map (Eastman, 2016b). AUC takes values from 0 to 1, where a value of 0 indicates a perfectly inaccurate test and a value of 1 reflects a perfectly accurate test (Mandrekar, 2010; Varma, 2021). The VALIDATE module computes kappa index statistics using the T'$_3$ hard prediction as a comparison map: kappa for grid cell level location ($K_{location}$), kappa for no information (K_{no}), kappa for stratum-level location ($K_{locationStrata}$), and kappa standard ($K_{standard}$) (Mishra et al., 2018). A strong and acceptable AUC and Kappa value is usually associated with values in the vicinity of 80% and above (Eastman, 2016b; Gharaibeh et al., 2020; Mandrekar, 2010). For future prediction, the images of 2003 and 2021 were taken as the dependent variable to simulate the LULC map of 2035 and 2050 based on business-as-usual (BAU) scenario. The reservoir was specified as a constraint feature and zoning was applied in the change allocation process so that the transition potentials associated with each transition were multiplied by the constraints map during the change prediction process.

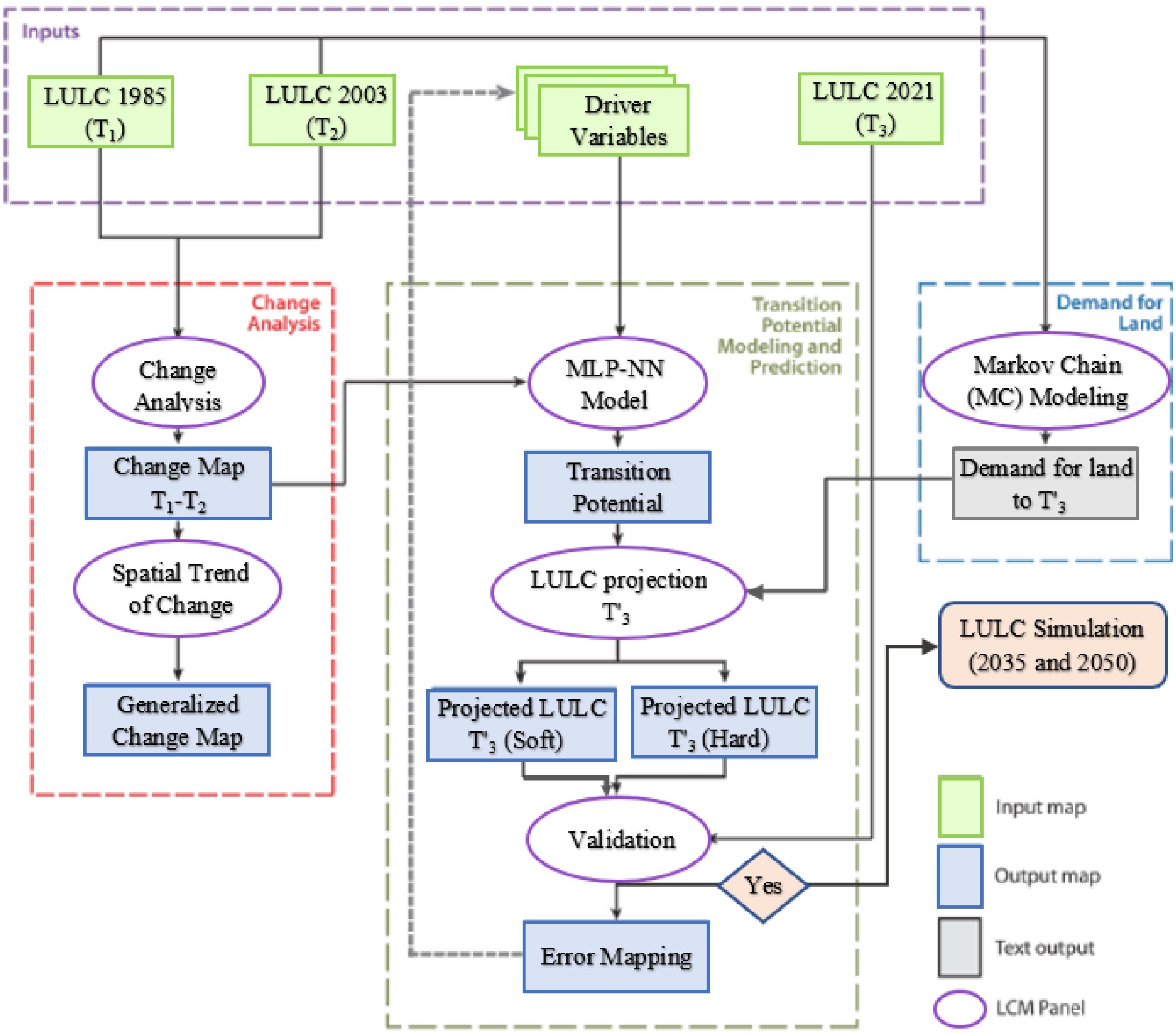

Figure 4. Flow chart for MLP-CA-MC modeling approach (Modified from Eastman (2016a))

2.3. Results and discussion

2.3.1. Historical changes in LULC

Assessing and understanding the historical changes in LULC dynamics is fundamental to forecast future trends for the coming decades (Regasa et al., 2021). Based on the hybrid classification approach, nine major LULC classes were identified viz, water body, grass land, forest, agriculture land, barren/bare land, settlement/built-up area, agroforestry, shrub, and marshy area. The OA and kappa analysis results (Table 3) were found much more than the substantial range ($\geq$ 80%) ensuring a strong level of acceptance (Dey et al., 2021; Wang et al., 2021). The study watershed experienced significant landscape alteration and various changes have been observed over the past 36 years (1985–2021) (Table 4 and Figure 5). In 1985, the largest land cover type was shrub land (24.3%) followed by forest (21.8%) and agriculture (19.8%). In the subsequent years (2003 and 2021), agricultural land has undergone a significant expansion and overturned the dominancy by 25% and 40% respectively. Similarly, the spatial extent of agroforestry was increased from 13% to 15% and 20% over the study years. While forest coverage continually decreases from 21.8% to 19.5%, and 11.2% during the same year.

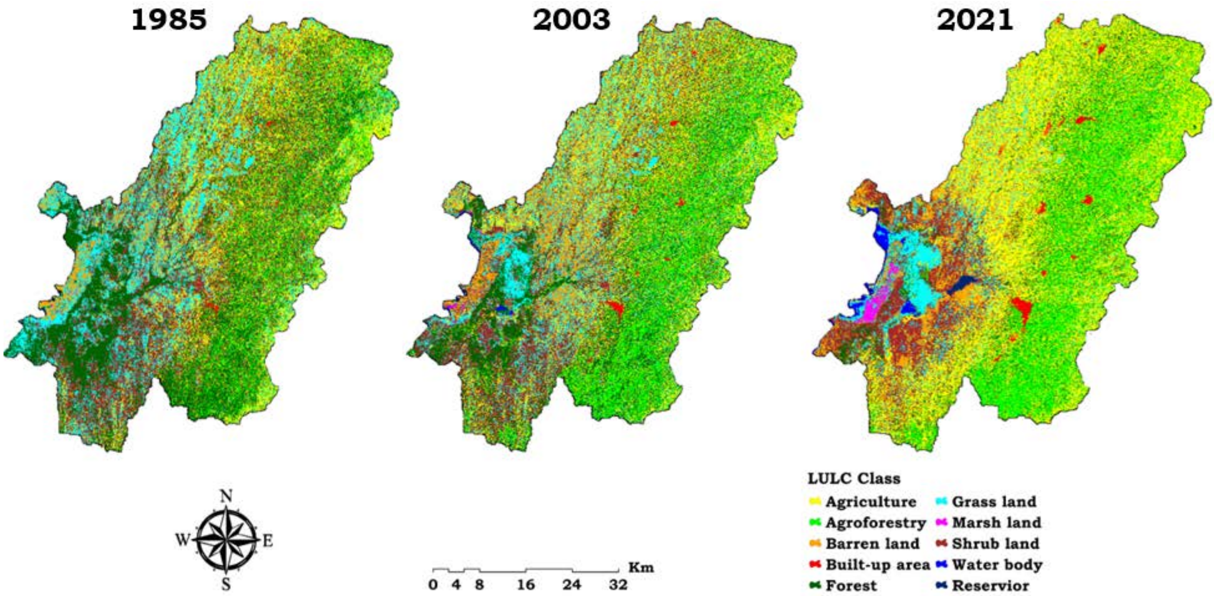

Figure 5. LULC map for 1985, 2003 and 2021

Table 3. Classification accuracy assessment result for 1985, 2003, and 2021

Year	LULC Class																			
	Water body		Grass land		Forest		Agriculture		Barren land		Built-up		Agroforestry		Shrub land		Marsh land			
	PA (%)	UA (%)	PA (%)	UA (%)	PA (%)	UA (%)	PA (%)	UA (%)	PA (%)	UA (%)	PA (%)	UA (%)	PA (%)	UA (%)	PA (%)	UA (%)	PA (%)	UA (%)	OA (%)	Kappa (%)
1985	93.6	96.7	80	80	78.8	86.7	77.1	90	88.9	80	87.1	90	85.7	80	89.7	86.7	96.2	83.3	85.9	0.84
2003	93.6	96.7	78.8	86.7	87.5	70.0	81.8	90.0	90.6	96.7	96.4	90.0	74.2	76.7	80.0	80.0	96.4	90	86.3	0.85
2021	96.4	90.0	77.1	90.0	76.5	86.7	93.6	96.7	90.3	93.3	96.6	93.3	75.9	73.3	91.7	73.3	89.7	86.7	87.04	0.85

Table 4. Area (ha) and net change (% of area) of historical LULC classes

LULC type	Area (ha)			Annual change (ha/yr)		Net change (% of area)	
	1985	2003	2021	1985-2003	2003-2021	1985-2003	2003-2021
Water body	91.44	601.8	3798.3	28.36	177.58	0.14	0.90
Grass land	61836.39	52727.9	30109.3	-506.03	-1256.6	-2.57	-6.37
Forest	77194.26	69172.7	39822.57	-445.65	-1630.7	-2.26	-8.27
Agriculture land	70326.99	89062	140869	1040.84	2878.2	5.28	14.59
Barren land	12507.75	18060.4	19397.3	308.48	74.27	1.56	0.38
Buit-up	478.44	1175.9	3179.6	38.75	111.32	0.20	0.56
Agroforestry	46207.17	54388.4	71109.5	454.51	928.96	2.30	4.71
Shrub land	86238.45	69517.8	44623.1	-928.93	-1383.04	-4.71	-7.01
Marsh land	85.41	259.5	2057.7	9.67	99.90	0.05	0.51

Table 5 represents the detailed transition area matrix in hectare (ha) of each category between 1985–2003 and 2003–2021. The analysis has shown there has been continuous annual deforestation (2.4% per year) with the expense of agroforestry (1.71% per year) and agricultural land (3.23% per year) expansion between 2003 and 2021. The other major rate of change was recorded in the built-up area from 8.1% to 9.5% between 1985–2003 and 2003–2021 respectively. Annual reduction in grass (2.4%) and shrub land (2%) has been noticed for the past 36 years remarkably after 2003. In the vicinity of GW, similar trends of change were observed by previous studies, what follows is as proof: According to Wolde et al. (2021), significant changes were occurred in agroforestry, bare land, settlements, and grass land from 1986 to 2019; study conducted by Aragaw et al. (2021), showed the increment in cultivated land and urban areas between 1988 and 2018 where as a decline in evergreen forest, grassland and agroforestry (exceptionally increased between 2000 and 2018) was observed in the same year; In the upper catchment of Gidabo, agriculture land and urban expansion was identified at the expense of loss of agroforest, grassland and forest between 1985 and 2018 (Belihu et al., 2020). In 2014, Worku confirmed the increments of cropland land and agroforestry while forest cover, grass land and shrub land decreased from 1986 to 2006 in Ameleke Watershed, tributary of Gidabo river.

According to WoldeYohannes et al. (2018), rapid reduction in shrubland and natural grassland, and an increase in arable land was observed in the Abaya-Chamo sub-basin between 1985 and 2010. A study conducted by Ariti et al. (2015) and Gebreslassie (2014), in the Ethiopian Central Rift Valley, revealed similar trends of change from grass, shrub, and forest to agricultural land. The expansion of marshy area and water body was observed in the south-western part i.e., shore side of Lake Abaya. Marsh land was increased from 21.96ha (1985) to 259.47ha (2003) and 2057.67ha (2021). Conspicuously, 3798.27ha area of land was accounted for water body in 2021. Out of which 23% is an artificial reservoir accredited to Gidabo irrigation dam. An attempt has been made and studies confirmed most of the Ethiopian Rift Valley lakes experienced unstable water level fluctuations. For instance, Lake Abaya experienced a significant and continuous increasing trend in water level (Dadi et al., 2015; Schütt, 2005). As stated by WoldeYohannes et al. (2018), the surface area of Lake Abaya was reduced by 1.2% between 1985 and 1995 and has increased by 2.9% since then. This might be one of the reasons for the expansion of marshy areas and water bodies. Therefore, the result of this study is consistent with past studies.

Table 5. Transition area matrix (ha) of LULC between 1985–2003 and 2003–2021

LULC Class		2003 Water body	Grass land	Forest	Agriculture land	Barren land	Built-up area	Agroforestry	Shrub land	Marsh land	Total
1985	Water body	88.29	1.08	0.99	0.09	0	0	0	0.99	0	91.44
	Grass land	95.22	21002.76	2590.65	14708.7	7834.05	80.01	574.29	14883.66	67.05	61836.39
	Forest	344.7	4499.55	32333	8690.58	125.19	137.88	20827.35	10163.16	72.81	77194.26
	Agriculture land	8.1	10312.47	8228.61	30688.11	1703.7	160.47	5995.71	13229.55	0.27	70326.99
	Barren land	25.38	2696.67	86.85	1044	6886.8	60.93	16.02	1634.85	56.25	12507.75
	Built-up area	0	0.18	2.25	0.09	0.18	474.93	0.09	0.72	0	478.44
	Agroforestry	4.68	1863	11446.74	10855.53	40.59	88.47	17835.21	4072.86	0.09	46207.17
	Shrub land	28.26	12347.82	14482.8	23070.24	1469.52	173.25	9139.68	25516.8	10.08	86238.45
	Marsh land	7.2	4.32	0.72	4.68	0.36	0	0	15.21	52.92	85.41
	Total	601.83	52727.85	69172.65	89062.02	18060.39	1175.94	54388.35	69517.8	259.47	354966.3

LULC Class		2021 Water body	Grass land	Forest	Agriculture land	Barren land	Built-up area	Agroforestry	Shrub land	Marsh land	Total
2003	Water body	516.96	30.87	16.47	16.02	4.32	0.36	0.27	15.84	0.72	601.83
	Grass land	671.4	10591.56	2573.55	22179.87	5150.61	294.93	2683.08	8014.41	568.44	52727.85
	Forest	1232.64	3326.13	12149.28	21027.06	1482.84	441.72	18520.92	10947.06	45	69172.65
	Agriculture land	185.31	5393.43	9449.46	48537.18	2797.29	570.69	15199.56	6794.1	135	89062.02
	Barren land	376.92	3470.58	209.34	5041.17	5761.8	160.47	73.35	2375.1	591.66	18060.39
	Built-up area	0	1.98	3.87	0.72	0.45	1166.13	0.27	2.52	0	1175.94
	Agroforestry	98.73	439.92	8711.64	14089.5	220.95	195.48	29096.1	1534.59	1.44	54388.35
	Shrub land	548.91	6844.77	6708.69	29977.47	3976.02	349.83	5535.99	14936.13	639.99	69517.80
	Marsh land	167.4	10.08	0.27	0	2.97	0	0	3.33	75.42	259.47
	Total	3798.3	30109.3	39822.6	140869.0	19397.3	3179.6	71109.5	44623.1	2057.7	354966.3

Among the land uses, agriculture and agroforestry are the dominant livelihood of the local community (Aragaw et al., 2021; Belihu et al., 2020), resulting in increased trends in the study area and could be a significant contributor to continuous deforestation and forest cover change. Besides agricultural practice, forest resources are the main contributor to the livelihood of rural households, for example; firewood, timber, and charcoal production for commercial and community use which trigger the losses (Dadi et al., 2015; Yemiru et al., 2010). Regasa et al. (2021) briefly reviewed, during the last decades, Ethiopian lands changed from natural to agricultural land use, waterbody, commercial farmland, and built-up/settlement. Forest land, grazing land, swamp/wetland, shrubland, rangeland, and bare cover class changed to other LULC class types, mainly as a consequence of the increasing anthropogenic pressure. Rapid population growth, internal migration, policy shifts, and regime change were identified as the key driving forces of LULC changes (WoldeYohannes et al., 2018).

2.3.2. Gains and losses in LULC types

Gains and losses for the respective study period were acquired from the LCM change analysis module and represented by a graph in Figure 6. The largest gain was observed in the case of agricultural land (Figure 6), besides shrub and forest cover was diminished predominantly over the entire period. Agriculture gained 8.42% and 13% of area in 2003 and 2021 respectively. Shrub land (1.42%), agroforestry (0.7%), and grass land (0.63%) were the largest agriculture's contributors between 1985 and 2003 (Figure 7). In this same year, agroforestry gained 1.35% and 0.73% area of land from forest and shrub land respectively. 0.74% grass cover was converted to barren land while receiving 0.47% from forest and agroforestry. Next to grass land, agriculture and shrub was the largest contributor to bare land (Figure 6). Grossly, 8.76% shrub and 6.47% forest cover have transformed to other land use between 1985 to 2003 (Figure 7). Between 2003-2021, majority of the area from shrub (3.34%), grass (2.42%), and forest (1.67%) were converted to agricultural land (Figure 8). Losses from forest (1.41%), shrub (0.58%), and grass (0.32%) cover were noticed with the expansion of agroforestry (Figure 8) in the same year respectively. Grass land (0.87%), forest (0.25%) and shrub (0.22%) were converted to barren land since 2003. By 2021, water body gained 0.31% by area of land (Figure 8) principally from forest cover taking into account the reservoir was situated in areas where forest cover was dominant in the preceding years.

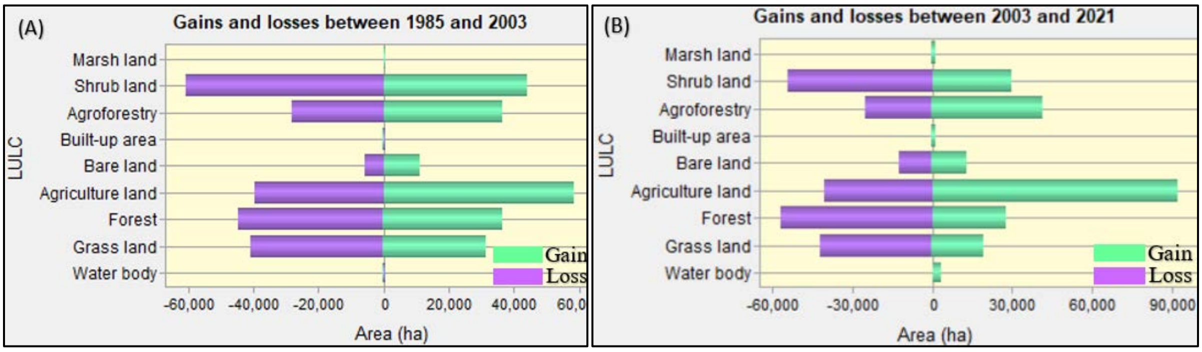

Figure 6. Gains and losses graph between 1985-2003 (A) and 2003-2021 (B)

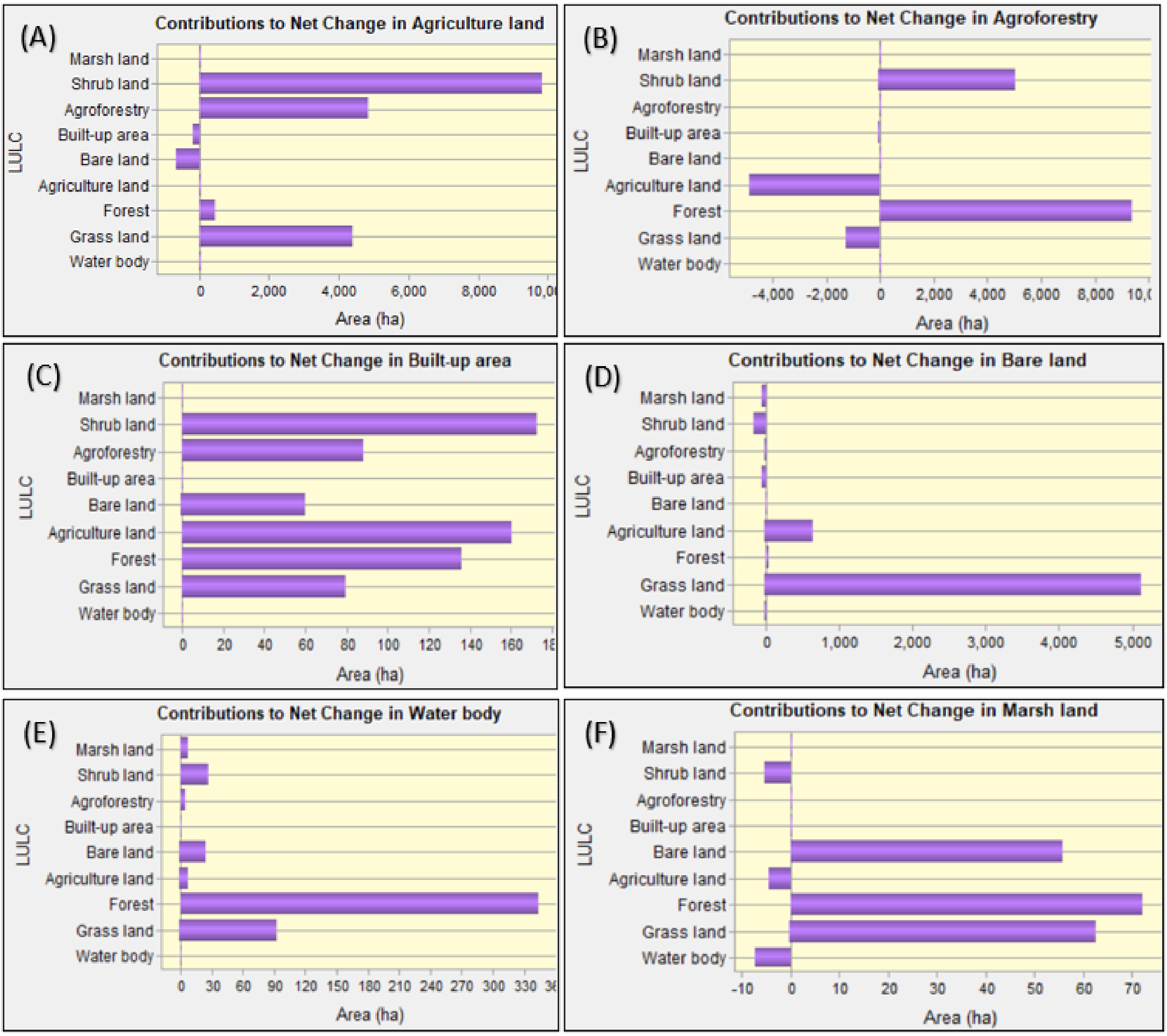

Figure 7. Contributions to net change (ha) in agriculture (A), agroforestry (B), built-up area (C), barren land (D), water body (E) and marsh land (F) between 1985 and 2003

Figure 8. Contributions to net change (ha) in agriculture (A), agroforestry (B), built-up area (C), barren land (D), water body (E) and marsh land (F) between 2003 and 2021

Over the entire period, the settlement gained mainly from shrub land, agriculture, grass land, and forest cover in sequential order. The statistical and graphical representation of net change by each category was also presented in Table 4 and Figure 9. A significant net increase was noticed in agriculture from 18735ha to 51807ha between 1985–2003 and 2003–2021 respectively. The next positive growth was marked in agroforestry from 8181ha to 16721ha in the same year whereas, the net change in barren land gradually decreased from 5553ha to 1137ha between 1985–2003, and 2003–2021 respectively. This is because bare land was converted to water body, marsh land between 2003-2021. Built-up area, water body, and marshy area show positive increment. On the contrary, a significant decline was observed in the case of shrub land (16721ha, 24895ha), forest cover (8022ha, 29350ha) and grass land (9109ha, 22619ha) between 1985–2003 and 2003–2021 respectively (Figure 9). Transformation maps (Figure 10) between 1985–2003 and 2003–2021 were created using image difference operator in ERDAS. Accordingly, unchanged value describes the percentage of persistence pixels; the decreased class represents transitions to water body, forest, and grass land whereas the expansion in agriculture, agroforestry, barren, and settlement by replacing, for example, forest and grass land indicated by increased class. Out of the total area (Figure 10), 38% is unchanged, 32% is in the decreased category while 30% is in the increased class between 1985 and 2003. Since 2003, both the unchanged and increased class accounted for 35%, whereas the remaining 30% is in the decreased category. The result indicated the gradual decrease of the persistence classes from 1985–2003 and 2003–2021.

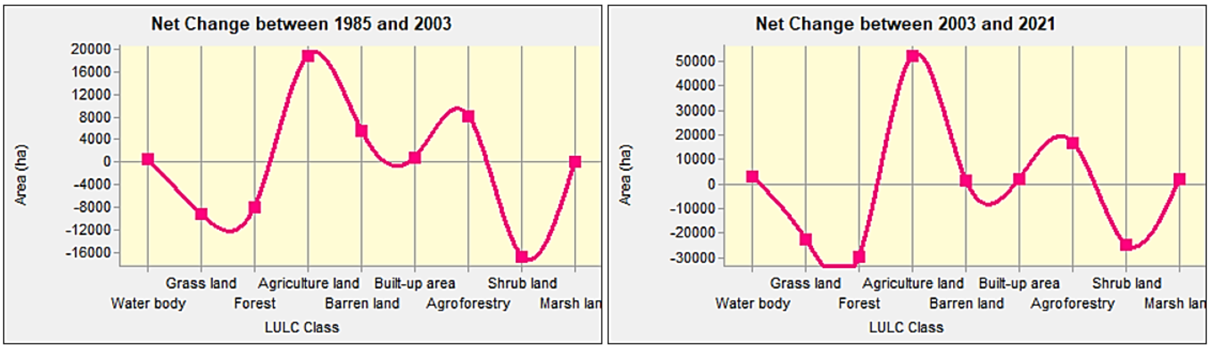

Figure 9. Net change graph between 1985-2003 and 2003-2021

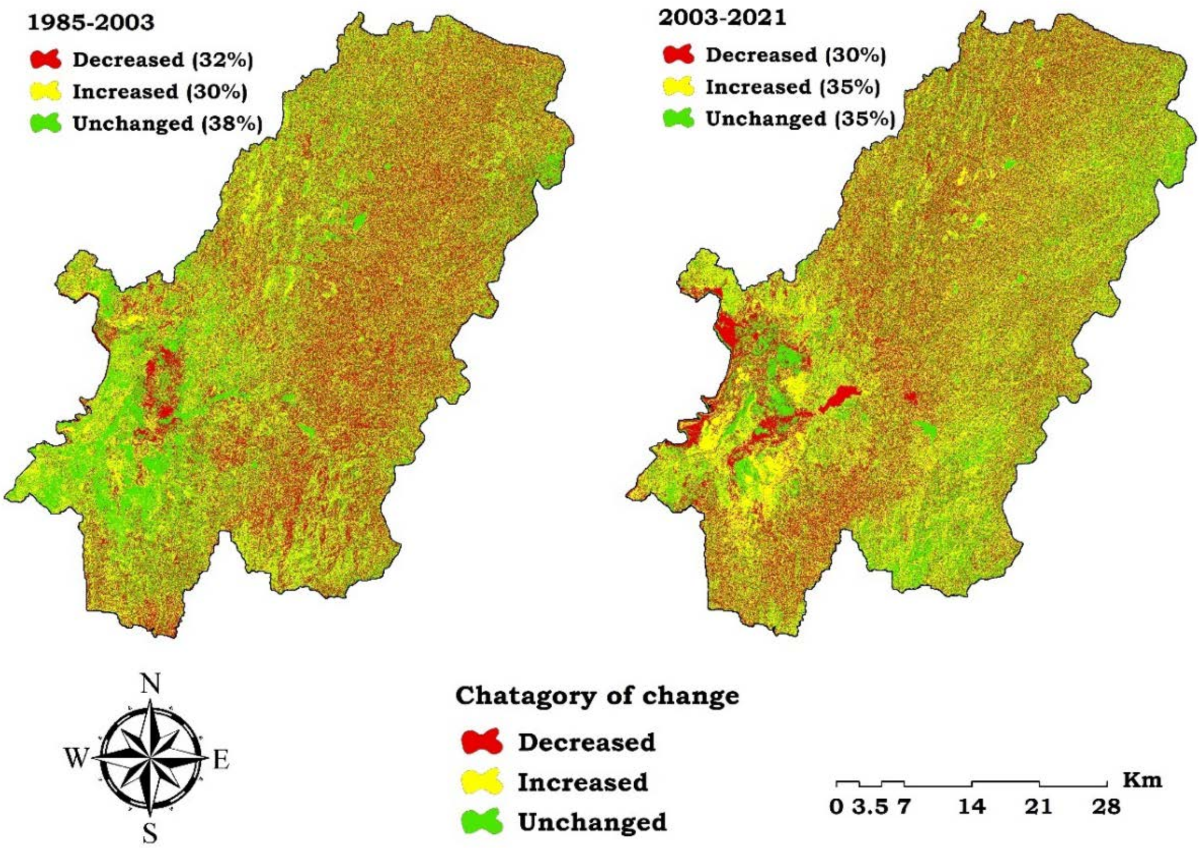

Figure 10. LULC transformation maps of the study area between 1985-2003 and 2003-2021

2.3.3. MLP skill measure

MLP is a machine learning technique capable to model complex patterns and behaviour (Gharaibeh et al., 2020). In the present study, a three-layer feedforward MLP was designed with one input layer, one hidden layer, and one output layer (Table 6). Each layer contains nodes (or neurons) connected by different weights: the input layer had seven nodes called driver variables; eight nodes were created in the hidden layer and nine nodes were associated in the output layer. The effect and influence order of each driver variable was statistically tested against the MLP skill using 10000 iterations, and three different sensitivity analysis techniques were executed as illustrated in the subsequent sub-sections. The purpose of training the network is to get the proper weights both for the connections between the input and hidden layers and between the hidden and the output layers for the classification of unknown pixels. The overall (with all variables) skill (0.9) and accuracy (93.52%) of the model is well beyond the permissible limit (80%) to accept the training result for future projection (Table 6).

Table 6. Parameter and model performance result

Application type	Classification
Input layer neurons	7
Hidden layers	1
Hidden layer 1 neurons	8
Output layer neurons	9
Requested samples per class	1000
Final learning rate	0.0003
Momentum factor	0.5
Sigmoid constant	1
Acceptable RMS	0.01
Iterations	10000
Training RMS	0.1312
Testing RMS	0.1363
Accuracy rate	93.52%
Skill measure	0.9271

Forcing a single independent variable to be constant

The model was tested holding a single variable constant at a time to determine which variable was the most influential and which one was the least influential. The result in Table 7 indicated that holding evidence likelihood constant significantly generates poor model accuracy (28%) and least skill measure (0.2). This implied the evidence likelihood is the most influential parameter while holding elevation constant has shown less impact and it was considered as the least influential parameter. However, the study watershed is characterized by its diverse biophysical composition therefore elevation variation can be a considerable driver of change (Rawat and Kumar, 2015; Simwanda et al., 2020). Leta et al. (2021) attained similar order for evidence likelihood in the western part of Ethiopia.

Table 7. The result of forcing a single independent variable to be constant

Model	Accuracy (%)	Skill measure	Influence order
With all variables	93.52	0.9271	N/A
Var. 1 constant	90.87	0.8973	6
Var. 2 constant	88.07	0.8658	3
Var. 3 constant	90.65	0.8948	5
Var. 4 constant	89.05	0.8768	4
Var. 5 constant	94.10	0.9336	7 (least influential)
Var. 6 constant	28.01	0.1901	1 (most influential)
Var. 7 constant	33.84	0.2557	2

Var. 1 is river proximity; Var. 2 is distance from road; Var. 3 is distance from urban; Var. 4 is Population density; Var. 5 is Elevation; Var. 6 is Evidence likelihood and Var. 7 is Slope

Forcing all independent variables except one to be constant

All variables are held constant except one in order to get information about each variable. In this case (Table 8), a considerable deviation of accuracy and skill measure was observed in each attempt except the first one (with all variables). Here, it is deducible to understand the presence of interaction effects as well as intercorrelations between input variables (Eastman, 2016b).

Table 8. The result obtained by forcing all independent variables except one to be constant

Model	Accuracy (%)	Skill measure
With all variables	93.52	0.9271
All constant but var. 1	11.29	0.0020
All constant but var. 2	11.64	0.0060
All constant but var. 3	11.29	0.0020
All constant but var. 4	11.29	0.0020
All constant but var. 5	11.29	0.0020
All constant but var. 6	33.99	0.2574
All constant but var. 7	22.48	0.1279

Backwards stepwise constant forcing

The training process was initially started using all variables, it then holds constant every variable, in turn, to figure out which pair, when held constant/removed, have the least effect on the skill. Thus, it can sometimes occur that the skill of the model slightly increases as some of the variables are removed. However, in this study all the variables (Table 9) were considered since model skill (step 1 and 2, Table 9) variation was insignificant.

Table 9. The output from backwards stepwise constant forcing

Model	Variables included	Accuracy (%)	Skill measure
With all variables	All variables	93.52	0.9271
Step 1: var.[5] constant	[1,2,3,4,6,7]	94.10	0.9336
Step 2: var.[5,1] constant	[2,3,4,6,7]	93.37	0.9254
Step 3: var.[5,1,4] constant	[2,3,6,7]	89.40	0.8808
Step 4: var.[5,1,4,2] constant	[3,6,7]	85.57	0.8377
Step 5: var.[5,1,4,2,3] constant	[6,7]	78.83	0.7618
Step 6: var.[5,1,4,2,3,7] constant	[6]	33.99	0.2574

2.3.4. Validation of simulated map

For validation, the MLP-CA-MC model was first applied to simulate the soft and hard LULC patterns in 2021 (T'_3) using the LULC maps of 1985 (T_1) and 2003 (T_2). Kappa statistic for quantity and location was derived based on the comparison between the hard simulation and the reference map of 2021. The statistics showed that K_{no} value is 87%, $K_{location}$ value is 87%, $K_{locationStrata}$ value is 85%, and $K_{standard}$ is 79.9%. All the kappa index values exceed the satisfactory range ($\geq$80%) (Eastman, 2016b; Gharaibeh et al., 2020; Mandrekar, 2010), ensuring good agreement between the simulated and observed LULC maps. Quantity disagreement occurs when cell quantity of the same category of T'_3 differs from T_3. Wherever cell's location of the same category of T'_3 differs from T_3, location disagreement will occur (Gharaibeh et al., 2020). The bar graph in Figure 11, presents the distribution of agreement and disagreement components, and the overall proportion correct (91.3%) for MLP-CA-MC. ROC measure was used to determine how well a continuous surface predicts the locations given the distribution of a Boolean variable (soft prediction). In the present study, an acceptable AUC value of 0.75 was attained (Mandrekar, 2010).

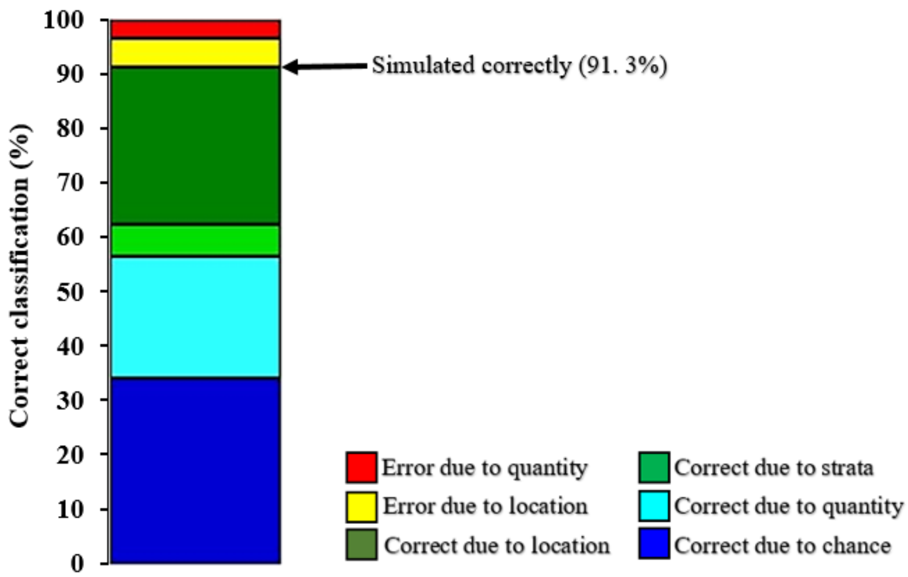

Figure 11. Successes and errors of the simulation

2.3.5. LULC prediction for 2035 and 2050

The appraisal of this study is to model LULC change and predict what the landscape might look like in the years 2035 and 2050 owing to the BAU scenario. The simulated areal extent and net change (%) by category are presented in Figure 12 and Table 10. The unceasing expansion of agriculture land (48.3%, 55%), agroforestry (23%, 25.2%), water body (1.7%, 2.5%), and built-up (1.4%, 2%) will be expected by 2035 and 2050 respectively. In contrast to this, grass land (6.5%, 3%), forest (7%, 2.6%) and shrub land (4.9%, 2.8%) will decrease drastically while marshy area and barren land will show a positive growth till 2035 (0.8% and 6.82% of area) and decreased by 2050. Agriculture will gain the largest share from shrub land (2.8%), grass land (1.4%), and forest cover (1.1%) in 2035. The growth in agroforestry will replace 0.8% of agriculture, 0.4% shrub, and 0.2% forest in the same year. Concurrently the expected expansion of built-up area will replace agricultural land, forest cover, agroforestry, shrub, and barren land by 2035. Almost 0.65% of shrub land will contribute to the net change of grass cover between 2021 and 2035.

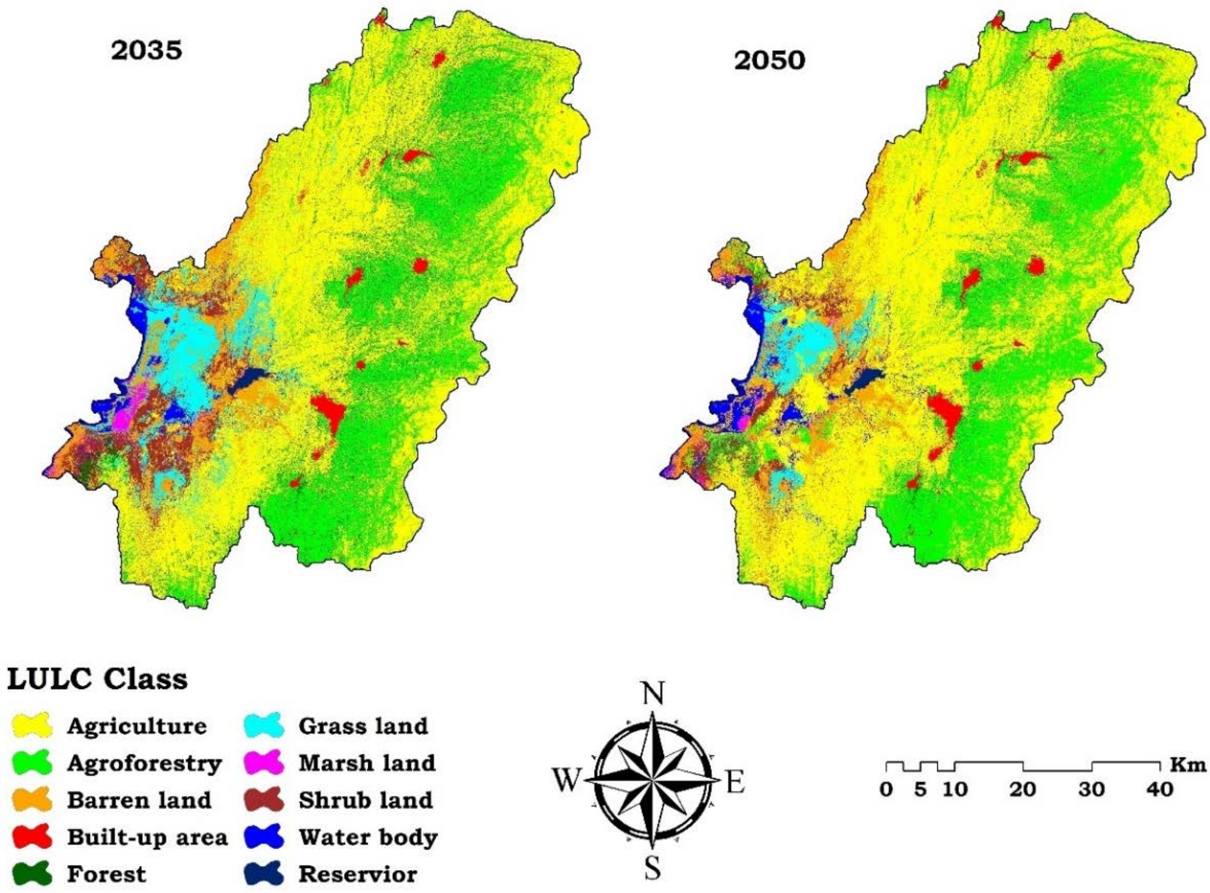

Figure 12. Projected LULC map for 2035 and 2050

Table 10. Area (ha) and net change (% of area) of LULC for 2035 and 2050

LULC type	Area (ha)			Annual change (ha/yr)		Net change (% of area)	
	2021	2035	2050	2021-2035	2035-2050	2021-2035	2035-2050
Water body	3798.3	6060.78	9018.45	161.6	197.18	0.33	0.43
Grass land	30109.3	23133.6	10589.22	-498.3	-836.29	-1.01	-1.81
Forest	39822.57	24984.63	9242.91	-1059.9	-1049.5	-2.14	-2.27
Agriculture land	140869	171316.53	194883.6	2174.8	1571.14	4.39	3.4
Barren land	19397.3	24193.35	23479.11	342.6	-47.62	0.69	-0.1
Buit-up	3179.6	4914.45	6712.92	123.9	119.90	0.25	0.26
Agroforestry	71109.5	80125.38	89306.28	644.0	612.06	1.3	1.32
Shrub land	44623.1	17381.52	9786.15	-1945.8	-506.36	-3.93	-1.1
Marsh land	2057.7	2856.06	1947.69	57.0	-60.56	0.12	-0.13

Table 11 and Table 12 represents the detailed transition probability matrix and transition area matrix (ha) of each category between 2021–2035 and 2035–2050. The interminable agricultural practice will gain mainly from grass (2%), forest (1.2%), and shrub (0.62%) cover sequentially between 2035 and 2050. The LULC projection shows water bodies will increase with the expense of marshy area (0.2%), agriculture (0.11%), barren (0.1%), and grass (0.1%) cover reduction between 2035 to 2050. Though marshy areas will be replaced by water bodies, simultaneously it will gain almost 0.1% from barren between 2035 and 2050. Agroforestry will gain 0.62%, 0.54%, and 0.27% respectively from forest, shrub, and agriculture classes in the same year. The expected expansion of built-up area will replace 0.12% agricultural land and 0.1% agroforestry. The 2035 and 2050 forecasted LULC change analysis indicated the annual expansion rate of agricultural land by 21% and 13%; settlement by 54.6% and 36.6%; agroforestry by 12.6% and 11.5%; water body by 59.6% and 48.8% respectively. The expected annual rate of loss by forest cover is 37.3% and 63%; grass land is 23% and 54%; shrub is 61% and 43.7% in the same year. The gains, losses, and net change (ha) by graph are represented in Figure 13 and Figure 14.

Similar to other watersheds in Ethiopia, GW experienced significant LULC dynamics and agricultural land showed a continuously increasing trend at the expense of forest, shrub, and grasslands to meet the ever-growing demands. According to this study, this trend of alteration will also be extended for the coming 30 years (2050). Though there were different causes, the anthropogenic pressure could take the lion's sharing part in aggravating the change. The rapidly increasing population, an average annual rate of around 2.61% according to (World Population Review, 2021), has led to declining availability of farmland and shifting to marginally unsuitable areas. Those changes in land use types and the related trend of increasing landscape fragmentation (triggered by scarce land resources) played a significant role in the increased rate of soil erosion, sediment load, hydrological imbalance, and land degradation. For instance, Bekele (2019) and WoldeYohannes et al. (2018) mentioned the remarkable effect of land-use change on soil erosion, surface runoff, and sediment transport; Aragaw et al. (2021) and Belihu et al. (2020) noted the impact of land-use change dynamics on the hydrological response emphasizing the negative effect of agriculture land expansion on baseflow, lateral flow, percolation, and evapotranspiration. The changes that occurred in major land use had significantly impacted hydrological behaviours, energy characteristics, and food production potential, resulting in food insecurity (Wolde et al., 2021). To minimize these adverse consequences of land-use change, environmentally-friendly management measures must be implemented in the future.

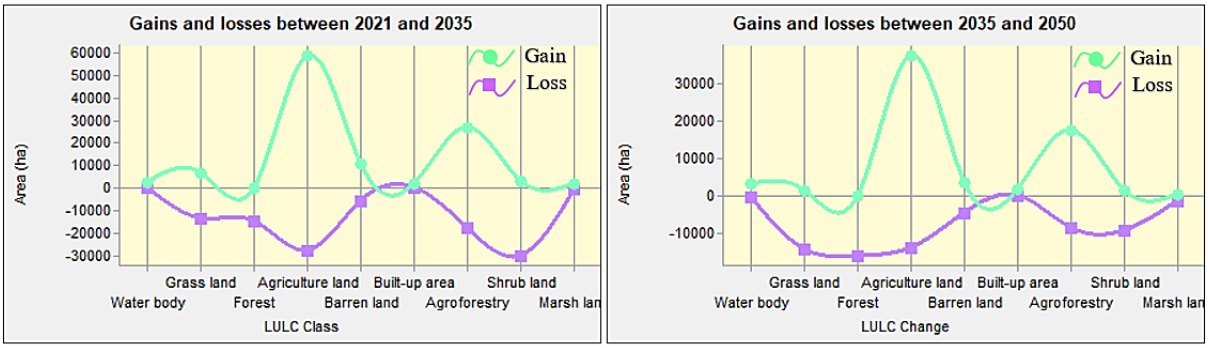

Figure 13. Gains and losses (ha) graph between 2021-2035 and 2035-2050

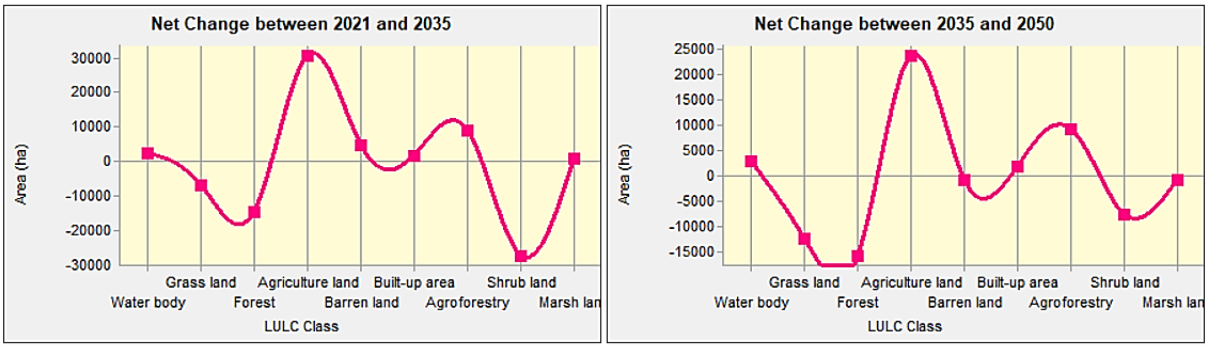

Figure 14. Net change (ha) graph between 2021-2035 and 2035-205

Table 11. Transition probability matrix of LULC between 2021–2035 and 2035–2050

LULC Class		2035								
		Water body	Grass land	Forest	Agriculture land	Barren land	Built-up area	Agroforestry	Shrub land	Marsh land
2021	Water body	1.0000	0.0000	0.0000	0.0000	0.0000	0.0000	0.0000	0.0000	0.0000
	Grass land	0.0117	0.5349	0.0000	0.3291	0.1046	0.0052	0.0033	0.0000	0.0112
	Forest	0.0183	0.0477	0.6078	0.2006	0.0206	0.0061	0.0300	0.0685	0.0003
	Agriculture land	0.0015	0.0000	0.0000	0.7907	0.0311	0.0061	0.1693	0.0000	0.0013
	Barren land	0.0072	0.0001	0.0000	0.2687	0.6780	0.0085	0.0026	0.0000	0.0348
	Built-up area	0.0000	0.0000	0.0000	0.0000	0.0000	1.0000	0.0000	0.0000	0.0000
	Agroforestry	0.0000	0.0000	0.0000	0.2562	0.0028	0.0032	0.7378	0.0000	0.0000
	Shrub land	0.0067	0.1003	0.0000	0.4405	0.0592	0.0047	0.0716	0.3074	0.0096
	Marsh land	0.3331	0.0366	0.0000	0.0013	0.0114	0.0000	0.0000	0.0101	0.6075
		2050								
		Water body	Grass land	Forest	Agriculture land	Barren land	Built-up area	Agroforestry	Shrub land	Marsh land
2035	Water body	0.9332	0.0183	0.0000	0.0050	0.0125	0.0001	0.0014	0.0279	0.0016
	Grass land	0.0243	0.2977	0.0000	0.6433	0.0093	0.0019	0.0118	0.0112	0.0006
	Forest	0.0016	0.0362	0.2759	0.4065	0.0230	0.0083	0.2019	0.0437	0.0028
	Agriculture land	0.0060	0.0001	0.0000	0.8965	0.0177	0.0068	0.0723	0.0006	0.0001
	Barren land	0.0277	0.0010	0.0000	0.1795	0.7681	0.0045	0.0021	0.0008	0.0163
	Built-up area	0.0007	0.0000	0.0000	0.0022	0.0031	0.9938	0.0000	0.0000	0.0000
	Agroforestry	0.0002	0.0000	0.0000	0.1241	0.0040	0.0087	0.8624	0.0000	0.0006
	Shrub land	0.0162	0.0230	0.0000	0.3051	0.0211	0.0122	0.2526	0.3693	0.0004
	Marsh land	0.5373	0.0041	0.0000	0.0086	0.0138	0.0001	0.0008	0.0178	0.4174

Table 12. Transition area matrix (ha) of LULC between 2021–2035 and 2035–2050

LULC Class		2035									
		Water body	Grass land	Forest	Agriculture land	Barren land	Built-up area	Agroforestry	Shrub land	Marsh land	Total
2021	Water body	3798.27	0	0	0	0	0	0	0	0	3798.27
	Grass land	328.23	16743.69	0	9526.59	3044.07	144.54	0	0	322.2	30109.32
	Forest	688.95	1831.86	24984.63	7534.44	756.63	226.98	1071.27	2719.89	7.92	39822.57
	Agriculture land	197.19	0	0	112737.51	4197.87	802.98	22764.42	0	169.02	140869
	Barren land	120.24	0	0	4992.84	13477.23	155.16	0	0	651.78	19397.25
	Built-up area	0	0	0	0	0	3179.61	0	0	0	3179.61
	Agroforestry	0	0	0	17386.29	156.42	213.3	53353.53	0	0	71109.54
	Shrub land	276.66	4484.61	0	19138.86	2539.08	191.88	2936.16	14640.84	414.99	44623.08
	Marsh land	651.24	73.44	0	0	22.05	0	0	20.79	1290.15	2057.67
	Total	6060.78	23133.6	24984.63	171316.53	24193.35	4914.45	80125.38	17381.52	2856.06	354966.3
		2050									
		Water body	Grass land	Forest	Agriculture land	Barren land	Built-up area	Agroforestry	Shrub land	Marsh land	Total
2035	Water body	5752.62	96.12	0	0.9	58.68	0	0	144.45	8.01	6060.78
	Grass land	472.5	9094.68	0	13111.29	138.96	20.88	21.96	260.37	12.96	23133.6
	Forest	3.6	960.39	9242.91	8633.52	480.24	159.57	4308.66	1128.78	66.96	24984.63
	Agriculture land	775.53	3.51	0	157583.7	2388.42	867.78	9610.56	86.4	0.63	171316.5
	Barren land	484.65	19.35	0	3420.54	19830.78	80.64	0	13.32	344.07	24193.35
	Built-up area	2.7	0	0	8.1	11.88	4891.68	0.09	0	0	4914.45
	Agroforestry	0	0	0	7709.67	234.18	523.62	71615.25	0	42.66	80125.38
	Shrub land	231.66	410.85	0	4397.58	305.19	168.57	3749.76	8113.41	4.5	17381.52
	Marsh land	1295.19	4.32	0	18.27	30.78	0.18	0	39.42	1467.9	2856.06
	Total	9018.45	10589.22	9242.91	194883.57	23479.11	6712.92	89306.28	9786.15	1947.69	354966.3

2.4. Conclusion

The GW LULC change dynamics between 1985 and 2050 were modelled using different geospatial techniques and the MLP machine learning algorithm. For this study different dependent/driver and independent spatial datasets were used. Using the hybrid image classification process, nine major land cover classes were identified where, in general, agriculture is dominant (For example 40% cover in 2021) and substantial classification accuracy result (>80%) was attained ensuring further consideration. Statistical and graphical LULC change detection such as gains, losses, and net changes were assessed both in ERDAS Imagine and TerrSet software. The results revealed noticeable landscape changes over the last 36 years between 1985–2021. The persistence/unchanged class percentage was gradually decreased from 38% to 35% between 1985–2003 and 2003–2021 respectively. Among the land uses, agriculture and agroforestry are the dominant contributors to the livelihood of the local community, resulting in increased trends with the expense of forest, shrub, and grass cover destruction.

Topography features, proximity variables, population density, and evidence likelihood were considered as the main drivers of LULC change. Prior to future prediction, the fundamental MLP model skill test and parameter sensitivity analysis were performed using three statistical approaches. The result generated an overall skill (0.9) and accuracy (93.52%) well beyond the permissible limit, and evidence likelihood is the most influential parameter while elevation has the least effect in this study. The 2021 hard and soft prediction result of the MLP-CA-MC model was further validated using the VALIDATE and ROC module based on the actual reference image (2021). Both the derived Kappa statistics (>80%) and AUC value (0.75) guaranty the reliability of the MLP-CA-MC model in predicting the future. Future LULC changes (2035 and 2050) were then predicted while taking into consideration the BAU scenario and the unceasing expansion of agricultural land, agroforestry, water body, and built-up will be expected between 2035 and 2050 with the reduction in forest, grass, and shrub land. Marshy area and barren land will show a positive growth till 2035 and decrease by 2050. Most, even to say all, of the past studies conducted in GW were mainly focused on historical land-use changes while ignoring the future change and revealing its impact from different perspectives.

The change in LULC is expected in the future, yet no study has attempted to simulate the future LULC dynamics and their effect in GW. A study on LULC change detection and prediction is required for proper planning and sustainable management. These unplanned LULC changes should be seen as a major and serious threat to the existing limited land resources in GW.

Therefore, to minimize these adverse consequences of land-use change, environmentally friendly natural resource management measures must be implemented by concerned authorities in the future. Since the combined effects of land use and climate changes, for example on hydrology, are different from the separate impacts therefore rather than relying only on projected climate variables this study highly recommends combining with future LULC changes which will be decisive for sustainable planning and management. The methods and findings of this study will be helpful for concerned stakeholders in providing the opportunity to develop adequate land and water resource conservation strategy and irrigation management plan for the future. Although the modified MLP-CA-MC model provides future LULC prediction with more accurate results, scarcity of dynamic variables data, for example; planned infrastructure changes, and proposed reserve areas are considered as limitations and further investigations to correlate future LULC prediction with different scenarios are appreciated.

3. Performance evaluation of CORDEX-Africa regional climate models in simulating climate variables over Ethiopian Rift Valley Lakes Basin: Evidence from Gidabo watershed for impact modeling studies

Abstract

Measuring the simulation skill of regional climate models (RCMs) is vital in selecting the best performing model that can be used for climate change studies. To that end, the performance of eleven Coordinated Regional Climate Downscaling Experiment (CORDEX) Africa RCMs were evaluated against observed datasets from 1991 to 2005. RCMs' outputs were evaluated using coefficient of variation (CV), percent of bias (PBIAS), Root Means Square Error (RMSE), Pearson's correlation coefficient (r), revised R-squared (RR^2), Taylor Skill Score (TSS), Mann-Kendall (MK) trend test and Sen's slope estimator. The results confirm the difference of RCMs in capturing the annual and seasonal climate variables. In relation to the spatial pattern of the rainfall, RACMO22T (EC-EARTH) strongly reproduced the mean annual rainfall. CCLM4-8 (MPI) and mean ensemble reproduced the annual patterns of the observed rainfall despite the fact with varying rainfall amounts reproduced. The seasonal rainfall pattern was satisfactorily captured by RACMO22T (EC-EARTH), CCLM4-8 (MPI) and REMO2009 (MPI). The agreement between the observed and modeled rainfall is superior in CCLM4-8 (MPI) and RACMO22T (EC-EARTH) at station level. CRCM5 (MPI) satisfactory replicated the patterns of both minimum and maximum temperature. RACMO22T (EC-EARTH) showed best performance in simulating annual and seasonal rainfall trends in the GW. In overall, models that performs better in replicating the observed climatology in the GW include RACMO22T (EC-EARTH), CCLM4-8 (MPI), CRCM5 (MPI), CCLM4-8 (CNRM), and REMO2009 (EC-EARTH). The study underscored the use of the mean ensemble of model simulation did not always guarantee better agreement with observation than individual models. Therefore prior to climate impact study, it is advisable to correct the systematic bias and employ the multi-model ensemble of best performing models for climate change impact and adaptation studies in the GW.

This chapter is originally published as:

Girma, R., Fürst, C., Moges, A., 2022. Performance evaluation of CORDEX-Africa regional climate models in simulating climate variables over Ethiopian main rift valley: Evidence from Gidabo river basin for impact modeling studies. Dynamics of Atmospheres and Oceans, 99: 101317. https://doi.org/10.1016/j.dynatmoce.2022.101317.

3.1. Introduction

The impacts of climate change are a major concern worldwide and becoming sever, particularly in developing countries (Asfaw et al., 2021; Babaousmail et al., 2021; Demissie and Sime, 2021). The changes in frequency and intensity of climate events have led to changes in the frequency, intensity, spatial extent, duration, and timing of weather and climate extremes (Seneviratne et al., 2012). This can result in unprecedented extremes such as severe climate-related disasters (e.g., droughts, floods) (Seneviratne et al., 2012; Ayugi et al., 2020a). In Sub-Saharan African region, climate change is expected to exacerbate the existing socioeconomic challenges due to its high exposure and low adaptive capacity (Intergovernmental Panel on Climate Change (IPCC), 2014a; Niang et al., 2014; Warnatzsch and Reay, 2019; Adenuga et al., 2021; Hamadalnel et al., 2022a). Increased frequency and intensity of droughts and floods over the East Africa region has threatened many people's livelihood and the economy at large (Asumadu-Sarkodie, 2015; Ayugi et al., 2020b; Umuhoza et al., 2021).

Climate change in the form of higher temperature, reduced rainfall, and increased rainfall variability adversely affects and resulted in significant impact on agricultural countries' leading economy like Ethiopia (Araya et al., 2010; Gezie, 2019), where around 90% is predominantly rain-fed agriculture. The main causes for vulnerability of Ethiopia to climate variability and change are very highly dependent on rain fed agriculture and underdevelopment of water resources (Belihu et al., 2018). Climate change impacts on are of major concern in view of the sustainability of water resources and agricultural production in Ethiopia (Conway and Schipper, 2011; Tesfaye et al., 2019).

Accurate climate information is necessary to evaluate the regional and local climate change effects, perform impact assessments and design adaptation strategies at regional or national level (IPCC, 2014b; Giorgi and Gutowski, 2015). Understanding the historical climate is of great importance for better estimating future climate change and assessing its influence from different perspectives (Hamadalnel et al., 2021; Pang et al., 2021). Numerical climate model has become an effective tool to understand the climate change and predict the climate at different time scales (Umuhoza et al., 2021). Since the invent of Global Climate Models (GCMs), several studies have used GCM outputs to assess global and regional climate changes (Ayugi et al., 2020b; Hamadalnel et al., 2022b). Nonetheless, many scholars proved coarse spatial resolutions GCMs have limitations in simulating hydrological variables at catchment scale and regional scale phenomena (Zanis et al., 2015; Dibaba et al., 2019; Stefanidis et al., 2020). Moreover, GCMs could not realistically capture extreme events (Worku et al., 2018).

GCMs based climate simulation represent changes over a relatively large area, however, to carry out context-specific impact and adaptation assessments, a more detailed local understanding is required (Kim et al., 2013; Warnatzsch and Reay, 2019). Thus, in regions particularly characterized by an uneven topography, downscaling climate models at regional spatial scale are vital to get accurate information for local climate impact studies (Flato et al., 2013; Worku et al., 2018). This have prompted the idea of employing downscaled and high-resolution regional climate models (RCMs) to describe climate variability at regional or local scale (Ayugi et al., 2020b). Downscaling techniques resolve scale disparity to translate large-scale climate model results to local climate (Dibike et al., 2007; Tesfaye et al., 2019). The downscaling techniques are divided into dynamic (Xue et al., 2014) and statistical (Sachindra et al., 2018) approaches as noted by Stefanidis et al. (2020). Dynamic downscaling approaches are physically based driven process and, complex and computationally demanding whereas statistical downscaling models are data driven and easy to apply and require much less computational time (Tesfaye et al., 2019).

In recent years, several institutions continue to use RCMs for varying applications in climate studies (IPCC, 2014b; Ayugi et al., 2020b). There are also different initiatives to produce large ensembles of RCM simulations that can be further used for varying applications in climate studies at regional spatial scales (IPCC, 2014b). This is attributed to, but not limited, CORDEX (Coordinated Regional Climate Downscaling Experiment) under the auspices of the World Climate Research Program (WCRP) (Ayugi et al., 2020b). CORDEX-Africa is an initiative to downscale different GCM outputs and to generate an ensemble of high resolution (~50km) historical and future climate projections for the African continent (Worku et al., 2018). RCMs add value to climate projections particularly in areas with variable topography, and extreme or small-scale climatic processes (Flato et al., 2013; Warnatzsch and Reay, 2019). Studies have shown that RCMs simulate the most reliable annual and seasonal climate variable estimations, and are also preferable in analyzing extreme rainfall distributions and frequency (Worku et al., 2018; Demissie and Sime, 2021).

Although, the use of outputs from RCMs has become a vital and effective tool for studying regional climate change and variability (Kisembe et al., 2019), it has also been found that the way the RCMs inherit the biases from the GCMs varies for different regions and variables within Africa (Kim et al., 2013; Warnatzsch and Reay, 2019). And equal in a localized study area, RCMs that achieve good results in some areas may have limitation in other places (Endris et al., 2013: Onyutha, 2020). According to Nikulin et al., 2012, RCMs simulate climatic variables with different levels of accuracy and significant biases can be found depending on region and season. Therefore, in order to select the appropriate RCMs for a specific watershed, it is necessary to evaluate the performance of multiple RCMs (Mutayoba and Kashaigili, 2017; Dibaba et al., 2019; Warnatzsch and Reay, 2019; Demissie and Sime, 2021).

Climate change impact and adaptation studies can benefit from an enhanced understanding about the performance of individual as well as ensemble simulations of RCMs (Alemseged and Tom, 2015). According to Anagnostopoulos et al. (2010) and Stefanidis et al. (2020), the ability of RCMs to represent climate conditions should be examined prior to their use in impact assessment studies. Since the performance of downscaled data differs either from location to location or from one RCM to another (Mutayoba and Kashaigili, 2017), gauging the skills of historical RCMs is crucial in selecting the best performing model that can be used for future climate projections and impacts studies (Umuhoza et al., 2021).

In the locality of GW, several studies revealed the impacts of climate change from different perspectives (Shanka, 2017; Belihu et al., 2018; Alehu et al., 2021). Such and other related studies have mostly based on either observed data or an individual RCM simulation. However, the effort made using multiple climate models/ensembles was rare. Furthermore, the extent of the differences among results from various RCMs and how these differences affect the projected results of climate change have rarely been attempted in the GW. The reasonableness of the future climate change projections depends on how accurate the climate models reproduce observed or historical climate variability (Onyutha et al., 2019). Though model performance assessment is not new in Ethiopia, it was not conducted in the study area. As a result, this study focuses on evaluating the performance of frequently used CORDEX-Africa RCMs and their mean ensemble in simulating rainfall and temperature (minimum and maximum) over GW for impact modeling studies. This is an important step to better understand how the individual RCMs perform in any climate impact assessment study, as the uncertainties in RCMs are characterized (Demissie and Sime, 2021).

3.2. Materials and methods

3.2.1. Data source and processing

In Ethiopia and particularly in GW, dearth of long meteorological time-series observed data were limited our reference time period from 1991 to 2005. According to Dibaba et al. (2019), climate analysis requires complete datasets with no gaps and missing records. Therefore, stations having small percentage of missing values with both precipitation and temperature record were considered for the evaluation purpose. For this study, the following five meteorological stations were selected: Dilla, Hagereselam, Haisawite, Yergalem and Yergacheffe (Figure 1 and Table 13). Daily rainfall and air temperature (minimum and maximum) data were collected from the National Meteorology Agency (NMA) of Ethiopia, which cover 15 years from 1991 to 2005 that is common period for the aforementioned stations.

Data imputation technique was used to estimate and complete the missing values prior to the analysis. The stations have random missing values of less than 5% (Table 13). Missing data were filled with multiple imputation algorithm based on the Markov Chain Monte Carlo (MCMC) approach using XLSTAT 2021 add-ins software package (Sattari et al., 2017; Ekeuwei et al., 2018; Banda et al., 2021). Moreover, homogeneity test was assessed through the application of the Standard Normal Homogeneity Test (SNHT) (Elzeiny et al., 2019) and double mass curve (DMC) analysis was executed to assess the consistency of rainfall (Gao et al., 2017). Accordingly, the annual rainfall in the area is found to be homogeneous as the computed p-value is greater than the significance level alpha=0.05 at 99% confidence interval (Table A1). Again, it was found that each station rainfall was consistent with the cumulative mean annual rainfall of all stations (Figure A1). Finally, the observed point data (rainfall and temperature) were transformed into spatial dataset using Thiessen Polygon method to calculate the areal average (Worku et al., 2018).

Table 13. Characteristics of the rain gauge stations

Meteorological station	Elevation (m)	Mean annual rainfall (mm/year)	Coefficient of variation (%)	Skewness	Percent of missing data
Dilla	1519	1290	15.3	0.57	0.4
Hagereselam	2809	1277	12.9	0.16	2.1
Haisawite	2240	1058	17.2	-0.48	1.1
Yergalem	1786	1215	19.3	0.24	0.3
Yergacheffe	1856	1316	20.9	1.61	0.1

RCMs simulations from CORDEX driven by MPI-ESM-LR (MPI-M: Max Planck Institute for Meteorology), CNRM-CM5 (CNRM-CERFACS: Centre National de Recherches Météorologiques) and EC-EARTH (ICHEC: Consortium of European research institution and researchers) were obtained from the publicly available Earth System Grid Federation (ESGF) (https://esgf-data.dkrz.de/search/esgf-dkrz/) (Table 14). According to Worku et al. (2018); Dibaba et al. (2019); Demissie and Sime (2021), these models have been evaluated in multiple studies on Africa, and have been found to perform well in simulating rainfall and air temperature. This study used 11 RCM outputs (Table *14*) and their mean ensemble (multi-model average) to attempt the evaluation. For each model, historical simulations and only the first ensemble member (r1) was used, except the EC-EARTH model from which the 12th ensemble member (r12) was used. The RCM network command data form (NetCDF) were being extracted using the latitude and longitude of the corresponding stations in ArcGIS 10.7 model builder as used by Demissie and Sime (2021) (Figure 15).

Table 14. Description of RCMs and deriving GCM used in this study

Description of the RCMs	Driving GCM	RCM short name	Reference
Climate Limited-Area Modeling Community version 4.8	CNRM-CM5 EC-EARTH MPI-ESM-LR	CCLM4-8 (CNRM) CCLM4-8 (EC-EARTH) CCLM4-8 (MPI)	Sørland et al., 2021
Fifth-generation Canadian Regional Climate Model	MPI-ESM-LR	CRCM5 (MPI)	Takhsha et al., 2018
High-Resolution Hamburg Climate Model 5	EC-EARTH	HIRHAM5 (EC-EARTH)	Christensen et al., 2007
Regional atmospheric climate model version 2.2	EC-EARTH	RACMO22T (EC-EARTH)	Wessem & Laffin, 2020
Rossby Centre Regional Atmospheric Model	CNRM-CM5 EC-EARTH MPI-ESM-LR	RCA4 (CNRM) RCA4 (EC-EARTH) RCA4 (MPI)	Samuelsson et al., 2011
REgional Model	EC-EARTH MPI-ESM-LR	REMO2009 (EC-EARTH) REMO2009 (MPI)	Demessie et al., 2023

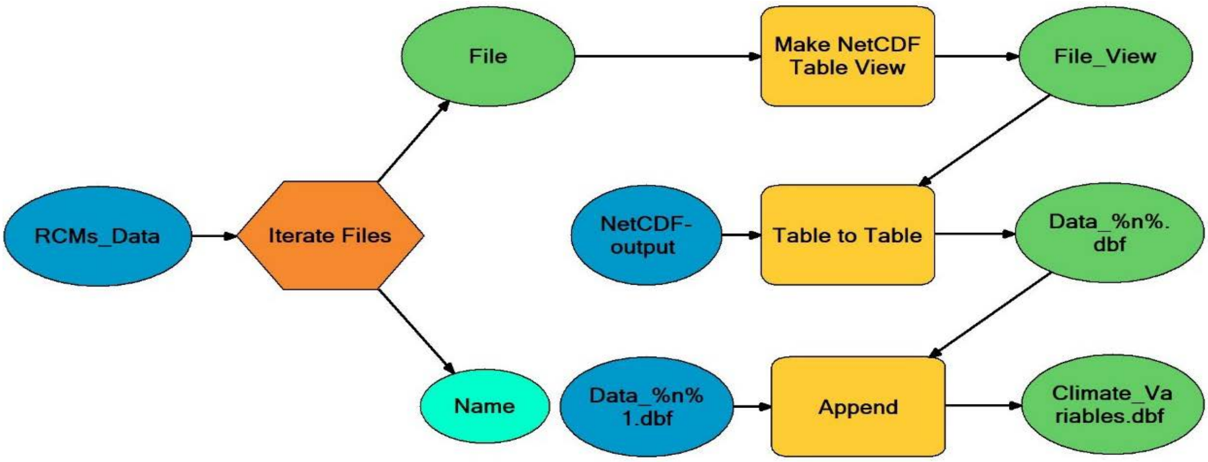

Figure 15. ArcGIS model used to extract the RCMs NetCDF (Source: https://help.arcgis.com)

3.2.2. Data analysis techniques

Comparison between CORDEX RCMs outputs and observed data was done to test the ability of the CORDEX RCMs to reproduce the seasonal, annual cycles, interannual variability, annual total and trends of rainfall. Hence, descriptive and statistical tests (Asfaw et al., 2018) were used for variability investigation and trend analysis as illustrated in the succeeding sub-sections:

Assessing the skill of RCMs output in reproducing GW climatology

The study used mean seasonal, annual and inter-annual variations to assess the skill of RCMs in reproducing the fundamental characteristics of rainfall and temperature over GW as used by other studies (Worku et al., 2018; Ayugi, et al., 2020b). Hence the regional models were evaluated through visual inspection by plots and spatial distribution maps of meteorological variables (observed and RCM simulated data) (Alemseged and Tom, 2015). Prior to spatial analysis, the observed point data collected from the five meteorological stations were converted into spatial datasets using inverse distance weight (IDW) interpolation algorithm in ArcGIS environment (Worku et al., 2018; Dibaba et al., 2019; Demissie and Sime, 2021).

Statistical validation of the RCMs

This study employed five statistical metrics (Equation 11–15) including percent of bias (PBIAS), Root Means Square Error (RMSE), Pearson's correlation coefficient (r), revised R-squared (RR^2) (Onyutha, 2022) and Coefficient of Variation (CV). These metrics were previously used in evaluation of climate models by a number of researchers such as Alemseged and Tom (2015), Asfaw et al. (2018), Worku et al. (2018), Dibaba et al. (2019), Ayugi et al. (2020b), Demissie and Sime (2021), Mengistu et al. (2021) and Onyutha (2022).

$$PBIAS = \frac{\sum_{i=1}^{n}(S_i - O_i)}{\sum_{i=1}^{n} O_i} \times 100 \qquad (11)$$

$$RMSE = \sqrt{n^{-1}\sum_{i=1}^{n}(S_i - O_i)^2} \qquad (12)$$

$$r = \frac{\sum_{i=1}^{n}(S_i - \bar{S})\,(O_i - \bar{O})}{\sqrt{\sum_{i=1}^{n}(S_i - \bar{S})^2}\,\sqrt{\sum_{i=1}^{n}(O_i - \bar{O})^2}} \qquad (13)$$

$$RR^2 = |r| \times \frac{min(S_O, S_S)}{max(S_O, S_S)} \times \frac{min(S_O^2, S_{SD}^2)}{max(S_O^2, S_{SD}^2)} \qquad (14)$$

$$CV = \frac{\sigma}{\mu} \times 100 \qquad (15)$$

Where S_i and O_i are the i^{th} model simulated and observed variables respectively; *n* represents the total number of pairs; the bar over the variables refers the average values over the analysis period; *min* and *max* denote the minimum and maximum, respectively, of observed and simulated variables; S_O and S_S is sample standard deviation of observed and simulated climate variables respectively; S_O^2 is sample variance of observed climate variable and S_{SD}^2 denotes the conditional variance of simulated variable with respect to $\bar{O}$ such that $S_{SD}^2 = (n - 1)^{-1} \sum_{i=1}^{n} (S_i - \bar{O})^2$ (Onyutha, 2022).

PBIAS measure the systematic bias or bias between the observed and model simulated climate variable using Eq. (12). A PBIAS value close to 0 indicates a minor systematic difference between RCM and observed amounts; a PBIAS value far from 0 suggests a deviation. A positive PBIAS indicates overestimation whereas a negative PBIAS indicates an underestimation of the observed variables (Alemseged and Tom, 2015; Worku et al., 2018; Mengistu et al., 2021). RMSE measures the difference between the observed and RCMs output. An RMSE value close to 0 indicates better performance. RMSE is elucidated mathematically as in Eq. (13) (Worku et al., 2018; Mengistu et al., 2021).

r, in Eq. (14), is often used to evaluate the existing linear relationship between the RCMs and observed data. r value is ranging between 1 and -1 (Luhunga et al., 2016); values close to 1 indicate a better linear relationship between the observed and modeled data whereas a value away from 1 indicates less agreement (Worku et al., 2018; Mengistu et al., 2021). RR^2 values range from 0 to 1 where the higher the RR^2, the better the model fits the observed data. CV (Eq. 16) was computed to evaluate the variability of seasonal and annual climatological events. A higher value is the indicator of larger variability, and vice versa (Asfaw et al., 2018). CV is used to classify the degree of variability of rainfall events as less (CV< 20%), moderate (20% < CV <30%), and high (CV >30%) (Mekonen and Berlie, 2019; Demissie and Sime, 2021).

In addition, standardized anomaly index (SAI) of the RCM and observed data (annual and seasonal records) have been computed, using equation 16, to show the consistence of model simulations to capture the deviation of the data from long term average (Alemseged and Tom, 2015; Asfaw et al., 2018; Dibaba et al., 2019; Anose et al., 2021). Standardized rainfall anomaly (SRA) describes extreme climate events viz, drought period (Asfaw et al., 2018). For instance, Agnew and Chappell (1999), classified droughts into extreme (SRA < –1.65), severe (–1.28 > SRA > –1.65), moderate (–0.84 > SRA > –1.28) and no drought (SRA > –0.84) which is also adopted in the Ethiopian context (Asfaw et al., 2018; Belay et al., 2021). Therefore, to evaluate the skill of RCMs to reproduce the interannual variability of hydrologic extreme events, it is vital to compute the SRA of climatological variables (Alemseged and Tom, 2015; Asfaw et al., 2018; Dibaba et al., 2019).

$$SAI = \frac{(x_i - \mu)}{\sigma} \tag{16}$$

Where, x_i is the rainfall or temperature data of a particular year; μ is long term mean annual rainfall or temperature over a period of observation and σ is the standard deviation of annual rainfall or temperature over the period of observation.

Furthermore, Taylor diagram and Taylor Skill Score (TSS) was employed (using R version 4.1.3) to evaluate the performance of RCM replicating monthly rainfall and temperature over the study area. Recalling previous studies (Taylor, 2001; Kusunoki et al., 2006; Kusunoki and Arakawa, 2015; Wang et al., 2018; Abbasian et al., 2019; Babaousmail et al., 2021; Shiru et al., 2021), Taylor diagram and TSS approach has been widely used to assess the correlation between different sets of data (Babaousmail et al., 2021). It can illustrate the statistical relationship between the RCM simulations and observations. Taylor diagram represent three different statistics viz, the centered root mean squared error (CRMSE), the linear correlation coefficient and the standard deviation (Abbasian et al., 2019). The TSS was calculated using equation 17 and the score vary from 0 (least skillful) to 1 (most skillful) (Taylor, 2001).

$$TSS = \frac{4(1+R)}{\left(\hat{\sigma}_f + 1/\hat{\sigma}_f\right)^2 (1+R_0)} \qquad (17)$$

where R is the spatial pattern correlation coefficient between the model outputs and observation; R_0 is the maximum correlation attainable (the threshold was assumed at 1 (Kusunoki and Arakawa, 2015; Babaousmail et al., 2021) and $\hat{\sigma}_f$ is normalized standard deviation of the simulated patterns.

Appraisal of RCMs skill to simulate trends in rainfall and temperature

Several approaches have been articulated to analyze the trend of climate time series data using either non-parametric or parametric statistical methods. The parametric methods, for example linear regression, are developed based on assumptions such as the normality, the stationarity and the independency of time series, while these assumptions are most uncommon to be satisfied in a hydrological time series (Mirabbasi et al., 2020). Moreover, the parametric tests are very sensitive to the presence of the outliers in the data series, which is not the case with the non-parametric methods (Mirabbasi et al., 2020) such as the Mann Kendall test (Mann, 1945; Kendall, 1975), Spearman's rho test (Spearman, 1904; Lehmann, 1975; Sneyers, 1990), Onyutha test (Onyutha, 2021), and Sen's Innovative Trend method (Sen, 2012).

Among the non-parametric methods, Mann-Kendall (MK) trend test method is the most commonly used techniques. The MK test has several advantages such as the handling of missing data, the requirement of few assumptions, and independence of the data distribution

(Öztopal and Sen, 2017; Ali et al., 2019). MK test is used for estimating trends having datasets with high variance and are less sensitive to outliers (Hamed, 2008). This method is also used for trend analysis of nominal, ordinal, ratio, or interval data series (Sarkar et al., 2021). Trend analysis of skewed data is also done by MK (Sarkar et al., 2021).

Prior to trend analysis, the autocorrelation function (ACF) plots for meteorological time series variables were developed using R to identify the presence of serial correlation. In the ACF plot significant serial correlation is depicted when the vertical lines extend beyond the blue horizontal band (at 5% significant level) at lag -1 (Mulugeta et al., 2019). Accordingly, Figure 16 illustrate there was no significant serial correlation for rainfall and temperature time series for the entire watershed. In 2019, Mulugeta et al. also reported similar result in Awash River basin, Ethiopia. Consequently, the ACF result attested to use the original Mann-Kendall (MK) trend test. In this regard, MK test and Sen's slope estimator were adopted to test the ability of the RCMs simulating trends and the magnitude of the trends respectively (Luhunga et al., 2016). MK, non-parametric statistical test, was employed to detect the time series trends of the RCMs output (Luhunga et al., 2016; Belihu et al., 2018). The Mann-Kendall test, rank based procedure, is used to discern the alternative hypothesis (H_1) that indicates the presence of trend, against the null hypothesis (H_0) of no trend (Mann, 1945; Kendall, 1975). The test was based on S statistics and each paired sequential data values, x_i and x_j,, were compared to find out whether $x_i > x_j$ or the vice versa (Mutayoba and Kashaigili, 2017; Belihu et al., 2018). Standardized Mann-Kendall S statistic were computed using equation 18 (Mann, 1945; Kendall, 1975):

$$S = \sum_{i=1}^{n-1} \sum_{j=i+1}^{n} sgn(x_j - x_i) \tag{18}$$

where x_i and x_j are sequential data for the i^{th} and j^{th} terms, n is the number of observation or sample size and the test of significant, sgn was calculated using equation 19:

$$sgn(x_j - x_i) = \begin{cases} +1 \; if \; x_j > x_i \\ 0 \; if \; x_j = x_i \\ -1 \; if \; x_j < x_i \end{cases} \tag{19}$$

S is approximately normally distributed with the mean and variance. The variance of *S, Var(S)* was calculated using equation 20 where m denotes the number of tied groups (a set of t_i sample time series data owning the same values).

$$Var(S) = \frac{n(n-1)(2n+5) - \sum_{i=1}^{p} t_i(t_i-1)(2t_i+5)}{18} \quad (20)$$

When n >10, a standardized Z statistic (Equation 21) was computed to measure the significance of trend. Negative Z-score values denote downward trend while positive Z-score values denote upward trend.

$$Z = \begin{cases} \frac{S-1}{\sqrt{Var(S)}} \; if \; S > 0 \\ 0 \; if \; S = 0 \\ \frac{S+1}{\sqrt{Var(S)}} \; if \; S < 0 \end{cases} \quad (21)$$

For a given level of significance α, H_1 is accepted if $|Z| > Z_{1-\alpha/2}$ implying significant trend in the time series data (either increased for positive Z-value or vice versa). $Z_{1-\alpha/2}$ is calculated from the standard normal distribution tables. In this study, the trend of RCM outputs in annual and seasonal time scale were tested at α=0.01, 0.05 and 0.1 significant levels.

Sen's slope estimator was used to estimate the gradient of the trends in meteorological variables. This method provides a more robust slope estimate because it is sensitive to the outliers or extreme values (Theil, 1950 and Sen, 1968). In 2018, Belihu et al. noted the slope estimator β_{ij} (Equation 22) is the median (Gan, 1998) over all possible combinations of pairs for the whole data set.

$$\beta_{ij} = Median\left[\frac{x_j - x_i}{j - i}\right], j > i \quad (22)$$

Where x_i and x_j are the time series of monthly climatology; i = 1, 2, 3, …, n – 1 and j = i +1, i + 2, i + 3, …, n; n is the number or length of the dataset.

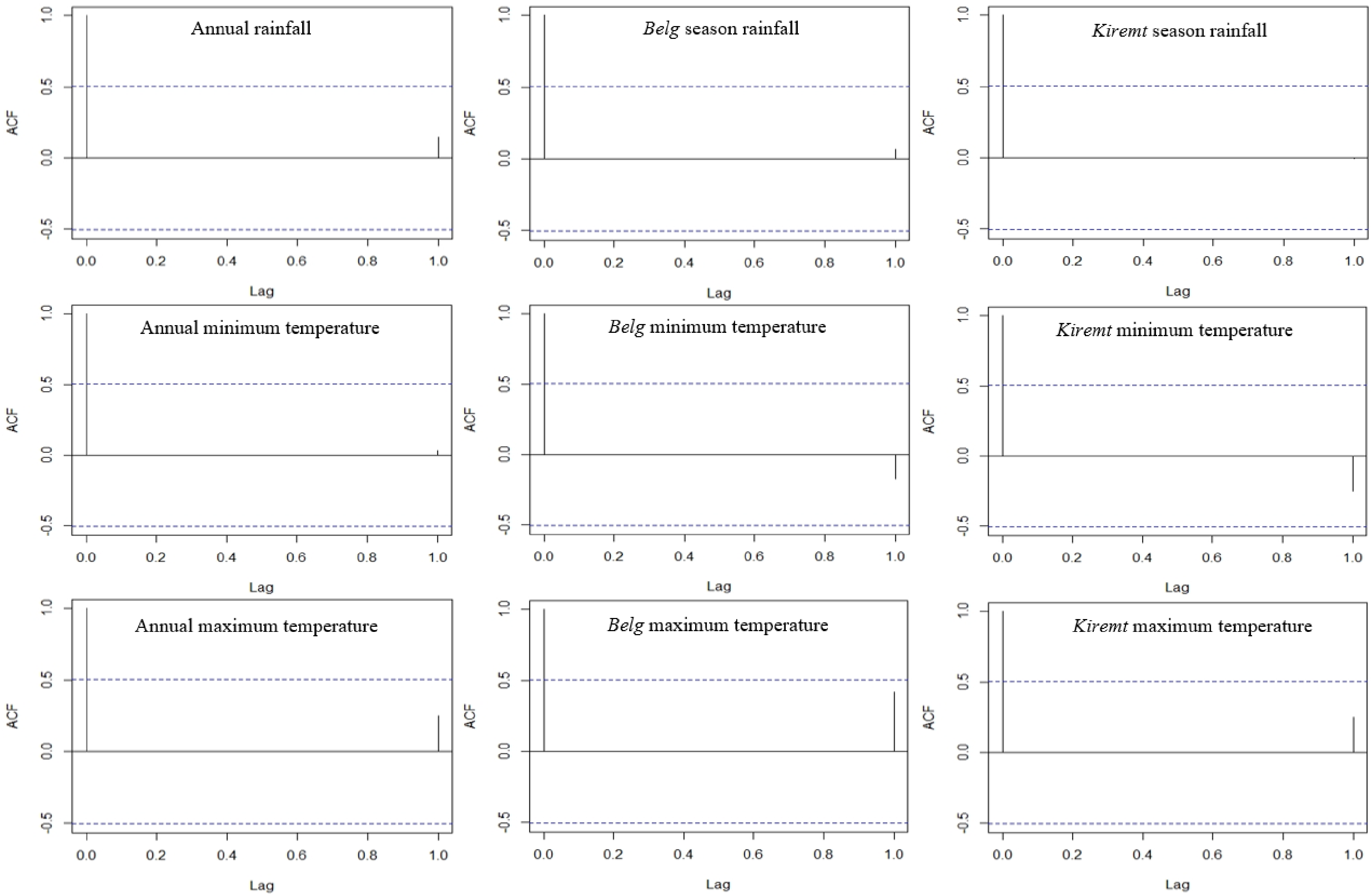

Figure 16. ACF plots for annual and seasonal rainfall and temperature

3.3. Results and discussion

The performance of eleven RCMs together with the mean ensemble were examined against their capability in reproducing the observed annual climatology, seasonal and interannual variability, and trends in rainfall and temperature over GW to select best performing model. Such assessment is vital to gain confidence in climate impact studies and analysis (Babaousmail et al., 2021).

3.3.1. Mean annual rainfall cycle

The spatial distribution of observed and simulated mean annual rainfall showed a distinct variation over the study watershed (Figure 17). In the upper region of the watershed, CCLM4-8 (CNRM) and CCLM4-8 (EC-EARTH) outputs were better in representing the observed mean annual rainfall. RACMO22T (EC-EARTH) robustly reproduce the mean annual rainfall both in the upper and middle regions as compared to other models. The RCA4 group and HIRHAM (EC-EARTH) simulate higher than the observed rainfall in the upper and central part of the watershed. The output attained from REMO2009 (EC-EARTH) underestimate the annual rainfall in the middle and lower region and REMO2009 (MPI) exhibit lower records than the observed mean annual rainfall over the entire watershed.

Rainfall and temperature are two of the most important meteorological variables that are frequently used to trace the extent and magnitude of climate change and variability (IPCC, 2007). The assessment of spatiotemporal dynamics of climatological variables, particularly in countries like Ethiopia where the economy is heavily dependent on low-productivity rainfed agriculture, is very crucial to assess climate-induced changes and suggest feasible adaptation strategies (Cheung et al., 2008; Asfaw et al., 2018). The existing geographical features and topographic complexity of Ethiopia are responsible for the spatiotemporal variability of climate in the country (National Meteorology Service Agency (NMSA), 1996; Zeleke et al., 2013; Alhamshry et al., 2020). Moreover, Berhanu et al. (2014) pointed out regional and global change of the weather systems along with the seasonal cycles have a strong impact on these variations over space and time.

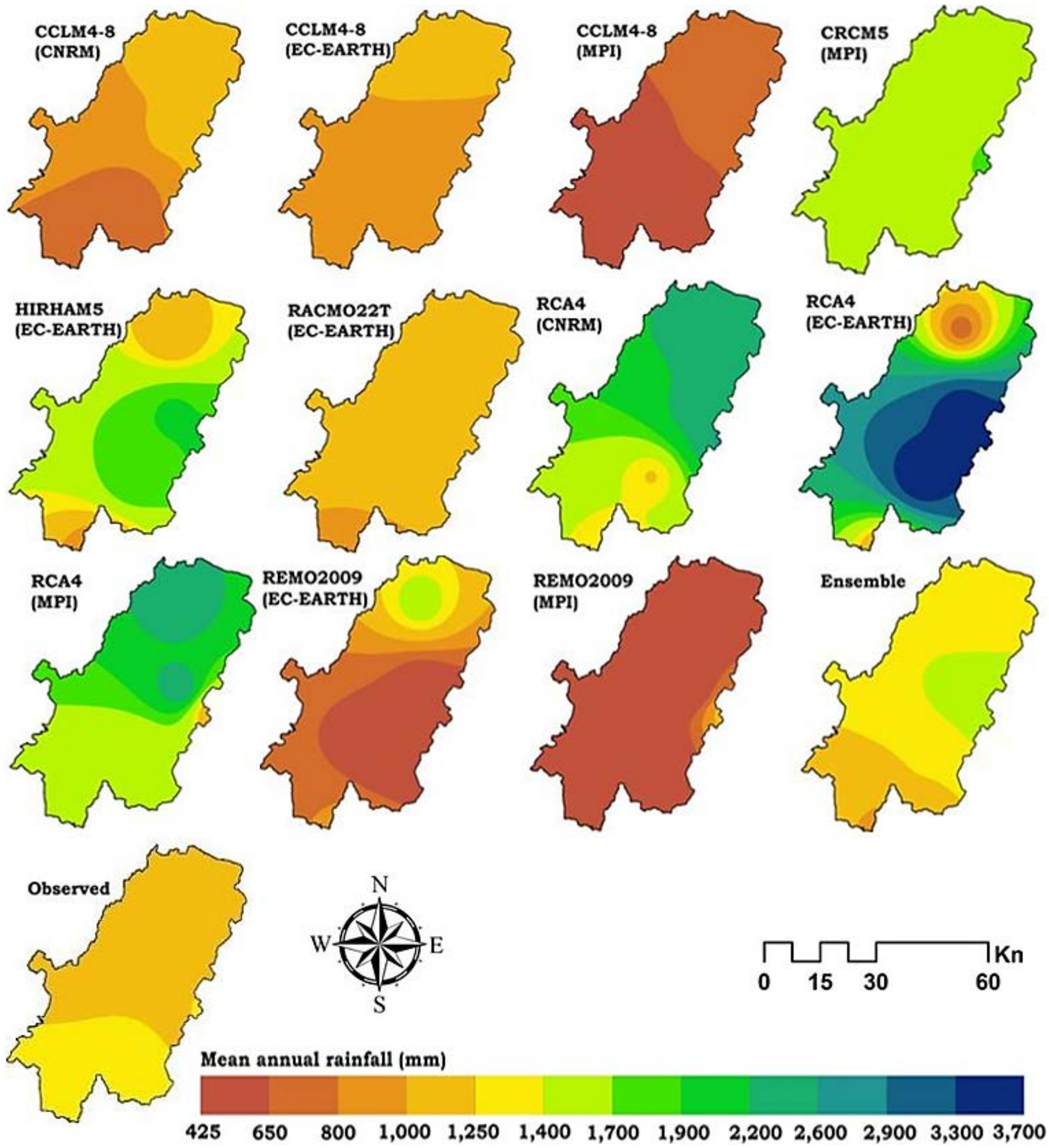

Figure 17. Spatial distribution of simulated and gauged mean annual rainfall

The performance of RCMs in simulating the mean annual rainfall cycle is graphically represented by Figure 18. The observed areal average rainfall exhibits two peaks of rainfall i.e., bimodal pattern in the entire GW; a primary maximum is in April/May, a secondary one is in September/October and the lowest amount is recorded in December. In agreement with this, Belihu et al. (2018) assembled the mean annual rainfall into high (March–May), moderate (August–October), low (June-July) and dry period (November–February). Likewise, Alhamshry et al. (2020) described the southern domain of Ethiopia (where the study area is located) experienced bimodal rainfall cycle viz, March to May (with rainfall peaks in April/May) and October to November.

As can be illustrated in Figure 18, most of the RCM's output reproduced the bimodal patterns of rainfall over all the stations while shifting the April/May peak period up to 2 months.

Congruently, Mengistu et al. (2021) attained similar results in Baro-Akobo basin. Some of the RCMs (i.e., CCLM4-8 (CNRM), CCLM4-8 (MPI), RACMO22T (EC-EARTH) and RCA4 (CNRM)) satisfactorily captured the timing of peak rainfall despite the fact with varying rainfall amounts reproduced. CCLM4-8 (MPI) model well captured the annual pattern of observed mean monthly rainfall. Similarly in 2021, Mengistu et al. stated CCLM4-8 model perform better to reproduce the observed mean monthly rainfall in Baro–Akobo basin, Ethiopia.

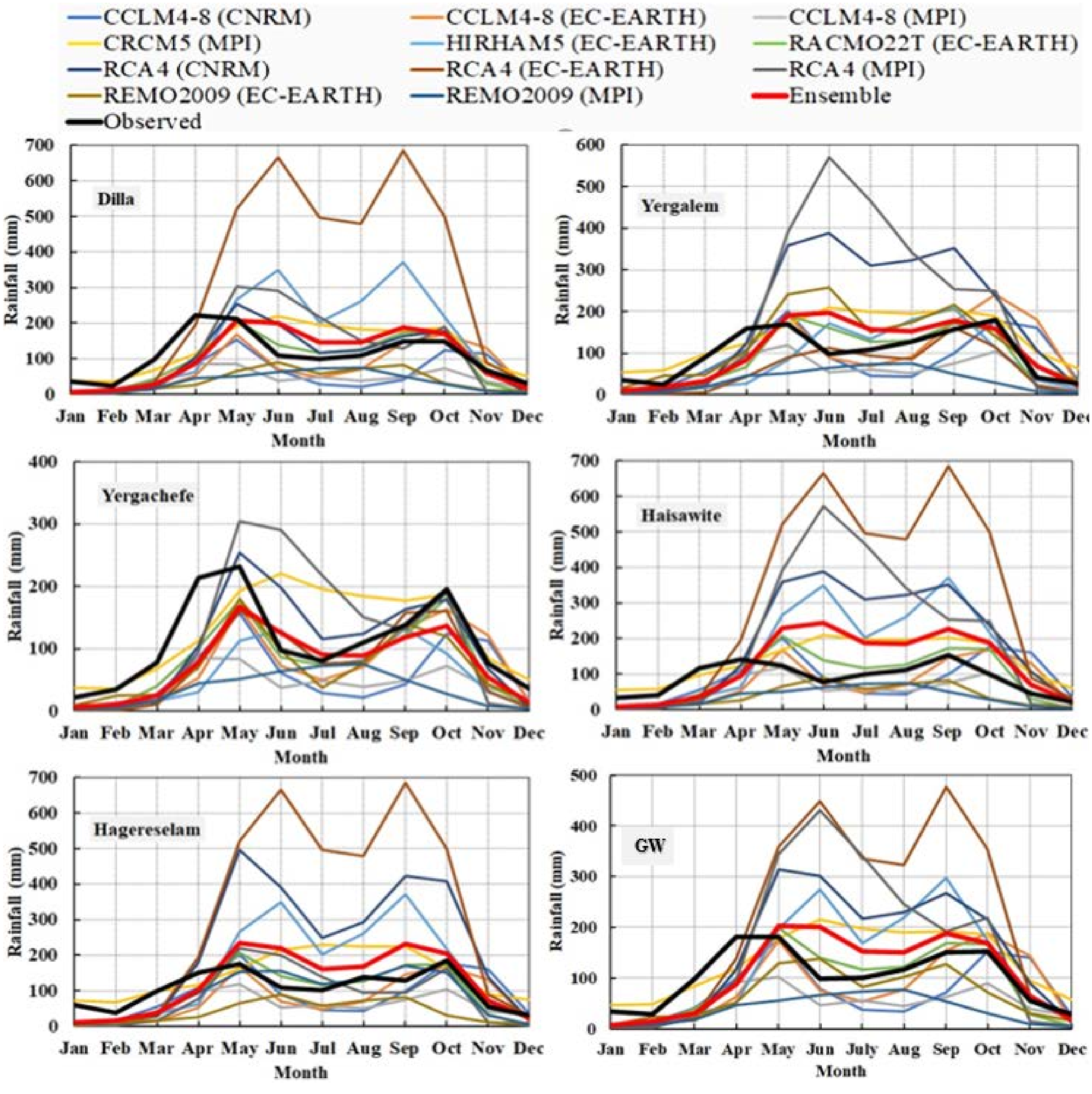

Figure 18. Observed and simulated mean annual rainfall (mm/month) cycle at each station and the entire GW (areal average).

CCLM4-8 and REMO2009 group underestimate the mean annual rainfall cycle all over the year while CRCM5, HIRHAM5, RACMO22T (EC-EARTH) (from May-October) and RCA4 overestimate the mean annual rainfall cycle. The mean ensemble reproduced the annual patterns of the observed rainfall more adequately than the individual RCMs over the study watershed. On the contrary, RCA4 group, characterized by overestimation, showed weak performance in capturing the mean annual rainfall distribution in the study domain (Figure *18*). Previous studies conducted in different parts of the country also attained similar results. For example, Worku et al. (2018); Demissie and Sime (2021) found the overestimation characteristics of RCA4 in the upper Gilgel Gibe districts and Jimma sub-basin respectively.

It is found that the RCMs inconsistently reproduced the magnitude and pattern of observed rainfall at each station (Figure *18*). For instance, CCLM4-8 (MPI) underestimate the peak annual rainfall cycle at Dilla while capturing the annual pattern satisfactorily. The peak simulated by CCLM4-8 (EC-EARTH) showed higher than the observed mean annual rainfall at Yergalem, on the contrary lower than the observed annual rainfall cycle at Hagereselam and Yergachefe stations. RCA4 from CNRM and MPI overestimate the observed peak while REMO2009 (EC-EARTH) and mean ensemble reproduced smaller peak at Yergachefe. Both HIRHAM5 (EC-EARTH) and RCA4 (EC-EARTH) exhibited a higher peak than the observed rainfall at Haisawite. At Yergachefe station, both RACMO22T (EC-EARTH) and RCA4 (CNRM) relatively captured the annual rainfall distribution well than the other stations.

Most of the derived RCMs (excluding CRCM5 (MPI), RACMO22T (EC-EARTH) and REMO2009 group) overestimate the annual cycle of minimum temperature (Figure 19). CRCM5 (MPI) satisfactory replicates the distribution of annual minimum temperature. On the other hand, almost the RCMs and mean ensemble showed lower records of maximum temperature cycle over the entire watershed. The annual pattern of maximum temperature over the study watershed is better captured by CRCM5 (MPI) and mean ensemble. At station level, each RCMs replicate the observed temperature with varying ranges. For example, most of the regional models and mean ensemble reproduce lower than the observed maximum temperature throughout the year at Dilla, Yergalem, Haisawite and Yergachefe stations while REMO2009 simulate higher than the observed maximum temperature at Haisawite and Yergachefe stations. All the derived RCMs and mean ensemble simulate higher than the observed minimum and maximum (apart from CRCM5) temperature at Hagereselam station. Outputs attained from CRCM5 (MPI) (at Dilla and Yergachefe stations), RCA4 of EC-EARTH and CNRM (at Yergalem station) and mean ensemble (at Hageresela, Dilla and Yergalem stations) satisfactorily captured the pattern of mean annual maximum temperature though it is failed to reproduce the magnitude.

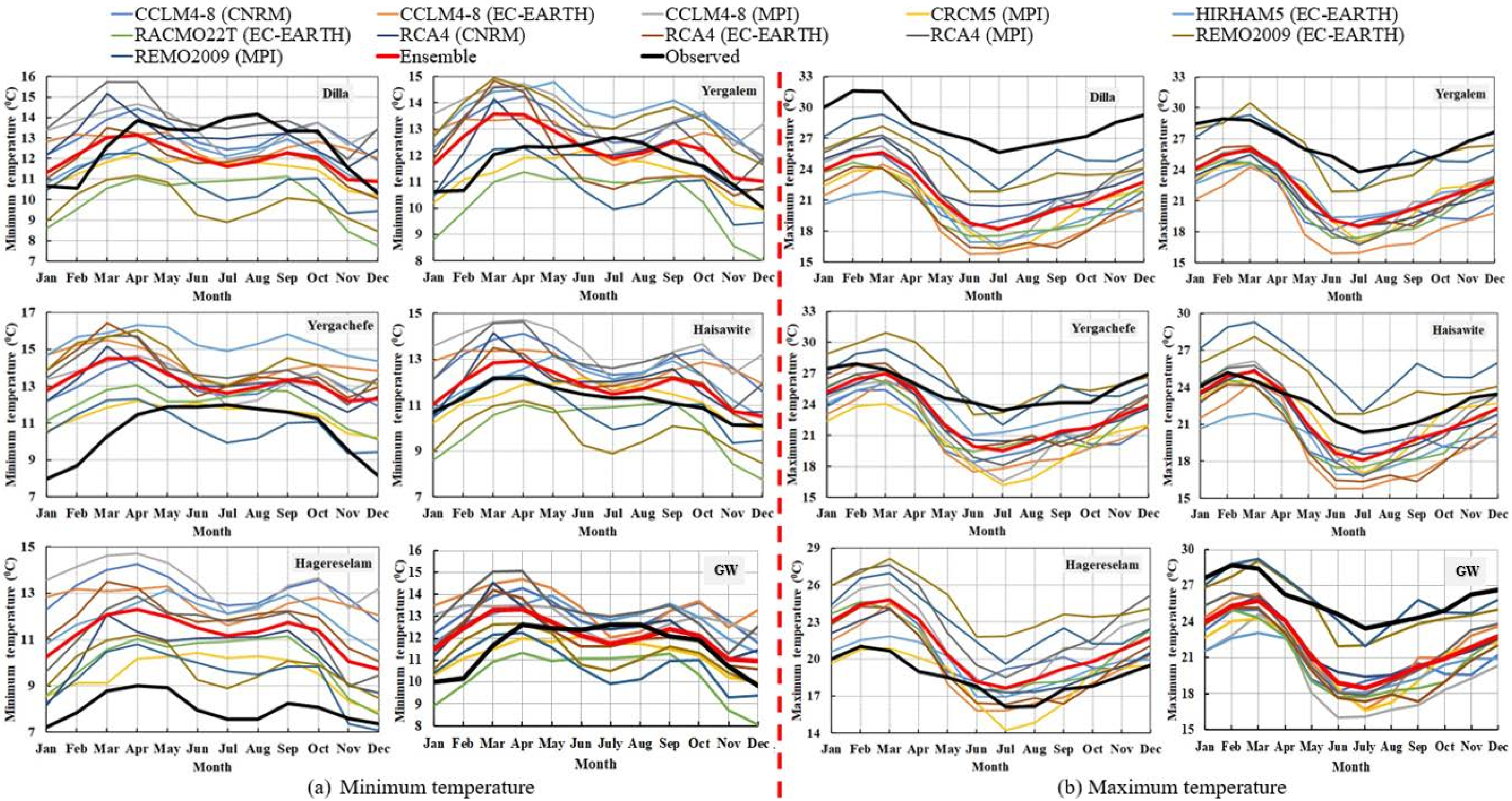

Figure 19. Observed and simulated mean annual cycle of minimum (a) and maximum (b) temperature at each station and in the entire GW.

3.3.2. Seasonal climatology

The study area (located in the southern Ethiopia) experienced two wet seasons viz Belg and Kiremt with short transition. Scholars argued that Ethiopian rainfall is characterized by both seasonal and interannual spatial variabilities (Alhamshry et al., 2020). Therefore, in the data set used in this study (Figure 18), the Belg season rainfall extends from March–May and the Kiremt season lasts from June–October. This corresponds with Tesfamariam et al. (2019) where the ERVLB is characterized by bimodal rainfall distributions with the short rainy season (Belg) extending from March to May and the long rainy season (Kiremt) ranges from June to September (and extends up to October in the southernmost parts). Whereas Belihu et al. (2018), segregated Kiremt season rainfall into June-July and August–October.

Based on rainfall occurrence, there are three major rainy seasons in most part of Ethiopia, namely *Kiremt* (long rainy season, also called Meher) which extends from June to September, *Belg* (short rainy season) which ranges from February to May and Bega (dry season) which lasts from October to January (NMA, 2007; Asfaw et al., 2018). Since majority of the mean annual rainfall totals in Ethiopia is accounted for *Kiremt* (summer) rain, it has high contribution to agricultural productivity and major water reservoirs. While *Belg* (spring) rain is important for *Belg* and long-season crops, as well as for Meher land preparation and in supplementing water for irrigation (Asfaw et al., 2018). Though most of the area in Ethiopia receives one main wet season i.e., *Kiremt*, the spatiotemporal distribution of rainfall has different characteristics from region to region (Berhanu et al., 2014; Belihu et al., 2018; Alhamshry et al., 2020).

Despite their diverse findings, several studies were attempted to subdivide Ethiopia into homogeneous zones relied on spatial homogeneity and seasonality of rainfall. For example, Diro et al. (2011); Tsidu (2012); Alhamshry et al. (2020) grouped Ethiopia into different regions/clusters, of which the southern part of the country is characterized with bimodal seasons of long rainfall (March–May) with rainfall peaks in April/May and another short rainfall (September/October–November). Whereas, Korecha and Sorteberg (2013) delineated Ethiopia into twelve homogenous rainfall regimes, among which the central Rift Valley and southern highlands receive continuous rains for two consecutive seasons (*Belg* and *Kiremt*), with a short spell in June. According to Degefu et al. (2017); Bekele-Biratu et al. (2018), *Belg* (from March to May) is the main rainfall seasons over southern and south-eastern Ethiopia contributing more than 50% of the rainfall. Moreover, Korecha and Sorteberg (2013) underscored both (*Belg* and *Kiremt)* seasons are more or less equally important for this region where the transition from *Belg* to *Kiremt* rainfall is short.

All regional models, except RCA4 (CNRM) and RCA4 (EC-EARTH), underestimate the *Belg* season rainfall while the *Kiremt* and annual rainfall replicated by the CCLM4-8 and REMO2009 group is underestimated over the entire watershed. *Belg* seasonal rainfall pattern is satisfactorily captured by CCLM4-8 (MPI) and REMO2009 (MPI). Besides, *Kiremt* seasonal rainfall distribution is well reproduced by RACMO22T (EC-EARTH). RCMs showed wide-ranging skills in reproducing the seasonal climatology at each station. For example, the RCA4's group (EC-EARTH at Dilla, Haisawite and Hagereselam; CNRM at Yergalem, Haisawite and Hagereselam; MPI at Yergalem and Haisawite) reproduced higher magnitude of *Belg* rainfall than the reference rainfall. While all the RCMs underestimate the *Belg* record at Yergachefe. The output attained from CRCM5 (MPI) overestimate the *Kiremt* rainfall at all stations and *Belg* rainfall at Haisawite station. HIRHAM5 (EC-EARTH) and mean ensemble reproduced higher *Kiremt* at Dilla, Yergalem, Haisawite and Hagereselam station. Whereas, the *Kiremt* rainfall replicated from RACMO22T (EC-EARTH) is higher at Dilla, Haisawite and Hageselam stations.

3.3.3. Interannual variability

SAI was used to compute the negative and positive anomalies (Anose et al., 2021; Belay et al., 2021) of rainfall and temperature fluctuation in the study watershed. The SRA in Figure 20 depicted the occurrence of interannual variability where the observed/gauged annual SRA ranges from –1.5 in 2003 to +2.1 in 1996. According to (Alemseged and Tom, 2015; Asfaw et al., 2018; Dibaba et al., 2019; Belay et al., 2021), SRA enables to reflect dry and wet years over the observation period and is used to examine interannual variability of hydrologic extreme events (e.g., frequency and severity of flood and droughts). In this regard, the study area has experienced both dry and wet years (Figure 20) where very low values of SRA (–1.5 in 2003) correspond to severe drought periods and 1996 was the wet year with high SRA value of 2.1. Previous studies (Gissila et al., 2004; Segele et al., 2009; Korecha and Sorteberg, 2013; Berhanu et al., 2014; Alemseged and Tom, 2015; Alhamshry et al., 2020) emphasized Ethiopia's significant interannual rainfall variability is linked to large-scale phenomena such as El Niño Southern Oscillation (ENSO) and the movement of the Inter-Tropical Convergence Zone (ITCZ).

Scholars witnessed, in Ethiopia, there were widespread droughts in frequency, severity and geospatial coverage in 1965, 1969, 1973/74, 1984/85, 1987/89, 1991/92, 1997–99, 2002–2004, 2008/09, 2012 and 2015/16 (Comenetz and Caviedes, 2002; Suryabhagavan, 2017; Asfaw et al., 2018; Mera, 2018; Bisrat and Berhanu, 2019; Kassaye et al., 2020). Thus, the annual gauged

SRA attained in Figure 7 (red colored column) reveals low SRA values (drought) in 1991, 1999/2000, and 2002-2004. Conversely, the country also experienced abundant amounts of rainfall (Seleshi and Zanke, 2004; Alhamshry et al., 2020). Of which, the year 1996 (Figure *20*) is a typical example of wet year that receives above-average rainfall and higher SRA value which is consistent with previous studies conducted by Seleshi and Zanke (2004); Alhamshry et al. (2020).

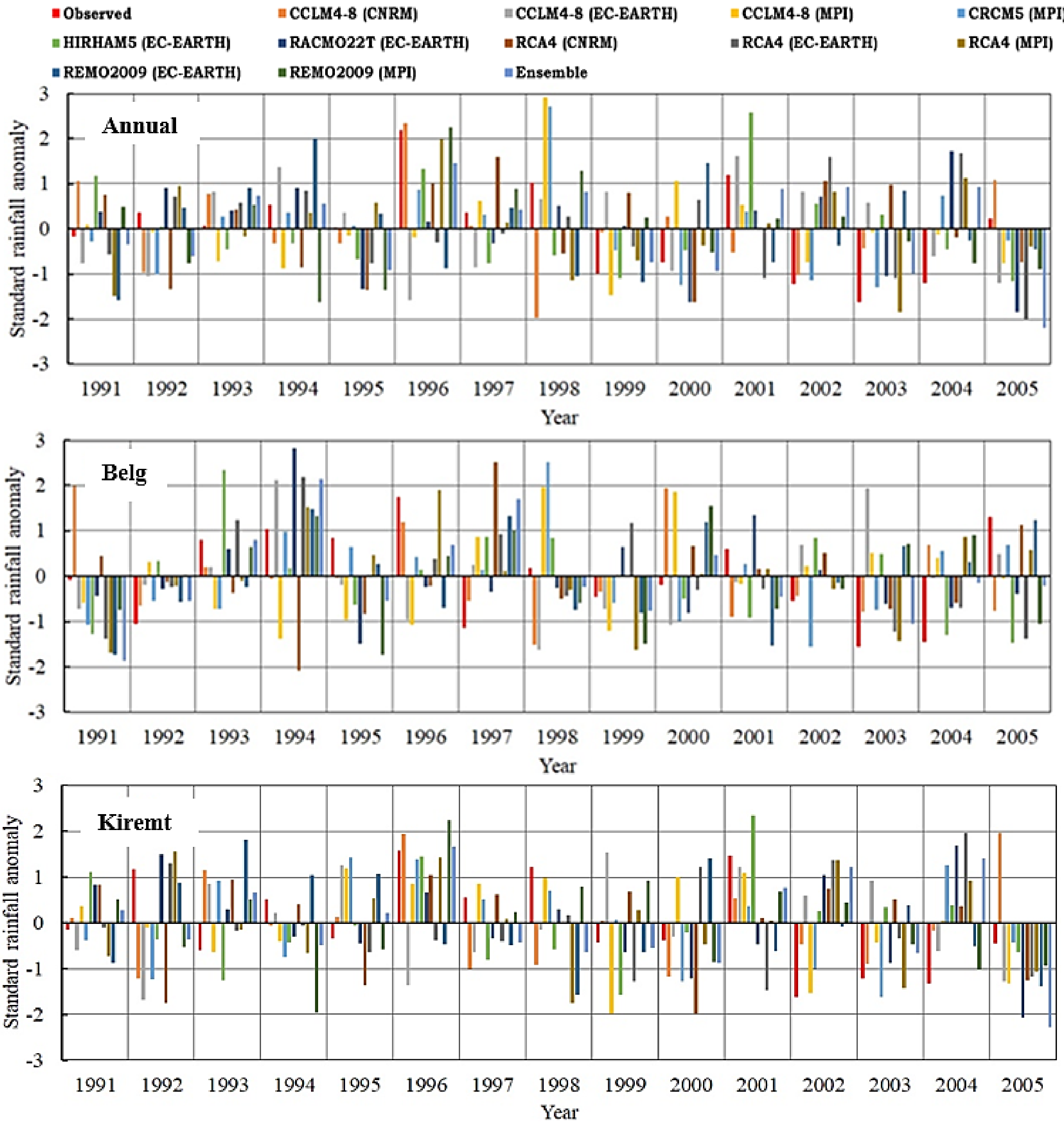

Figure 20. Interannual variability of SRA (mm) over GW for gauged data and RCMs' estimates.

As proved in Figure 20, the performance of regional models to reproduce the rainfall anomalies is varied widely and most of the models and mean ensemble well captured the wet years (e.g., 1996 in the annual and *Belg* season) than the dry years. In line with this, Dibaba et al. (2019)

reported similar results in the Upper Blue Nile Basin, Ethiopia. Most of the models (refer Figure *20*) replicated the 2003 drought episode satisfactorily. Zeleke et al. (2017) uncovered the drying trend over the south and southwestern regions of the country is dominated by the spring season, which corresponds to the season of maximum precipitation. Owing to such drought years, the *Belg* and *Kiremt* seasons were highly affected. Subsequently, both crop and livestock production were highly affected (Belay et al., 2021).

Regards to gauged temperature anomaly, Figure 21 depicted that there were significant interannual variations in minimum and maximum temperature over the study period. It has been noticed that GW experienced both positive and negative standard temperature anomalies (STA). A positive anomaly denotes that the temperature was warmer than normal; a negative anomaly indicates that the temperature was cooler than normal. The deviation of negative minimum STA is highest during *Kiremt* season (–3.1 in 1999). In *Kiremt*, positive minimum STA as high as 1.8 in 1993. The highest above-average deviation (i.e., +2.4 in 2002) of maximum temperature anomaly is observed during *Kiremt* season. There was inter-model skill variability to reproduce the temperature anomaly over the study area. Majority of the RCMs exhibited better performance in capturing the interannual variability of maximum temperature over the GW.

3.3.4. Statistical evaluation of RCMs

The replication capability of individual RCM and their mean ensemble were evaluated using different statistical metrics. The statistical result attained in Table 15 and Table 16, at each station and areal average respectively, confirms the difference in the skill of RCMs in capturing annual and seasonal rainfall over GW. For instance (Table 15), CRCM5 (MPI) overestimated the annual rainfall while CCLM4-8's group and REMO2009 (MPI) underestimated the annual rainfall all over the stations. Though it was in different location, Dibaba et al. (2019) reported similar results in the Upper Blue Nile Basin. Outputs from RCA4's family, marked with high PBIAS and RMSE values, overestimated the annual rainfall at stations of higher altitude (e.g., Hagereselam and Haisawite stations) and underestimated at stations of lower altitude (e.g., Yergachefe). In agreement to this study, Alemseged and Tom (2015); Worku et al. (2018); Dibaba et al. (2019) ascertained GCMs downscaled by RCA4 model were characterized by overestimation in the higher altitudes and vice versa in Ethiopia. The agreement between the observed and modeled rainfall is superior in CCLM4-8 (MPI) and RACMO22T (EC-EARTH) at majority of the stations. RACMO22T (EC-EARTH) do extremely well at Yergachefe station with respect to RR^2.

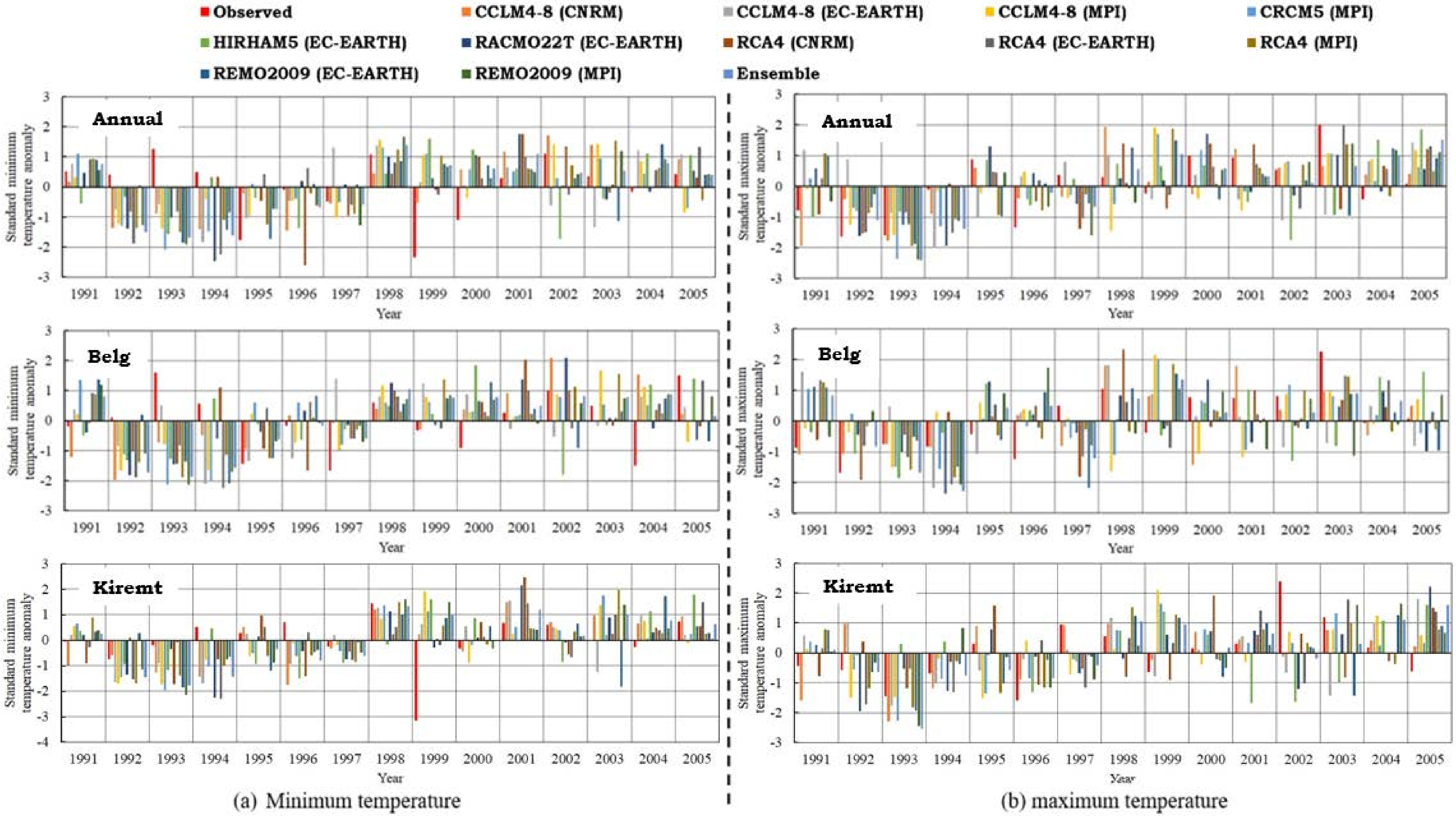

Figure 21. Interannual variability of minimum and maximum temperature anomalies over GW for gauged data and RCMs' estimates.

The annual and seasonal average rainfall variability (CV, Table 16) is less in the case of CRCM5 (MPI), RACMO22T (EC-EARTH), mean ensemble (least CV value) datasets. Whereas, high variation is observed in rainfall climatology produced by CCLM4-8 of EC-EARTH and MPI. Similarly, *Belg* rainfall simulated by RCA4 of EC-EARTH and MPI also showed high variation. Seasonal (*Belg* and *Kiremt*) rainfall captured by HIRHAM5 (EC-EARTH) exhibited moderate variation. Similarly, annual and *Belg* outputs attained from CCLM4-8 (CNRM) showed moderate variation. The CV s indicated the mean ensemble showed the least variation, hence variability is stifled as compared to all separate models (Alemseged and Tom, 2015).

The PBIAS in areal averaged rainfall (Table 16) extended from –74.12% in REMO2009 (MPI) to 174.38% in RCA4 (EC-EARTH). The systematic bias in *Belg* ranged from –74.12% in REMO2009 (MPI) to +12.77% in RCA4 (EC-EARTH). Similarly, the PBIAS in *Kiremt* lasts from –61.44% in REMO2009 (MPI) to +174.38% in RCA4 (EC-EARTH). Hence, the highest wet PBIAS is accounted for RCA4 (EC-EARTH). In line with this, a study conducted by Worku et al. (2018) also underscored GCMs downscaled using RCA4 showed higher wet PBIAS and higher RMSE compared to other models. The mean ensemble replicated the annual rainfall with the lowest PBIAS (4.9%). However, the ensemble underestimated the *Belg* rainfall while overestimated the *Kiremt* rainfall with higher PBIAS as compared to some individual models. This underscore, the mean ensemble of simulated rainfall will never always result better accuracy than using simulations of individual models. Congruently, Alemseged and Tom (2015) reported the poor performance of the ensemble in the Upper Blue Nile basin, Ethiopia.

Majority of the RCMs, except RCA4 (EC-EARTH) and RCA4 (MPI), underestimated the *Belg* seasonal rainfall. Annual, *Belg* and *Kiremt* rainfall reproduced by mean ensemble, RCA4 (MPI) and CCLM4-8 (EC-EARTH) respectively showed minor systematic bias as elucidated in Table 16. In overall, the annual and seasonal rainfall climatology were underestimated by CCLM4-8 group and overestimated by RCA4 family. PBIAS in rainfall is highly associated with the physiographic features such as complex topography (Dibaba et al., 2019; Ayugi et al., 2020b). RACMO22T (EC-EARTH) and mean ensemble showed better performance in capturing the annual and *Kiremt* rainfall while CRCM5 (MPI) replicate the *Belg* rainfall better than other models. RCA4 (EC-EARTH) exhibited poor replication capacity with higher PBIAS (except *Belg*) and RMSE value over all the seasons. CCLM4-8 (MPI) showed better correlation with the observed data to simulate annual and seasonal rainfall. CRCM5 (MPI), RCA4 (MPI) and REMO2009's group were inversely correlated with the observed *Kiremt* rainfall. CCLM4-8 (MPI) and CRCM5 (MPI) *Belg* outputs fitted better than others with high RR^2 value.

Table 15. Statistical indices between the observed and RCMs mean annual rainfall climatology at each station

	Performance statistics	CCLM4-8 (CNRM)	CCLM4-8 (EC-EARTH)	CCLM4-8 (MPI)	CRCM5 (MPI)	HIRHAM5 (EC-EARTH)	RACMO22T (EC-EARTH)	RCA4 (CNRM)	RCA4 (EC-EARTH)	RCA4 (MPI)	REMO2009 (EC-EARTH)	REMO2009 (MPI)	Ensemble
Dilla	PBIAS	-47.4	-31.5	-61.7	18.4	44.2	-13.9	-5.4	183.0	8.2	-63.5	-67.4	-3.4
	RMSE	69.4	64.2	78.1	59.8	121.8	44.5	53.2	304.8	85.2	88.1	90.1	56.1
	r	0.7	0.6	0.9	0.6	0.5	0.8	0.8	0.6	0.6	0.5	0.6	0.7
	RR^2	0.33	0.68	0.07	0.50	0.06	0.57	0.34	0.01	0.12	0.06	0.04	0.39
Hagereselam	PBIAS	-18.7	-29.9	-46.6	36.3	47.5	-11.9	107.3	189.4	-20.3	-62.6	-15.9	15.8
	RMSE	52.5	55.9	55.7	64.1	117.3	36.9	178.0	305.2	54.2	78.5	37.8	58.1
	r	0.6	0.7	0.9	0.6	0.6	0.9	0.8	0.7	0.8	0.6	0.8	0.8
	RR^2	0.33	0.37	0.28	0.31	0.04	0.32	0.02	0.00	0.21	0.12	0.43	0.15
Haisawite	PBIAS	-2.8	-16.2	-36.1	55.2	76.2	5.3	110.7	245.8	126.6	-55.4	-60.2	40.8
	RMSE	59.5	57.2	44.5	66.1	129.9	47.1	161.7	322.7	213.7	60.3	62.5	79.7
	r	0.4	0.5	0.7	0.7	0.6	0.8	0.6	0.6	0.4	0.6	0.7	0.6
	RR^2	0.13	0.16	0.36	0.25	0.02	0.17	0.01	0.00	0.00	0.21	0.15	0.07
Yergachefe	PBIAS	-47.8	-33.3	-62.0	17.5	-45.7	-30.0	-6.2	-33.3	7.4	-36.2	-67.7	-30.7
	RMSE	66.5	58.9	80.9	62.8	75.6	42.5	51.0	56.1	85.6	55.2	95.7	52.2
	r	0.8	0.7	1.0	0.6	0.6	0.9	0.8	0.8	0.6	0.8	0.5	0.8
	RR^2	0.30	0.43	0.05	0.59	0.55	0.89	0.46	0.59	0.15	0.37	0.03	0.37
Yergalem	PBIAS	-14.5	-1.1	-43.8	36.5	-18.7	-12.5	85.3	-39.5	99.3	22.8	-65.0	4.4
	RMSE	53.4	55.3	52.8	54.0	62.5	40.8	144.9	54.4	198.1	61.8	78.7	45.1
	r	0.6	0.7	0.9	0.8	0.6	0.8	0.7	0.8	0.6	0.7	0.7	0.8
	RR^2	0.45	0.28	0.21	0.64	0.27	0.41	0.04	0.65	0.01	0.23	0.07	0.38

Table 16. Statistical indices between areal average observed and RCMs rainfall (annual and seasonal) climatology over GW

	CV (%)			PBIAS (%)			RMSE			r			RR^2		
	Annual	*Belg*	*Kiremt*	Annual	*Belg*	*Kiremt*	Annual	*Belg*	*Kiremt*	Annual	*Belg*	*Kiremt*	Annual	*Belg*	*Kiremt*
Observed	13.63	19.64	20.43	–	–	–	–	–	–	–	–	–	–	–	–
CCLM4-8 (CNRM)	23.69	27.58	31.86	-28.6	-30.47	-38.39	54.3	57.71	65.64	0.65	0.81	0.79	0.59	0.27	0.11
CCLM4-8 (EC-EARTH)	30.65	31.74	41.86	-20.0	-45.01	-0.36	54.2	83.24	31.03	0.65	0.72	0.97	0.39	0.15	0.09
CCLM4-8 (MPI)	40.59	37.95	47.17	-51.3	-53.14	-53.25	59.9	81.71	75.23	0.92	0.99	0.83	0.16	0.76	0.23
CRCM5 (MPI)	14.49	18.62	16.46	31.2	-16.93	35.31	56.5	36.82	52.49	0.69	0.78	-0.46	0.44	0.76	0.05
HIRHAM5 (EC-EARTH)	12.29	29.53	23.90	22.4	-40.27	64.61	87.6	86.36	104.46	0.58	0.60	0.10	0.08	0.09	0.01
RACMO22T (EC-EARTH)	11.68	19.87	16.37	-11.5	-28.40	9.03	37.9	62.89	13.59	0.85	0.75	1.00	0.42	0.15	0.67
RCA4 (CNRM)	15.11	23.89	19.59	46.2	-2.52	69.35	98.4	97.25	100.15	0.71	0.76	0.19	0.07	0.02	0.10
RCA4 (EC-EARTH)	12.18	32.49	17.32	107.4	12.77	174.38	184.4	113.89	251.13	0.67	0.76	0.60	0.02	0.02	0.01
RCA4 (MPI)	14.83	32.60	18.62	55.9	0.05	56.06	139.9	115.80	86.81	0.56	0.68	-0.82	0.03	0.02	0.02
REMO2009 (EC-EARTH)	12.04	28.48	16.20	-34.1	-54.95	-28.31	54.1	90.17	49.28	0.67	0.71	-0.12	0.79	0.52	0.20
REMO2009 (MPI)	16.91	19.88	35.02	-63.7	-74.12	-61.44	77.5	116.26	92.53	0.64	0.98	-0.89	0.32	0.06	0.27
Ensemble	6.04	10.75	9.27	4.9	-30.27	20.64	50.9	67.81	30.51	0.73	0.75	0.81	0.28	0.12	0.13

The result in Table 17 unveiled majority of the RCMs overestimated the minimum temperature all over the stations. Likewise, Dibaba et al. (2019) also found similar results in the Upper Blue Nile Basin. The output from CCLM4-8 (MPI), at Hagereselam station, showed the weakest performance to replicate the observed minimum annual temperature with highest PBIAS (68.4%) and RMSE (5.5^{0}C) values. Whereas, CCLM4-8 and RCA4 downscaled from EC-EARTH strongly captured the minimum temperature at Dilla station with the lowermost PBIAS (0.1%) and RMSE (0.4^{0}C) value. The r statistics showed better correlation between gauged and majority of RCM outputs (minimum temperature) at Hageresam and Haisawite stations. Unlike to minimum temperature, majority of the RCMs underestimated the maximum temperature. At Hagereselam station, REMO2009 (EC-EARTH) exhibited the poorest skill to simulate maximum temperature due to its uppermost overestimation PBIAS (32%). Similarly, CCLM4-8 (EC-EARTH) showed weak performance to replicate maximum temperature at Dilla station due to high PBIAS (31.5%) and RMSE (9^{0}C). Contrary to that, CRCM5 (MPI) is superior in replicating the observed maximum temperature with minimum PBIAS (-1.1%) and RMSE (1^{0}C) value at Hagereselam station. The existing linear relationship between gauged and all RCM estimates (maximum temperature) revealed the presence of strong agreement. The PBIAS, in Table 17, depicts all RCM outputs overestimated both minimum and maximum temperature at station of higher altitude (e.g., Hagereselam station) and underestimated stations of lower altitude (e.g., Dilla). In agreement with this, Flato et al. (2013); Kim et al. (2013); Dibaba et al. (2019) indicated PBIAS is much larger at station of higher altitudes.

The areal average annual and seasonal variation of both minimum and maximum temperature is very low (CV < 20%) (Table 18). Minimum temperature was relatively more variable than the maximum average temperature. This is consistent with earlier studies (Lambe and Kundapura, 2021; Teshome et al., 2022). Most of the RCMs output overestimated minimum temperature except CRCM5 (MPI), RACMO22T (EC-EARTH) and REMO2009 (MPI). Whereas, the areal maximum temperature is underestimated by majority of the RCMs except of REMO2009 (EC-EARTH). The annual and seasonal minimum temperature correlation between observed and CRCM5 (MPI) output is stronger than the others. 50% of RCM outputs and mean ensemble were inversely correlated with the observed minimum temperature in the Belg and Kiremt season. Moreover, almost all RCM outputs (excepting CCLM4-8 (CNRM) and REMO2009 (MPI)) and mean ensemble outshined with a strong linear relationship (r > 0.7) with the reference maximum temperature. Similarly, Kim et al. (2013) and Dibaba et al. (2019) revealed RCM skill is higher for maximum temperature than minimum temperature.

Table 17. Statistical indices between the observed and RCMs mean annual temperature (minimum and maximum) at each station

Minimum temperature	Performance measures	CCLM4-8 (CNRM)	CCLM4-8 (EC-EARTH)	CCLM4-8 (MPI)	CRCM5 (MPI)	HIRHAM5 (EC-EARTH)	RACMO22T (EC-EARTH)	RCA4 (CNRM)	RCA4 (EC-EARTH)	RCA4 (MPI)	REMO2009 (EC-EARTH)	REMO2009 (MPI)	Ensemble
Dilla	PBIAS	3.7	0.0	6.5	-9.3	-4.6	-20.2	3.5	0.0	10.3	-22.4	-14.2	-4.2
	RMSE	0.5	0.0	0.8	-1.2	-0.6	-2.5	0.4	0.0	1.3	-2.8	-1.8	-0.5
	r	0.5	-0.2	-0.1	0.8	0.9	0.9	0.3	-0.2	0.2	0.4	0.3	0.5
	RR^2	0.08	0.01	0.02	0.09	0.16	0.50	0.09	0.01	0.07	0.09	0.09	0.05
Hagereselam	PBIAS	63.3	57.5	68.4	18.7	50.2	25.6	30.0	48.4	41.0	22.2	17.0	40.2
	RMSE	5.1	4.6	5.5	1.5	4.0	2.1	2.4	3.9	3.3	1.8	1.4	3.2
	r	0.9	0.7	0.7	0.5	0.7	0.6	0.7	0.8	0.7	0.9	0.8	0.9
	RR^2	0.51	0.46	0.25	0.17	0.29	0.09	0.09	0.21	0.09	0.30	0.11	0.37
Haisawite	PBIAS	15.3	13.1	20.4	0.4	7.3	-10.2	6.8	6.0	14.9	-12.7	-3.5	5.2
	RMSE	1.7	1.5	2.3	0.0	0.8	-1.1	0.8	0.7	1.7	-1.4	-0.4	0.6
	r	0.8	0.5	0.6	0.8	0.7	0.8	0.9	0.9	0.9	0.8	0.9	0.9
	RR^2	0.53	0.40	0.26	0.54	0.37	0.14	0.23	0.30	0.22	0.32	0.26	0.62
Yergachefe	PBIAS	24.0	35.0	27.3	8.4	45.6	13.7	23.7	31.0	31.8	35.4	2.5	25.3
	RMSE	2.5	3.7	2.9	0.9	4.8	1.4	2.5	3.3	3.4	3.7	0.3	2.7
	r	0.5	-0.4	-0.1	0.8	0.5	0.7	0.3	-0.1	0.1	0.1	0.3	0.3
	RR^2	0.06	0.05	0.02	0.07	0.04	0.15	0.06	0.05	0.04	0.02	0.07	0.03
Yergalem	PBIAS	12.1	8.7	15.7	-3.5	16.8	-12.0	2.6	2.5	10.5	15.1	-7.2	5.6
	RMSE	1.4	1.0	1.8	-0.4	2.0	-1.4	0.3	0.3	1.2	1.8	-0.8	0.6
	r	0.5	-0.1	0.0	0.9	0.7	0.9	0.6	0.1	0.5	0.6	0.4	0.6
	RR^2	0.28	0.03	0.01	0.58	0.62	0.39	0.40	0.03	0.28	0.46	0.28	0.44
Maximum temperature	Performance measures	CCLM4-8 (CNRM)	CCLM4-8 (EC-EARTH)	CCLM4-8 (MPI)	CRCM5 (MPI)	HIRHAM5 (EC-EARTH)	RACMO22T (EC-EARTH)	RCA4 (CNRM)	RCA4 (EC-EARTH)	RCA4 (MPI)	REMO2009 (EC-EARTH)	REMO2009 (MPI)	Ensemble
Dilla	PBIAS	-24.1	-31.5	-22.3	-27.3	-31.0	-27.4	-19.0	-30.3	-19.4	-13.4	-8.5	-23.1
	RMSE	6.9	9.0	6.5	7.8	8.8	7.8	5.4	8.7	5.7	3.9	2.6	6.6
	r	0.9	0.9	0.9	0.9	0.9	1.0	1.0	1.0	0.9	0.9	0.9	1.0
	RR^2	0.47	0.25	0.21	0.38	0.63	0.35	0.58	0.26	0.21	0.73	0.71	0.45
Hagereselam	PBIAS	12.2	4.3	17.5	-1.1	5.2	10.6	6.9	6.2	24.6	32.0	23.7	12.9
	RMSE	2.6	1.9	3.6	1.0	1.2	2.4	1.7	2.0	4.9	6.0	4.6	2.6
	r	0.8	0.9	0.9	0.9	0.9	0.9	0.9	0.9	0.9	0.9	0.9	0.9
	RR^2	0.26	0.12	0.14	0.31	0.64	0.18	0.26	0.13	0.11	0.37	0.28	0.25
Haisawite	PBIAS	-8.8	-14.6	-3.8	-4.7	-13.9	-9.4	-5.8	-13.0	-5.4	8.1	14.2	-5.2
	RMSE	2.4	3.7	1.7	1.5	3.2	2.5	1.6	3.3	2.0	2.1	3.4	1.5
	r	0.8	0.9	1.0	0.9	0.9	0.9	0.9	1.0	1.0	0.9	0.9	1.0
	RR^2	0.27	0.13	0.14	0.23	0.70	0.18	0.29	0.14	0.12	0.39	0.37	0.26
Yergachefe	PBIAS	-15.8	-17.3	-13.8	-19.3	-7.5	-12.0	-10.1	-8.6	-10.6	5.0	1.6	-9.8
	RMSE	4.2	4.7	3.9	5.1	2.2	3.3	2.7	2.7	3.2	2.0	1.2	2.8
	r	0.9	0.9	0.9	0.9	0.8	1.0	0.9	1.0	1.0	0.8	0.8	0.9
	RR^2	0.25	0.13	0.11	0.20	0.70	0.18	0.31	0.13	0.11	0.18	0.36	0.23
Yergalem	PBIAS	-21.3	-17.6	-27.2	-18.4	-17.4	-20.9	-19.3	-16.8	-19.0	-2.3	-2.2	-16.6
	RMSE	5.8	4.9	7.3	5.0	4.7	5.7	5.2	4.6	5.2	1.4	1.1	4.5
	r	0.8	1.0	0.9	0.9	0.9	1.0	1.0	1.0	1.0	0.9	0.9	1.0
	RR^2	0.40	0.21	0.22	0.32	0.85	0.24	0.43	0.23	0.18	0.25	0.54	0.35

Table 18. Statistical indices between gauged and simulated areal mean annual and seasonal temperature (minimum and maximum) over GW

Minimum temperature	CV (%)			PBIAS (%)			RMSE			r			RR^2		
	Annual	*Belg*	*Kiremt*	Annual	*Belg*	*Kiremt*	Annual	*Belg*	*Kiremt*	Annual	*Belg*	*Kiremt*	Annual	*Belg*	*Kiremt*
Observed	4.47	5.35	4.97	–	–	–	–	–	–	–	–	–	–	–	–
CCLM4-8 (CNRM)	2.47	2.20	2.50	12.5	14.07	7.58	1.7	1.77	1.18	0.50	0.33	-0.99	0.17	0.06	0.23
CCLM4-8 (EC-EARTH)	2.46	3.11	2.86	10.5	9.89	3.11	1.8	1.28	0.76	-0.13	0.17	-0.96	0.02	0.00	0.25
CCLM4-8 (MPI)	2.15	2.89	4.25	16.1	18.19	7.19	2.3	2.27	1.25	-0.03	0.14	-0.90	0.02	0.01	0.06
CRCM5 (MPI)	3.84	6.05	2.95	-2.8	-3.92	-5.89	0.6	0.53	0.73	0.90	0.98	0.70	0.25	0.11	0.78
HIRHAM5 (EC-EARTH)	2.09	2.58	2.16	10.7	10.49	8.22	1.4	1.31	1.08	0.84	0.75	-0.34	0.31	0.39	0.27
RACMO22T (EC-EARTH)	2.49	2.33	3.29	-11.0	-9.61	-10.4	1.4	1.22	1.32	0.91	0.70	0.59	0.78	0.06	0.30
RCA4 (CNRM)	2.57	3.38	2.23	7.1	9.92	1.91	1.3	1.72	0.43	0.52	-0.78	0.42	0.36	0.08	0.25
RCA4 (EC-EARTH)	3.40	4.10	2.90	4.4	9.84	-1.91	1.3	1.60	0.37	0.38	-0.51	-0.42	0.36	0.08	0.10
RCA4 (MPI)	4.72	6.28	3.53	14.7	18.62	7.60	2.1	2.47	0.99	0.37	-0.31	0.20	0.33	0.06	0.19
REMO2009 (EC-EARTH)	4.11	3.25	3.17	-2.5	2.08	-7.10	1.1	0.55	1.00	0.42	-0.18	-0.76	0.25	0.02	0.26
REMO2009 (MPI)	3.59	3.70	4.91	-7.1	-1.99	-12.3	1.4	0.61	1.65	0.37	-0.25	-0.96	0.27	0.08	0.24
Ensemble	2.30	2.63	2.22	4.8	7.05	-0.19	1.0	1.02	0.42	0.56	-0.25	-0.73	0.19	0.06	0.35
Maximum temperature	**CV (%)**			**PBIAS (%)**			**RMSE**			**r**			**RR^2**		
	Annual	*Belg*	*Kiremt*	Annual	*Belg*	*Kiremt*	Annual	*Belg*	*Kiremt*	Annual	*Belg*	*Kiremt*	Annual	*Belg*	*Kiremt*
Observed	1.28	2.56	1.98	–	–	–	–	–	–	–	–	–	–	–	–
CCLM4-8 (CNRM)	3.04	3.40	3.76	-18.5	-16.22	-18.30	4.9	4.55	4.51	0.87	0.90	0.03	0.35	0.13	0.01
CCLM4-8 (EC-EARTH)	3.18	3.76	6.02	-24.6	-17.63	-28.80	6.5	5.11	7.03	0.91	0.82	0.63	0.18	0.07	0.16
CCLM4-8 (MPI)	3.16	3.99	4.27	-15.5	-11.58	-18.07	4.3	3.35	4.53	0.95	0.91	0.77	0.17	0.14	0.02
CRCM5 (MPI)	2.44	3.28	3.06	-18.8	-14.27	-21.15	5.0	3.86	5.31	0.92	0.89	0.91	0.28	0.86	0.03
HIRHAM5 (EC-EARTH)	1.99	3.06	3.74	-20.3	-16.38	-20.29	5.3	4.44	4.96	0.89	0.86	0.65	0.87	0.16	0.16
RACMO22T (EC-EARTH)	1.71	3.97	2.10	-19.4	-17.30	-23.78	5.2	4.81	5.80	0.96	0.87	0.56	0.24	0.14	0.43
RCA4 (CNRM)	1.84	2.83	2.99	-14.9	-11.30	-17.05	3.9	3.24	4.16	0.95	0.91	0.84	0.39	0.17	0.75
RCA4 (EC-EARTH)	2.24	4.29	2.93	-19.8	-15.04	-25.87	5.3	4.17	6.33	0.97	0.93	0.64	0.19	0.18	0.47
RCA4 (MPI)	2.46	3.65	3.56	-14.8	-13.19	-17.47	4.1	3.74	4.30	0.96	0.94	0.69	0.18	0.14	0.04
REMO2009 (EC-EARTH)	2.55	2.52	4.45	-2.9	2.90	-3.01	1.3	0.87	0.76	0.89	0.96	0.56	0.38	0.80	0.11
REMO2009 (MPI)	1.85	2.29	2.61	-0.3	3.33	1.57	1.0	0.97	0.85	0.89	0.95	0.73	0.49	0.80	0.05
Ensemble	1.57	1.92	1.95	-15.4	-11.52	-17.47	4.1	3.22	4.27	1.0	0.90	0.75	0.33	0.25	0.16

3.3.5. Trends in observed and simulated rainfall and temperatures

The trends of rainfall and temperature based on the original MK test and Sen's slope estimator are presented in Table 19 and Table 20, respectively. The observed trend analysis in Table 19 indicates that rainfall experienced significant decreasing trends (at 10% level of significance) both in the annual (-13.38 mm) and *Kiremt* (-12.1 mm) time scale. On the other hand, *Belg* season rainfall exhibited a non-significant decreasing tendency with a magnitude of about ~4 mm. The result agrees with the findings of earlier studies reported in different parts of Ethiopia. For example, Belihu et al. (2018) revealed rainfall in GW exhibited a significant decreasing trend around 12 mm per annum between 1982 and 2014. Cheung et al. (2008) and Mulugeta et al. (2019) underscored the significant decreasing trend of Kiremt rainfall at watershed, sub-basin and basin level in Ethiopia while annual and Belg rainfall showed no significant trends in the period 1960 – 2002 and 1902 – 2016, respectively. Moreover, the annual rainfall over GW (Alehu et al., 2021) and ERVLB (Kassie et al., 2014) decreased insignificantly, whereas Ademe et al. (2020a) highlighted the decline trend in Kiremt rainfall and absence of annual rainfall trends in the ERVLB.

Likewise, Tesfamariam et al. (2019), stated the declining tendency in majority of the months constituting the *Belg* and *Kiremt* seasons over the ERVLB despite the fact that the significant declining trends were found to be rare. Besides, Viste et al. (2013) uncovered the decreasing trends of annual and *Kiremt* seasonal rainfall over the eastern, southern and the southwestern areas of Ethiopia. In addition, the areal weighted average rainfall shows negligible declining trend over Bilate basin of RVLB in Ethiopia (Lambe and Kundapura, 2021). Nevertheless, the results are different from the findings of Belay et al. (2021) where an increasing trend of annual and *Kiremt* rainfall were recorded in the Southern Ethiopia. This contrast indicates the country, Ethiopia, experienced spatio-temporal climate sensitivities.

The result in Table 19 depicts majority of the RCMs exhibit non-significant declining trends of both annual and seasonal rainfall. Despite of that, the *Belg* and *Kiremt* season rainfall tendency captured by RCA4 (EC-EARTH) and RACMO22T (EC-EARTH) outputs showed statistically significant decline trend at 5% significant level respectively. However, increasing trends (positive Z-score) of RCM outputs such as CCLM4-8 (EC-EARTH), RCA4 (CNRM), CCLM4-8 (MPI), CRCM5 (MPI), RCA4 (MPI), REMO2009 (EC-EARTH), REMO2009 (MPI) and CCLM4-8 (CNRM) is in contrast to the observed pattern. In general, the output attained from RACMO22T (EC-EARTH) showed best performance in simulating annual and seasonal rainfall trends in GW.

Table 19. Mann–Kendall test results for annual and seasonal rainfall

RCM	Annual			*Belg*			*Kiremt*		
	P-Value	Z-Score	Sen's slope	P-Value	Z-Score	Sen's slope	P-Value	Z-Score	Sen's slope
Observed	0.117***	-1.39	-13.38	0.187	-0.89	-3.981	0.0688***	-1.485	-12.1
CCLM4-8 (CNRM)	0.383	-0.297	-2.446	0.117	-1.19	-5.979	0.422	0.198	0.545
CCLM4-8 (EC-EARTH)	0.461	0.099	0.558	0.161	0.99	4.11	0.383	0.297	5.903
CCLM4-8 (MPI)	0.346	-0.396	-1.531	0.161	0.99	7.147	0.346	-0.396	-2.746
CRCM5 (MPI)	0.422	-0.198	-2.99	0.422	0.198	1.262	0.214	-0.792	-4.438
HIRHAM5 (EC-EARTH)	0.214	-0.792	-8.823	0.0829***	-1.386	-5.708	0.31	0.495	9.692
RACMO22T (EC-EARTH)	0.187	-0.891	-6.074	0.346	-0.396	-0.919	0.0374**	-1.782	-15.47
RCA4 (CNRM)	0.422	0.198	3.427	0.244	0.693	5.667	0.244	-0.693	-7.907
RCA4 (EC-EARTH)	0.31	-0.495	-13.34	0.0462**	-1.683	-21.56	0.422	-0.198	-5.392
RCA4 (MPI)	0.422	-0.198	-3.286	0.31	0.495	3.242	0.346	-0.396	-5.833
REMO2009 (EC-EARTH)	0.461	-0.099	-3.247	0.187	0.891	5.331	0.138	-1.089	-6.112
REMO2009 (MPI)	0.187	-0.891	-4.551	0.422	0.198	0.521	0.187	-0.891	-2.648
Ensemble	0.422	-0.198	-1.25	0.346	-0.396	-1.228	0.187	-0.891	-2.104

, * mean significant trends at alpha (α) = 0.05 and 0.1 respectively.

Table 20. Mann–Kendall test results for annual and seasonal temperature

Minimum temperature	Annual			*Belg*			*Kiremt*		
	P-Value	Z-Score	Sen's slope	P-Value	Z-Score	Sen's slope	P-Value	Z-Score	Sen's slope
Observed	0.31	-0.049	-0.003	0.383	0.297	0.014	0.244	0.693	0.0118
CCLM4-8 (CNRM)	0.00504*	2.573	0.056	5.45E-4*	3.266	0.056	0.00877*	2.375	0.0449
CCLM4-8 (EC-EARTH)	0.187	0.891	0.027	0.187	0.89	0.025	0.0462**	1.683	0.0243
CCLM4-8 (MPI)	0.0566***	1.58	0.030	0.0147**	2.18	0.054	0.0239**	1.979	0.072
CRCM5 (MPI)	0.214	0.792	0.039	0.31	0.495	0.0156	0.0188**	2.078	0.0511
HIRHAM5 (EC-EARTH)	0.0566***	1.58	0.030	0.0374**	1.78	0.0455	0.0147**	2.177	0.0283
RACMO22T (EC-EARTH)	0.0991	1.29	0.032	0.03**	1.881	0.042	0.0239**	1.979	.041
RCA4 (CNRM)	0.0829***	1.386	0.028	0.117	1.19	0.042	0.0147**	2.177	0.0328
RCA4 (EC-EARTH)	0.0462*	1.683	0.038	0.187	0.891	0.058	0.0114**	2.276	0.0453
RCA4 (MPI)	0.03**	1.881	0.089	0.0188**	2.078	0.129	0.03**	1.881	0.065
REMO2009 (EC-EARTH)	0.138	1.09	0.017	0.422	0.198	0.008	0.0991***	1.287	0.0304
REMO2009 (MPI)	0.0188**	2.078	0.0615	0.0147**	2.177	0.064	0.0188**	2.078	0.0641
Ensemble	0.0374**	1.782	0.047	0.0114**	2.276	0.052	0.0114**	2.276	0.047
Maximum temperature	Annual			*Belg*			*Kiremt*		
	P-Value	Z-Score	Sen's slope	P-Value	Z-Score	Sen's slope	P-Value	Z-Score	Sen's slope
Observed	0.024*	2.63	0.054	0.00279*	2.77	0.106	0.0829***	1.386	0.042
CCLM4-8 (CNRM)	0.00279*	2.771	0.0898	0.0188**	2.08	0.087	0.276	0.594	0.0998
CCLM4-8 (EC-EARTH)	0.461	0.099	0.003	0.276	-0.59	-0.039	0.214	0.792	0.0722
CCLM4-8 (MPI)	0.0374**	1.782	0.0822	0.138	1.089	0.0616	0.0114**	2.276	0.116
CRCM5 (MPI)	0.0239**	1.979	0.0614	0.346	0.396	0.0337	0.0566**	1.584	0.0624
HIRHAM5 (EC-EARTH)	0.0566***	1.584	0.058	0.0566***	1.58	0.091	0.31	0.495	0.0275
RACMO22T (EC-EARTH)	0.187	0.891	0.030	0.383	0.297	0.018	0.0374**	1.782	0.0593
RCA4 (CNRM)	0.0374**	1.782	0.0498	0.0688***	1.485	0.0385	0.138	1.089	0.0245
RCA4 (EC-EARTH)	0.00877*	2.375	0.0712	0.0829***	1.386	0.109	0.0239*	1.979	0.069
RCA4 (MPI)	0.0147**	2.177	0.0749	0.138	1.089	0.0539	0.0566***	1.584	0.0739
REMO2009 (EC-EARTH)	0.0566***	1.585	0.0766	0.461	-0.10	-0.007	0.0829***	1.386	0.0901
REMO2009 (MPI)	0.00108*	3.068	0.072	0.422	0.198	0.019	0.0147*	0.098	0.098
Ensemble	0.00108***	1.64	0.058	0.187	0.89	0.028	0.00279*	2.771	0.0637

*,**, *** mean significant trends at alpha (α) = 0.01, 0.05, and 0.1 respectively.

As can be illustrated in Table 20, minimum mean temperature declined (annual) and increased (Belg and Kiremt) insignificantly at 10% level of significance over the study period. Contrary to this, the mean annual and *Belg* season maximum temperature exhibited a significant increasing trend at 1% level of significance whereas *Kiremt* season maximum temperature showed significant increasing trend at 10% level of significance. The overall result revealed, GW experienced warming trends attributed to a significant increase in maximum temperature. The findings of this study are consistent with previous studies appraised in different parts of Ethiopia. To give an instance, a study by Belihu et al. (2018) documented the overall increments of temperature in GW. Ademe et al. (2020b) disclosed that maximum temperature showed higher warming trend than the minimum temperature in the highlands of Ethiopia. Getahun et al. (2021) deduced a significant increasing trend in temperature both on annual and seasonal basis in Awash River basin. In the north east Ethiopia, a non-significant warming trend of minimum temperature was observed during annual and *Kiremit* season (Abegaz and Abera, 2020; Teshome et al., 2022).

3.3.6. Taylor skill score and ranking

Mentioning Figure 22a, CCLM4-8 (MPI) and REMO2009 (MPI) models scored low variability compared to the observed rainfall. In contrast, the RCA4 family and HIRHAM5 (EC-EARTH) show higher variability against the observed rainfall. REMO2009 (EC-EARTH), CCLM4-8 (CNRM), CRCM5 (MPI) and CCLM4-8 (EC-EARTH) exhibit a close agreement in terms of rainfall variability relative to reference rainfall. In comparison, HIRHAM5 (EC-EARTH) and RCA4 (MPI) scored the weakest correlation (~ 0.6) while CCLM4-8 (MPI) scored the highest (~ 0.92). Based on CRMSE, CCLM4-8 (MPI) and RACMO22T (EC-EARTH) showed good performance resulting in a low CRMSE value whereas the highest value was scored by RCA4 (EC-EARTH), which results in the weakest performance compared to the other models.

In the same way, the performance of each RCMs for simulation of mean minimum and maximum temperature is displayed in Figure 22b and Figure 22c, respectively. Majority of the models exhibit low variation against the reference minimum temperature. CCLM4-8 (EC-EARTH) scored the least variation to capture the observed minimum temperature over GW while RACMO22T (EC-EARTH) showed the highest variation. It has been noticed that (Figure 22b), RACMO22 (EC-EARTH) and CRCM5 (MPI) exhibit a strong correlation score (0.9) and low CRMSE value indicate good simulation skill. On the other hand, CCLM4-8 (EC-EARTH) and CCLM4-8 (MPI) indicate inverse correlation (< 0) and high CRMSE value ensuing weak performance compared to the other models. Figure 22c demonstrate all the RCMs exhibit higher variability against the observed maximum temperature. Figure 22c demonstrate all the RCMs exhibit higher variability against the observed maximum temperature. Whereas, the correlation coefficient ranges between 0.87 (CCLM4-8 (CNRM)) and 0.97 (RCA4 (EC-EARTH)) reveal strong relationship. In terms of CRMSE majority of the models showed weak simulation performance except HIRHAM5 (EC-EARTH) and RCA4 (CNRM).

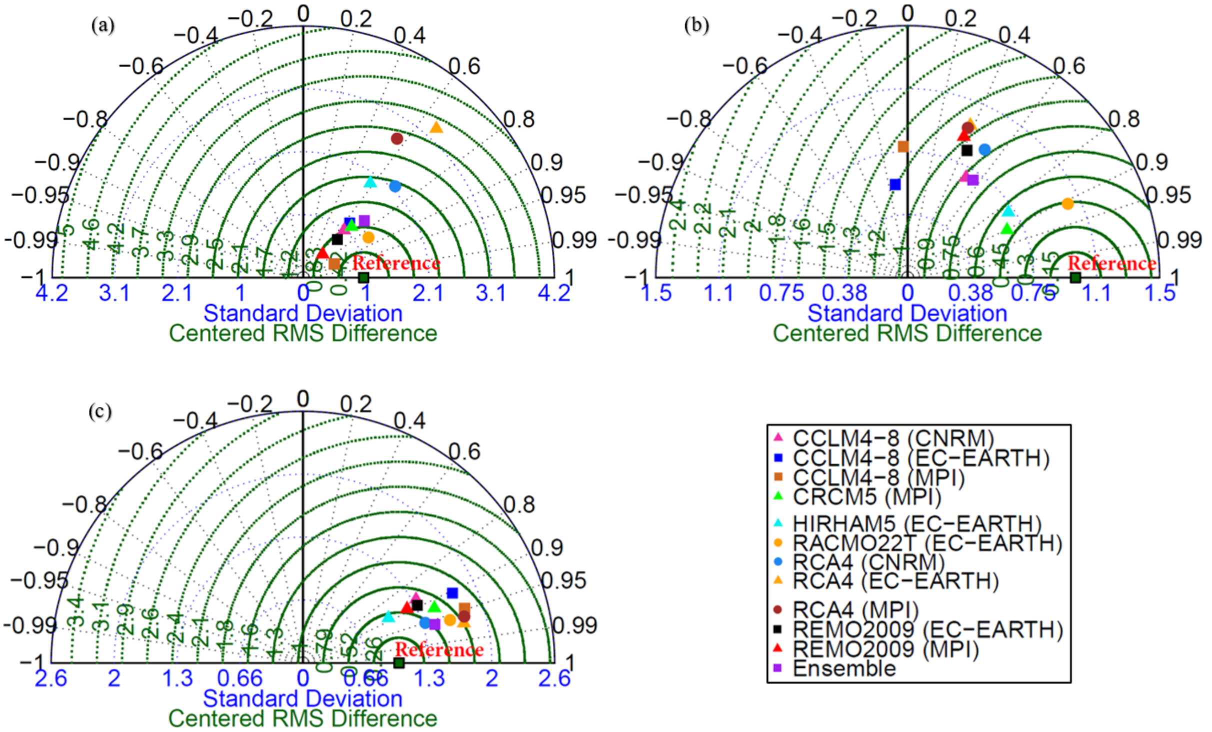

Figure 22. Taylor diagram of RCMs, ensemble and reference datasets for rainfall, mm/month (a) and temperature, ^{0}C (minimum (b) and maximum (c)).

The overall status/ranking of model performance is executed using TSS metrics as shown in Figure 23. RACMO22T (EC-EARTH) surpasses the other models with TSS value of 0.88 (rainfall) and 0.95 (minimum temperature). HIRHAM5 (EC-EARTH) outperforms in the case of maximum temperature with the highest TSS value (0.94) whereas the TSS score of the other models extends from 0.71 to 0.91. Other models that perform better in replicating rainfall include CRCM5 (MPI), CCLM4-8 (CNRM) and REMO2009 (EC-EARTH). The lowest TSS is scored by RCA4 (EC-EARTH) (0.26) and CCLM4-8 (EC-EARTH) (0.31) for rainfall and minimum temperature respectively. The Taylor diagram provides a concise statistical summary of how well patterns match each other (Taylor, 2001). The effectiveness of the Taylor diagram is due to its compact representation where a single diagram is used showing three statistical metrics (CRMSE, correlation and standard deviation) (Singh et al., 2013). Moreover, Taylor (2001), boldly underscored the diagram is useful in evaluating complex models.

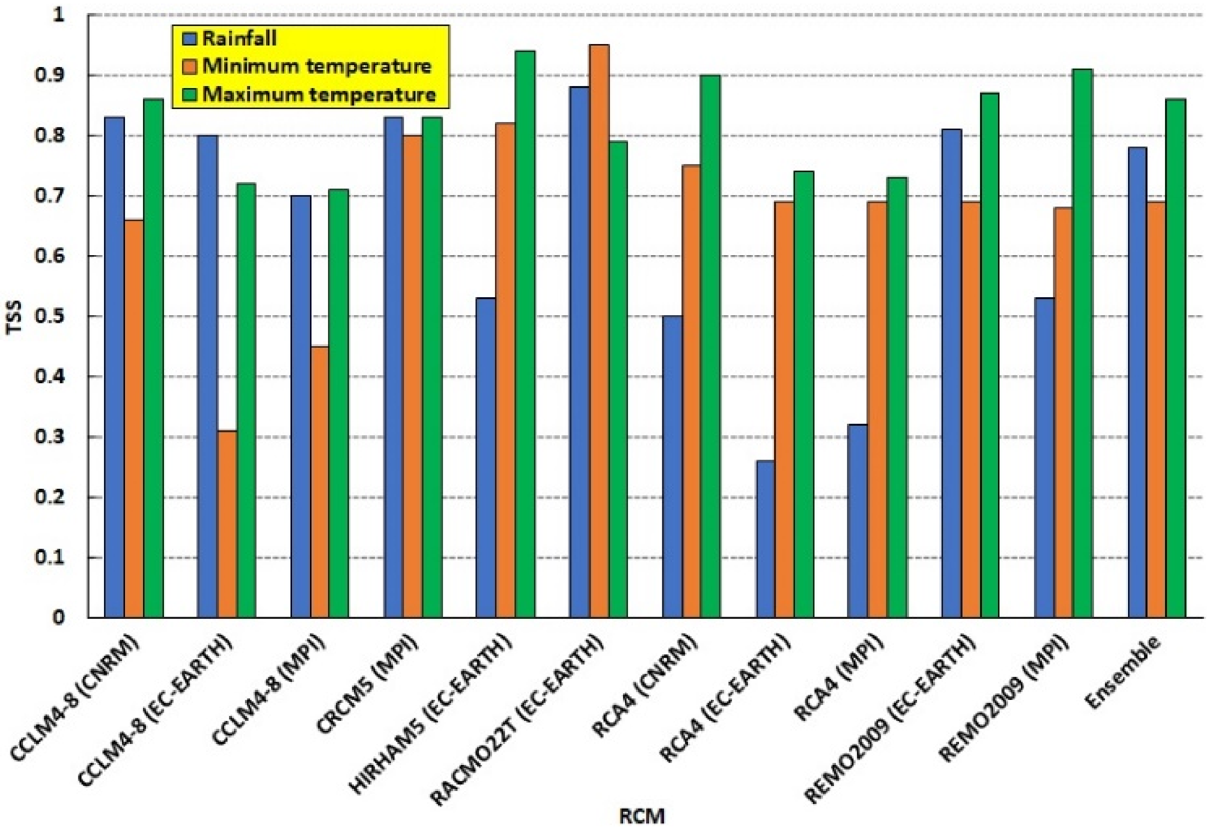

Figure 23. Taylor skill score (TSS) and ranking of RCM outputs performance

3.4. Conclusion

The performance of 11 CORDEX-Africa RCMs and their mean ensemble were evaluated in reproducing the spatial and temporal distribution of rainfall and temperature over GW. Statistical metrics such as PBIAS, RMSE, r, CV and TSS are utilized to assess model performance in reproducing seasonal, annual and inter-annual time scale against the gauged dataset. Additionally, MK test and Sen's slope estimator were adopted to investigate the capability of RCMs in replicating the trends of meteorological variables. The overall results depict the performance of RCMs varies according to different sets of data, topographic feature and climatic variables. Thus, replication of rainfall and temperature by downscaled RCMs is characterized by overestimation and underestimation over the study area. RACMO22T (EC-EARTH) robustly reproduced the spatial rainfall variability. CCLM4-8 (MPI) model and mean ensemble well captured the annual pattern of observed mean monthly rainfall. The *Belg* season rainfall is underestimated by majority of the models. Most of the models and mean ensemble well captured the wet years than the dry years. In overall, the annual and seasonal rainfall climatology were underestimated by CCLM4-8 group and overestimated by RCA4 family. In addition, RCA4 (EC-EARTH) exhibited poor replication capacity with higher RMSE value over all the seasons. Most of the derived RCMs exhibited higher and lower records than the observed minimum and maximum temperature cycle respectively. Whereas, CRCM5 (MPI) satisfactory replicated the annual distribution of minimum and maximum temperature. Majority of the RCMs exhibited better performance in capturing the interannual variability of maximum temperature. Moreover, almost all RCM outputs and mean ensemble outshined with a strong linear relationship with the reference maximum temperature. Majority of the RCMs captured the non-significant declining trends of both annual and seasonal rainfall. In this case, RACMO22T (EC-EARTH) showed strong performance in simulating annual and seasonal rainfall trends. Majority of the models reproduced the increasing tendency of both minimum and maximum temperature. In terms of TSS, RACMO22T (EC-EARTH) surpasses the other models with the highest TSS value for rainfall and minimum temperature. Whereas, HIRHAM5 (EC-EARTH) outperforms in the case of maximum temperature with the highest TSS value. The lowest TSS is scored by RCA4 (EC-EARTH) and CCLM4-8 (EC-EARTH) for rainfall and minimum temperature respectively. Altogether, models that performs better in replicating the observed climate variables include RACMO22T (EC-EARTH), CRCM5 (MPI), CCLM4-8 (CNRM) and REMO2009 (EC-EARTH). Generally, the analysis indicates a need to correct the systematic bias of RCM outputs and built an ensemble by using best performing models prior to employing further climate change impact studies.

4. Integrated modeling of land degradation dynamics and insights on the possible future management alternatives in the Gidabo watershed, Ethiopian Rift Valley Lakes Basin

Abstract

Land degradation is a pivotal environmental concern, bearing substantial impacts in the GW, prompting a critical need for effective mitigation strategies. In this study, we aimed to assess the dynamics of land degradation pathways in the context of change in climate and land use. The identification of potential erosion hotspots and the appraisal of management strategies was also carried out. The Soil and Water Assessment Tool (SWAT) and the Good Practice Guidance (GPG) framework was employed. The results revealed a compelling synergy between land use dynamics and climate changes, asserting joint and individual prevalence in influencing surface runoff and sediment yield. The past simulation revealed 4–5.9% and 24–43% increments in mean annual runoff and sediment yield, respectively. While the near (2021–2040) and mid (2041–2060) future scenarios displayed varying trends under RCP4.5 and RCP8.5. Furthermore, sub-basins prone to soil erosion risk were identified, thereby enabling targeted conservation efforts. The assessment of trends in land degradation neutrality (LDN) unveiled the expansion of land degradation trajectories (by 26%) from 1985–2003 to 2003–2021. This might be attributed to the dynamic interplay between climate and LULC change, with croplands and bare land emerging as high-risk degraded areas. Addressing these concerns, soil/stone bund, terracing, contour farming, and reforestation practice can significantly reduce the annual sediment yield in the future. The integration of soil erosion indicators with LDN sub-indicators can provide a more comprehensive approach that can lead to more effective land management and restoration strategies in the GW. The findings of this study could contribute crucial insights and substantial implications for policymakers, land managers, and conservationists. Moreover, future efforts should be directed to expand investigations into diverse land degradation pathways and mitigation measures.

This chapter is originally published as:

Girma, R., Fürst, C., Moges, A., 2023. Integrated modeling of land degradation dynamics and insights on the possible future management alternatives in the Gidabo river basin, Ethiopian rift valley. Land, 12, 1809. https://doi.org/10.3390/land12091809.

4.1. Introduction

Land has the potential to provide a full suite of goods and services at local, landscape and global scale (Sanz, 2017; UNCCD, 2019a). Nevertheless, land is coming under growing pressure from ever-increased competing uses (Orr et al., 2017) and subjected to increasing degradation trends (UNCCD, 2019a). Land degradation has diverse and wide-reaching impacts on the provision of vital ecosystem services, causing economic and social consequences more severely than ever before (Akça et al., 2022; IPBES, 2018; Pricope et al., 2023; Verburg et al., 2019). These impacts, however, are worse in developing countries, where the majority of the population directly depends on land resources for its livelihood (Shitu, 2022; UNCCD, 2019b). Most of East Africa, including Ethiopia, has experienced severe land degradation problems that pose a challenge to people's livelihoods (Kirui et al., 2021; Moges and Gebregiorgis, 2013; UNCCD, 2019b). Different approaches have been used to assess land degradation including expert opinions, field measurement, biophysical modeling and remote sensing, or a combination thereof (García et al., 2019; Kirui et al., 2021; Nzuza et al., 2021).

The expert opinion approach highly relied on the people consulted and is considered subjective, inconsistent and replicable with difficulty (Gibbs and Salmon, 2015; Nzuza et al., 2021). Field measurement involves local sampling techniques and surveys to provide detailed objective information, for example, at a plot level (Nzuza et al., 2021). However, this approach is often criticized for being time-consuming, labour intensive, costly and applicable to small areas (Nzuza et al., 2021). The biophysical modeling approach integrate biophysical variables to assess land degradation. Though it is globally consistent and quantitative, its accuracy might be influenced by inherent error (Gibbs and Salmon, 2015; Nzuza et al., 2021). The remote sensing approach is vital in measuring land degradation, especially over a larger scale (Kirui et al., 2021; Yang et al., 2023). Remote sensing provides a plausible, consistent and useful alternative for multi-temporal and operational scale monitoring of land degradation. This approach is considered a cost-effective, reputable and time-efficient (Gibbs and Salmon, 2015).

Most recently, the United Nations Convention to Combat Desertification (UNCCD) introduced the concept of "Land Degradation Neutrality" (LDN) to combat and recover the current trends in land degradation (Feng et al., 2022). LDN that refers to a condition of "zero net land degradation" became one of the significant targets of the Sustainable Development Goal (SDG 15.3). An extensive description of LDN is provided in [17,18]. The LDN assessment is based on three significant biophysical sub-indicators: (i) land productivity (LP), (ii) land cover (LC) and (iii) soil organic carbon (SOC) (Sims et al., 2019). The three indicators follow the principle of “The One-Out, All-Out (1OAO)” (Schillaci et al., 2023; Zhao et al., 2023). This principle enables the identification of land degradation more accurately with three dimensions of land status including aboveground, below-ground, and surface change (Zhao et al., 2023). Trends.Earth, a QGIS plugin, is working in combination with the Google Earth Engine to facilitate data preparation and processing for generating both the sub-indicators and the final SDG indicator 15.3.1 (Giuliani et al., 2020).

Soil erosion is a widely distributed land degradation pathway and an important complement to the three global LDN indicators that interacts with other environmental issues (Borrelli et al., 2018; Tsymbarovich et al., 2020). In recent decades, with the well-established use of geospatial technologies, models are becoming increasingly important in the identification of erosion prone areas at different time and spatial scales (Gao et al., 2020; Lemma et al., 2019; Ricci et al., 2018). Process-based hydrological models are very accurate owing to their capabilities to simulate and describe the spatial distribution of land degradation (IPBES, 2018). These models can depict the spatial characters of meteorological conditions, topography, land cover and soil properties (Gao et al., 2020). The soil and water assessment tool (SWAT) model, the most widely used model (Ricci et al., 2018), considers these factors to identify areas susceptible to soil erosion (dos Santos et al., 2023). SWAT model provides spatial and temporal distribution and magnitude of surface runoff and sediment yield (IPBES, 2018). Both runoff and sediment yield are closely tied to soil erosion, which is a key component of land degradation (Dutta, 2016). Moreover, the SWAT model allows to quantify the impact of land management practices and is capable of assessing the best management alternatives in large and complex watersheds (Lemma et al., 2019).

The study demonstrated an integrated approach to assess the trends of land degradation in the GW. The watershed has been subjected to substantial landscape alteration, climatic variability and drastic ecological change (Alehu et al., 2021; Belihu et al., 2018; Girma et al., 2022a; Mana and Abebe, 2023; Mechal et al., 2015; Worako et al., 2022). These changes, triggered by dynamic population growth, exacerbate soil erosion, excessive sedimentation and eutrophication of waterbodies, hydrological imbalance and land–water–energy–food nexus resource degradation (Aragaw et al., 2022; Belihu et al., 2020; Serur and Adi, 2022; Wolde et al., 2021; WoldeYohannes et al., 2018). The explicit quantification of spatial and temporal trends of land degradation and its trajectory help to achieve LDN (Yang et al., 2023). Moreover, decisions addressing land degradation problems are not only based on an assessment of the current land degradation but also on the expected future state of the land (IPBES, 2018).

Climate and land use change are intertwined with soil erosion and land degradation. Understanding these interactions is crucial for developing effective strategies to achieve LDN goals. It is notable that land degradation can take many forms and that some methods are not appropriate for measuring all forms of land degradation pathways (Kirui et al., 2021). However, previous studies lack spatial and temporal information on the extent and magnitude of land degradation in the GW. Therefore, this study aimed at the integration of SWAT model and Trends.Earth platform to assess land degradation pathways in the GW. The specific objectives were to (1) extensively evaluate the individual and joint impacts of climate and land use land cover (LULC) change on runoff and sediment yield during the temporal span of 1990 to 2060, (2) conduct an in-depth assessment of trends in land degradation neutrality, (3) identify erosion hotspots necessitating intensified attention, and (4) evaluate potential management alternatives aimed at curtailing sediment production.

4.2. Materials and methods

4.2.1. Data source and processing

Climate data

The observed data of daily rainfall, temperature, solar radiation, relative humidity and wind speed were collected from 5 stations (Figure 1). The data were acquired from the Ethiopian Meteorology Institute (EMI) for the period of 1990–2021 and Dilla station was used to establish the weather generator database. Filling of missed meteorological data and temporal homogeneity test was performed using XLSTAT 2021 statistical software as used by previous studies (Demissie and Sime, 2021; Dibaba et al., 2019). Moreover, double mass curve (DMC) analysis was executed to assess the consistency of rainfall (Gao et al., 2017).

Projected climate data for near (2021–2040) and mid (2041–2060) future were acquired from RCM of Coordinated Regional Climate Downscaling Experiment (CORDEX) (https://esgf-data.dkrz.de/search/esgf-dkrz/ (accessed on 11 April 2022)). Two representative concentration pathways (RCP), i.e., moderate emission (RCP4.5) and highest emission (RCP8.5) were considered as future scenarios (IPCC, 2023). According to the performance study in chapter 3 (Girma et al., 2022b), RACMO22T (ECEARTH), CCLM4–8 (MPI), CRCM5 (MPI), CCLM4–8 (CNRM) and REMO2009 (EC-EARTH) were chosen. Thus, the ensemble of these RCMs was used and bias corrected using distribution mapping (DM) method. DM method provided better result in the study watershed (Worako et al., 2022). Moreover, Mann–Kendall (MK) test and Sen's slope estimator were used to test the trends in climate variables. A detailed description of these trend test methods can also be found in chapter 3 or Girma et al. (2022b).

Spatial data

The long-term LULC dynamics for the baseline years (1985, 2003 and 2021) and projected years (2035 and 2050) were adopted from Chapter 2 (Girma et al., 2022a). For erosion modeling, soil data were extracted from the latest FAO Harmonized World Soil Database version 2.0 (https://gaez.fao.org/pages/hwsd (accessed on 2 June 2023)) (FAO & IIASA, 2023). Additionally, the SoilGrids raster layer at 250 m spatial resolution developed by the International Soil Reference Information Center (ISRIC) was used for SOC estimation (https://soilgrids.org/ (accessed on 15 July 2023)). Topographic data were extracted from the Alaskan Satellite Facility digital elevation model (DEM) (12.5 m resolution) available at https://search.asf.alaska.edu/#/ (accessed on 20 June 2023).

Hydrology data

For SWAT model calibration and validation, 18 years (1997–2014) daily streamflow data at Aposto and Bedessa gaging stations (Figure 1) were used. The two stations were considered since they have the longest period of flow data. The data were acquired from the Ministry of Water and Energy (MoWE) of Ethiopia. Due to the lack of continuous-time step sediment records, sediment yield data were generated using sediment rating curve (SRC). The SRC is extensively used to overcome the scarcity of temporal sediment data (Adi et al., 2023; Assfaw, 2020; Dananto et al., 2022; Gadissa et al., 2018; Toma et al., 2023). Hence, the suspended sediment load for Aposto and Bedessa gauging stations was generated using the sediment discharge rating curve developed by Adi et al. (2023) with an R^2 value of 0.96 and 0.91, respectively.

4.2.2. Assessment of land degradation indicators

Surface runoff and sediment yield modeling using SWAT

To evaluate the effects of climate and LULC change, we applied 20 different simulations (individual and combined scenarios), as shown in Table 21. Prior to simulation, the study area was divided into sub-basins using the DEM as input in SWAT2012 (interface of ArcGIS10.8). Furthermore, each sub-basin was further subdivided into several number of hydrologic response units (HRUs)[2] with a unique combination of 5% land cover, 10% soil type and 10% slope thresholds. Then, all the required climatic variables were fed to the model and a three-year warming-up period was given during simulation. Details of SWAT model procedure is given in SWAT theoretical documentation (Neitsch et al., 2011).

[2] Changes in land use resulted in variations in the number and distribution of HRUs in the GW. Therefore, 261 HRUs for 1985, 237 HRUs for 2003, 175 HRUs for 2021, 178 HRUs for 2035 and 163 HRUs for 2050 were created.

Table 21. SWAT model simulation setup

Simulation	LULC	Climate	RCP
Past period			
S1 *	1985	1990–2005	–
S2	2003	1990–2005	–
S3	2021	1990–2005	–
S4	1985	2006–2020	–
S5	2003	2006–2020	–
S6 **	2021	2006–2020	–
Future LULC change scenario			
S7	2035	2006–2020	–
S8	2050	2006–2020	–
Future climate change scenario			
S9	2021	2021–2040	RCP4.5
S10	2021	2041–2060	RCP4.5
S11	2021	2021–2040	RCP8.5
S12	2021	2041–2060	RCP8.5
Future combined (LULC and climate change) scenario			
S13	2035	2021–2040	RCP4.5
S14	2035	2041–2060	RCP4.5
S15	2035	2021–2040	RCP8.5
S16	2035	2041–2060	RCP8.5
S17	2050	2021–2040	RCP4.5
S18	2050	2041–2060	RCP4.5
S19	2050	2021–2040	RCP8.5
S20	2050	2041–2060	RCP8.5

*, ** represents baseline for past period and future scenario, respectively.

Surface runoff was estimated using the soil conservation service curve number (SCS-CN) method (Equation 23) (Neitsch et al., 2011).

$$\mathrm{Q_{surf}} = \frac{\left(\mathrm{R_{day}} - \mathrm{I_a}\right)^2}{\left(\mathrm{R_{day}} - I_a + \mathrm{S}\right)}, \tag{23}$$

where Q_{surf} is the accumulated runoff or rainfall excess (mm water), R_{day} is the daily rainfall depth (mm water), I_a is the initial abstractions which includes surface storage, interception and infiltration period to runoff (mm water), and S is the retention parameter (mm water) mathematical expressed using the curve number (CN) (Equation 24) (Neitsch et al., 2011).

$$\mathrm{S} = 25.4\left(\frac{1000}{\mathrm{CN}} - 10\right), \tag{24}$$

The CN is governed mainly by LULC, soil permeability and a hydraulic group of soils (Neitsch et al., 2011). The initial abstractions, I_a, is commonly approximated as 0.2S and equation 24 becomes (Equation 25) (Neitsch et al., 2011):

$$\mathrm{Q_{surf}} = \frac{\left(\mathrm{R_{day}} - 0.2\mathrm{S}\right)^2}{\left(\mathrm{R_{day}} + 0.8\mathrm{S}\right)}, \tag{25}$$

Sediment yield was estimated using the Modified Universal Soil Loss Equation (MUSLE) (Equation 26) (Arnold et al., 2012).

$$SY = 11.8 \times \left(Q_{surf} \times Q_{peak} \times area_{hru}\right)^{0.56} \times K \times C \times P \times LS \times CFRG, \quad (26)$$

where SY is the sediment yield on a day (metric tons), Q_{surf} is the surface runoff volume (mm ha−1), Q_{peak} is the peak runoff rate ($m^3\ s^{-1}$) (Equation 27), $area_{hru}$ is the area of the HRU (ha), K is the soil erodibility factor, C is the cover and management factor, P is the support practice factor, LS is the topographic factor, CFRG is the coarse fragment factor, and 0.56 is the delivery ratio.

$$Q_{peak} = \frac{C \times i \times area}{3.6}, \quad (27)$$

Where Q_{peak} is peak runoff rate ($m^3\ s^{-1}$), c is the runoff coefficient, i is the rainfall intensity (mm/hr.), sub-basin area (km^2) and 3.6 is conversion factor.

SWAT calibration, validation and performance measures

Multi-site calibration was performed using the sequential uncertainty fitting (SUFI-2) algorithm in SWAT-CUP. SWAT simulates total sediment load, i.e., suspended load plus bedload (Neitsch et al., 2011). In most rivers, bed load to suspended load ranges between 10 and 30% (Church, 2006). Since most (81%) of the study area was characterized as gentle to moderate steep slopes, 10% of the suspended sediment load obtained from the rating curve were considered as bedload. Similar assumptions were employed in the Ethiopian rift valley (Aga et al., 2018; Dananto et al., 2022). Parameters to be calibrated were initially selected by reviewing previously used parameters in the GW (Adi et al., 2023; Aragaw et al., 2022; Dananto et al., 2022; Serur and Adi, 2022), and SWAT theoretical documentation (Neitsch et al., 2011).

Afterwards, sensitivity analysis was performed and the most sensitive parameters were identified based on Lenhart et al., (2002) sensitivity classes. Furthermore, model performance was evaluated using Nash–Sutcliffe efficiency (NSE) coefficient, coefficient of determination (R^2) and percent bias (PBIAS) according to the ratings given by Moriasi et al., (2015). The iteration was run for the simulation period of 1997–2014 and the first 3 years were used for warm-up period. A split sample test was employed to split the remaining years into calibration period (2000–2009) and validation period (2010–2014) on a monthly basis (Abraham et al., 2022).

Assessing and monitoring LDN indicators

The assessment and monitoring of LDN was carried out based on the Good Practice Guidance

(GPG) prepared for the Sustainable Development Goal (SDG15) (Sims et al., 2019). Accordingly, QGIS3.28 Trends.Earth plugin and Google Earth engine was used to quantify the following sub-indicators.

The LP sub-indicator (in kg/ha/year) were determined from a time series of annual normalized difference vegetation index (NDVI) dataset (Schillaci et al., 2023; Teich et al., 2023). In this study, two NDVI data sources were used to monitor the entire period from 1985 to 2021: (i) the Advanced Very-High-Resolution Radiometer (AVHRR) data obtained from Global Inventory Modeling and Mapping Studies (GIMMS) were used to assess trends from 1985 to 2003, and (ii) data provided by the Terra Moderate Resolution Imaging Spectroradiometer (MODIS) Vegetation Indices (MOD13Q1) Version 6 was used to determine trends from 2003 to 2021 (Trends.Earth, 2022). Moreover, Water Use Efficiency (WUE) correlation method was employed to correct the effects of climate on LP (Schillaci et al., 2023).

To assess the LC sub-indicator, custom LULC data (1985, 2003, 2021) were used and reclassified to forestlands, grasslands, croplands, wetlands, artificial areas, bare land and waterbodies using UNCCD reporting and IPCC land classification (Trends.Earth, 2022). Afterwards, the land cover transition matrix between 1985–2003 and 2003–2021 were analyzed to identify which pixels remained in the same land cover class, and which ones changed (Sims et al., 2019). Based on expertise and local knowledge of the conditions in the study area, table of degradation typologies was created to identify which transitions correspond to degradation, improvement, or no change (Trends.Earth, 2022). Finally, Trends.Earth combined the information from the LULC maps and the table of degradation typologies by LC transition to compute the LC degradation between 1985–2003 and 2003–2021.

For SOC sub-indicator, the relative change in SOC (t/ha) was determined using a combined LULC/SOC method in Trends.Earth. Area which experienced a loss in SOC of >10% during the reporting period (2003 and 2021) was considered potentially degraded, and areas experiencing a gain of >10% as potentially improved (Trends.Earth, 2022).

The sub-indicators were then combined using the 1OAO principle to determine the extent of land that is degraded as a percentage of the total area (Sims et al., 2019). The 1OAO principle implies that a significant reduction or negative change in any one of the three sub-indicators is considered to comprise land degradation in a land unit, then the final indicator is assessed as degraded for the specific land unit (Giuliani et al., 2020; Sims et al., 2019).

Soil conservation scenarios

The SWAT model simulates the efficiency of land management interventions by adjusting both erosion and runoff parameters (Gashaw et al., 2017; Lemma et al., 2019; Qiu et al., 2020). Thus, five soil conservation scenarios were examined including filter strips, terracing, soil/stone bund, contour farming and reforestation. The filter strips scenario was implemented on croplands by changing the width of the filter strip (i.e., FILTERW) into 1 m (Admas et al., 2022; Hurni, 2016). Likewise, terracing, contour farming and soil/stone bund scenarios were evaluated by modifying the corresponding CN2, USLE_P, the slope length (SLSUBBSN) and slope steepness (HRU_SLP) on croplands (Admas et al., 2022; Hurni, 2016). The reforestation scenario assumes that all the cultivated lands above 15% slope as well as bare land will be changed into forest (Admas et al., 2022; Gashaw et al., 2017). Thus, the implementation of the reforestation scenario was made by changing the land use map (Admas et al., 2022).

4.3. Results and discussion

4.3.1. Biophysical characteristics

More than 70% of the GW is covered by three soil groups (Figure 24a): Eutric Vertisols (29%) characterized by a significant proportion of clay-sized particles and vetric property (FAO-UNESCO, 1988), Lithic Leptosols (25%) dominated in the eastern escarpment and have limited agricultural potential due to their shallow depth, low fertility and poor water-holding capacity (FAO-UNESCO, 1988), and Chromic Luvisols (22%) are soils with subsurface accumulation of high activity clays and high base saturation (Nachtergaele et al., 2012). The altitude of the study area ranged from 1133 to 3197 m above sea level (a.s.l) (Figure 24b) and most (81%) of the watershed exhibited gentle to moderate steep slopes (Figure 24c). The eastern part of the watershed is characterized by longest and very steep slopes (having >45% slope), while the lower part is dominantly characterized by flat terrain (<3% slope). On the bases of topographic features, the study area was subdivided in to 35 sub-basins (Figure 24d).

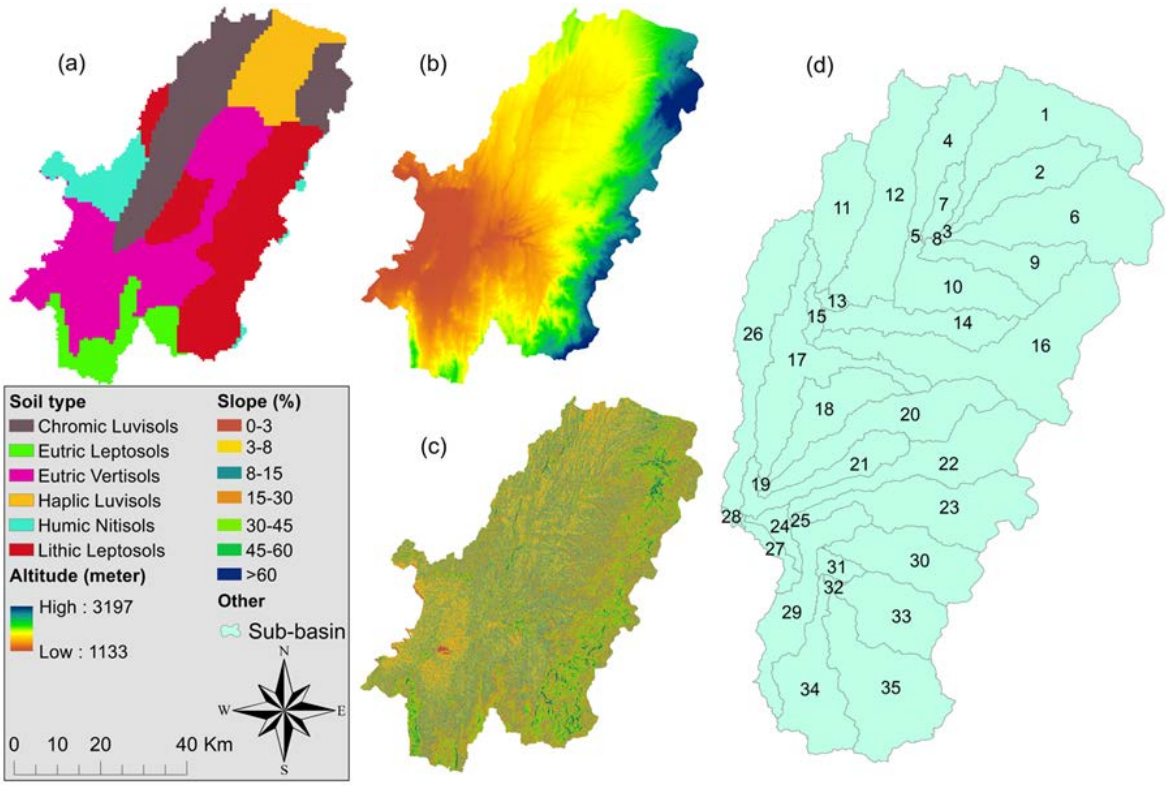

Figure 24. (a) major soil groups, (b) altitude, (c) slope classes and (d) sub-basin in the GW.

4.3.2. Trends in rainfall and temperature

The trend analysis indicated that the observed mean annual rainfall experienced decreasing trend with a magnitude of about 13.4 mm/year from 1990 to 2005 (significantly) and 0.44 mm/year from 2006 to 2021 (insignificantly) (Table 22). While there has been a significant decline in rainfall in the earlier past (1990–2005), the trend in the more recent years (2005–2021) was relatively stable. The observed mean annual maximum temperature showed a significant increasing trend, whereas minimum temperature declined insignificantly. Under RCP4.5, the projected mean annual rainfall showed a non-significant decreasing trend with a magnitude of about 4.5 and 6.4 mm/year (2021–2040 and 2041–2060, respectively). However, both mean annual minimum and maximum temperature showed statistically significant evidences of increasing trends (Table 22). Under high emission scenario (RCP8.5), the annual rainfall will decrease (at a rate of 5.4 mm/year during the near future) and increase (at a rate of 7.8 mm/year during the mid future) insignificantly, while both the annual minimum and maximum temperature will increase significantly.

This indicates that the watershed is likely to experience warmer conditions in the future, which can have various implications for ecosystems, water resources and human activities. For example, rising temperatures will amplify the impact of droughts, reducing soil moisture availability and cropland productivity (Shigute et al., 2023). Since majority of the livelihoods were primarily dependent on subsistence rainfed agriculture (Wolde et al., 2021), these trends could have significant effects on agricultural practices and might be the determinant factor for various socio-economic problems in the watershed. These findings emphasize the need for robust climate monitoring and adaptation strategies to address the potential impacts of changing climate conditions on water resources, agriculture and overall environmental sustainability in the region. The results were consistent with the findings of previous studies (Alehu et al., 2021; Aragaw et al., 2022; Belihu et al., 2018; Mana and Abebe, 2023). The spatial pattern of projected mean annual rainfall and temperature were included in the annex (Figure A2 and Figure A3).

Table 22. The Mann–Kendall and the Sen's slope test results for rainfall and temperature.

Variable	Trend Test	Observed		RCP4.5		RCP8.5	
		1990–2005	2006–2021	2021–2040	2041–2060	2021–2040	2041–2060
Rainfall	Z-Score	−1.39***	−0.22	−0.55	−0.49	−0.88	1.14
	Sen's slope	−13.4	−0.44	−4.5	−6.4	−5.4	7.8
Minimum temperature	Z-Score	−0.05	0.88	2.63*	1.46***	3.15*	3.36*
	Sen's slope	−0.003	0.02	0.1	0.02	0.1	0.1
Maximum temperature	Z-Score	2.63*	−0.44	2.17**	0.81	2.95*	1.72**
	Sen's slope	0.1	−0.01	0.04	0.02	0.04	0.03

*, **, *** means significant trend at alpha (α) = 0.01, 0.05, and 0.1, respectively.

4.3.3. Land use land cover dynamics

Nine LULC classes were identified, including waterbody, grasslands, forestlands, agriculture lands, bare land, settlements, agroforestry, shrublands and marshy area (Figure 25). A detailed description of the LULC classification and change analysis can also be found in Chapter 2 (Girma et al., 2022a). In 1985, the largest land cover type was shrublands (24.3%) followed by forestlands (21.8%) and agriculture lands (19.8%) (Table 4). However, agricultural lands, agroforestry and bare land showed increments and overturned the dominancy in 2003 and 2021 (Table 5). These unceasing expansion and trends will also be expected by 2035 and 2050 at the expense of forest, shrub and grasslands loss (Table 11). Moreover, the expansion of waterbodies (Figure 5), particularly along the shore side of Lake Abaya might be attributed to the displacement and lateral expansion of the lake's water due to the increase in sediment load, resulting from soil erosion (Dadi Belete et al., 2015; Schütt, 2005; Zekarias et al., 2021). Rapid population growth, social instability, land policy, unproductive land and climate change were identified as the key driving forces of LULC changes in the area (Hassen et al., 2021a; WoldeYohannes et al., 2018). Inappropriate land use practices played a significant role in triggering land degradation (IPCC, 2022). To minimize these adverse consequences of land use change, it is recommended that adequate land use planning and management strategies must be implemented.

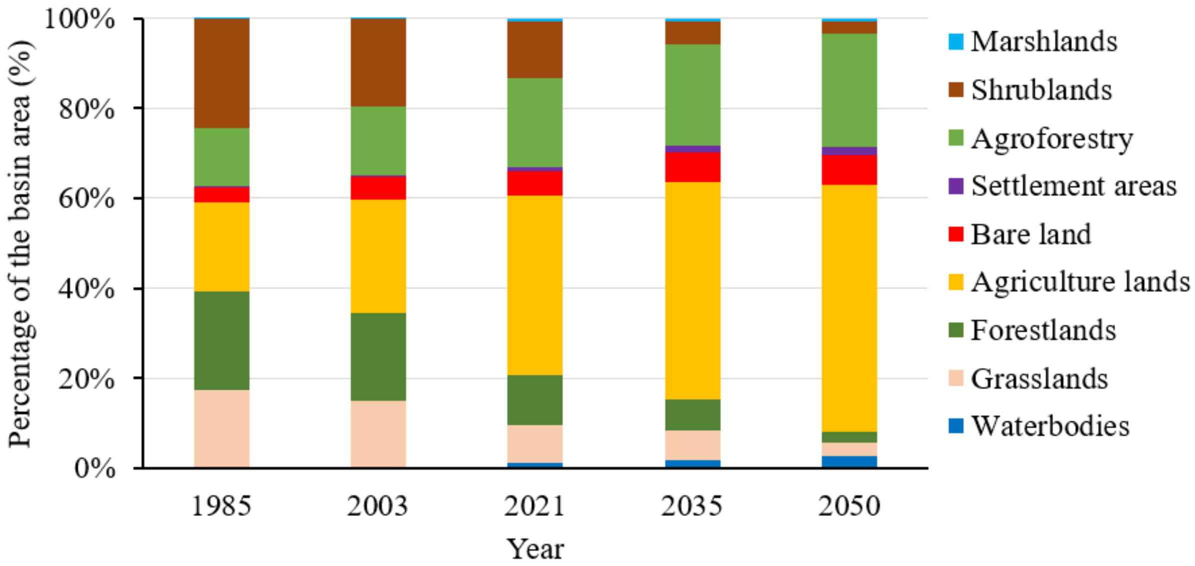

Figure 25. The relative proportion of each land use.

The existing diverse range of LULC types reflects the complex nature of the landscape and its susceptibility to change. The results revealed significant shifts in land cover over the past several years (1985–2021). The "from–to" analysis in Table 5 showed a substantial conversion of natural landscapes into cultivable areas and settlements. By 2035 and 2050, it is expected that agricultural lands, agroforestry and bare land will continue to expand at the expense of forest, shrub and grasslands (Table 11). These projections are indicative of ongoing land use changes that could have far-reaching environmental and socio-economic consequences (Mekuria et al., 2021). The increase in human population often leads to higher demands for land, particularly for agriculture and settlements (WoldeYohannes et al., 2018). Effective land-use planning and management are critical for achieving sustainable and resilient landscapes.

4.3.4. Sensitivity analysis, calibration and validation

A total of fifteen parameters listed in Table 23 with very high to high sensitivity were selected. The sensitivity result showed the SCS runoff curve number (CN2) as a major key parameter with highest t-stat and lowest p-value (Table 24), while USLE_C and USLE_P are the two most important parameters for sediment calibration (Figure A4). The graphical representation in Figure 26 and Figure 27 showed that the magnitude and temporal variation of simulated and measured streamflow and sediment yield matched closely. As shown in Table 24, the R^2 values ($R^2 > 0.74$) were satisfactory, as indicated by the goodness-of-fit between the measured and simulated dataset. The NSE values indicated good model performance for stream flow and sediment yield simulation at both stations. The PBIAS showed slight underestimation at Aposto (streamflow) and overestimation at Bedessa. However, all the PBIAS values are less than ±15%

indicating a good simulation (Moriasi et al., 2015). Hence, all the statistical indices are in the acceptable range.

Table 23. Selected parameters, allowable range and fitted values for SWAT calibration

Parameters	Description	Sensitivity			Allowable	Fitted
		t-Stat	*p*-Value	Rank	Range	Value
Streamflow						
CN2	SCS runoff curve number	−21	0	1	-0.2–0.2	0.15
ALPHA_BF	Baseflow alpha factor	−9.6	0	2	0–1	0.3
SOL_BD	Moist bulk density	−7.4	0	3	0.9–2.5	1.01
GW_DELAY	Groundwater delay	4.5	0.04	4	0–500	272
CH_K2	Effective hydraulic conductivity	3.8	0.1	5	−0.01–500	67
SOL_K	Saturated hydraulic conductivity	−3.7	0.16	6	0–2000	32
SOL_AWC	Available water capacity of the soil layer	1.6	0.34	7	0–1	0.6
Sediment						
USLE_P	USLE support practice factor	−8.4	0	1	0–1	0.57
USLE_C	USLE cover factor	−5.8	0	2	0.001–0.5	0.05
CH_COV1	Channel erodibility factor	1.6	0.11	3	−0.05–0.6	0.03
SPCON	Linear factor for the channel sediment routing	1.3	0.25	4	0.0001–0.01	0.01
CH_EQN	Sediment routing method	1.2	0.27	5	0–4	3.0
SPEXP	Exponential factor for channel sediment routing	−0,68	0.49	6	1–2	1.2
CH_COV2	Channel cover factor	−0.64	0.51	7	−0.001–1	0.75
HRU_SLP	Average slope steepness	0.59	0.55	8	0–1	0.17

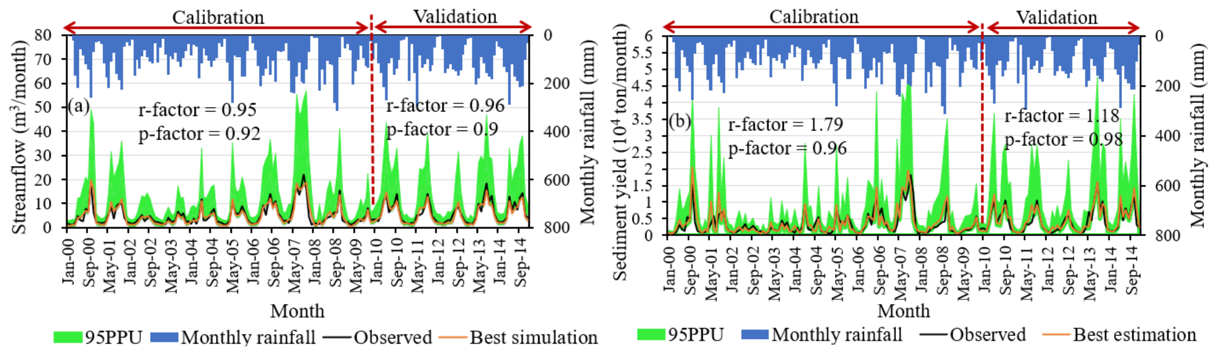

Figure 26. Monthly streamflow (a) and sediment yield (b) hydrograph during calibration and validation period at Aposto gauging station.

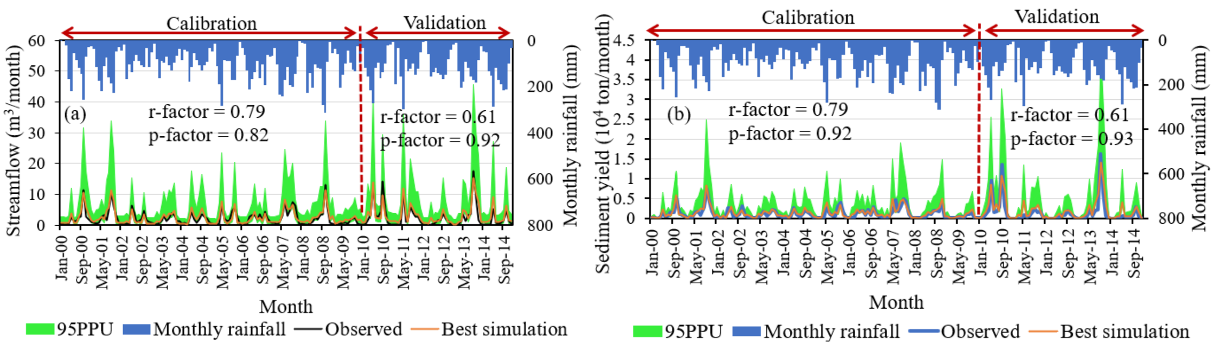

Figure 27. Monthly streamflow (a) and sediment yield (b) hydrograph during calibration and validation period at Bedessa gauging station.

Table 24. Statistical indices for the SWAT model performance measure

Model simulation	Period	Aposto			Bedessa		
		R^2	NSE	PBIAS (%)	R^2	NSE	PBIAS (%)
Streamflow	Calibration	0.89	0.80	−1.5	0.79	0.76	8.9
	Validation	0.81	0.75	−3.9	0.84	0.8	11.1
Sediment yield	Calibration	0.74	0.67	4.9	0.76	0.72	8.1
	Validation	0.8	0.76	3.6	0.84	0.77	13.8

4.3.5. Estimation of surface runoff and sediment yield

Impacts of land use change on surface runoff and sediment yield

The simulations that were driven from LULC change in the past indicated that the mean annual surface runoff increased by 15.3 mm (4.5%) and 23.4 mm (6.8%) during S2 and S3, respectively, compared to S1 (base period for past). Similarly, the sediment yield increased by 7.1 t/ha/year (28.8%) and 11.4 t/ha/year (46.2%) during S2 and S3, respectively. Despite lower precipitation, surface runoff and sediment yield were increased in the past. This could be attributed to the changes in LULC particularly the expansion of agricultural land at a rate of 3.23% per year at the expense of natural vegetation (deforestation at a rate of 2.4% per year) between 1985 and 2021 (Girma et al., 2022a). Moreover, significant changes were observed in settlement areas ranged between 1.5 and 9.5%.

Simulations driven by future modeled LULC and observed climate data (S7 and S8) showed an increase in surface runoff by 64.7 mm (17.8%) and 114.4 mm (31.5%), respectively, compared to S6 (baseline for future simulations). Likewise, the annual sediment yield increased by 5.1 t/ha/year (14.4%) and 8 t/ha/year (22.8%) during S7 and S8 compared to S6. Consequently, the predicted LULC change will lead to an increased surface runoff and sediment yield assuming a similar climate development as observed in S6. This could be due to the unceasing expansion of, for example, agriculture land (48.3%, 55%) and settlements (1.4%, 2%) by 2035 and 2050, respectively (Figure 25). The findings revealed that land-use changes alone have a more positive synergy on surface runoff and sediment yield. The results were consistent with those in the previous studies (Adi et al., 2023; Aragaw et al., 2022). The degradation of soil and vegetation may increase the area of impervious surface, leave the soil exposed to the erosive forces of water and leading to more water reaching the ground, lowers the infiltration capacity of the soil and increases the surface runoff (Nyatuame et al., 2020; Tan et al., 2022). Additionally, land-use changes can modify natural drainage patterns, leading to the concentration of runoff into specific areas. This might result in localized flooding and erosion (Sugianto et al., 2022).

Impacts of climate change on surface runoff and sediment yield

Simulation obtained from climate change in the past (S4) depicted a decline in surface runoff by 3.9 mm (1.1%) and sediment yield by 0.9 t/ha/year (3.7%), as compared to S1. The near-term (S9) and mid-term (S10) simulations driven by future climate data (RCP4.5) and observed LULC (2021) decreased the surface runoff by 17.7 mm (4.9%) and 20.2 mm (5.6%), respectively, compared to S6. Likewise, the sediment yield will be reduced by 2.9 t/ha/year (8.3%) and 3.1 t/ha/year (8.9%) during the S9 and S10, respectively. Under RCP8.5, the surface runoff will decrease by 64.9 mm (17.9%) in the near-term (S11) and increase by 6.7 mm (1.9%) during the mid-term (S12), compared to S6. Correspondingly, the sediment yield will decrease by 4.6 t/ha/year (13%) in the S11 and increase by 1.7 t/ha/year (4.9%) in the S12. These results might be attributed to the dynamic trends in climate variables (decrease in precipitation and increase in temperature), as described in Table 22. The findings were consistent with the results of other studies in the ERVLB (Aragaw et al., 2022; Gadissa et al., 2018).

The impacts of climate change on surface runoff and sediment yield are interconnected. For example, Mana and Abebe (2023) revealed the reduction in stream flow in the future due to the decrease in precipitation and an increase in evapotranspiration (associated with an increase in temperature). It has also been shown that there is a significant relationship between streamflow and sediment yield (Adi et al., 2023; Gadissa et al., 2018). Thus, the result implies that the reduction in sediment yield (S9, S10 and S11) in the future period might also be associated with the reduction in streamflow, which is, in turn, linked with climate changes.

Combined impacts of land use and climate change on surface runoff and sediment yield

Under the combined effect of land use and climate change, there is high variation in annual surface runoff and sediment yield as compared to the individual effect. The result obtained from past simulation (S5 and S6) indicated that the annual runoff increased by 13.9 mm (4%) and 20.1 mm (5.9%), respectively, as compared to S1. Under these same scenarios, the sediment yield increased by 6 t/ha/year (24.2%) and 10.5 t/ha/year (42.7%), respectively, for S5 and S6. Urbanization and deforestation associated with land use change reduce the ability of land to absorb water, leading to increased surface runoff (Nyatuame et al., 2020; Tan et al., 2022). Climate change can intensify this effect by causing more frequent and intense rainfall events, resulting in even higher rates of sediment yield (Li and Fang, 2016).

Despite increased impervious surface through increased settlement areas and bare land, most of the combined future scenarios indicated a decrease in surface runoff and sediment yield as compared to base period (S6). Under RCP4.5, for example, the S13 (near-term) and S14 (mid-term) scenario showed a decrease in surface runoff by 10.3 mm (2.9%) and 13.6 mm (3.7%). Likewise, the sediment yield decreased by 2.4 t/ha/year (6.9%) and 2.6 t/ha/year (7.4%), respectively, in the S13 and S14. Under RCP8.5, S15 (near-term) showed a decrease in surface runoff and sediment yield by 41.5 mm (11.4%) and 3.1 t/ha/year (8.8%), respectively. Similarly, S17, S18 and S19 indicated a decrease in surface runoff and sediment yield. Thus, the percentage decrease in surface runoff ranged from 1.6% (S17) to 10.2% (S19). Similarly, the percentage decrease in sediment yield ranged from 1.1% (S18) to 5.4% (S19). This could be due to the offset of runoff and sediment reduction by climate change (i.e., lower precipitation and higher temperature projections) in the coupled climate and land-use change scenario.

However, S16 and S20 showed an increase in surface runoff by 13.2 mm (3.6%) and 19.8 mm (5.5%), sediment yield by 2.5 t/ha/year (7.2%) and 3.96 mm (11.3%) into the future, respectively. This might be attributed to the expected increasing trends in the annual rainfall (7.8 mm/year) under the RCP8.5 scenario (Table 22). It is clearly evident that a little rise in annual precipitation is resulting in a higher surface flow. This indicates that climate change has greater contribution on hydrological process compared to land use. These findings were supported by previous studies on hydrological processes and sediment yield (Aragaw et al., 2022; Giri et al., 2019).

4.3.6. Identification of soil erosion hotspots

The identification of erosion hotspot areas is crucial for effective land and water resource management, as well as for developing targeted erosion control and mitigation strategies. Hence, the average annual sediment yield of GW was classified into five sediment severity classes (Table 25). The classes were adapted from Dananto et al., (2022); Guduru and Jilo (2023). Table 25 indicated that most (>77%) of the study area experienced high to severe sediment yield in a given scenario. The past analysis depicted that a mean annual sediment yield of 42.9 t/ha/year and 45.6 t/ha/year was accounted for in S1 and S5, respectively. Moreover, Figure 28 showed the spatial variability of mean annual sediment yield at sub-basin scale under the different scenarios. The highest amount of sediment yield was showed in the southern as well as in eastern part of the watershed (Figure 28, S1 and S5), characterized by widespread steep slopes and more often, the southern part received high amount of rainfall (Guduru and Jilo, 2023). On the contrary, most of the sub-basins in the western and northern part experienced low to high sediment yield. The results are consistent with Adi et al. (2023); Dananto et al. (2022); Guduru and Jilo (2023).

Table 25. The percentage of erosion severity areas (Area %) in the past and future scenarios

Severity Class	Description	Past		Near Future		Mid Future	
		S1	S5	S13	S15	S18	S20
0–5	Low	4.9	4.9	0.7	0.7	0.7	0.6
5–10	Moderate	18.6	13.6	0.9	0.9	4.1	0.1
10–25	High	38.8	33.7	26.9	32.8	51.5	10.5
25–50	Very high	32.7	40.1	51.3	52	26.2	60.8
>50	Severe	5	7.7	20.2	13.6	17.5	28

Furthermore, the spatial variability of sediment yield was identified for future combined scenarios. The combined scenario analysis depicted the insignificant intra-variability within each RCP scenario. Hence, we used a combination of one future period (2021–2040, 2041–2060) correspondingly for each projected land use (LULC 2035, LULC 2050) under each RCP (2 LULC×2 pathways×1 climate = 4). In this line, S13 and S15 as well as S18 and S20 were considered for near and mid future scenario, respectively. Thus, the near future average annual sediment yield varied between 28.25 t/ha/year and 29.57 t/ha/year (S13 and S15, respectively), while the mid future average annual sediment yield ranged from 30.71 t/ha/year to 43.5 t/ha/year (S18 and S20, respectively). Among the 35 sub-basins (Figure 28), sub-basins 6, 19, 25, 27, 29, 30, 33, 34 and 35 will generate the highest amount of surface runoff and sediment yield in to the future (S13, S15, S18 and S20); thus, they were categorized under critical sub-basins.

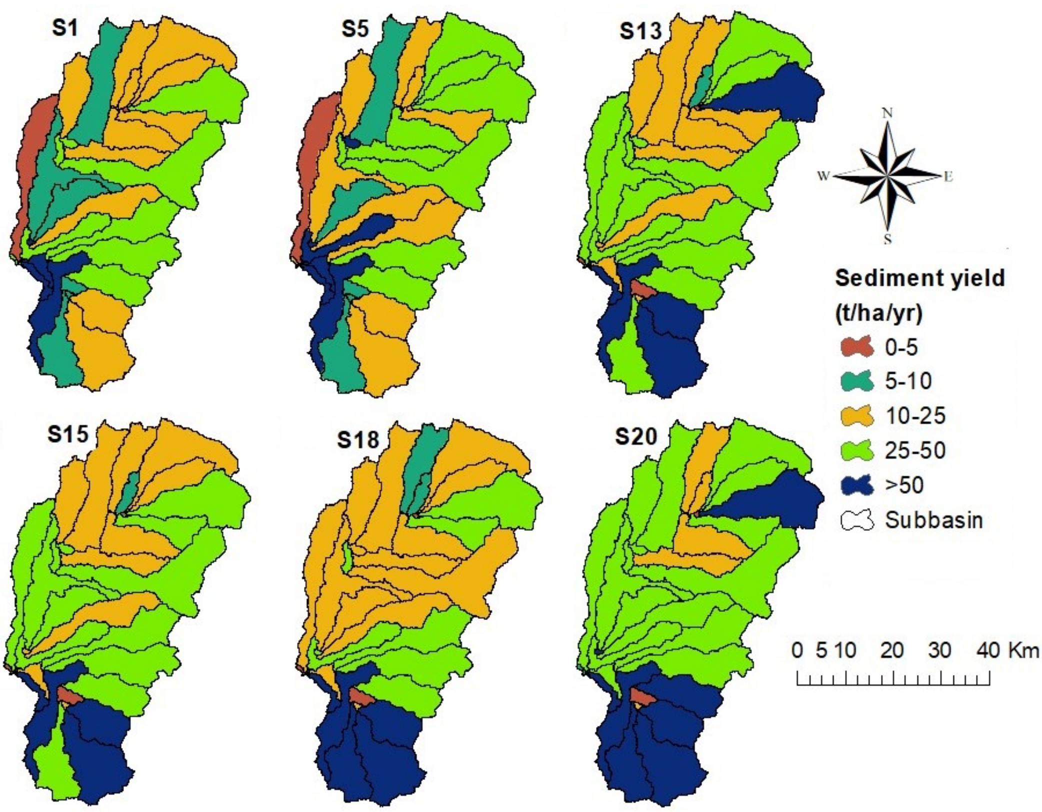

Figure 28. The spatial pattern of sediment yield at the given scenario.

Most of the critical sub-basins (28% of the total area) were characterized by shallow (Leptosols) and clay dominant soils (Vertisols), dominated by agriculture and grasslands, and very steep slopes. Moreover, the southern part of the GW will receive high amount of rainfall under both RCPs (Figure A2 and Figure A3). Regardless of differences in rainfall, surface runoff and soil erosion were much higher on croplands and grazing lands (Ebabu et al., 2023). This is largely due to excessive tillage operations and intense grazing by livestock which lead to increased soil disruption and vulnerability to erosion. Moreover, high values of surface runoff were correlated with Vertisols owing to slow internal drainage and low infiltration capacity after getting wet (Garg et al., 2022; Tibebe and Bewket, 2011). On the contrary, sub-basins 4, 7, 8, 28 and 31, which represented 4.7% of the total area, were under low sediment severity class. These sub-basins were dominated by shrublands and forestlands with a slope ranged between 3 and 12%.

4.3.7. LDN indicators

Land productivity dynamics

From 1985 to 2003, most (83.2%) of the study area was characterized under stable productivity class and smaller (1.6%) proportion of the study area showed improvements in productivity (Table A2). The LP trend showed early signs of decline in 13.2% of the area. Another 1.4% of the study area showed decline land productivity and insignificant proportion (0.01%) of the study area characterized as stressed. Based on the LP trend analysis applied between 2003 and 2021, 67% of the study area was marked as stable (Table A2). Furthermore, 18.4% and 14.1% of the study area were under early signs of decline and decline, respectively. Similar to the previous years, an insignificant proportion (0.03%) of the study area was characterized as stressed between 2003 and 2021.

The stress or pressure on land productivity varied with land use and land cover (Figure 29). For example, out of the total stressed area, 48% were found in croplands. Similarly, the largest share of early signs of decline (68%) and decline (71%) categories were contributed from croplands between 1985 and 2003. Furthermore, the share of the area with early signs of decline (52%) and decline (53.8%) were higher in croplands from 2003 to 2021 (Figure 29), while around 57% of the stressed category were found in artificial areas between 2003 to 2021. Overall, croplands accounted for 68.4% and 53% of the LP declined area in 1985–2003 and 2003–2021, respectively. These areas are characterized by lower tree cover, unsustainable land management practices, accelerated carbon decomposition and erosion (Zomer et al., 2016; Lorenz and Lal, 2018, Ebabu et al., 2023).

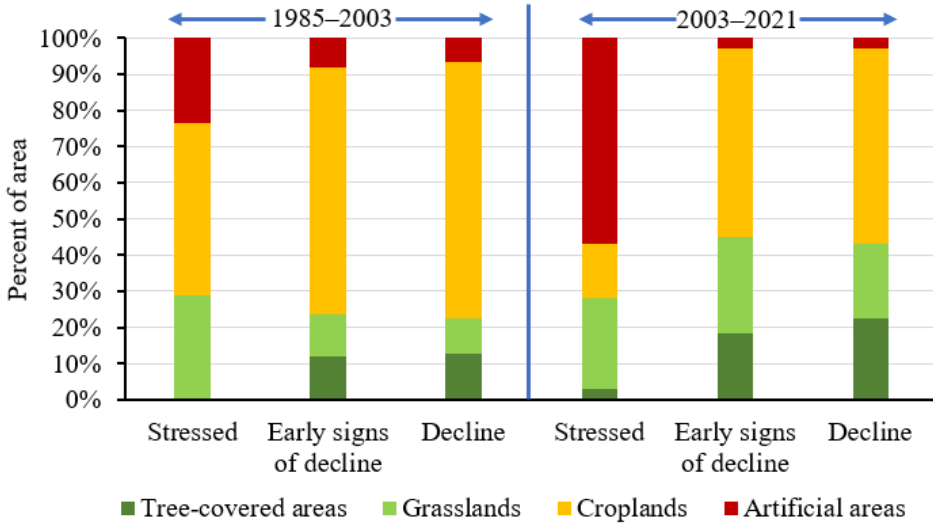

Figure 29. The distribution of LP sub-indicator across the different land use and land cover types.

From 1985–2003 to 2003–2021, the area where LP was improved and stable were reduced while the land area degraded were increased (Figure 30a,d, respectively). In line with this, Degefa (2007); Hassen et al. (2021b); Regassa Debelo et al. (2017) indicated that trend in agricultural productivity has declined over the last decades given that climate change, soil erosion, and poor soil and water conservation (SWC) practices were mentioned as the main drivers. This, in turn, resulted in increased demand for farm inputs (e.g., fertilizer, pesticides) and increased production costs. As a result of the expansion of land degradation over time, agricultural productivity has decreased and worsened food insecurity and poverty in the GW (Wolde et al., 2021).

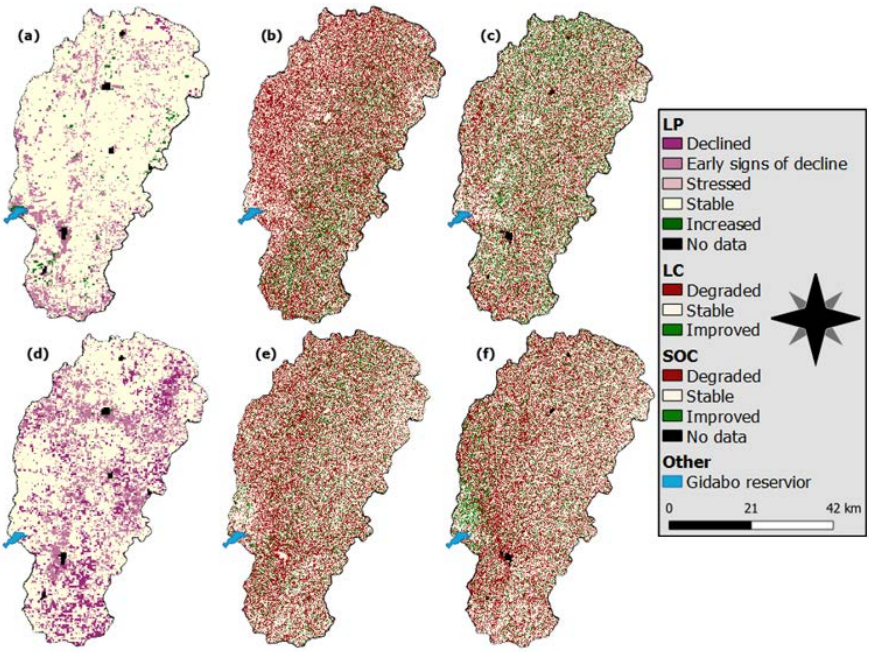

Figure 30. Land degradation sub-indicators LP (a,d), LC (b,e), SOC (c,f) between 1985–2003 and 2003–2021, respectively.

Land cover degradation

The outputs for the land cover sub-indicator revealed that land area with stable land cover were dominant (52% and 47%) in both periods (1985–2003 and 2003–2021, respectively). Additionally, the degraded land cover was increased from 36% during the 1985–2003 to 42% during the 2003–2021 (Figure 30b,e). However, land area with improved land cover was slightly reduced from 12% during the 1985–2003 to 11% during the 2003–2021 (Table A2). The long-term LULC dynamics indicated that GW experienced significant landscape alteration between 1985 and 2021 (Table 4). Croplands covering 20% of the study area (in 1985) experienced the highest relative expansion by 25% and 40% (in 2003 and 2021, respectively). Similarly, the spatial extent of agroforestry was increased from 13% to 15% and 20% over the study years. The other major rate of change was recorded in the residential areas from 1.5% to 9.5% between 1985–2003 and 2003–2021, respectively. This reflects the intensification of agricultural practice and urbanization activity in the GW. Furthermore, the expansion of agroforestry was mainly attributed to cultural values and traditional beliefs in the study area (Hassen et al., 2021a). Studies identified that human and livestock population in regions of limited resources, unsustainable farming techniques, an insecure land tenure system, poverty and climate change as major drivers of LULC and land degradation (Desta and Fetene, 2020; Mekuria et al., 2021; Mesfin et al., 2020; Meshesha et al., 2012).

Soil organic carbon loss

Figure 30c,f showed the spatial distribution of SOC over the two periods (1985–2003 and 2003–2021, respectively). The results indicated that 13% and 12% of the study area showed improvement in SOC, 53% and 49% of the GW displayed stable condition during 1985–2003 and 2003–2021, respectively (Table A2). In addition, it appeared that the percentage of degraded areas were increased from 35% in 1985–2003 to 39% in 2003–2021. This could be attributed to the significant conversion of forestlands (–1.16%, –4.23%), grasslands (–1.31%, –3.26%) and shrublands (–2.41%, –3.59%) to other land uses, mainly croplands (Table 5) and extractive nature of the farming practice. In line with this, Negasa (2020) and Okolo et al. (2019) indicated that conversion of native forest to other land uses and the intensification of agricultural activities resulted in a significant decrease in the SOC stocks across Ethiopia.

Land degraded status

Combining all the three sub-indicators, 45% and 56% of the study area were under degraded status, 41% and 31% unchanged, 14% and 12% improved over the periods between 1985–2003 and 2003–2021, respectively (Table 26). From 1985–2003 to 2003–2021, the proportion of degraded land was increased by 26%, while stable and improved land areas were reduced by 25% and 9%, respectively. The expansion of degraded area might be attributed to the dynamic interplay of climate and LULC change. The high-risk degraded land was mainly located in areas dominated by croplands and bare land (Figure 31).

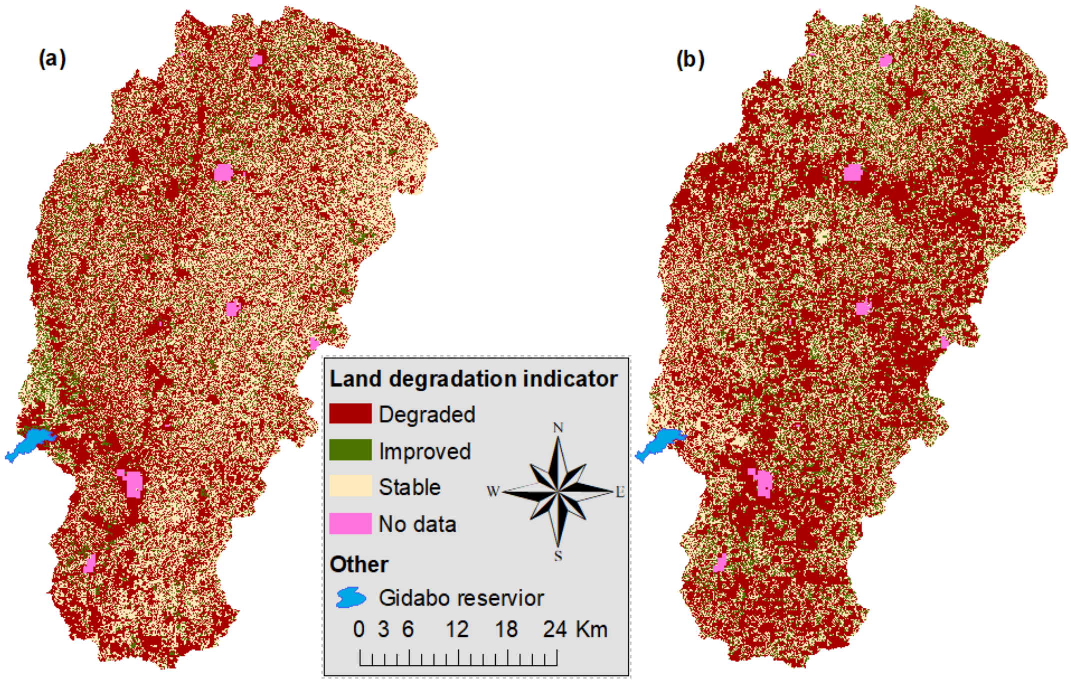

Figure 31. Land degradation neutrality indicator map between 1985–2003 (a) to 2003–2021 (b) in the Gidabo watershed.

Table 26. The extent of degraded, stable, and improved land according to the SDG 15.3.1 indicator

Land Degradation Status	1985–2003 (% of Land)	2003–2021 (% of Land)
Stable	40.9	30.9
Improved	13.7	12.3
Degraded	44.6	56
No data	0.8	0.8

4.3.8. Sediment yields under soil conservation scenarios

The average annual sediment yield reduction (% reduction) with respect to the soil conservation practices was presented in Table 27. The result revealed that soil/stone bund generated the lowest value of sediment yield (5.7–10.3 t/ha/year), then terracing (6.4–12.7 t/ha/year) and contour farming (7–12.6 t/ha/year), followed by reforestation (9.1–16.1 t/ha/year) and filter strip of 1 m (16.8–29.1 t/ha/year). Furthermore, Figure 32 shows the distribution of average sediment yield (t/ha/year) in critical sub-basins under the proposed conservation scenario. At the implementation of terracing, for example, there are no areas within the severe sediment yield category. Accordingly, 64.8% and 59.4% (Low), 21.6% and 27% (moderate), 13.6% (high to very high) were classified during S13 and S15, respectively. Likewise, 36.4% and 29.2% of the study area were accounted for low severity class during S18 and S20, respectively, while 51.9% and 47.2% were identified as moderate class. The remaining (11.7% and 23,6%) were grouped under high to very high class during S18 and S20, respectively. The results attained are comparable with the findings of previous studies in GW (Adi et al., 2023; Dananto et al., 2022). Similarly, Admas et al. (2022); Gashaw et al. (2020); Lemma et al (2019); Leta et al. (2023) quantified the significant contribution of the aforementioned conservation scenarios in different part of the country.

Table 27. Mean annual sediment reduction in soil conservation scenarios over the entire GW

Conservation Scenarios	Sediment Yield (% Reduction) *			
	S13	S15	S18	S20
Terracing	77.2	63.1	78.9	70.8
Contour farming	72	58.4	77.1	71
Filter strip	38.7	38.4	45.2	33.1
Stone/soil bund	79.8	67.9	81.1	76.2
Reforestation	67.9	55.7	70.4	63

* Compared to the corresponding “without SWC” scenario

While these conservation practices had varying levels of effectiveness, the analysis justified that soil conservation practices used in each scenario could significantly reduce the annual sediment yield and will help to achieve the LDN in the future. In line with this, Hassen et al. (2021c) revealed the positive correlation between soil conservation practice, agroecology and soil physicochemical properties in the GW. Particularly, the traditional agroforestry system and plantation work has a significant contribution to soil fertility improvement and local communities’ livelihood (Hassen et al., 2021b; Temesgen et al., 2018). Apparently, the integration of the proposed conservation scenarios with the traditional practice might reduce the soil erosion and also improve the LDN indicators, thereby reducing related degradations.

4.3.9. Enhancing land degradation assessment

Soil erosion, as a key driver of land degradation, directly impacts soil quality and land productivity. Soil erosion assessment provides insights into erosion extent, severity and vulnerability of areas that may not be fully captured by the LDN sub-indicators alone. Moreover, soil erosion indicators such as runoff and sediment yield can help to evaluate the success of land restoration activities, providing valuable feedback on the effectiveness of LDN interventions, and ultimately supports land management and conservation efforts. Therefore, the integration of soil erosion indicator into LDN assessments can complement the existing sub-indicators, allows for more comprehensive understanding of land degradation dynamics and watershed management measures.

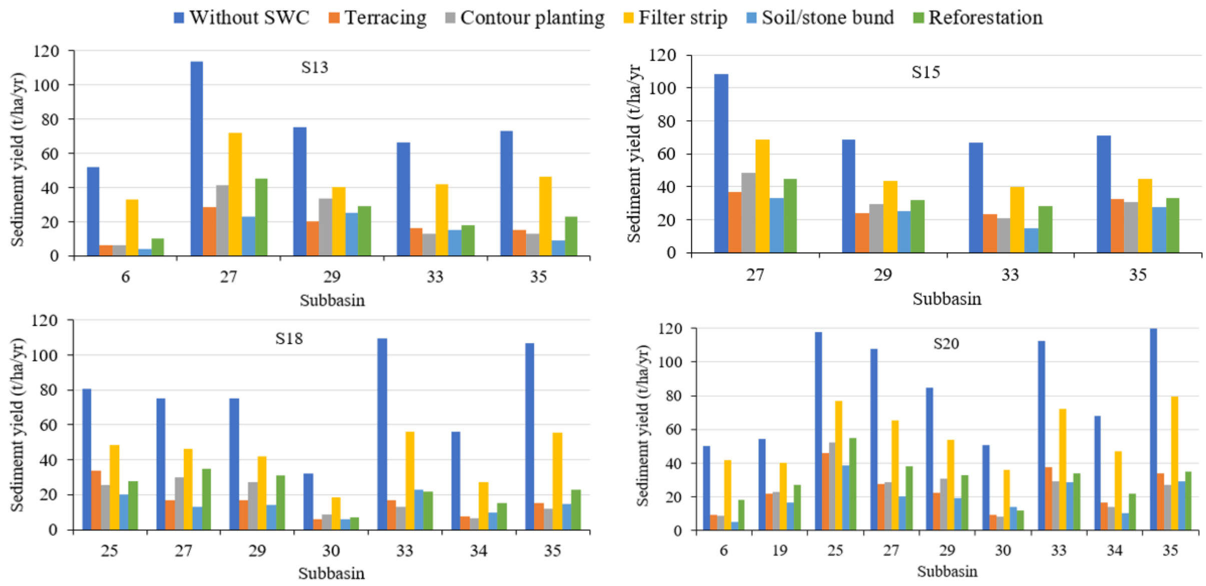

Figure 32. Comparison of the conservation practices in critical sub-basins under a given scenario.

4.4. Conclusion

The study employed an integrated approach combining the SWAT model and the Trends.Earth. The GW faces substantial landscape alteration and climatic variability, and significant challenges related to soil erosion and land degradation. Historical changes in LULC led to an increase in mean annual surface runoff and sediment yield despite lower precipitation. This increase is attributed to the expansion of agricultural land and deforestation, which reduced the land's ability to absorb water and increased surface runoff. Future projection showed further increases in surface runoff and sediment yield due to the ongoing expansion of agriculture and settlements. Past simulations as well as future climate change scenarios under the RCP4.5 showed a decline in surface runoff and sediment yield, while under RCP8.5, results showed decreases in the near-term (2021–2040) and increases in the mid-term (2041–2060) in surface runoff and sediment yield. The interplay between land use and climate change led to varied outcomes, with some scenarios (e.g., S5 and S6) showed increases in surface runoff and sediment yield, indicating a synergy between land use change and climate change, while certain future scenarios (e.g., S13, S14, S15) showed decreases in surface runoff and sediment yield. The findings revealed that significant portion of the study area, particularly the southern and eastern parts of the watershed, exhibited high to severe soil erosion rates. The LP dynamics indicated that the proportion of land categorized as stable were decreased, while areas displayed early signs of decline and decline were increased from 1985–2003 to 2003–2021. Concurrently, land-cover degradation and SOC loss was also increased. Overall, the proportion of degraded land expanded significantly emphasizing the need for sustainable land management practices to mitigate further degradation. The study evaluated various soil conservation practices in the context of sediment yield reduction, with soil/stone bund emerging as the most effective measure, followed by terracing, contour farming and reforestation. These practices exhibited the potential to significantly reduce annual sediment yield and are crucial for achieving LDN goals.

5. Synthesis

5.1. Overview

Soil erosion and vegetation degradation are interrelated environmental issues that have significant implications for ecosystems, agriculture, and human well-being in Ethiopia (Wassie, 2020). The GW features diverse biophysical characteristics and provides essential resources for industrial and domestic use (Wolde et al., 2020). However, the watershed faces significant challenges related to soil erosion and land degradation attributed to substantial landscape alteration, climatic variability and drastic ecological change (Belihu et al., 2020; Mana et al., 2023; Worako et al., 2022). Modeling the long-term impact of LULC and climate change on soil erosion, and evaluating land degradation dynamics is essential to understand the past and future state of the landscapes (Kidane et al., 2019). Ultimately, this provides insights into vulnerable areas, the effectiveness of different management practices to make management decisions to protect GW and ensure the long-term sustainability. Therefore, this study makes a contribution to understanding and addressing soil erosion and land degradation challenges towards sustainable land management in the GW.

The overall aim of this study is to investigate the dynamic patterns of land degradation indicators in the context of climate and land use changes, and suggests potential management alternatives to address these critical environmental challenges. To achieve these goals, a multidisciplinary approach was employed, integrating hydrological modeling, remote sensing, and geospatial analysis. As described, chapter 2 to 4 endeavored to address the specific objectives related to LULC studies, performance assessment of climate models, and land degradation trajectories in the GW. The aim of this final chapter is to synthesize the findings and provide a cohesive understanding of the research outcomes from various perspectives. Moreover, it provides insights for future investigation and exploration, thus providing a comprehensive closure to the study and guiding further research endeavors.

5.2. Brief answer to the research questions

This section provides synthesis of the previous chapters, presenting a cohesive overview that aligns with the core essence of the six research questions.

I. *What are the major LULC classes in the study area, and how evolved from 1985 to present and the future to 2050?*

The major LULC classes identified in the study area were waterbodies, grasslands, forestlands, agriculture lands, barren/bare land, settlement areas, agroforestry, shrublands, and marshy area. The study area underwent significant changes in LULC from 1985 to 2021, with notable trends and impacts on the landscape. In 1985, the dominant land cover type was shrub land (24.3%), followed by forest (21.8%) and agriculture (19.8%). However, over the years, there was a significant expansion of agricultural land, which surpassed other land cover types, reaching 40% by 2021. This expansion came at the expense of forest cover, which decreased from 21.8% in 1985 to 11.2% in 2021. Similar trends were observed in agroforestry, which increased from 13% to 20% over the study period, while grassland and shrub land experienced significant declines.

The transition matrix between 1985–2003 and 2003–2021 revealed continuous deforestation, with an annual deforestation rate of 2.4%. This deforestation was driven by the expansion of agricultural land, which increased at a rate of 3.23% per year. Additionally, there was a notable increase in the settlement areas from 1.5% in 1985 to 9.5% in 2021, indicating urban expansion. Similar trends of land cover change were observed in previous studies in the region (Aragaw et al., 2022; Belihu et al., 2020; Wolde et al., 2021), emphasizing the ongoing transformation of land use driven by factors like population growth, agricultural practices, and policy shifts.

Looking into the future, the study projected LULC changes for 2035 and 2050 under a BAU scenario. The results forecasted further expansion of agriculture, agroforestry, waterbodies, and settlement areas, while grasslands, forestlands, and shrublands were expected to decrease significantly. Marshy areas and barren land were projected to show positive growth until 2035 and then decrease by 2050. These predictions are in line with the observed historical trends and indicate a continuation of current practices, with agriculture playing a dominant role in shaping the landscape.

II. *What are the observed trends in climate variables and how different regional climate models (RCMs) perform in simulating these variables?*

Rainfall, a critical factor for rainfed agriculture-dependent economy, displays distinct variations temporal patterns. The results indicated a significant decreasing trend in annual and Kiremt season rainfall, while Belg rainfall showed non-significant decreasing trends. This declining trend in the primary rainy season has substantial implications for agricultural productivity and water resources. In contrast, temperature trends indicated warming in the watershed. Both annual and Belg season maximum temperatures showed significant increasing trends, with the annual maximum temperature exhibiting a particularly pronounced rise. Minimum temperature, on the other hand, experienced non-significant decreases annually but exhibited significant increases during the Belg and Kiremt seasons. The warming trend observed in temperatures revealed the influence of climate change in the study area.

The findings revealed that the performance of RCMs in simulating rainfall and temperature varies widely across different models. RACMO22T (EC-EARTH) perform well in representing observed annual rainfall patterns, particularly in the upper and central part of the GW. However, other models like CCLM4-8 (EC-EARTH) and RCA4 (EC-EARTH) overestimate annual rainfall, while REMO2009 (MPI) underestimates it, especially in the middle and lower part. The mean ensemble approach generally reproduces observed annual rainfall patterns more accurately than individual RCMs.

Regarding mean annual rainfall cycle, some models capture the timing of peak rainfall in April/May and September/October, such as CCLM4-8 (CNRM), CCLM4-8 (MPI), RACMO22T (EC-EARTH), and RCA4 (CNRM), despite variations in the rainfall amounts they reproduce. However, CCLM4-8 (EC-EARTH) shifted the peak period by up to two months. In terms of the seasonal rainfall patterns, it is observed that most RCMs tend to underestimate the Belg season rainfall, with notable exceptions like CCLM4-8 (MPI) and REMO2009 (MPI), which perform better in replicating the Belg season rainfall. Similarly, for the Kiremt season, RCMs exhibit varied performance, with some overestimating and others underestimating rainfall. RACMO22T (EC-EARTH) is identified as performing well in simulating Kiremt seasonal rainfall.

In terms of temperature simulations, most RCMs overestimate minimum temperature and underestimate maximum temperature at station level. CRCM5 (MPI) showed relatively better performance in replicating the observed minimum temperature patterns, while RCA4 (EC-EARTH) performs poorly. In terms of maximum temperature, CRCM5 (MPI) and mean ensemble show better performance. The correlation between observed and simulated temperature varies by station, but CRCM5 (MPI) consistently exhibits strong performance for minimum temperature, and most RCMs achieve good correlations for maximum temperature.

Taylor diagram and Skill Score (TSS) provides a comprehensive view of the RCMs' performance by considering multiple statistical metrics. In terms of rainfall, CCLM4-8 (MPI) and REMO2009 (MPI) models showed low variability compared to observations, while RCA4 (EC-EARTH) and HIRHAM5 (EC-EARTH) exhibited higher variability. CCLM4-8 (MPI) had the highest correlation with observations, while RCA4 (MPI) showed the weakest correlation and high CRMSE, indicating weaker performance. For temperature, RACMO22T (EC-EARTH) and CRCM5 (MPI) demonstrated strong correlations and low CRMSE, indicating good performance in capturing temperature trends. In contrast, CCLM4-8 (EC-EARTH) and CCLM4-8 (MPI) had inverse correlations and high CRMSE, indicating weaker performance.

III. How climate change and land use dynamics influence surface runoff and sediment yield?

In the past, simulations showed that mean annual surface runoff increased by 4.5% (S2) and 6.8% (S3) compared to the base period (1985), along with a corresponding increase in sediment yield (28.8% and 46.2%, respectively). These changes were largely attributed to shifts in land use, including the expansion of agricultural land and deforestation. Moreover, future simulations (S7 and S8) predicted even greater increases in surface runoff and sediment yield due to continued land use changes, particularly in agriculture and settlements. These findings indicated that land-use changes can significantly impact surface runoff and sediment yield. Simulations driven by past climate data (S4) showed a decline in surface runoff and sediment yield, However, future climate projections indicated varied effects, with some scenarios (S9–S11) showing a decrease in surface runoff and sediment yield, while others demonstrated an increase (S12). These variations were attributed to the dynamic trends in precipitation and temperature.

Furthermore, the results revealed that the joint impact of these factors led to high variations in annual surface runoff and sediment yield compared to their individual effects. The results obtained from past simulation (S5 and S6) indicated that both annual runoff and sediment yield were increased. In some scenarios, the combined influence of projected land use changes and climate change resulted in a decrease in surface runoff and sediment yield, particularly under the RCP4.5 scenario. However, other scenarios showed an increase in surface runoff and sediment yield, primarily due to expected increases in annual rainfall under the RCP4.5 scenario. These findings emphasized the complex relationship between land use, climate change, and their combined impact on hydrological processes and sediment yield.

IV. Where are critical sub-basins in terms of sediment yield and what are the common characteristics of these critical sub-basins?

The identification of erosion hotspots is crucial for effective land and water resource management and for developing targeted strategies to control and mitigate erosion. In this study, the average annual sediment yield was categorized into five sediment severity classes, revealing that more than 77% of the study area faced high to severe sediment yield under different scenarios. Additionally, the study identified critical sub-basins (6, 19, 25, 27, 29, 30, 33, 34 and 35) that generate the highest surface runoff and sediment yield. Most of these critical sub-basins were primarily characterized by shallow and clay-dominant soils, intensive agricultural and grassland use, receive high rainfall, and steep and long slopes. Conversely, sub-basins with shrublands, forestlands and gentle slopes exhibited lower sediment severity.

V. *What are the trends in land degradation neutrality indicators in the study area from 1985 to 2021?*

In the context of land productivity dynamics, between 1985 and 2003, the majority (83%) of the study area exhibited stable land productivity, while a small portion showed improvements. However, there were early signs of decline in 13.2% of the area, and a minor proportion showed stressed conditions. From 2003 to 2021, 67% of the study area remained stable, but there was an increase in areas showing early signs of decline and decline, especially in croplands. This indicated that over time, the study area experienced a reduction in land areas with improved or stable productivity and an increase in degraded lands.

Regarding land cover degradation, the results indicated that the land area with stable land cover was dominant in 1985–2003 (52%) and 2003–2021 (47%). However, the proportion of degraded land cover increased from 36% (1985–2003) to 42% (2003–2021). This shift can be attributed to significant changes in LULC dynamics, such as the expansion of croplands and agroforestry, reflecting intensified agricultural practices and deforestation. While there was a slight reduction in improved land cover areas, the most noticeable change was the increase in degraded land cover.

Soil Organic Carbon loss is another critical aspect of land degradation. The analysis showed that while some areas experienced improvements in SOC, a significant portion of the study area remained stable in terms of SOC levels. However, there was an increase in degraded areas from 35% to 39% between 1985–2003 and 2003–2021. This degradation is attributed to the conversion of forestlands, grasslands, and shrublands into other land uses, particularly croplands. These findings align with previous studies that link the conversion of native forests and intensification of agriculture to decreased SOC stocks in Ethiopia (Negasa et al., 2017 and Okolo et al., 2019).

When considering all three sub-indicators together, the study area saw an expansion in degraded land from 1985–2003 (45%) to 2003–2021 (56%), particularly in cropland-dominated areas. In overall, the study revealed concerning trends in LDN indicators in the study area over the reference periods. There has been a decline in land productivity, an increase in land cover degradation, and a rise in soil organic carbon loss. These trends indicated that land degradation is on the rise, with the expansion of degraded areas primarily associated with changes in land use, particularly the expansion of croplands and urbanization. These findings emphasize the importance of sustainable land management practices to mitigate further degradation of the study area's land resources.

VI. Can the implementation of soil conservation scenarios lead to a reduction in sediment yield?

The study investigated the comparative effectiveness of five commonly implemented soil conservation scenarios (filter strips, terracing, soil/stone bund, contour farming and reforestation) in reducing annual sediment yield. The results revealed that soil/stone bund exhibited the highest effectiveness with the lowest sediment yield values ranging from 5.7 to 10.3 t/ha/year. Terracing and contour farming also demonstrated significant effectiveness in sediment yield reduction, with values ranging from 6.4 to 12.7 t/ha/year and 7 to 12.6 t/ha/year, respectively. Reforestation showed a moderate level of effectiveness, with sediment yield values between 9.1 and 16.1 t/ha/year, while the filter strip of 1 m was the least effective, yielding sediment values ranging from 16.8 to 29.1 t/ha/year. These findings were consistent with previous studies (Adi et al., 2023; Admas et al., 2022; Dananto et al., 2022; Leta et al., 2023) and underscored the importance of implementing soil/stone bunds, terracing, contour farming, and reforestation to reduce annual sediment yield. Moreover, the study emphasized the potential of integrating these conservation practices with traditional methods to further enhance soil fertility and improve local communities' livelihoods. Traditional agroforestry systems and plantation work were found to positively correlate with soil conservation practices and soil physicochemical properties in the GW (Hassen, 2021; Temesgen et al., 2018). This integration could contribute to achieve the LDN goals by reducing soil erosion and related degradations.

5.3. The multifaceted implications of land use and climate change

Overall, this study revealed that GW experienced substantial challenges due to climate and LULC changes. These interconnected factors pose a serious threat to both the environment and the socio-economic well-being of the local communities. The subsequent sub-sections illustrate these implications from various perspectives, including environmental, socio-economic, and management related considerations.

5.3.1. Environmental perspectives

The study unveiled substantial landscape changes over the past three decades while underscoring the future projections are of great concern. Deforestation, agricultural expansion, and urbanization are significantly continued at alarming rates, with potentially dire consequences for the environment. The continuous deforestation and reduction in natural land covers are indicative of land degradation (increase in degraded land cover from 36% to 42% between 1985–2003 and 2003–2021), which can have long-term adverse effects on ecosystem stability. The projections for future LULC changes (2035 and 2050) indicate a further expansion of agriculture and built-up areas, accompanied by a decline in forest and grasslands. These trends revealed an ongoing challenge for sustainable land management and ecosystems conservation. The relentless conversion of forest, shrub, and grassland cover into agricultural land poses a serious threat to habitat loss and fragmentation, threatening biodiversity and ecosystem stability (Ma et al., 2023).

The results in chapter 4 showed that LULC changes led to an increase in mean annual surface runoff and sediment load. This increase in runoff and sediment yield can be attributed to the expansion of agricultural land and deforestation, which reduced the land's ability to absorb water and often leads to changes in water availability, increasing the risk of flooding and a hydrological imbalance (Nyatuame et al., 2020; Tan et al., 2022; Zhai et al., 2016). This, in turn, can result in reduced soil fertility, loss of topsoil, and decreased agricultural productivity. The expansion of agriculture land likely driven by the need to meet the demands of a growing population may result in increased use of pesticides and fertilizers (Dhankhar & Kumar, 2023), which can affect water quality and aquatic ecosystem health in the downstream (Dhankhar & Kumar, 2023; Tudi et al., 2021).

Additionally, agricultural expansion (e.g., irrigation practices) and intensification (e.g., increased water demand for crops) may lead to the depletion of water resources or alter the natural flow of rivers and streams (Berhe et al., 2022; Ma et al., 2023). Similarly, rapid urban expansion can increase water demand for domestic and industrial purposes. This demand can strain local water supplies, potentially leading to over-extraction of groundwater or surface water (Ayele et al., 2023). Furthermore, urbanization contribute to both point source and non-point source pollution. This pollution can induce contaminants such as nutrients, pesticides, and heavy metals into water bodies, degrading water quality (Agrawal et al., 2021).

Forests play a crucial role in carbon sequestration and maintaining ecosystem services, and their conversion to other land uses releases stored carbon (SOC) into the atmosphere, contributing to global warming (Ameray et al., 2021; Hurteau, 2021). Thus, land use changes especially deforestation and increased agricultural activities can contribute to greenhouse gas emissions and exacerbate climate-related challenges. The reduction in SOC in significant proportions of the study area (from 35% to 39%) indicated a loss of soil fertility, reduced carbon sequestration capacity, and increased risk of soil degradation and vulnerability to erosion (de Blécourt et al., 2019; Sheng et al., 2015). This is a critical concern for agriculture, as healthy soils are essential for crop productivity.

LULC can affect local microclimates, thereby leading to changes in precipitation patterns and temperature extremes (Khan et al., 2020). The observed trends in climate variables, such as declining rainfall and increasing maximum temperature, indicated the watershed's vulnerability to climate change. This, in turn, may influences water availability (Konapala et al., 2020) and drive changes in land use practices, such as shifting crop calendars or altering the suitability of land for specific agricultural activities and reduced vegetation cover making the soil even more vulnerable to erosion (Abdulmana et al., 2021; Mall et al., 2017). Similarly, intensified rainfall events, often associated with climate change, can increase the risk of flooding and exacerbate soil erosion (Tabari, 2020).

Moreover, the significant increases in temperature can exacerbate drought conditions, higher evaporation rates from reservoir (e.g., Gidabo dam), reduce soil moisture and making it less cohesive and more susceptible to erosion (Grillakis, 2019; Hermans & McLeman, 2021). As a result, soil erosion is increased, leading to the loss of fertile topsoil which is detrimental to agriculture, and the sedimentation of rivers and waterbodies that can degrade water quality and disrupt aquatic ecosystems (e.g., lake Abaya), damage infrastructure and affect the functioning of Gidabo irrigation reservoir. These changes can have far-reaching consequences for agriculture, water resources, and the overall climate resilience of the watershed.

The variation in biophysical characteristics such as soil type, altitude and slope across the watershed resulted in substantial influence on runoff patterns and soil erosion dynamics. Different soil types have varying permeability, water-holding capacity and soil erodibility (Mallick et al., 2016; Osman, 2013). Higher altitudes (e.g., southern and eastern part of the watershed) receive more precipitation, and coupled with steeper slopes, intensified the runoff velocity and increased erosion hazards as well as sediment transport while diminishing soil stability. The results revealed the pivotal role of biophysical heterogeneity on runoff patterns and identification of erosion susceptible areas within the watershed.

5.3.2. Socio-economic perspectives

The dominance of agriculture and agroforestry as livelihoods in the GW signifies their importance to the local community. However, the assessment of land degradation using LDN indicators indicated that a significant portion of the study area, particularly croplands experienced a decrease in land productivity. The increase in soil degradation due to land use changes can diminishes the nutrient-rich layer necessary for agricultural productivity (Du et al., 2022). This can have adverse socio-economic impacts on local communities that depend on agriculture for their livelihoods (Vávra et al., 2019). Declining soil fertility leads to reduced crop yields, increased production costs to maintain agricultural production, and potential economic losses for rural communities (Mosier et al., 2021). Additionally, the sedimentation of waterbodies can harm fisheries and water quality, affecting livelihoods and food sources (Fetahi, 2019; Kjelland et al., 2015; Reddy & Osborne, 2022). Furthermore, as land becomes less productive, there might be increased competition for the remaining arable land and water resources, potentially leading to conflicts and social instability within local communities (Ariti et al., 2015; Mekuria et al., 2018).

The continuous expansion of agricultural land can lead to short-term gains but may compromise long-term sustainability of these practices and their impact on food security and rural livelihoods if not managed carefully. This is because, the rapid population growth can lead to increased land demand, competition for arable land, urbanization, and the conversion of marginal lands into agriculture and settlements (Wassie, 2020). These trends may put additional pressure on land resources, land disputes and could affect living conditions in the GW. Moreover, the trend of increasing landscape fragmentation could exacerbate land degradation.

Rainfall and temperature are crucial meteorological variables for monitoring climate change and its impacts (Stott & Strangeways, 2018). In Ethiopia, where rainfed agriculture plays a significant role in the economy, understanding the spatial and temporal variability of climate variables is essential for developing effective adaptation strategies. The decreasing trends in mean annual rainfall results potential water scarcity issues in the watershed (Alehu et al., 2021; Belihu et al., 2018; Mana & Abebe, 2023). This may lead to stress on local flora and fauna, reduce crop yields and agricultural productivity, increased vulnerability to extreme weather events, especially for rainfed agriculture, which is crucial for the livelihoods of many in the watreshed. Additionally, climate change can negatively impact the availability of grazing land for livestock (Godde et al., 2021), which is another vital component of the local economy. The observed trends in climate variables can exacerbate the existing challenges and could be a determining factor for various socio-economic issues affecting both rural and urban populations, including food insecurity, poverty, income loss, migration, and unemployment.

5.3.3. Pathway to sustainable land management

The findings showed the complex interplay between climate change, land use change, and their environmental consequences. Addressing these challenges requires effective land management strategies, conservation practices, and adaptation measures to promote sustainable land use and environmental resilience in the GW. Moreover, variations in biophysical attributes like soil type, altitude, and slope exert substantial influence on runoff dynamics and soil erosion. This implies, understanding the local conditions of the study area and their interactions were crucial for effective land and water resource management. For example, information such as soil types, soil properties, and topographic features provides a baseline for assessing the suitability of land for various uses, guide land use planning and conservation efforts.

Monitoring trends in rainfall and temperature is essential for climate change adaptation on soil and water resources management. The decreasing trend in annual rainfall and the significant increase in temperature are great concerns in the study area. The findings underscored the urgency of climate monitoring and the development of adaptation strategies. These includes, the implementation of sustainable water management activities such as water harvesting techniques to store water for agricultural use during dry spells, and water-efficient methods (e.g., drip irrigation) can help farmers adapt to erratic rainfall patterns and prolonged droughts (Chartzoulakis & Bertaki, 2015; Srivastav et al., 2021). Moreover, promote climate-resilient agriculture, planting a variety of drought-tolerant crops and diversify livelihoods to cope with vulnerability to climate change (Acevedo et al., 2020). The implementation of crop rotation and intercropping practices can enhance the resilience of the agricultural system to changing precipitation patterns and temperature extremes, maintain soil health and reduce the risk of soil degradation, and increase overall yield stability (Huss et al., 2022). Moreover, the inclusion of future projections under different emission scenarios (RCP4.5 and RCP8.5) can help scenario-based planning and preparedness for different climate change outcomes.

The findings on LDN indicators have significant importance in the context of sustainable land management activities aimed at achieving LDN in the studied area. As a standard methodology the findings can easily be compared with present and future findings elsewhere. To address the land degradation issues in the GW, a comprehensive management strategy such as improving land productivity, reducing land cover degradation, and enhancing SOC should be considered. This includes the implementation of soil management and conservation techniques such as terracing, cover cropping, crop rotation, the adoption of organic farming practices and conservation agriculture practices that minimize soil disturbance and maintain crop residues could help to retain SOC. Moreover, unplanned LULC change have far-reaching environmental (e.g., land cover degradation and SOC loss) and socio-economic consequences in the GW. Therefore, it is essential to implement adequate land-use planning strategies that balance agricultural expansion with conservation efforts to ensure food security and sustainable land use. This might include the implementation of afforestation and reforestation programs to restore degraded areas, as forests can contribute significantly to stabilize land productivity, carbon sequestration as well as counteract deforestation trends (Ameray et al., 2021; Hurteau, 2021). Moreover, encouraging agroforestry practices that integrate trees with agriculture can provides multiple benefits, including improved soil fertility, enhanced water retention, and increased resilience to extreme weather events (Hassen, 2021; Temesgen et al., 2018). Trees also provide shade and windbreaks, which can protect crops from climate change stress, stabilize land cover and enhance ecosystem services.

The identification of spatial variability in soil erosion is critical for long-term planning and management of land and water resources (Shivhare et al., 2018). This information allows for the prioritization of resources and interventions in critical sub-basins to reduce soil erosion and land degradation (Sinshaw et al., 2021). The fact that over 77% of the study area experiences high to severe soil erosion rates indicates a pressing need for intervention. Particularly, most of the southern and eastern parts of the watershed characterized as high-risk areas due to steep slopes and relatively high rainfall. These findings emphasize the importance of targeted management efforts in these areas to prevent further soil loss and its associated consequences. Moreover, evaluating the effectiveness of different soil conservation practices in reducing sediment yield is crucial for decision-making. This can help to identify the most effective conservation measures for specific areas and informs resource allocation for soil erosion control. In this context, the implementation of effective soil conservation practices, such as terracing and contour farming (on sloping lands), soil/stone bund, and reforestation can reduce runoff velocity and soil erosion, optimize water retention and stabilize the soil, and provide socio-economic opportunities through sustainable land management.

Lake buffer zone management plays a crucial role in preserving the ecological integrity of lake Abaya and its surrounding ecosystems while addressing the socio-economic problems associated with it (Li et al., 2019; Wang et al., 2020). Therefore, proper buffer zone management such as controlled land use practices (e.g., limiting agriculture and deforestation) and zoning regulations can reduce fragmentation and maintain the natural balance of the critical ecosystem. Moreover, the establishment of vegetative buffer strips along the lake's shoreline comprising native plants and grasses can act as a natural filter and barrier, preventing pollutants such as sediments, nutrients, and chemicals from entering the lake, and also stabilize the soil (Cole et al., 2020; Mander et al., 2017). In essence, effective lake buffer zone management is a fundamental strategy in ensuring the long-term sustainability of lake Abaya and the broader environment it is a part of, benefiting both nature and human communities that rely on this valuable resource.

The effects of land use and climate change on surface runoff and soil erosion demonstrated the need for integrated land management strategies. Some scenarios show reduced surface runoff and sediment yield, likely due to the offsetting effects of climate changes. However, other scenarios indicated increased runoff and erosion, emphasizing the importance of considering both factors in mitigation and adaptation strategies. Therefore, effective land and water resource management strategies should consider the biophysical characteristics, climate trends, land use changes, and the impacts of both land use and climate change. Additionally, soil erosion indicators play a crucial role in assessing and addressing land degradation, and integration in LDN assessments can enhance the overall understanding of the degradation processes, allows for the identification of areas at risk of erosion-induced land degradation and the formulation of targeted strategies to mitigate erosion, enhance soil conservation, and ultimately achieve LDN goals. Eventually, this helps policymakers and land managers to develop effective strategies and policies to combat land degradation.

In general, the implementation of sustainable land management (SLM) activities requires participatory approaches that balances environmental conservation with socioeconomic development (Etsay et al., 2019; Haregeweyn et al., 2023). Collaboration and partnerships between different stakeholders, including governments and non-governmental organizations, local communities, and the private sector are essential. Particularly, community engagement and active involvement in decision-making processes is crucial for the success of SLM initiatives (Mengistu & Assefa, 2020). This can be achieved through education and awareness campaigns, training programs, and the establishment of local conservation groups. Additionally, it is essential to consider the cultural and socio-economic context of each community to adapt SLM interventions that align with their needs and traditions (Mengistu & Assefa, 2020).

5.4. The nexus of land use change, climate dynamics, and land degradation

Land use, climate change, and land degradation are linked in a complex web of environmental processes (IPCC, 2022; Simonsen, 2019). The interlinkage between LULC change study, performance assessment of climate models, and land degradation trajectories is a crucial framework to understand the intricate cause-and-effect relationships between these environmental dynamics in the GW.

The results in chapter 2 revealed substantial LULC dynamics, with a significant expansion of agriculture land and settlement at the expense of natural vegetations. This land use change can alter the characteristics of the land surface, such as albedo, evapotranspiration, and carbon cycle (Bai et al., 2023; Chu et al., 2022; Houghton, 2018). These changes gradually have direct impacts on regional climate, such as temperature and precipitation, which are essential variables to evaluate the RCMs as discussed in chapter 3. This, in turn, can affect the performance of regional climate models (RCMs) in capturing the observed climate patterns (Lakku and Behera, 2022; Sylla et al., 2013; Wu et al., 2020). Therefore, the findings from the LULC study can provide valuable insights into the factors influencing the performance of RCMs in the GW, as land use changes are one of the drivers of climate change. On the other hand, climate change can also influence land use patterns. As temperature rise and extreme weather events become more frequent, this can lead to shifts in land use in response to climate change (Sleeter et al., 2018). Studies have shown that land and climate interact in complex ways through multiple biophysical feedbacks (Jia et al., 2022). These feedbacks can create a self-reinforcing cycle, where climate change induces further land use changes (Abdulmana et al., 2021; Mall et al., 2017), which, in turn, exacerbate climate impacts, indicating the intricate and interconnected relationship between land use and climate change.

Moreover, land use changes and unsustainable land management are the direct causes of land degradation, with agriculture being a dominant sector driving degradation (IPCC, 2022), which is a central concern discussed in chapter 4. Thus, the integration of LULC data into land degradation assessments, can provide valuable inputs for models used to assess the extent of land degradation processes. Moreover, it helps in predicting potential future scenarios, enabling policymakers and land managers to implement land management strategies to mitigate land degradation. Therefore, LULC modeling serves as an essential tool in the broader context of land degradation assessments, as well as supporting sustainable land management and conservation efforts (Gaur and Singh, 2023). The evaluation of climate models reveals varying degrees of accuracy in replicating climate variables such as rainfall and temperature, which are critical for assessing land degradation pathways, as discussed in chapter 4. Inadequate climate modeling can lead to misinformed land use decisions and an increased risk of land degradation, emphasizing the significance of selecting accurate models for impact assessments (Giorgi and Gutowski, 2015; IPCC, 2014). This information is vital for selecting the most accurate models that represent climate-related factors for impact assessment in the GW. The land degradation assessment was relied on this to predict potential land degradation pathways, as changes in precipitation and temperature can influence erosion and sediment yield. Therefore, the results obtained from the RCM evaluation were crucial for understanding the links between climate and land degradation in the watershed.

Land degradation, in turn, can intensify land use change, as deteriorating land quality may necessitate further shifts in land use patterns, such as conversion of forests to cropland to compensate for declining agricultural productivity (Hermans and McLeman, 2021). Additionally, in areas experiencing severe land degradation, rural populations may migrate to urban areas in search of better livelihoods (Hermans et al., 2023). This can lead to increased urbanization and changes in land use patterns. Land degradation resulted in the loss of valuable ecosystem services, reduced carbon sequestration capacity, and increased vulnerability to extreme weather events (IPCC, 2022). This, in turn, contributes to climate change through the release of stored carbon, exacerbating greenhouse gas emissions and alterations in climate patterns (Shukla et al., 2019). Simultaneously, changes in land use and climate can exacerbates land degradation process. This feedback loop creates a vicious cycle, resulted in significant ecological, economic, and social consequences as discussed in section 5.3.

In conclusion, the interconnection between land use, climate change, and land degradation implies the need for integrated and sustainable land and water resource management strategies (as discussed in section 5.3.3), policies and practices to protect the watershed's land and water resources. Therefore, the study provides valuable insights for policymakers, land managers, and conservationists in addressing the challenges posed by these interconnected environmental issues and developing effective strategies for adaptation and mitigation.

5.5. Scientific contributions

This study employed a comprehensive methodology and provided scientific foundation to understand, monitor, and mitigate soil erosion and land degradation processes. The primary contribution of this study lies in its forward-looking approach to model and simulate future LULC changes in the GW, employing advanced geospatial techniques, and revealing the environmental and socio-economic implications of these changes. While previous studies had provided valuable insights into historic LULC changes, this study goes a step further to simulate LULC dynamics for the future. In this context, the study addressed a critical gap in the existing literature by focusing not only on historical LULC changes but also on predicting future trends for the years 2035 and 2050. This future-oriented perspective is crucial for decision-making in land and water resource management.

Moreover, the study employed advanced geospatial techniques and machine learning algorithms (MLP) to model the future LULC changes. The study considered various driver variables, including topography features, proximity variables, and population density to understand the factors influencing LULC changes in the GW. The use of MLP allows for the modeling of complex patterns and behaviors in LULC dynamics, provides a more accurate and robust prediction of future changes. The high classification accuracy (>80%) ensured the reliability of the results, making them valuable for policymakers, land-use planners, and hydrologists.

The findings of the study provided valuable insights into the performance of multiple RCMs in replicating key meteorological variables, such as rainfall and temperature patterns. The assessment revealed variations in model performance, with some models better replicating observed patterns while others exhibit overestimation or underestimation. Importantly, the study underscored the significance of understanding how different RCMs perform in climate impact assessment studies, as model uncertainties can greatly influence projections of climate change. Additionally, the study identified trends in rainfall and temperature, indicating changes in climate conditions over time. These insights can contribute to a better understanding of climate dynamics in the GW and aid in developing strategies for mitigating the impacts of climate change.

The other notable contribution in this study lies in its integrated approach to assess the land degradation pathways from 1990 to 2060. The study considered the individual and combined effects of climate and land use change on surface runoff and soil erosion, identified erosion hotspots, assessed LDN indicators, and evaluated the effectiveness of soil conservation practices in reducing sediment yield. These findings provided valuable insights and guidance for conservation efforts in the study area at present, near and mid-term while indicating what need to be done in the future based on the scenarios considered. This will contribute to the broader scientific knowledge on the complex interactions between climate, land use, and soil degradation.

5.6. Conclusions

The study presented a detailed understanding of the LULC changes, climate variability and their impacts on soil erosion indicators, and land degradation dynamics. The study encompasses historical perspective from 1985 to 2021 and extends into future predictions up to 2060, employing multidisciplinary approach integrating remote sensing, statistical and geospatial analysis, and hydrological modeling. The observed LULC changes over the past 36 years indicated a significant shift, with agriculture and agroforestry dominating at the expense of forests, shrubs, and grasslands. The study predicted continued expansion of agricultural land, agroforestry, and built-up areas, accompanied by a reduction in forest, grass, and shrub land between 2021 and 2050. Furthermore, the evaluation of 11 CORDEX-Africa RCMs and their mean ensemble in reproducing rainfall and temperature patterns over GW revealed varying performance across different models. Despite overestimations and underestimations in replicating observed climate variables, certain models, such as RACMO22T (EC-EARTH), CRCM5 (MPI), CCLM4-8 (CNRM), and REMO2009 (EC-EARTH), exhibited better overall performance. The findings revealed the importance of correcting systematic biases in RCM outputs and building ensembles with the best-performing models for accurate climate change impact assessments studies.

The integrated approach using the SWAT model and Trends.Earth elucidated the environmental challenges faced by GW, including soil erosion and land degradation indicators. Historical LULC changes contributed to increased surface runoff and sediment yield, driven by agricultural expansion and deforestation. Future projections also indicated further increases in runoff and sediment yield due to ongoing land-use changes. However, most of the climate change scenarios under the RCP4.5 and RCP8.5 showed a decline in surface runoff and sediment yield. The interplay between land use and climate change yields varied outcomes with some scenarios showed increases in surface runoff and sediment yield, indicating a synergy between land use change and climate change, while certain future scenarios showed decreases in surface runoff and sediment yield, indicating the offset effect of climate changes. Additionally, the LP showed a decline, and LC degradation and SOC loss were increased from 1985–2003 to 2003–2021. The integration of soil erosion indicator into LDN assessments can complement the existing sub-indicators.

Furthermore, the study evaluated soil conservation practices and identified soil/stone bund as the most effective measure for reducing sediment yield, followed by terracing, contour farming, and reforestation. Overall, the findings emphasized the critical need for proactive measures to address the adverse consequences of unplanned LULC changes, climate variability, and soil erosion in the GW. This might include the integration of LULC and climate change considerations for comprehensive planning and sustainable management to address the complex challenges faced by the watershed. The outputs attained in this study provide valuable information for stakeholders, enabling the development of effective land and water resources conservation strategies in the future.

5.7. Limitations of the research and future directions

The study covered a range of topics and provided valuable insights into the land degradation trajectories and potential management alternatives in the GW. Additionally, the following issues and recommendations should be considered for further research to fully understand and enhance the robustness of the findings:

- The future LULC predictions were performed based on a Business-As-Usual (BAU) scenario which assumes a continuation of current trends. Moreover, the study used limited key drivers of LULC change, such as topography, proximity, and population density due to the scarcity of dynamic variables. Thus, future research in this area could delve to incorporate additional variables, such as policy changes and economic factors, and explore different scenarios beyond the BAU model, including sustainable development and conservation scenarios into the modeling process. This would provide a more wide-ranging picture of the LULC changes and future possibilities.
- Though climate change and land use change are interconnected processes, the study did not directly investigate the synergetic effects of the two factors. Therefore, future research efforts should aim to investigate the synergetic effects of climate change and land use change, ultimately informing more effective strategies for sustainable land management and adaptation to environmental change.
- RCMs are subjected to ongoing development and improvements. Focusing solely on frequently used RCMs may overlook the potential benefits of less frequently used models or newer models that address known issues or provide better performance. Therefore, pursuing comparative studies that evaluate the CORDEX-Africa RCMs alongside other RCMs can provide a comprehensive insight into model strengths and weaknesses. The findings were limited by observed data availability. Extending the analysis to longer timeframes is essential for understanding long-term climate trends and their implications. Thus, future research could explore alternative data sources like remote sensing data.
- While the use of the SWAT model and Trends.Earth platform is a valuable approach, these models rely on various input parameters and the accuracy of the results is highly dependent on the quality and availability of data. Therefore, future research should focus on validating the model outputs through field measurements and ground-truthing to improve the accuracy of the predictions.
- The study evaluated the effectiveness of various soil conservation practices in reducing sediment yield. While this is important information, it would be valuable to assess the economic feasibility and social acceptability of implementing these practices. Understanding the barriers to adoption and the socio-economic implications of conservation measures can help in designing more effective land management strategies.
- The study primarily focused on the biophysical aspects of land degradation, such as soil erosion and LDN indicators driven by climate and land use changes. However, land degradation is a multidimensional issue often influenced by socio-economic factors and

policy decisions. To develop integrated strategies that address multiple aspects of land degradation simultaneously, future research should expand its scope to include socio-economic variables and policy scenarios. This would involve assessing the human drivers of land degradation, such as population growth, land management practices, and policy interventions. These future analyses can be of crucial importance for gaining a more detailed understanding of the multidimensional pattern of land degradation.

- LDN indicators are typically designed to assess trends in land degradation and restoration. While these indicators can provide valuable information about the state of the land, they may not directly capture all the chemical, physical, and biological changes occurring within the ecosystem. Similarly, soil erosion assessment primarily addresses the physical aspect of land degradation by focusing on the loss of soil. While soil erosion can indirectly affect chemical and biological characteristics of the soil, it may not directly capture all the changes occurring within the soil. Therefore, it's important to complement these approaches with other indicators that capture a broader range of changes in chemical, physical, and biological characteristics of the landscape. Such a deep understanding is vital for enhancing the scientific support used in the implementation of policies designed to protect, restore and rehabilitate degraded lands.

References

Abbasian, M., Moghim, S., Abrishamchi, A., 2019. Performance of the general circulation models in simulating temperature and precipitation over Iran. Theoretical and Applied Climatology 135, 1465–1483. https://doi.org/10.1007/S00704-018-2456-Y.

Abdulmana, S., Lim, A., Wongsai, S., Wongsai, N., 2021. Land surface temperature and vegetation cover changes and their relationships in Taiwan from 2000 to 2020. Remote Sens Appl 24, 100636. https://doi.org/10.1016/J.RSASE.2021.100636

Abegaz, W.B., Abera, E.A., 2020. Temperature and Rainfall Trends in North Eastern Ethiopia. International Journal of Environmental Sciences & Natural Resources 25, 49–57. https://doi.org/10.19080/IJESNR.2020.25.556163.

Abraham, T., Liu, Y., Tekleab, S., Hartmann, A., 2022. Prediction at Ungauged Catchments through Parameter Optimization and Uncertainty Estimation to Quantify the Regional Water Balance of the Ethiopian Rift Valley Lake Basin. Hydrology 9. https://doi.org/10.3390/hydrology9080150

Aburas, M.M., Ho, Y.M., Ramli, M.F., Ash'aari, Z.H., 2017. Improving the capability of an integrated CA-Markov model to simulate spatio-temporal urban growth trends using an Analytical Hierarchy Process and Frequency Ratio. International Journal of Applied Earth Observation and Geoinformation 59, 65–78. https://doi.org/10.1016/J.JAG.2017.03.006

Acevedo, M., Pixley, K., Zinyengere, N., Meng, S., Tufan, H., Cichy, K., Bizikova, L., Isaacs, K., Ghezzi-Kopel, K., Porciello, J., 2020. A scoping review of adoption of climate-resilient crops by small-scale producers in low- and middle-income countries. Nature Plants 2020 6:10 6, 1231–1241. https://doi.org/10.1038/s41477-020-00783-z

Ademe, D., Ziatchik, B.F., Tesfaye, K., Simane, B., Alemayehu, G., Adgo, E., 2020b. Climate trends and variability at adaptation scale: Patterns and perceptions in an agricultural region of the Ethiopian Highlands. Weather and Climate Extremes 29, 100263. https://doi.org/10.1016/J.WACE.2020.100263.

Ademe, F., Kibret, K., Beyene, S., Mitike, G., Getinet, M., 2020a. Rainfall analysis for rain-fed farming in the Great Rift Valley Basins of Ethiopia. Journal of Water and Climate Change 11, 812–828. https://doi.org/10.2166/WCC.2019.242.

Adenuga, Kayode I, Mahmoud, S., Dodo, Yakubu Aminu, Albert, Moutlen, Kori, A., Danlami, Nusa Jibril, Adenuga, K I, Mahmoud, A.S., Dodo, Y A, Albert, M, Kori, S.A., Danlami, N J, 2021. Climate Change Adaptation and Mitigation in Sub-Saharan African Countries. Advanced Sciences and Technologies for Security Applications 393–409. https://doi.org/10.1007/978-3-030-63654-8_16.

Adi, K.A., Serur, A.B., Meskele, D.Y., 2023. Sediment yield responses to land use land cover change and developing best management practices in the upper Gidabo dam watershed. Sustain Water Resour Manag 9. https://doi.org/10.1007/s40899-023-00850-1

Admas, B.F., Gashaw, T., Adem, A.A., Worqlul, A.W., Dile, Y.T., Molla, E., 2022. Identification of soil erosion hot-spot areas for prioritization of conservation measures using the SWAT model in Ribb watershed, Ethiopia. Resources, Environment and Sustainability 8, 100059. https://doi.org/10.1016/J.RESENV.2022.100059.

Adnan, M., 2020. Land Degradation and its Management: A Review. International Journal of Environmental Sciences & Natural Resources 25. https://doi.org/10.19080/IJESNR.2020.25.556157

Adugna, T. M., & Cherie, D. A. (2021). A Review on Reservoirs Sedimenation Problems in Ethiopia. Asian Journal of Advanced Research and Reports, 15(3), 1–8. https://doi.org/10.9734/ajarr/2021/v15i330372

Aga, A.O., Chane, B., Melesse, A.M., 2018. Soil erosion modelling and risk assessment in data Scarce Rift Valley Lake Regions, Ethiopia. Water (Switzerland) 10. https://doi.org/10.3390/w10111684

Agnew, C.T., Chappell, A., 1999. Drought in the Sahel. GeoJournal 1999 48:4 48, 299–311. https://doi.org/10.1023/A:1007059403077.

Agrawal, K.K., Panda, C., Bhuyan, M.K. (2021). Impact of Urbanization on Water Quality. In: Acharya, S.K., Mishra, D.P. (eds) Current Advances in Mechanical Engineering. Lecture Notes in Mechanical Engineering. Springer, Singapore. https://doi.org/10.1007/978-981-33-4795-3_60

Akça, E., Büyük, G., İnan, M., Kırpık, M., 2022. Sustainable management of land degradation through legume-based cropping system, in: Advances in Legumes for Sustainable Intensification. https://doi.org/10.1016/B978-0-323-85797-0.00029-X

Alehu, B.A., Desta, H.B., Daba, B.I., 2021. Assessment of climate change impact on hydro-climatic variables and its trends over Gidabo Watershed. Modeling Earth Systems and Environment 2021 1–23. https://doi.org/10.1007/S40808-021-01327-W.

Alemseged, T.H., Tom, R., 2015. Evaluation of regional climate model simulations of rainfall over the Upper Blue Nile basin. Atmospheric Research 161–162, 57–64. https://doi.org/10.1016/J.ATMOSRES.2015.03.013.

Alhamshry, A., Fenta, A.A., Yasuda, H., Kimura, R., Shimizu, K., 2020. Seasonal Rainfall Variability in Ethiopia and Its Long-Term Link to Global Sea Surface Temperatures. Water 2020, Vol. 12, Page 55 12, 55. https://doi.org/10.3390/W12010055.

Ali, R., Kuriqi, A., Abubaker, S., Kisi, O., 2019. Long-Term Trends and Seasonality Detection of the Observed Flow in Yangtze River Using Mann-Kendall and Sen's Innovative Trend Method. Water. 2019; 11(9):1855. https://doi.org/10.3390/w11091855.

Almagro, M., de Vente, J., Boix-Fayos, C. et al., 2016. Sustainable land management practices as providers of several ecosystem services under rainfed Mediterranean agroecosystems. Mitig Adapt Strateg Glob Change 21, 1029–1043 (2016). https://doi.org/10.1007/s11027-013-9535-2.

Ameray, A., Bergeron, Y., Valeria, O., Montoro Girona, M., Cavard, X., 2021. Forest Carbon Management: a Review of Silvicultural Practices and Management Strategies Across Boreal, Temperate and Tropical Forests. Current Forestry Reports. https://doi.org/10.1007/s40725-021-00151-w

Anagnostopoulos, G.G., Koutsoyiannis, D., Christofides, A., Efstratiadis, A., Mamassis, N., 2010. A comparison of local and aggregated climate model outputs with observed data. 55, 1094–1110. https://doi.org/10.1080/02626667.2010.513518.

Anose, F.A., Beketie, K.T., Terefe Zeleke, T., Yayeh Ayal, D., Legese Feyisa, G., 2021. Spatio-temporal hydro-climate variability in Omo-Gibe river Basin, Ethiopia. Climate Services 24, 100277. https://doi.org/10.1016/J.CLISER.2021.100277.

Anurag, Saxena, A., Pradhan, B., 2018. Land Use/ Land Cover Change Modelling: Issues and Challenges. J Rural Dev 37, 413. https://doi.org/10.25175/jrd/2018/v37/i2/129708.

Aragaw, H.M., Goel, M.K., Mishra, S.K., 2021. Hydrological responses to human-induced land use/land cover changes in the Gidabo River basin, Ethiopia. 66, 640–655. https://doi.org/10.1080/02626667.2021.1890328.

Aragaw, H.M., Goel, M.K., Mishra, S.K., 2021. Hydrological responses to human-induced land use/land cover changes in the Gidabo River basin, Ethiopia. 66, 640–655. https://doi.org/10.1080/02626667.2021.1890328.

Aragaw, H.M., Mishra, S.K., Goel, M.K., 2022. Responses of water balance component to land use/land cover and climate change using geospatial and hydrologic modeling in the Gidabo River basin, Ethiopia. Geocarto Int 37. https://doi.org/10.1080/10106049.2022.2123956

Araya, A., Keesstra, S.D., Stroosnijder, L., 2010. A new agro-climatic classification for crop suitability zoning in northern semi-arid Ethiopia. Agricultural and Forest Meteorology 150, 1057–1064. https://doi.org/10.1016/j.agrformet.2010.04.003.

Ariti, A.T., Vliet, J. van, Verburg, P.H., 2015. Land-use and land-cover changes in the Central Rift Valley of Ethiopia: Assessment of perception and adaptation by stakeholders. Applied Geography 65, 28–37. https://doi.org/10.1016/J.APGEOG.2015.10.002.

Arnold, J.G., Moriasi, D.N., Gassman, P.W., Abbaspour, K.C., White, M.J., Srinivasan, R., Santhi, C., Harmel, R.D., Van Griensven, A., Van Liew, M.W., Kannan, N., Jha, M.K., 2012. SWAT: Model use, calibration, and validation. Trans ASABE 55.

Asfaw, A., Bantider, A., Simane, B., Hassen, A., 2021. Smallholder farmers' livelihood vulnerability to climate change-induced hazards: agroecology-based comparative analysis in Northcentral Ethiopia (Woleka Sub-basin). Heliyon 7. https://doi.org/10.1016/J.HELIYON.2021.E06761.

Asfaw, A., Simane, B., Hassen, A., Bantider, A., 2018. Variability and time series trend analysis of rainfall and temperature in northcentral Ethiopia: A case study in Woleka sub-basin. Weather and Climate Extremes 19, 29–41. https://doi.org/10.1016/J.WACE.2017.12.002

Assfaw, A.T., 2020. Modeling Impact of Land Use Dynamics on Hydrology and Sedimentation of Megech Dam Watershed, Ethiopia. Scientific World Journal 2020. https://doi.org/10.1155/2020/6530278

Asumadu-Sarkodie, S., 2015. Situational Analysis of Flood and Drought in Rwanda. International Journal of Scientific and Engineering Research 6, 960–970. https://doi.org/10.14299/IJSER.2015.08.013.

Ayele, S., Getaneh, Z., Tekola, B., 2023. Water challenges of Dire Dawa city of Ethiopia: An assessment of urban growth and groundwater supply. https://doi.org/10.1016/j.envc.2023.100738.

Ayugi, B., Tan, G., Gnitou, G.T., Ojara, M., Ongoma, V., 2020b. Historical evaluations and simulations of precipitation over East Africa from Rossby centre regional climate model. Atmospheric Research 232, 104705. https://doi.org/10.1016/J.ATMOSRES.2019.104705.

Ayugi, B., Tan, G., Ruoyun, N., Babaousmail, H., Ojara, M., Wido, H., Mumo, L., Ngoma, N.H., Nooni, I.K., Ongoma, V., 2020a. Quantile Mapping Bias Correction on Rossby Centre Regional Climate Models for Precipitation Analysis over Kenya, East Africa. Water 2020a, Vol. 12, Page 801 12, 801. https://doi.org/10.3390/W12030801.

Azari, M., Tayyebi, A., Helbich, M., Reveshty, M.A., 2016. Integrating cellular automata, artificial neural network, and fuzzy set theory to simulate threatened orchards: application to Maragheh, Iran. http://dx.doi.org/10.1080/15481603.2015.1137111 53, 183–205. https://doi.org/10.1080/15481603.2015.1137111.

Babaousmail, H., Hou, R., Ayugi, B., Ojara, M., Ngoma, H., Karim, R., Rajasekar, A., Ongoma, V., 2021. Evaluation of the Performance of CMIP6 Models in Reproducing Rainfall Patterns over North Africa. Atmosphere 2021, Vol. 12, Page 475 12, 475. https://doi.org/10.3390/ATMOS12040475.

Bai, T., Fan, L., Song, G., Song, H., Ru, X., Wang, Y., Zhang, H., Min, R., Wang, W., 2023. Effects of Land Use/Cover and Meteorological Changes on Regional Climate under Different SSP-RCP Scenarios: A Case Study in Zhengzhou, China. Remote Sensing 2023, Vol. 15, Page 2601 15, 2601. https://doi.org/10.3390/RS15102601

Balogun, I.A., Ishola, K.A., 2017. Projection of Future Changes in Landuse/Landcover Using Cellular Automata/Markov Model over Akure City, Nigeria. Journal of Remote Sensing Technology 5, 22–31. https://doi.org/10.18005/JRST0501003.

Banda, V.D., Dzwairo, R.B., Singh, S.K., Kanyerere, T., 2021. Trend analysis of selected hydro-meteorological variables for the Rietspruit sub-basin, South Africa. Journal of Water and Climate Change 1 November 2021; 12 (7): 3099–3123. https://doi.org/10.2166/wcc.2021.260.

Bekele, T., 2019. Effect of Land Use and Land Cover Changes on Soil Erosion in Ethiopia. International Journal of Agricultural Science and Food Technology 026–034. https://doi.org/10.17352/2455-815X.000038.

Bekele-Biratu, E., Thiaw, W.M., Korecha, D., 2018. Sub-seasonal variability of the Belg rains in Ethiopia. International Journal of Climatology 38, 2940–2953. https://doi.org/10.1002/JOC.5474.

Belay, A., Demissie, T., Recha, J.W., Oludhe, C., Osano, P.M., Olaka, L.A., Solomon, D., Berhane, Z., 2021. Analysis of Climate Variability and Trends in Southern Ethiopia. Climate 2021, Vol. 9, Page 96 9, 96. https://doi.org/10.3390/CLI9060096.

Belayneh, M., Yirgu, T., Tsegaye, D., 2019. Effects of soil and water conservation practices on soil physicochemical properties in Gumara watershed, Upper Blue Nile Basin, Ethiopia. Ecol Process 8, 1–14. https://doi.org/10.1186/S13717-019-0188-2/TABLES/7

Belihu, M., Abate, B., Tekleab, S., Bewket, W., Belihu, M., Abate, B., Tekleab, S., Bewket, W., 2018. Hydro-meteorological trends in the Gidabo catchment of the Rift Valley Lakes Basin of Ethiopia. Physics and Chemistry of the Earth, Parts A/B/C 104, 84–101. https://doi.org/10.1016/J.PCE.2017.10.002.

Belihu, M., Tekleab, S., Abate, B., Bewket, W., 2020. Hydrologic response to land use land cover change in the Upper Gidabo Watershed, Rift Valley Lakes Basin, Ethiopia. HydroResearch 3, 85–94. https://doi.org/10.1016/J.HYDRES.2020.07.001.

Berhanu, B., Seleshi, Y., Melesse, A.M., 2014. Surface water and groundwater resources of Ethiopia: Potentials and challenges of water resources development. Nile River Basin: Ecohydrological Challenges, Climate Change and Hydropolitics 9783319027203, 97–117. https://doi.org/10.1007/978-3-319-02720-3_6.

Berhe, G., Baartman, J., Veldwisch, G., Grum B., Ritsema, C., 2022. Irrigation development and management practices in Ethiopia: a systematic review on existing problems, sustainability issues and future directions. Agric Water Manag 274(September):107959. https://doi.org/10.1016/j.agwat.2022.107959

Berihun, M.L., Tsunekawa, A., Haregeweyn, N., Meshesha, D.T., Adgo, E., Tsubo, M., et al., 2019. Exploring land use/land cover changes, drivers and their implications in contrasting agro-ecological environments of Ethiopia.

Bewket, W., Abebe, S., 2013. Land-use and land-cover change and its environmental implications in a tropical highland watershed, Ethiopia. 70, 126–139. https://doi.org/10.1080/00207233.2012.755765.

Bisrat, E., Berhanu, B., 2019. Drought in Ethiopia: Temporal and spatial characteristics. Extreme Hydrology and Climate Variability: Monitoring, Modelling, Adaptation and Mitigation 263–274. https://doi.org/10.1016/B978-0-12-815998-9.00021-X.

Borrelli, P., Alewell, C., Alvarez, P., Anache, J.A.A., Baartman, J., Ballabio, C., Bezak, N., 2021. Soil erosion modelling: A global review and statistical analysis. Science of The Total Environment 780, 146494. https://doi.org/10.1016/J.SCITOTENV.2021.146494

Borrelli, P., Robinson, D.A., Panagos, P., Lugato, E., Yang, J.E., Alewell, C., Wuepper, D., Montanarella, L., Ballabio, C., 2020. Land use and climate change impacts on global soil erosion by water (2015-2070). Proc Natl Acad Sci U S A 117, 21994–22001. https://doi.org/10.1073/PNAS.2001403117/SUPPL_FILE/PNAS.2001403117.SAPP.PDF

Borrelli, P., Van Oost, K., Meusburger, K., Alewell, C., Lugato, E., Panagos, P., 2018. A step towards a holistic assessment of soil degradation in Europe: Coupling on-site erosion with sediment transfer and carbon fluxes. Environ Res 161. https://doi.org/10.1016/j.envres.2017.11.009

Burnicki, A.C., Brown, D.G., Goovaerts, P., 2010. Propagating error in land-cover-change analyses: impact of temporal dependence under increased thematic complexity. 24, 1043–1060. https://doi.org/10.1080/13658810903279008.

Chartzoulakis, K., Bertaki, M., 2015. Sustainable Water Management in Agriculture under Climate Change. Agriculture and Agricultural Science Procedia 4, 88–98. https://doi.org/10.1016/J.AASPRO.2015.03.011

Cheung, W.H., Senay, G.B., Singh, A., 2008. Trends and spatial distribution of annual and seasonal rainfall in Ethiopia. International Journal of Climatology 28, 1723–1734. https://doi.org/10.1002/JOC.1623.

Chowdhury, M., Hasan, M.E., Abdullah-Al-Mamun, M.M., 2020. Land use/land cover change assessment of Halda watershed using remote sensing and GIS. The Egyptian Journal of Remote Sensing and Space Science 23, 63–75. https://doi.org/10.1016/J.EJRS.2018.11.003.

Christensen, O.B., Drews, M., Dethloff, K., Ketelsen, K., Hebestadt, I., Rinke, A., 2007. Technical report 06-17 the HIRHAM regional climate model version 5 ($β$) Jens Hesselbjerg Christensen Danish climate Centre, DMI Foundation Polar Marine Res. Colophon 5 (January) (2007) 1–22. Danish Meteorol. Inst., Copenhagen, Denmark.

Chu, X. lei, Lu, Z., Wei, D., Lei, G. ping, 2022. Effects of land use/cover change (LUCC) on the spatiotemporal variability of precipitation and temperature in the Songnen Plain, China. J Integr Agric 21, 235–248. https://doi.org/10.1016/S2095-3119(20)63495-5

Church, M., 2006. Bed material transport and the morphology of alluvial river channels. Annu Rev Earth Planet Sci. https://doi.org/10.1146/annurev.earth.33.092203.122721

Cole, L.J., Stockan, J., Helliwell, R., 2020. Managing riparian buffer strips to optimise ecosystem services: A review. Agric Ecosyst Environ 296, 106891. https://doi.org/10.1016/J.AGEE.2020.106891

Comenetz, J., Caviedes, C., 2002. Climate variability, political crises, and historical population displacements in Ethiopia. Global Environmental Change Part B: Environmental Hazards 4, 113–127. https://doi.org/10.1016/J.HAZARDS.2003.08.001.

Conway, D., Schipper, E.L.F., 2011. Adaptation to climate change in Africa: Challenges and opportunities identified from Ethiopia. Global Environmental Change 21, 227–237. https://doi.org/10.1016/J.GLOENVCHA.2010.07.013.

Cowie, A.L., Orr, B.J., Castillo Sanchez, V.M., Chasek, P., Crossman, N.D., Erlewein, A., Louwagie, G., Maron, M., Metternicht, G.I., Minelli, S., Tengberg, A.E., Walter, S., Welton, S., 2018. Land in balance: The scientific conceptual framework for Land Degradation Neutrality. Environ Sci Policy 79, 25–35.

Dadi Belete, M., Diekkrüger, B., Roehrig, J., 2015. Characterization of Water Level Variability of the Main Ethiopian Rift Valley Lakes. https://doi.org/10.3390/hydrology3010001.

Dananto, M., Aga, A.O., Yohannes, P., Shura, L., 2022. Assessing the Water-Resources Potential and Soil Erosion Hotspot Areas for Sustainable Land Management in the Gidabo Watershed, Rift Valley Lake Basin of Ethiopia. Sustainability (Switzerland) 14. https://doi.org/10.3390/su14095262

Das, N., Mondal, P., Sutradhar, S., Ghosh, R., 2021. Assessment of variation of land use/land cover and its impact on land surface temperature of Asansol subdivision. The Egyptian Journal of Remote Sensing and Space Science 24, 131–149.

https://doi.org/10.1016/J.EJRS.2020.05.001.

de Blécourt, M., Gröngröft, A., Baumann, S., Eschenbach, A., 2019. Losses in soil organic carbon stocks and soil fertility due to deforestation for low-input agriculture in semi-arid southern Africa. J Arid Environ 165, 88–96. https://doi.org/10.1016/J.JARIDENV.2019.02.006

de Nijs, E.A., Cammeraat, E.L.H., 2020. The stability and fate of Soil Organic Carbon during the transport phase of soil erosion. Earth Sci Rev 201, 103067. https://doi.org/10.1016/J.EARSCIREV.2019.103067

Degefa, S., 2007. Home garden agroforestry practices in the Gedeo zone, Ethiopia: a sustainable land management system for socio-ecological benefits. Socio-ecological Production Landscapes and Seascapes (SEPLS) in Africa.

Degefu, M.A., Rowell, D.P., Bewket, W., 2017. Teleconnections between Ethiopian rainfall variability and global SSTs: observations and methods for model evaluation. Meteorology and Atmospheric Physics 129, 173–186. https://doi.org/10.1007/S00703-016-0466-9.

Demessie, S.F., Dile, Y.T., Bedadi, B. et al., 2023. "Evaluations of regional climate models for simulating precipitation and temperature over the Guder sub-basin of Upper Blue Nile Basin, Ethiopia". Model. Earth Syst. Environ. 9, 4455–4476 (2023). https://doi.org/10.1007/s40808-023-01751-0

Demissie, T.A., Sime, C.H., 2021. Assessment of the performance of CORDEX regional climate models in simulating rainfall and air temperature over southwest Ethiopia. Heliyon 7. https://doi.org/10.1016/j.heliyon.2021.e07791.

Desta, H., Fetene, A., 2020. Land-use and land-cover change in Lake Ziway watershed of the Ethiopian Central Rift Valley Region and its environmental impacts. Land use policy 96. https://doi.org/10.1016/J.LANDUSEPOL.2020.104682.

Desta, H.B., Belayneh, M.Z., 2021. Dam breach analysis: a case of Gidabo dam, Southern Ethiopia. International Journal of Environmental Science and Technology 18, 107–122. https://doi.org/10.1007/S13762-020-03008-0/METRICS.

Dey, N.N., al Rakib, A., Kafy, A.- al, Raikwar, V., 2021. Geospatial modelling of changes in land use/land cover dynamics using Multi-layer perception Markov chain model in Rajshahi City, Bangladesh. Environmental Challenges 4, 100148. https://doi.org/10.1016/J.ENVC.2021.100148.

Dhankhar, N., Kumar, J., 2023. Impact of increasing pesticides and fertilizers on human health: A review. Mater Today Proc. https://doi.org/10.1016/J.MATPR.2023.03.766

Dibaba, W.T., Miegel, K., Demissie, T.A., 2019. Evaluation of the CORDEX regional climate models performance in simulating climate conditions of two catchments in Upper Blue Nile Basin. Dynamics of Atmospheres and Oceans 87, 101104. https://doi.org/10.1016/J.DYNATMOCE.2019.101104.

Dibike, Y.B., Gachon, P., St-Hilaire, A., Ouarda, T.B.M.J., Nguyen, V.T.V., 2007. Uncertainty analysis of statistically downscaled temperature and precipitation regimes in Northern Canada. Theoretical and Applied Climatology 2007 91:1 91, 149–170. https://doi.org/10.1007/S00704-007-0299-Z.

Diro, G.T., Grimes, D.I.F., Black, E., 2011. Teleconnections between Ethiopian summer rainfall and sea surface temperature: Part I-observation and modelling. Climate Dynamics 37, 103–119. https://doi.org/10.1007/S00382-010-0837-8.

dos Santos, F.M., de Souza Pelinson, N., de Oliveira, R.P., Di Lollo, J.A., 2023. Using the SWAT model to identify erosion prone areas and to estimate soil loss and sediment transport in Mogi Guaçu River basin in Sao Paulo State, Brazil. Catena (Amst) 222. https://doi.org/10.1016/j.catena.2022.106872

Du, X., Jian, J., Du, C., Stewart, R.D., 2022. Conservation management decreases surface runoff and soil erosion. International Soil and Water Conservation Research 10, 188–196. https://doi.org/10.1016/J.ISWCR.2021.08.001

Dutta, S. Soil erosion, sediment yield and sedimentation of reservoir: a review. Model. Earth Syst. Environ. 2, 123 (2016). https://doi.org/10.1007/s40808-016-0182-y.

Eastman, J.R., 2016a. TerrSet Manual, Geospatial Monitoring and Modeling System. Clark University, Worcester, USA. Clark University, Worcester, USA. http://www.clarklabs.org/

Eastman, J.R., 2016b. TerrSet Tutorial, Geospatial Monitoring and Modeling System. Clark University, Worcester, USA. http://www.clarklabs.org/ (accessed 8.22.21).

Ebabu, K., Taye, G., Tsunekawa, A., Haregeweyn, N., Adgo, E., Tsubo, M., Fenta, A.A., Meshesha, D.T., Sultan, D., Aklog, D., Admasu, T., van Wesemael, B., Poesen, J., 2023. Land use, management and climate effects on runoff and soil loss responses in the highlands of Ethiopia. J Environ Manage 326. https://doi.org/10.1016/j.jenvman.2022.116707.

Eekhout, J.P.C., de Vente, J., 2022. Global impact of climate change on soil erosion and potential for adaptation through soil conservation. Earth Sci Rev 226, 103921. https://doi.org/10.1016/J.EARSCIREV.2022.103921

Ekeu-wei, I.T., Blackburn, G.A., Pedruco, P., 2018. Infilling Missing Data in Hydrology: Solutions Using Satellite Radar Altimetry and Multiple Imputation for Data-Sparse Regions. Water 2018, 10, 1483. https://doi.org/10.3390/w10101483.

Elçiçek, H., Akdoğan, E., Karagöz, S., 2014. The use of artificial neural network for prediction of dissolution kinetics. Scientific World Journal 2014. https://doi.org/10.1155/2014/194874.

Elzeiny, R., Khadr, M., Zahran, S., & Rashwan, E. (2019). Homogeneity Analysis of Rainfall Series in the Upper Blue Nile River Basin, Ethiopia. Journal of Engineering Research, 3(September), 46-53. doi: 10.21608/erjeng.2019.125704

Endris, H.S., Omondi, P., Jain, S., Lennard, C., Hewitson, B., Chang'a, L., Awange, J.L., Dosio, A., Ketiem, P., Nikulin, G., Panitz, H.J., Büchner, M., Stordal, F., Tazalika, L., 2013. Assessment of the performance of CORDEX regional climate models in simulating East Africa rainfall. J Clim 26:8453-8475. https://doi.org/10.1175/JCLI-D-12-00708.1.

Etsay, H., Negash, T., Aregay, M., 2019. Factors that influence the implementation of sustainable land management practices by rural households in Tigrai region, Ethiopia. Ecol Process 8, 1–16. https://doi.org/10.1186/S13717-019-0166-8/TABLES/9.

FAO & IIASA, 2023. Harmonized World Soil Database version 2.0. FAO: Rome, Itaiy; IIASA: Laxenburg. https://doi.org/10.4060/cc3823en.

FAO, 2016. Manual for local level assessment of land degradation and sustainable land management - Part 1. Planning and methodological approach, analysis and reporting. https://landportal.org/node/48851 (accessed 8.30.23).

FAO 2017. Sustainable Land Management (SLM) in practice in the Kagera Basin. Lessons learned for scaling up at landscape level - Results of the Kagera Transboundary Agro-ecosystem Management Project. FAO, Rome, Italy. 440 pp.

FAO-UNESCO, 1988. Soils Map of the World: Revised Legend; FAO-UNESCO: Rome, Italy.

Feng, S., Zhao, W., Zhan, T., Yan, Y., Pereira, P., 2022. Land degradation neutrality: A review of progress and perspectives. Ecol Indic 144. https://doi.org/10.1016/j.ecolind.2022.109530

Fenta, A.A., Tsunekawa, A., Haregeweyn, N., Tsubo, M., Yasuda, H., Kawai, T., Ebabu, K., Berihun, M.L., Belay, A.S., Sultan, D., 2021. Agroecology-based soil erosion assessment for better conservation planning in Ethiopian river basins. Environ Res 195, 110786. https://doi.org/10.1016/J.ENVRES.2021.110786

Fetahi, T., 2019. Eutrophication of Ethiopian water bodies: a serious threat to water quality, biodiversity and public health. Afr J Aquat Sci 44, 303–312. https://doi.org/10.2989/16085914.2019.1663722

Flato, G., J. Marotzke, B. Abiodun, P. Braconnot, S.C. Chou, W. Collins, P. Cox, F. Driouech, S. Emori, V. Eyring, C. Forest, P. Gleckler, E. Guilyardi, C. Jakob, V. Kattsov, C. Reason and M. Rummukainen, 2013: Evaluation of Climate Models. In: Climate Change 2013: The Physical Science Basis. Contribution of Working Group I to the Fifth Assessment Report of the Intergovernmental Panel on Climate Change.

Gadissa, T., Nyadawa, M., Behulu, F., Mutua, B., 2018. The effect of climate change on loss of lake volume: Case of sedimentation in Central Rift Valley Basin, Ethiopia. Hydrology 5. https://doi.org/10.3390/hydrology5040067

Gan, T.Y., 1998. Hydroclimatic trends and possible climatic warming in the Canadian Prairies. Water Resources Research 34, 3009–3015. https://doi.org/10.1029/98WR01265.

Gao, P., Li, P., Zhao, B., Xu, R., Zhao, G., Sun, W., Mu, X., 2017. Use of double mass curves in hydrologic benefit evaluations. Hydrol Process 31. https://doi.org/10.1002/hyp.11377

Gao, X., Yan, C., Wang, Y., Zhao, X., Zhao, Y., Sun, M., Peng, S., 2020. Attribution analysis of climatic and multiple anthropogenic causes of runoff change in the Loess Plateau—A case-study of the Jing River Basin. Land Degrad Dev 31. https://doi.org/10.1002/ldr.3557

García, C.L., Teich, I., Gonzalez-Roglich, M., Kindgard, A.F., Ravelo, A.C., Liniger, H., 2019. Land degradation assessment in the Argentinean Puna: Comparing expert knowledge with satellite-derived information. Environ Sci Policy 91. https://doi.org/10.1016/j.envsci.2018.10.018

Garedew, E., Sandewall, M., Söderberg, U., Campbell, B.M., 2009. Land-Use and Land-Cover Dynamics in the Central Rift Valley of Ethiopia. Environmental Management 2009 44:4 44, 683–694. https://doi.org/10.1007/S00267-009-9355-Z

Garg, K.K., Anantha, K.H., Dixit, S., Nune, R., Venkataradha, A., Wable, P., Budama, N., Singh, R., 2022. Impact of raised beds on surface runoff and soil loss in Alfisols and Vertisols. Catena (Amst) 211. https://doi.org/10.1016/j.catena.2021.105972

Gashaw, T., Dile, Y.T., Worqlul, A.W., Bantider, A., Zeleke, G., Bewket, W., Alamirew, T., 2021. Evaluating the Effectiveness of Best Management Practices on Soil Erosion Reduction Using the SWAT Model: for the Case of Gumara Watershed, Abbay (Upper Blue Nile) Basin. Environ Manage 68, 240–261. https://doi.org/10.1007/S00267-021-01492-9/METRICS.

Gashaw, T., Tulu, T., Argaw, M., Worqlul, A.W., 2017. Evaluation and prediction of land use/land cover changes in the Andassa watershed, Blue Nile Basin, Ethiopia. Environmental Systems Research 2017 6:1 6, 1–15. https://doi.org/10.1186/S40068-017-0094-5

Gashaw, T., Worqlul, A.W., Dile, Y.T., Addisu, S., Bantider, A., Zeleke, G., 2020. Evaluating potential impacts of land management practices on soil erosion in the Gilgel Abay watershed, upper Blue Nile basin. Heliyon 6. https://doi.org/10.1016/j.heliyon.2020.e04777.

Gaur, S., Singh, R., 2023. A Comprehensive Review on Land Use/Land Cover (LULC) Change Modeling for Urban Development: Current Status and Future Prospects. Sustainability 15.

Gebreslassie, H., 2014. Land Use-Land Cover dynamics of Huluka watershed, Central Rift Valley, Ethiopia. International Soil and Water Conservation Research 2, 25–33. https://doi.org/10.1016/S2095-6339(15)30055-1

Getahun, Y.S., Li, M.H., Pun, I.F., 2021. Trend and change-point detection analyses of rainfall and temperature over the Awash River basin of Ethiopia. Heliyon 7. https://doi.org/10.1016/J.HELIYON.2021.E08024.

Gezie, M., 2019. Farmer's response to climate change and variability in Ethiopia: A review. 5. https://doi.org/10.1080/23311932.2019.1613770.

Gharaibeh, A., Shaamala, A., Obeidat, R., Al-Kofahi, S., 2020. Improving land-use change modeling by integrating ANN with Cellular Automata-Markov Chain model. Heliyon 6, e05092. https://doi.org/10.1016/J.HELIYON.2020.E05092.

Gibbs, H.K., Salmon, J.M., 2015. Mapping the world's degraded lands. Applied Geography 57, 12–21. https://doi.org/10.1016/J.APGEOG.2014.11.024

Gidey, E., Dikinya, O., Sebego, R., Segosebe, E., Zenebe, A., 2017. Cellular automata and Markov Chain (CA_Markov) model-based predictions of future land use and land cover scenarios (2015–2033) in Raya, northern Ethiopia. Modeling Earth Systems and Environment 2017 3:4 3, 1245–1262. https://doi.org/10.1007/S40808-017-0397-6

Giorgi, F., Gutowski, W.J., 2015. Regional Dynamical Downscaling and the CORDEX Initiative. http://dx.doi.org/10.1146/annurev-environ-102014-021217 40, 467–490. https://doi.org/10.1146/ANNUREV-ENVIRON-102014-021217.

Giri, S., Arbab, N.N., Lathrop, R.G., 2019. Assessing the potential impacts of climate and land use change on water fluxes and sediment transport in a loosely coupled system. J Hydrol (Amst) 577. https://doi.org/10.1016/j.jhydrol.2019.123955

Girma, R., Fürst, C., Moges, A., 2022a. Land use land cover change modeling by integrating artificial neural network with cellular Automata-Markov chain model in Gidabo river basin, main Ethiopian rift. Environmental Challenges 6, 100419. https://doi.org/10.1016/J.ENVC.2021.100419

Girma, R., Fürst, C., Moges, A., 2022b. Performance evaluation of CORDEX-Africa regional climate models in simulating climate variables over Ethiopian main rift valley: Evidence from Gidabo river basin for impact modeling studies. Dynamics of Atmospheres and

Oceans 99. https://doi.org/10.1016/j.dynatmoce.2022.101317

Gissila, T., Black, E., … D.G.-I.J. of, 2004, undefined, 2004. Seasonal forecasting of the Ethiopian summer rains. Wiley Online Library 24, 1345–1358. https://doi.org/10.1002/joc.1078.

Giuliani, G., Chatenoux, B., Benvenuti, A., Lacroix, P., Santoro, M., Mazzetti, P., 2020. Monitoring land degradation at national level using satellite Earth Observation time-series data to support SDG15–exploring the potential of data cube. Big Earth Data 4. https://doi.org/10.1080/20964471.2020.1711633

Godde, C.M., Mason-D'Croz, D., Mayberry, D.E., Thornton, P.K., Herrero, M., 2021. Impacts of climate change on the livestock food supply chain; a review of the evidence. Glob Food Sec 28, 100488. https://doi.org/10.1016/J.GFS.2020.100488

Grillakis, M.G., 2019. Increase in severe and extreme soil moisture droughts for Europe under climate change. Science of The Total Environment 660, 1245–1255. https://doi.org/10.1016/J.SCITOTENV.2019.01.001

Guan, D.J., Li, H.F., Inohae, T., Su, W., Nagaie, T., Hokao, K., 2011. Modeling urban land use change by the integration of cellular automaton and Markov model. Ecol Modell 222, 3761–3772. https://doi.org/10.1016/J.ECOLMODEL.2011.09.009

Guduru, J.U., Jilo, N.B., 2023. Assessment of rainfall-induced soil erosion rate and severity analysis for prioritization of conservation measures using RUSLE and Multi-Criteria Evaluations Technique at Gidabo watershed, Rift Valley Basin, Ethiopia. Ecohydrology and Hydrobiology 23. https://doi.org/10.1016/j.ecohyd.2022.09.002

Halmy, M.W.A., Gessler, P.E., Hicke, J.A., Salem, B.B., 2015. Land use/land cover change detection and prediction in the north-western coastal desert of Egypt using Markov-CA. Applied Geography 63, 101–112. https://doi.org/10.1016/J.APGEOG.2015.06.015

Hamad, R., Balzter, H., Kolo, K., 2018. Predicting Land Use/Land Cover Changes Using a CA-Markov Model under Two Different Scenarios. Sustainability 2018, Vol. 10, Page 3421 10, 3421. https://doi.org/10.3390/SU10103421

Hamadalnel, M., Zhu, Z., Gaber, A., Iyakaremye, V., Ayugi, B., 2022b. Possible changes in Sudan's future precipitation under the high and medium emission scenarios based on bias adjusted GCMs. Atmospheric Research, (2022), 106036269. https://doi.org/10.1016/j.atmosres.2022.106036.

Hamadalnel, M., Zhu, Z., Lu, R., Almazroui, M., Shahid, S., 2022a. Evaluating the Aptitude of GCMs from CMIP5 and CMIP6 in Capturing the Historical Observations of Monsoon Rainfall over Sudan from 1946-2005. International Journal of Climatology, (2022), 2717-

2738, 42(5). https://doi.org/10.1002/joc.7387.

Hamadalnel, M., Zhu, Z., Lu, R., Shahid, S., Ali, M., Abdalla, I., Elkanzi, M., Bilal, M., Bleiweiss, M., 2021. Spatio-temporal Investigations of Monsoon Precipitation and Its Historical and Future Trend over Sudan. Earth Syst Environ 5, 519–529 (2021). https://doi.org/10.1007/s41748-021-00236-3.

Hamed, K.H., 2008. Trend detection in hydrologic data: The Mann–Kendall trend test under the scaling hypothesis. Journal of Hydrology (349), 350-363. https://doi.org/10.1016/j.jhydrol.2007.11.009.

Haregeweyn, N., Tsunekawa, A., Nyssen, J., Poesen, J., Tsubo, M., Tsegaye Meshesha, D., Schütt, B., Adgo, E., Tegegne, F., 2015. Soil erosion and conservation in Ethiopia. 39, 750–774. https://doi.org/10.1177/0309133315598725

Haregeweyn, N., Tsunekawa, A., Tsubo, M., Fenta, A.A., Ebabu, K., Vanmaercke, M., Borrelli, P., Panagos, P., Berihun, M.L., Langendoen, E.J., Nigussie, Z., Setargie, T.A., Maurice, B.N., Minichil, T., Elias, A., Sun, J., Poesen, J., 2023. Progress and challenges in sustainable land management initiatives: A global review. Science of The Total Environment 858, 160027. https://doi.org/10.1016/J.SCITOTENV.2022.160027.

Hassan, Z., Shabbir, R., Ahmad, S.S., Malik, A.H., Aziz, N., Butt, A., Erum, S., 2016. Dynamics of land use and land cover change (LULCC) using geospatial techniques: a case study of Islamabad Pakistan. SpringerPlus 2016 5:1 5, 1–11. https://doi.org/10.1186/S40064-016-2414-Z

Hassen, G., Bantider, A., Legesse, A., and Maimbo, M., 2021c. The Effect of Soil and Water Conservation Structures on the Soil Physical and Chemical Properties in the Gidabo River Sub-basin, Ethiopian Rift Valley," International Journal of Environmental Science and Development vol. 12, no. 12, pp. 363-371, 2021.

Hassen, G., Bantider, A., Legesse, A., Maimbo, M. and Likissa, D., 2021a. Land Use and Land Cover Change for Resilient Environment and Sustainable Development in the Ethiopian Rift Valley Region. Environmental Protection and Natural Resources. 32. 1-18. https://doi.org/10.2478/oszn-2021-0007.

Hassen, G., Bantider, A., Legesse, A., Maimbo, M., 2021b. Assessment of Design and Constraints of Physical Soil and Water Conservation Structures in respect to the standard in the case of Gidabo sub-basin, Ethiopia, Cogent Food & Agriculture, 7:1, 1855818, https://doi.org/10.1080/23311932.2020.1855818.

Hermans, K., McLeman, R., 2021. Climate change, drought, land degradation and migration: exploring the linkages. Curr Opin Environ Sustain 50, 236–244. https://doi.org/10.1016/J.COSUST.2021.04.013

Hermans, K., Müller, D., O'Byrne, D., Olsson, L., Stringer, L.C., 2023. Land degradation and migration. Nature Sustainability 2023 1–3. https://doi.org/10.1038/s41893-023-01231-4

Hishe, S., Bewket, W., Nyssen, J., Lyimo, J., 2019. Analysing past land use land cover change and CA-Markov-based future modelling in the Middle Suluh Valley, Northern Ethiopia. 35, 225–255. https://doi.org/10.1080/10106049.2018.1516241

Houghton, R.A., 2018. Interactions Between Land-Use Change and Climate-Carbon Cycle Feedbacks. Current Climate Change Reports 2018 4:2 4, 115–127. https://doi.org/10.1007/S40641-018-0099-9

Hsieh, Y.P., 2022. A field technology for soil erosion research: Conceptual analysis and preliminary results. Catena 210, 105924. https://doi.org/10.1016/J.CATENA.2021.105924

Hurni, H., Berhe, W.A., Chadhokar, P., Daniel, D., Gete, Z., Grunder, M., Kassaye, G., 2016. Soil and Water Conservation in Ethiopia: Guidelines for Development Agents. Ministry of Agriculture (MoA): Addis Ababa, Ethiopia

Hurni, K., Zeleke, G., Kassie, M., Tegegne, B., Kassawmar, T., Teferi, E., Amdihun, A., Mekuriaw, A., Debele, B., Deichert, G., Hurni, H., Schauer, M., 2015. Economics of Land Degradation (ELD) Ethiopia Case Study: Soil degradation and sustainable land management in the rainfed agricultural areas of Ethiopia.

Hurteau, M.D., 2021. The role of forests in the carbon cycle and in climate change. Climate Change: Observed Impacts on Planet Earth, Third Edition 561–579. https://doi.org/10.1016/B978-0-12-821575-3.00027-X

Huss, C.P., Holmes, K.D., Blubaugh, C.K., 2022. Benefits and Risks of Intercropping for Crop Resilience and Pest Management. J Econ Entomol 115, 1350–1362. https://doi.org/10.1093/JEE/TOAC045

IPBES, 2018. The IPBES assessment report on Land degradation and restoration. Montanarella, L., Scholes, R., and Brainich, A. (eds.)., Secretariat of the Intergovernmental Science-Policy Platform on Biodiversity and Ecosystem Services.

IPCC, 2007. Climate change 2007 impacts adaptation and vulnerability working group ii contribution fourth assessment report IPCC | Climatology and climate change | Cambridge University Press.

IPCC, 2014a. Climate Change 2014: Impacts, Adaptation and Vulnerability. Chapter 22, Africa.

IPCC, 2014b. Climate Change 2014: Synthesis Report of the IPCC Fifth Assessment Report

(AR5) | weADAPT | Climate change adaptation planning, research and practice https://www.weadapt.org/knowledge-base/national-adaptation-planning/climate-change-2014-synthesis-report.

IPCC, 2022. Land–climate interactions. In: Climate Change and Land: an IPCC special report on climate change, desertification, land degradation, sustainable land management, food security, and greenhouse gas fluxes in terrestrial ecosystems, in: Climate Change and Land.

IPCC, 2023. Sections. In Climate Change 2023: Synthesis Report. Contribution of Working Groups I, II and III to the Sixth Assessment Report of the Intergovernmental Panel on Climate Change; Core Writing Team, Lee, H., Romero, J., Eds.; IPCC: Geneva, Switzerland.

Islam, K., Jashimuddin, M., Nath, B., Nath, T.K., 2018. Land use classification and change detection by using multi-temporal remotely sensed imagery: The case of Chunati wildlife sanctuary, Bangladesh. The Egyptian Journal of Remote Sensing and Space Science 21, 37–47. https://doi.org/10.1016/J.EJRS.2016.12.005

Ivetić, V., 2021. Reforestation and Sustainable Development. In: Leal Filho, W., Azul, A.M., Brandli, L., Lange Salvia, A., Wall, T. (eds) Life on Land. Encyclopedia of the UN Sustainable Development Goals. Springer, Cham. https://doi.org/10.1007/978-3-319-95981-8_31

Jia, S., Yang, C., Wang, M., Failler, P., 2022. Heterogeneous Impact of Land-Use on Climate Change: Study from a Spatial Perspective. Front Environ Sci 10, 840603. https://doi.org/10.3389/FENVS.2022.840603/BIBTEX

Kafy, A. al, Rahman, M.S., Faisal, A. al, Hasan, M.M., Islam, M., 2020. Modelling future land use land cover changes and their impacts on land surface temperatures in Rajshahi, Bangladesh. Remote Sens Appl 18, 100314. https://doi.org/10.1016/J.RSASE.2020.100314

Kafy, A.-A., Naim, Md.N.H., Subramanyam, G., Faisal, A.-A.-, Ahmed, N.U., Rakib, A. al, Kona, M.A., Sattar, G.S., 2021. Cellular Automata approach in dynamic modelling of land cover changes using RapidEye images in Dhaka, Bangladesh. Environmental Challenges 4, 100084. https://doi.org/10.1016/J.ENVC.2021.100084

Kantakumar, L.N., Neelamsetti, P., 2015. Multi-temporal land use classification using hybrid approach. Egyptian Journal of Remote Sensing and Space Science 18, 289–295. https://doi.org/10.1016/J.EJRS.2015.09.003

Kassawmar, T., Zeleke, G., Bantider, A., Desta Gessesse, G., Abraha, L., 2018. A synoptic land change assessment of Ethiopia's Rainfed Agricultural Area for evidence-based agricultural ecosystem management. cell.comT Kassawmar, G Zeleke, A Bantider, GD Gessesse, L AbrahaHeliyon, 2018•cell.com 4, e00914. https://doi.org/10.1016/j.heliyon.2018.

Kassaye, A.Y., Shao, G., Wang, X., Wu, S., 2020. Quantification of drought severity change in Ethiopia during 1952–2017. Environment, Development and Sustainability 2020 23:4 23, 5096–5121. https://doi.org/10.1007/S10668-020-00805-Y.

Kassie, B.T., Rötter, R.P., Hengsdijk, H., Asseng, S., van Ittersum, M.K., Kahiluoto, H., van Keulen, H., 2014. Climate variability and change in the Central Rift Valley of Ethiopia: challenges for rainfed crop production. The Journal of Agricultural Science 152, 58–74. https://doi.org/10.1017/S0021859612000986.

Keesstra, S., Nunes, J.P., Saco, P., Parsons, T., Poeppl, R., Masselink, R., Cerdà, A., 2018. The way forward: Can connectivity be useful to design better measuring and modelling schemes for water and sediment dynamics? Science of The Total Environment 644, 1557–1572. https://doi.org/10.1016/J.SCITOTENV.2018.06.342

Kendall, M.G., 1975. Rank correlation methods, 4th edn. Charles Griffin, London.

Khan, M.S., Ullah, S., Sun, T., Rehman, A.U., Chen, L., 2020. Land-Use/Land-Cover Changes and Its Contribution to Urban Heat Island: A Case Study of Islamabad, Pakistan. Sustainability 2020, Vol. 12, Page 3861 12, 3861. https://doi.org/10.3390/SU12093861

Kidane, M., Bezie, A., Kesete, N., Tolessa, T., 2019. The impact of land use and land cover (LULC) dynamics on soil erosion and sediment yield in Ethiopia. Heliyon 5, e02981. https://doi.org/10.1016/J.HELIYON.2019.E02981

Killeen, P.G., Mwenifumbo, C.J., Ford, K.L., 2015. Tools and Techniques: Radiometric Methods. Treatise on Geophysics: Second Edition 11, 447–524. https://doi.org/10.1016/B978-0-444-53802-4.00209-8

Kim, J., Waliser, D.E., Mattmann, C.A., Goodale, C.E., Hart, A.F., Zimdars, P.A., Crichton, D.J., Jones, C., Nikulin, G., Hewitson, B., Jack, C., Lennard, C., Favre, A., 2013. Evaluation of the CORDEX-Africa multi-RCM hindcast: systematic model errors. Climate Dynamics 2013 42:5 42, 1189–1202. https://doi.org/10.1007/S00382-013-1751-7.

Kim, Y., Newman, G., Güneralp, B., 2020. A Review of Driving Factors, Scenarios, and Topics in Urban Land Change Models. Land 2020, Vol. 9, Page 246 9, 246. https://doi.org/10.3390/LAND9080246.

Kindu, M., Schneider, T., Teketay, D., Knoke, T., 2013. Land Use/Land Cover Change Analysis Using Object-Based Classification Approach in Munessa-Shashemene Landscape of the Ethiopian Highlands. Remote Sensing 2013, Vol. 5, Pages 2411-2435 5, 2411–2435. https://doi.org/10.3390/RS5052411

Kirui, O.K., Mirzabaev, A., von Braun, J., 2021. Assessment of land degradation 'on the ground' and from 'above.' SN Appl Sci 3. https://doi.org/10.1007/s42452-021-04314-z

Kisembe, J., Favre, A., Dosio, A., Lennard, C., Sabiiti, G., Nimusiima, A., 2019. Evaluation of rainfall simulations over Uganda in CORDEX regional climate models. Theoretical and Applied Climatology 137, 1117–1134. https://doi.org/10.1007/S00704-018-2643-X/FIGURES/7.

Kjelland, M.E., Woodley, C.M., Swannack, T.M., Smith, D.L., 2015. A review of the potential effects of suspended sediment on fishes: potential dredging-related physiological, behavioral, and transgenerational implications. Environ Syst Decis 35, 334–350. https://doi.org/10.1007/S10669-015-9557-2/FIGURES/1

Konapala, G., Mishra, A.K., Wada, Y., 2020. Climate change will affect global water availability through compounding changes in seasonal precipitation and evaporation. Nat Commun 11, 3044 (2020). https://doi.org/10.1038/s41467-020-16757-w.

Korecha, D., Sorteberg, A., 2013. Validation of operational seasonal rainfall forecast in Ethiopia. Water Resources Research 49, 7681–7697. https://doi.org/10.1002/2013WR013760.

Kumar, M., Denis, D.M., Kundu, A. et al., 2022. Understanding land use/land cover and climate change impacts on hydrological components of Usri watershed, India. Appl Water Sci 12, 39 (2022). https://doi.org/10.1007/s13201-021-01547-6

Kumar, S., Radhakrishnan, N., Mathew, S., 2013. Geomatics, Natural Hazards and Risk Land use change modelling using a Markov model and remote sensing Land use change modelling using a Markov model and remote sensing.

Kura, A.L., Beyene, D.L., 2020. Cellular automata Markov chain model based deforestation modelling in the pastoral and agro-pastoral areas of southern Ethiopia. Remote Sens Appl 18. https://doi.org/10.1016/J.RSASE.2020.100321

Kusunoki, S., Arakawa, O., 2015. Are CMIP5 Models Better than CMIP3 Models in Simulating Precipitation over East Asia? Journal of Climate 28, 5601–5621. https://doi.org/10.1175/JCLI-D-14-00585.1.

Kusunoki, S., Yoshimura, J., Yoshimura, H., Noda, A., Oouchi, K., Mizuta, R., 2006. Change of Baiu Rain Band in Global Warming Projection by an Atmospheric General Circulation Model with a 20-km Grid Size. Journal of the Meteorological Society of Japan. Ser. II 84, 581–611. https://doi.org/10.2151/JMSJ.84.581.

Lakku, N.K.G., Behera, M.R., 2022. Skill and Inter-Model Comparison of Regional and Global Climate Models in Simulating Wind Speed over South Asian Domain. Climate 10, 85.

https://doi.org/10.3390/CLI10060085/S1

Lambe, B.T., Kundapura, S., 2021. Analysis of meteorological variability and tendency over Bilate basin of Rift Valley Lakes basins in Ethiopia. Arabian Journal of Geosciences 2021 14:23 14, 1–22. https://doi.org/10.1007/S12517-021-08962-8.

Lambin, E.F., Geist, H.J., Lepers, E., 2003. Dynamics of Land-Use and Land-Cover Change in Tropical Regions. https://doi.org/10.1146/annurev.energy.28.050302.105459 28, 205–241. https://doi.org/10.1146/ANNUREV.ENERGY.28.050302.105459

Lawler, J.J., Lewis, D.J., Nelson, E., Plantinga, A.J., Polasky, S., Withey, J.C., Helmers, D.P., Martinuzzi, S., Pennington, D., Radeloff, V.C., 2014. Projected land- use change impacts on ecosystem services in the United States. Proc. Natl. Acad. Sci. U.S.A. 111, 7492–7497. doi:10.1073/PNAS.1405557111.

Lehmann, E.L., 1975. Nonparametric, Statistical Methods Based on Ranks; Holden-Day Inc.: San Francisco, CA, USA.

Leisz, S.J., Rounds, E., An, N.T., Yen, N.T.B., Bang, T.N., Douangphachanh, S., Ninchaleune, B., 2016. Telecouplings in the east-west economic corridor within borders and across. Remote Sens (Basel) 8. https://doi.org/10.3390/RS8121012

Lemma, H., Frankl, A., van Griensven, A., Poesen, J., Adgo, E., Nyssen, J., 2019. Identifying erosion hotspots in Lake Tana Basin from a multisite Soil and Water Assessment Tool validation: Opportunity for land managers. Land Degrad Dev 30. https://doi.org/10.1002/ldr.3332

Lenhart, T., Eckhardt, K., Fohrer, N., Frede, H.G., 2002. Comparison of two different approaches of sensitivity analysis. Physics and Chemistry of the Earth 27, 645–654.

Leta, M.K., Demissie, T.A., Tränckner, J., 2021. Modeling and prediction of land use land cover change dynamics based on land change modeler (Lcm) in nashe watershed, upper blue nile basin, Ethiopia. Sustainability (Switzerland) 13. https://doi.org/10.3390/SU13073740

Leta, M.K., Waseem, M., Rehman, K., Tränckner, J., 2023. Sediment yield estimation and evaluating the best management practices in Nashe watershed, Blue Nile Basin, Ethiopia. Environ Monit Assess 195. https://doi.org/10.1007/s10661-023-11337-z

Li, C. hua, Wang, Y. kong, Ye, C., Wei, W. wei, Zheng, B. hui, Xu, B., 2019. A proposed delineation method for lake buffer zones in watersheds dominated by non-point source pollution. Science of The Total Environment 660, 32–39. https://doi.org/10.1016/J.SCITOTENV.2018.12.468

Li, Z., Fang, H., 2016. Impacts of climate change on water erosion: A review. Earth Sci Rev 163, 94–117. https://doi.org/10.1016/J.EARSCIREV.2016.10.004

Lorenz, K., Lal, R., 2018. Agricultural Land Use and the Global Carbon Cycle. In: Carbon Sequestration in Agricultural Ecosystems. Springer, Cham. https://doi.org/10.1007/978-3-319-92318-5_1.

Lu, X.X., Ran, L.S., Liu, S., Jiang, T., Zhang, S.R., Wang, J.J., 2013. Sediment loads response to climate change: A preliminary study of eight large Chinese rivers. International Journal of Sediment Research 28, 1–14. https://doi.org/10.1016/S1001-6279(13)60013-X

Luhunga, P., Botai, J., Kahimba, F., 2016. Evaluation of the performance of CORDEX regional climate models in simulating present climate conditions of Tanzania. Journal of Southern Hemisphere Earth Systems Science 66, 32–54. https://doi.org/10.22499/3.6601.005.

Ma, L., Li, M., Ma, X., Cheng, L., Du, P., Liu, Y., 2017. A review of supervised object-based land-cover image classification. ISPRS Journal of Photogrammetry and Remote Sensing 130, 277–293. https://doi.org/10.1016/J.ISPRSJPRS.2017.06.001

Ma, S., Wang, L.J., Jiang, J., Zhao, Y.G., 2023. Direct and indirect effects of agricultural expansion and landscape fragmentation processes on natural habitats. Agric Ecosyst Environ 353, 108555. https://doi.org/10.1016/J.AGEE.2023.108555

Ma, X., Zhao, C., Zhu, J., 2021. Aggravated risk of soil erosion with global warming – A global meta-analysis. Catena (Amst) 200, 105129. https://doi.org/10.1016/J.CATENA.2020.105129

Mahata, S., Sharma, V.N., 2021. The global problem of land degradation: A review. National Geographical Journal of India 67, 216–231. https://doi.org/10.48008/NGJI.1773

Mall, R.K., Gupta, A., Sonkar, G., 2017. Effect of Climate Change on Agricultural Crops. Current Developments in Biotechnology and Bioengineering: Crop Modification, Nutrition, and Food Production 23–46. https://doi.org/10.1016/B978-0-444-63661-4.00002-5

Mallick, J., Al-Wadi, H., Rahman, A., Ahmed, M., Abad Khan, R., 2016. Spatial variability of soil erodibility and its correlation with soil properties in semi-arid mountainous watershed, Saudi Arabia. Geocarto Int 31, 661–681. https://doi.org/10.1080/10106049.2015.1073368

Mana, T.T., Abebe, B.W., 2023. Assessment of hydro-meteorological regimes of Gidabo river basin under representative concentration pathway scenarios. Model Earth Syst Environ 9. https://doi.org/10.1007/s40808-022-01516-1

Mana, T.T., Abebe, B.W., Hatiye, S.D., 2023. Effect of climate change on reservoir water balance and irrigation water demand: a case of Gidabo irrigation project, Rift Valley Basin, Ethiopia. Environ Monit Assess 195, 1–27. https://doi.org/10.1007/S10661-023-11484-3/METRICS

Mander, Ü., Tournebize, J., Tonderski, K., Verhoeven, J.T.A., Mitsch, W.J., 2017. Planning and establishment principles for constructed wetlands and riparian buffer zones in agricultural catchments. Ecol Eng 103, 296–300. https://doi.org/10.1016/J.ECOLENG.2016.12.006

Mandrekar, J.N., 2010. Receiver Operating Characteristic Curve in Diagnostic Test Assessment. Journal of Thoracic Oncology 5, 1315–1316. https://doi.org/10.1097/JTO.0B013E3181EC173D

Mann, H.B., 1945. Nonparametric tests against trend. Econometrica 13(3):245-259.

Mas, J.F., Kolb, M., Paegelow, M., Camacho Olmedo, M.T., Houet, T., 2014. Inductive pattern-based land use/cover change models: A comparison of four software packages. Environmental Modelling & Software 51, 94–111. https://doi.org/10.1016/J.ENVSOFT.2013.09.010.

Mechal, A., Biruk, S., Winkler, G., Wagner, T., Mogessie, A., 2016. Characterizing regional groundwater flow in the Ethiopian rift: A multimodel approach applied to Gidabo river basin. Austrian Journal of Earth Sciences 109. https://doi.org/10.17738/AJES.2016.0005

Mechal, A., Wagner, T., Biruk, S., 2015. Recharge variability and sensitivity to climate: The example of Gidabo river basin, Main Ethiopian Rift. Journal of Hydrology: Regional Studies 4, 644–660. https://doi.org/10.1016/J.EJRH.2015.09.001

Mekonen, A.A., Berlie, A.B., 2019. Spatiotemporal variability and trends of rainfall and temperature in the Northeastern Highlands of Ethiopia. Modelling Earth Systems Environment 6, 285–300. https://doi.org/10.1007/s40808-019-00678-9.

Mekuria, W., Diyasa, M., Tengberg, A., Haileslassie, A., 2021. Effects of long-term land use and land cover changes on ecosystem service values: An example from the central rift valley, Ethiopia. Land (Basel) 10. https://doi.org/10.3390/land10121373

Mekuria, W., Mekonnen, K., Thorne, P., Bezabih, M., Tamene, L., Abera, W., 2018. Competition for land resources: driving forces and consequences in crop-livestock production systems of the Ethiopian highlands. Ecol Process 7, 1–15. https://doi.org/10.1186/S13717-018-0143-7/FIGURES/5

Mekuriaw, A., Heinimann, A., Zeleke, G., Hurni, H., 2018. Factors influencing the adoption of physical soil and water conservation practices in the Ethiopian highlands. International Soil and Water Conservation Research 6, 23–30. https://doi.org/10.1016/J.ISWCR.2017.12.006

Mengistu, A.G., Woldesenbet, T.A., Dile, Y.T., 2021. Evaluation of the performance of bias-corrected CORDEX regional climate models in reproducing Baro–Akobo basin climate. Theoretical and Applied Climatology 2021 144:1 144, 751–767.

https://doi.org/10.1007/S00704-021-03552-W.

Mengistu, F., Assefa, E., 2020. Towards sustaining watershed management practices in Ethiopia: A synthesis of local perception, community participation, adoption and livelihoods. Environ Sci Policy 112, 414–430. https://doi.org/10.1016/J.ENVSCI.2020.06.019

Mengistu, F., Assefa, E., 2021. Community participation in watershed management: analysis of the status and factors affecting community engagement in the upper Gibe basin, South West Ethiopia, Journal of Environmental Planning and Management, 64:2, 252-288, DOI: 10.1080/09640568.2020.1762550

Mera, G.A., 2018. Drought and its impacts in Ethiopia. Weather and Climate Extremes 22, 24–35. https://doi.org/10.1016/J.WACE.2018.10.002.

Mesfin, D., Simane, B., Belay, A., Recha, J.W., Taddese, H., 2020. Woodland cover change in the central rift valley of Ethiopia. Forests 11. https://doi.org/10.3390/F11090916

Meshesha, D.T., Tsunekawa, A., Tsubo, M., 2012. Continuing land degradation: Cause-effect in Ethiopia's Central Rift Valley. Land Degrad Dev 23. https://doi.org/10.1002/ldr.1061

Mi, J., Yang, Y., Zhang, S., An, S., Hou, H., Hua, Y., Chen, F., 2019. Tracking the Land Use/Land Cover Change in an Area with Underground Mining and Reforestation via Continuous Landsat Classification. Remote Sensing 2019, Vol. 11, Page 1719 11, 1719.

Mirabbasi, R., Ahmadi, F., Jhajharia, D., 2020. Comparison of parametric and non-parametric methods for trend identification in groundwater levels in Sirjan plain aquifer, Iran. Hydrology Research 2020; 51 (6): 1455–1477. doi: https://doi.org/10.2166/nh.2020.041.

Mishra, V.N., Rai, P.K., Prasad, R., Punia, M., Nistor, M.-M., 2018. Prediction of spatio-temporal land use/land cover dynamics in rapidly developing Varanasi district of Uttar Pradesh, India, using geospatial approach: a comparison of hybrid models. Applied Geomatics 2018 10:3 10, 257–276. https://doi.org/10.1007/S12518-018-0223-5

Moges, S.A., Gebregiorgis, A.S., 2013. Climate Vulnerability on the Water Resources Systems and Potential Adaptation Approaches in East Africa: The Case of Ethiopia, in: Climate Vulnerability: Understanding and Addressing Threats to Essential Resources. https://doi.org/10.1016/B978-0-12-384703-4.00517-7

Mohamed, A., Worku, H., 2020. Simulating urban land use and cover dynamics using cellular automata and Markov chain approach in Addis Ababa and the surrounding. Urban Clim 31. https://doi.org/10.1016/J.UCLIM.2019.100545

Mohammady, S., Delavar, M.R., Pahlavani, P., Mohammady, S., Delavar, M.R., Pahlavani, P., 2014. Urban Growth Modeling Using AN Artificial Neural Network a Case Study of

Sanandaj City, Iran. ISPAr XL2, 203–208. https://doi.org/10.5194/ISPRSARCHIVES-XL-2-W3-203-2014

Moriasi, D.N., Zeckoski, R.W., Arnold, J.G., Baffaut, C.B., Malone, R.W., Daggupati, P., Guzman, J.A., Saraswat, D., Yuan, Y., Wilson, B.W., Shirmohammadi, A., Douglas-Mankin, K.R., 2015. Hydrologic and water quality models: Key calibration and validation topics. Trans ASABE 58. https://doi.org/10.13031/trans.58.11075

Mosier, S., Córdova, S.C., Robertson, G.P., 2021. Restoring Soil Fertility on Degraded Lands to Meet Food, Fuel, and Climate Security Needs via Perennialization. Front Sustain Food Syst 5, 706142. https://doi.org/10.3389/FSUFS.2021.706142/BIBTEX

Mueller, E.N., Wainwright, J., Parsons, A.J., Turnbull, L., 2014. Land Degradation in Drylands: An Ecogeomorphological Approach. Patterns of Land Degradation in Drylands 1–9.

Mulugeta, S., Fedler, C., Ayana, M., 2019. Analysis of Long-Term Trends of Annual and Seasonal Rainfall in the Awash River Basin, Ethiopia. Water 2019, Vol. 11, Page 1498 11, 1498. https://doi.org/10.3390/W11071498.

Mutayoba, E., Kashaigili, J.J., 2017. Evaluation for the Performance of the CORDEX Regional Climate Models in Simulating Rainfall Characteristics over Mbarali River Catchment in the Rufiji Basin, Tanzania. Journal of Geoscience and Environment Protection 5, 139–151. https://doi.org/10.4236/GEP.2017.54011.

Nachtergaele, F.O.; van Velthuizen, H.; Verelst, L.; Wiberg, D.; Batjes, N.H.; Dijkshoorn, J.A.; van Engelen, V.W.P.; Fischer, G.; Jones, A.; Montanarella, L.; et al., 2012. Harmonized World Soil Database (Version 1.2); FAO and ISRIC: Rome, Italy.

Negasa, D.J., 2020. Major Constraints of Watershed Management Practices in Ethiopia and Ways Forward. http://www.sciencepublishinggroup.com 8, 70. https://doi.org/10.11648/J.IJEPP.20200804.11

Neitsch, S.L., Arnold, J.G., Kiniry, J.R., Williams, J.R., 2011. Soil & Water Assessment Tool Theoretical Documentation Version 2009. Texas Water Resources Institute. https://doi.org/10.1016/j.scitotenv.2015.11.063

Niang, I., Ruppel, O.C., Abdrabo, M.A., Essel, A., Lennard, C., Padgham, J., Urquhart, P., 2014. Africa. Climate Change 2014: Impacts, Adaptation and Vulnerability: Part B: Regional Aspects: Working Group II Contribution to the Fifth Assessment Report of the Intergovernmental Panel on Climate Change 1199–1266. https://doi.org/10.1017/CBO9781107415386.002.

Nikulin, G., Jones, C., Giorgi, F., Asrar, G., Büchner, M., Cerezo-Mota, R., Christensen, O. B., Déqué, M., Fernandez, J., Hänsler, A., van Meijgaard, E., Samuelsson, P., Sylla, M. B., &

Sushama, L., 2012. Precipitation Climatology in an Ensemble of CORDEX-Africa Regional Climate Simulations, Journal of Climate, 25(18), 6057-6078. https://doi.org/10.1175/JCLI-D-11-00375.1.

NMA, 2007. NMA: Climate change national adaptation programme.

NMSA, 1996. Climatic and Agroclimatic Resources of Ethiopia.

Nouri, J., Gharagozlou, A., Arjmandi, R., Faryadi, S., Adl, M., 2014. Predicting Urban Land Use Changes Using a CA–Markov Model. Arabian Journal for Science and Engineering 2014 39:7 39, 5565–5573. https://doi.org/10.1007/S13369-014-1119-2

Novara, A., Cerda, A., Barone, E., Gristina, L., 2021. Cover crop management and water conservation in vineyard and olive orchards. Soil Tillage Res 208, 104896.

Nyatuame, M., Amekudzi, L.K., Agodzo, S.K., 2020. Assessing the land use/land cover and climate change impact on water balance on Tordzie watershed. Remote Sens Appl 20. https://doi.org/10.1016/j.rsase.2020.100381

Nzuza, P., Ramoelo, A., Odindi, J., Kahinda, J.M., Madonsela, S., 2021. Predicting land degradation using Sentinel-2 and environmental variables in the Lepellane catchment of the Greater Sekhukhune District, South Africa. Physics and Chemistry of the Earth 124. https://doi.org/10.1016/j.pce.2020.102931

Okolo, C.C., Gebresamuel, G., Retta, A.N., Zenebe, A., Haile, M., 2019. Advances in quantifying soil organic carbon under different land uses in Ethiopia: a review and synthesis. Bull Natl Res Cent 43. https://doi.org/10.1186/s42269-019-0120-z

Onyutha, C., 2020. Analyses of rainfall extremes in East Africa based on observations from rain gauges and climate change simulations by CORDEX RCMs. Clim Dyn 54, 4841–4864 (2020). https://doi.org/10.1007/s00382-020-05264-9.

Onyutha, C., 2021. Graphical-statistical method to explore variability of hydrological time series. Hydrology Research (2021) 52 (1): 266-283. https://doi.org/10.2166/nh.2020.111.

Onyutha, C., 2022. A hydrological model skill score and revised R-squared. Hydrology Research (2022) 53 (1): 51-64. https://doi.org/10.2166/nh.2021.071.

Onyutha, C., Rutkowska, A., Nyeko-Ogiramoi, P., Willems, P., 2019. How well do climate models reproduce variability in observed rainfall? A case study of the Lake Victoria basin considering CMIP3, CMIP5 and CORDEX simulations. Stoch Environ Res Risk Assess 33, 687–707 (2019). https://doi.org/10.1007/s00477-018-1611-4.

Orr, B.J., Cowie, A.L., Castillo Sanchez, V.M., Chasek, P., Crossman, N.D., Erlewein, A., Louwagie, G., Maron, M., Metternicht, G.I., Minelli, S., et al., 2017. Scientific Conceptual Framework for Land Degradation Neutrality; A Report of the Science-Policy Interface;

United Nations Convention to Combat Desertification (UNCCD): Bonn, Germany

Osman, K.T., 2013. Physical Properties of Soil. Soils 49–65. https://doi.org/10.1007/978-94-007-5663-2_5

Öztopal, A., and Şen, Z., 2017. Innovative Trend Methodology Applications to Precipitation Records in Turkey. Water Resour Manage 31, 727–737 (2017). https://doi.org/10.1007/s11269-016-1343-5.

Panagos, P., Imeson, A., Meusburger, K., Borrelli, P., Poesen, J., Alewell, C., 2016. Soil Conservation in Europe: Wish or Reality? Land Degrad Dev 27, 1547–1551. https://doi.org/10.1002/LDR.2538

Pang, G., Wang, X., Chen, D., Yang, M., Liu, L., 2021. Evaluation of a climate simulation over the Yellow River Basin based on a regional climate model (REMO) within the CORDEX. Atmospheric Research 254, 105522. https://doi.org/10.1016/J.ATMOSRES.2021.105522.

Pimentel, D., Burgess, M., 2013. Soil Erosion Threatens Food Production. Agriculture 2013, Vol. 3, Pages 443-463 3, 443–463. https://doi.org/10.3390/AGRICULTURE3030443

Poesen, J., 2018. Soil erosion in the Anthropocene: Research needs. Earth Surf Process Landf 43, 64–84. https://doi.org/10.1002/ESP.4250

Prăvălie, R., 2021. Exploring the multiple land degradation pathways across the planet. Earth Sci Rev. https://doi.org/10.1016/j.earscirev.2021.103689

Pricope, N.G., Daldegan, G.A., Zvoleff, A., Mwenda, K.M., Noon, M., Lopez-Carr, D., 2023. Operationalizing an integrative socio-ecological framework in support of global monitoring of land degradation. Land Degrad Dev 34. https://doi.org/10.1002/ldr.4447

Qiu, J., Shen, Z., Hou, X., Xie, H., Leng, G., 2020. Evaluating the performance of conservation practices under climate change scenarios in the Miyun Reservoir Watershed, China. Ecol Eng 143. https://doi.org/10.1016/j.ecoleng.2019.105700

Rawat, J.S., Kumar, M., 2015. Monitoring land use/cover change using remote sensing and GIS techniques: A case study of Hawalbagh block, district Almora, Uttarakhand, India. The Egyptian Journal of Remote Sensing and Space Science 18, 77–84. https://doi.org/10.1016/J.EJRS.2015.02.002.

Rehman, A., Farooq, M., Lee, DJ. et al. Sustainable agricultural practices for food security and ecosystem services. Environ Sci Pollut Res **29**, 84076–84095 (2022). https://doi.org/10.1007/s11356-022-23635-z

Reddy, S., Osborne, W.J., 2022. Effect of pollution on sediments and their impact on the aquatic ecosystem. Relationship Between Microbes and the Environment for Sustainable Ecosystem Services, Volume 2: Microbial Mitigation of Waste for Sustainable Ecosystem

Services 5, 1–16. https://doi.org/10.1016/B978-0-323-89937-6.00001-2
Regasa, M.S., Nones, M., Adeba, D., 2021. A Review on Land Use and Land Cover Change in Ethiopian Basins. Land 2021, Vol. 10, Page 585 10, 585. https://doi.org/10.3390/LAND10060585
Regassa Debelo, A., Legesse, A., Milstein, T., Orkaydo, O.O., 2017. "Tree Is Life": The Rising of Dualism and the Declining of Mutualism among the Gedeo of Southern Ethiopia. Front Commun, 2. https://doi.org/10.3389/fcomm.2017.00007
Ricci, G.F., De Girolamo, A.M., Abdelwahab, O.M.M., Gentile, F., 2018. Identifying sediment source areas in a Mediterranean watershed using the SWAT model. Land Degrad Dev 29. https://doi.org/10.1002/ldr.2889
Rodrigo-Comino, J., 2018. Five decades of soil erosion research in "terroir". The State-of-the-Art. Earth Sci Rev 179, 436–447. https://doi.org/10.1016/J.EARSCIREV.2018.02.014
Roy, S., Farzana, K., Papia, M., Hasan, M., 2015. Monitoring and Prediction of Land Use/Land Cover Change using the Integration of Markov Chain Model and Cellular Automation in the Southeastern Tertiary Hilly Area of Bangladesh. undefined.
Rozario, P.F., Oduor, P., Kotchman, L., Kangas, M., 2017. Transition Modeling of Land-Use Dynamics in the Pipestem Creek, North Dakota, USA. Journal of Geoscience and Environment Protection 05, 182–201. https://doi.org/10.4236/gep.2017.53013
Sachindra, D.A., Ahmed, K., Rashid, M.M., Shahid, S., Perera, B.J.C., 2018. Statistical downscaling of precipitation using machine learning techniques. Atmospheric Research 212, 240–258. https://doi.org/10.1016/J.ATMOSRES.2018.05.022.
Sahour, H., Gholami, V., Vazifedan, M., Saeedi, S., 2021. Machine learning applications for water-induced soil erosion modeling and mapping. Soil Tillage Res 211, 105032.
Salazar, A., Baldi, G., Hirota, M., Syktus, J., McAlpine, C., 2015. Land use and land cover change impacts on the regional climate of non-Amazonian South America: A review. Glob Planet Change 128, 103–119. https://doi.org/10.1016/J.GLOPLACHA.2015.02.009
Samuelsson, P., Jones, C.G., Willén, U., Ullerstig, A., Gollvik, S., Hansson, U., Jansson, C., Kjellström, E., Nikulin, G. And Wyser, K., 2011. The Rossby Centre Regional Climate model RCA3: model description and performance. Tellus A, 63: 4-23. https://doi.org/10.1111/j.1600-0870.2010.00478.x
Sang, L., Zhang, C., Yang, J., Zhu, D., Yun, W., 2011. Simulation of land use spatial pattern of towns and villages based on CA–Markov model. Math Comput Model 54, 938–943.
Sanz, M.J., de Vente, J., Chotte, J.L., Bernoux, M., Kust, G., Ruiz, I., Almagro, M., Alloza, J.A., Vallejo, R., Castillo, V., et al., 2017. Sustainable Land Management contribution to

successful land-based climate change adaptation and mitigation: A Report of the Science-Policy Interface; United Nations Convention to Combat Desertification (UNCCD): Bonn, Germany.

Saputra, M.H., Lee, H.S., 2019. Prediction of Land Use and Land Cover Changes for North Sumatra, Indonesia, Using an Artificial-Neural-Network-Based Cellular Automaton. Sustainability 2019, Vol. 11, Page 3024 11, 3024. https://doi.org/10.3390/SU11113024

Sarkar, D., Sarkar, T., Saha, S., and Mondal, P., 2021. Compiling non-parametric tests along with CA-ANN model for precipitation trends and variability analysis: A case study of Eastern India, Water Cycle, Volume 2, 2021, Pages 71-84, ISSN 2666-4453, https://doi.org/10.1016/j.watcyc.2021.11.002.

Sartori, M., Philippidis, G., Ferrari, E., Borrelli, P., Lugato, E., Montanarella, L., Panagos, P., 2019. A linkage between the biophysical and the economic: Assessing the global market impacts of soil erosion. Land use policy 86, 299–312.

Sattari, M.T., Rezazadeh-Joudi, A., and Kusiak, A., 2017. Assessment of different methods for estimation of missing data in precipitation studies. Hydrology Research, 48(4), 1032-1044. https://doi.org/10.2166/nh.2016.364.

Schillaci, C., Jones, A., Vieira, D., Munafò, M., Montanarella, L., 2023. Evaluation of the United Nations Sustainable Development Goal 15.3.1 indicator of land degradation in the European Union. Land Degrad Dev 34. https://doi.org/10.1002/ldr.4457

Schütt, B., Thiemann, S., Wenclawiak, B., 2005. Deposition of modern fluvio-lacustrine sediments in Lake Abaya, South Ethiopia—A case study from the delta areas of Bilate river and Gidabo river, Northern Basin. Geomorphol. NF 2005, 138, 131–151

Segele, Z.T., Lamb, P.J., Leslie, L.M., 2009. Seasonal-to-interannual variability of Ethiopia/horn of Africa monsoon. Part I: Associations of wavelet-filtered large-scale atmospheric circulation and global sea surface temperature. Journal of Climate 22, 3396–3421. https://doi.org/10.1175/2008JCLI2859.1.

Seleshi, Y., Zanke, U., 2004. Recent changes in rainfall and rainy days in Ethiopia. International Journal of Climatology 24, 973–983. https://doi.org/10.1002/JOC.1052.

Sen, P.K., 1968. Estimates of the Regression Coefficient Based on Kendall's Tau, Journal of the American Statistical Association, 63:324, 1379-1389, DOI: 10.1080/01621459.1968.10480934.

Sen, Z., 2012. Innovative trend analysis methodology. J. Hydrol. Eng. 2012, 17, 1042-1046.

Seneviratne, S. I., Nicholls, N., Easterling, D., Goodess, C. M., Kanae, S., Kossin, J., Luo, Y., (2012). Changes in climate extremes and their impacts on the natural physical environment. In Managing the Risks of Extreme Events and Disasters to Advance Climate Change Adaptation: Special Report of the Intergovernmental Panel on Climate Change (pp. 109-230). Cambridge University Press. https://doi.org/10.1017/CBO9781139177245.006.

Serur, A.B., Adi, K.A., 2022. Multi-site calibration of hydrological model and the response of water balance components to land use land cover change in a rift valley Lake Basin in Ethiopia. Sci Afr 15. https://doi.org/10.1016/j.sciaf.2022.e01093

Shafizadeh-Moghadam, H., Tayyebi, A., Helbich, M., 2017. Transition index maps for urban growth simulation: application of artificial neural networks, weight of evidence and fuzzy multi-criteria evaluation. Environ Monit Ass. https://doi.org/10.1007/S10661-017-5986-3

Shanka, A.S., 2017. Evaluation of Climate Change Impacts on Run-Off in the Gidabo River Basin: Southern Ethiopia. Environment Pollution and Climate Change 01. https://doi.org/10.4172/2573-458X.1000129.

Sheng, H., Zhou, P., Zhang, Y., Kuzyakov, Y., Zhou, Q., Ge, T., Wang, C., 2015. Loss of labile organic carbon from subsoil due to land-use changes in subtropical China. Soil Biol Biochem 88, 148–157. https://doi.org/10.1016/J.SOILBIO.2015.05.015

Shigute, M., Alamirew, T., Abebe, A., Ndehedehe, C.E., Kassahun, H.T., 2023. Analysis of rainfall and temperature variability for agricultural water management in the upper Genale river basin, Ethiopia. Sci Afr 20. https://doi.org/10.1016/j.sciaf.2023.e01635

Shiru, Mohamed Sanusi, Shiru, Mohammed Sanusi, Chung, E.-S., 2021. Performance Evaluation of CMIP6 Global Climate Models for Selecting Models for Climate Projection over Nigeria. https://doi.org/10.21203/RS.3.RS-642786/V1.

Shitu, D., 2022. Cause of Land Degradation and Rehabilitation Practices in Case of Amba Sidist Western Ethiopia. American Journal of Chemistry and Pharmacy 1. https://doi.org/10.54536/ajcp.v1i1.419

Shivhare, N., Rahul, A.K., Omar, P.J., Chauhan, M.S., Gaur, S., Dikshit, P.K.S., Dwivedi, S.B., 2018. Identification of critical soil erosion prone areas and prioritization of micro-watersheds using geoinformatics techniques. Ecol Eng 121, 26–34. https://doi.org/10.1016/J.ECOLENG.2017.09.004

Shukla, P., Skea, J., Buendia, E.C., 2019. IPCC, 2019: Climate Change and Land: an IPCC special report on climate change, desertification, land degradation, sustainable land management, food.

Silva, L.P. e., Xavier, A.P.C., da Silva, R.M., Santos, C.A.G., 2020. Modeling land cover change based on an artificial neural network for a semiarid river basin in northeastern Brazil. Glob

Ecol Conserv 21. https://doi.org/10.1016/J.GECCO.2019.E00811.

Simonsen, N., 2019. Modelling the effects of land cover and climate change on watershed hydrology in south-western Ethiopia. Student thesis series INES; (2019).

Sims, N.C., England, J.R., Newnham, G.J., Alexander, S., Green, C., Minelli, S., Held, A., 2019. Developing good practice guidance for estimating land degradation in the context of the United Nations Sustainable Development Goals. Environ Sci Policy 92. https://doi.org/10.1016/j.envsci.2018.10.014

Simwanda, M., Murayama, Y., Ranagalage, M., 2020. Modeling the drivers of urban land use changes in Lusaka, Zambia using multi-criteria evaluation: An analytic network process approach. Land use policy 92. https://doi.org/10.1016/J.LANDUSEPOL.2019.104441

Singh, A., Acharya, N., Mohanty, U.C., Mishra, G., 2013. Performance of Multi Model Canonical Correlation Analysis (MMCCA) for prediction of Indian summer monsoon rainfall using GCMs output. Comptes Rendus Geoscience 345, 62–72. https://doi.org/10.1016/J.CRTE.2012.11.003.

Sinshaw, B.G., Belete, A.M., Tefera, A.K., Dessie, A.B., Bizuneh, B.B., Alem, H.T., Atanaw, S.B., Eshete, D.G., Wubetu, T.G., Atinkut, H.B., Moges, M.A., 2021. Prioritization of potential soil erosion susceptibility region using fuzzy logic and analytical hierarchy process, upper Blue Nile Basin, Ethiopia. Water-Energy Nexus 4, 10–24. https://doi.org/10.1016/J.WEN.2021.01.001

Sleeter, B., Loveland, T.R., Domke, G.M., Herold, N., Wickham, J., Wood, N.J., 2018. Chapter 5 : Land Cover and Land Use Change. Impacts, Risks, and Adaptation in the United States: The Fourth National Climate Assessment, Volume II. https://doi.org/10.7930/NCA4.2018.CH5.

Sneyers, R., 1990. On the Statistical Analysis of Series of Observations; Technical Note no. 143, WMO no. 415; Secretariat of the World Meteorological Organization: Geneva, Switzerland, 1990.

Sørland, S. L., Brogli, R., Pothapakula, P. K., Russo, E., et al., 2021. COSMO-CLM regional climate simulations in the Coordinated Regional Climate Downscaling Experiment (CORDEX) framework: a review, Geosci. Model Dev., 14, 5125–5154, https://doi.org/10.5194/gmd-14-5125-2021.

Spearman, C., 1904. The proof and measurement of association between two things. Am. J. Psychol., 15, 72-101. https://doi.org/10.2307/1412159.

Srivastav, A.L., Dhyani, R., Ranjan, M., Madhav, S., Sillanpää, M., 2021. Climate-resilient strategies for sustainable management of water resources and agriculture. Environmental

Science and Pollution Research 2021 28:31 28, 41576–41595. https://doi.org/10.1007/S11356-021-14332-4

Stefanidis, S., Dafis, S., Stathis, D., 2020. Evaluation of Regional Climate Models (RCMs) Performance in Simulating Seasonal Precipitation over Mountainous Central Pindus (Greece). Water 2020, Vol. 12, Page 2750 12, 2750. https://doi.org/10.3390/W12102750.

Stott, P., Strangeways, I., 2018. Measuring meteorological variables for studying the climate. Weather 73, 332–332. https://doi.org/10.1002/WEA.3369

Subedi, P., Subedi, K., Thapa, B., 2013. Application of a Hybrid Cellular Automaton – Markov (CA-Markov) Model in Land-Use Change Prediction: A Case Study of Saddle Creek Drainage Basin, Florida. Applied Ecology and Environmental Sciences 1, 126–132. https://doi.org/10.12691/AEES-1-6-5

Sugianto, S., Deli, A., Miswar, E., Rusdi, M., Irham, M., 2022. The Effect of Land Use and Land Cover Changes on Flood Occurrence in Teunom Watershed, Aceh Jaya. Land 2022, 11, 1271. https://doi.org/10.3390/land11081271

Suryabhagavan, K. v., 2017. GIS-based climate variability and drought characterization in Ethiopia over three decades. Weather and Climate Extremes 15, 11–23. https://doi.org/10.1016/J.WACE.2016.11.005.

Sylla, M.B., Diallo, I., Pal, J.S., Sylla, M.B., Diallo, I., Pal, J.S., 2013. West African Monsoon in State-of-the-Science Regional Climate Models. Climate Variability - Regional and Thematic Patterns. https://doi.org/10.5772/55140

Tabari, H. Climate change impact on flood and extreme precipitation increases with water availability. Sci Rep 10, 13768 (2020). https://doi.org/10.1038/s41598-020-70816-2

Tadese, S., Soromessa, T., Bekele, T., 2021. Analysis of the Current and Future Prediction of Land Use/Land Cover Change Using Remote Sensing and the CA-Markov Model in Majang Forest Biosphere Reserves of Gambella, Southwestern Ethiopia. Scientific World Journal 2021. https://doi.org/10.1155/2021/6685045

Takhsha, M., Nikiéma, O., Lucas-Picher, P. et al., 2018. Dynamical downscaling with the fifth-generation Canadian regional climate model (CRCM5) over the CORDEX Arctic domain: effect of large-scale spectral nudging and of empirical correction of sea-surface temperature. Clim Dyn 51, 161–186 (2018). https://doi.org/10.1007/s00382-017-3912-6

Tan, X., Liu, S., Tian, Y., Zhou, Z., Wang, Y., Jiang, J., Shi, H., 2022. Impacts of Climate Change and Land Use/Cover Change on Regional Hydrological Processes: Case of the Guangdong-Hong Kong-Macao Greater Bay Area. Front Environ Sci 9. https://doi.org/10.3389/fenvs.2021.783324.

Terefe, H., Argaw, M., Tamene, L. et al., 2020. Effects of sustainable land management interventions on selected soil properties in Geda watershed, central highlands of Ethiopia. Ecol Process 9, 14. https://doi.org/10.1186/s13717-020-0216-2

Taylor, K.E., 2001. Summarizing multiple aspects of model performance in a single diagram. Journal of Geophysical Research: Atmospheres 106, 7183–7192. https://doi.org/10.1029/2000JD900719.

Tayyebi, A., Pijanowski, B.C., Tayyebi, A., Pijanowski, B.C., 2014. Modeling multiple land use changes using ANN, CART and MARS: Comparing tradeoffs in goodness of fit and explanatory power of data mining tools. IJAEO 28, 102–116. https://doi.org/10.1016/J.JAG.2013.11.008

Teich, I., Harari, N., Caza, P., Henao-Henao, J.P., Lopez, J.C., Raviolo, E., Díaz-González, A.M., González, H., Bastidas, S., Morales-Opazo, C., García, C.L., 2023. An interactive system to map land degradation and inform decision-making to achieve Land Degradation Neutrality via convergence of evidence across scales: a case study in Ecuador. Land Degrad Dev. https://doi.org/10.1002/ldr.4645

Temesgen, H., Wu, W., Legesse, A., Yirsaw, E., Bekele, B., 2018. Landscape-based upstream-downstream prevalence of land-use/cover change drivers in southeastern rift escarpment of Ethiopia. Environ Monit Assess 190. https://doi.org/10.1007/s10661-018-6479-8

Tesfamariam, B.G., Gessesse, B., Melgani, F., 2019. Characterizing the spatiotemporal distribution of meteorological drought as a response to climate variability: The case of rift valley lakes basin of Ethiopia. Weather and Climate Extremes 26, 100237. https://doi.org/10.1016/J.WACE.2019.100237.

Tesfaye, S., Taye, G., Birhane, E., van der Zee, S.E., 2019. Observed and model simulated twenty-first century hydro-climatic change of Northern Ethiopia. Journal of Hydrology: Regional Studies 22, 100595. https://doi.org/10.1016/J.EJRH.2019.100595.

Teshome, H., Tesfaye, K., Dechassa, N., Tana, T., Huber, M., 2022. Analysis of Past and Projected Trends of Rainfall and Temperature Parameters in Eastern and Western Hararghe Zones, Ethiopia. Atmosphere 2022, Vol. 13, Page 67 13, 67. https://doi.org/10.3390/ATMOS13010067.

Thakur, J.K., Singh, S.K., Ekanthalu, V.S., 2017. Integrating remote sensing, geographic information systems and global positioning system techniques with hydrological modeling. Appl Water Sci 7, 1595–1608.

Theil, H., 1950. A rank-invariant method of linear and polynomial regression analysis. Nederl. Akad. Wetench. Ser. A, 53, 386-392.

Tibebe, D., Bewket, W., 2011. Surface runoff and soil erosion estimation using the SWAT model in the Keleta Watershed, Ethiopia. Land Degrad Dev 22. https://doi.org/10.1002/ldr.1034

Toma, M.B., Belete, M.D., Ulsido, M.D., 2023. Hydrological Components and Sediment Yield Response to Land Use Land Cover Change in The Ajora-Woybo Watershed of Omo-Gibe Basin, Ethiopia. Air, Soil and Water Research 16. https://doi.org/10.1177/11786221221150186

Trends.Earth, 2022. Trends Earth User Guide 2.1.8. Conservation International. Available online: http://trends.earth (accessed on 20 June 2023).

Tsidu, G.M., 2012. High-resolution monthly rainfall database for Ethiopia: Homogenization, reconstruction, and gridding. Journal of Climate 25, 8422–8443. https://doi.org/10.1175/JCLI-D-12-00027.1.

Tsymbarovich, P., Kust, G., Kumani, M., Golosov, V., Andreeva, O., 2020. Soil erosion: An important indicator for the assessment of land degradation neutrality in Russia. International Soil and Water Conservation Research 8. https://doi.org/10.1016/j.iswcr.2020.06.002

Tudi, M., Ruan, H.D., Wang, L., Lyu, J., Sadler, R., Connell, D., Chu, C., Phung, D.T., 2021. Agriculture Development, Pesticide Application and Its Impact on the Environment. International Journal of Environmental Research and Public Health 2021, Vol. 18, Page 1112 18, 1112. https://doi.org/10.3390/IJERPH18031112

Umuhoza, J., Chen, L., Mumo, L., Umuhoza, J., Chen, L., Mumo, L., 2021. Assessing the Skills of Rossby Centre Regional Climate Model in Simulating Observed Rainfall over Rwanda. Atmospheric and Climate Sciences 11, 398–418. https://doi.org/10.4236/ACS.2021.113023.

UNCCD, 2019a. Land Degradation Neutrality Transformative Projects and Programs: Operational Guidance for Country Support. Bonn, Germany.

UNCCD, 2019b. The Global Land Outlook, East Africa Thematic Report. Bonn, Germany.

Van Lynden, G.W.J., Mantel, S., 2001. The role of GIS and remote sensing in land degradation assessment and conservation mapping: some user experiences and expectations. International Journal of Applied Earth Observation and Geoinformation 3, 61–68.

Vanmaercke, M., Panagos, P., Vanwalleghem, T., Hayas, A., Foerster, S., Borrelli, P., Rossi, M., 2021. Measuring, modelling and managing gully erosion at large scales: A state of the art. Earth Sci Rev 218, 103637. https://doi.org/10.1016/J.EARSCIREV.2021.103637

Varma, P.K., 2021. Application of EuroSCORE II and STS score for risk assessment in Indian patients—are they useful? Indian Journal of Thoracic and Cardiovascular Surgery 2021 1–

2. https://doi.org/10.1007/S12055-021-01232-Y
Vávra, J., Duží, B., Lapka, M., Cudlínová, E., Rikoon, J.S., 2019. Socio-economic context of soil erosion: A comparative local stakeholders' case study from traditional agricultural region in the Czech Republic. Land use policy 84, 127–137. https://doi.org/10.1016/J.LANDUSEPOL.2019.03.005
Verburg, P.H., Metternicht, G., Allen, C., Debonne, N., Akhtar-Schuster, M., Cunha, M.I. da, Karim, Z., Pilon, A., Raja, O., Santivañez, M.S., Şenyaz, A., 2019. Creating an Enabling Environment for Land Degradation Neutrality: and its potential contribution to enhancing well-being, livelihoods and the environment, Uniwersytet śląski.
Viste, E., Korecha, D., Sorteberg, A., 2013. Recent drought and precipitation tendencies in Ethiopia. Theoretical and Applied Climatology 2012 112:3 112, 535–551. https://doi.org/10.1007/S00704-012-0746-3.
Wang, B., Zheng, L., Liu, D.L., Ji, F., Clark, A., Yu, Q., 2018. Using multi-model ensembles of CMIP5 global climate models to reproduce observed monthly rainfall and temperature with machine learning methods in Australia. International Journal of Climatology 38, 4891–4902. https://doi.org/10.1002/JOC.5705.
Wang, C., Yu, M., Gao, Q., 2017. Continued Reforestation and Urban Expansion in the New Century of a Tropical Island in the Caribbean. Remote Sensing 2017, Vol. 9, Page 731 9, 731. https://doi.org/10.3390/RS9070731
Wang, M., Duan, L., Wang, J., Peng, J., Zheng, B., 2020. Determining the width of lake riparian buffer zones for improving water quality base on adjustment of land use structure. Ecol Eng 158, 106001. https://doi.org/10.1016/J.ECOLENG.2020.106001
Wang, S.W., Munkhnasan, L., Lee, W.K., 2021. Land use and land cover change detection and prediction in Bhutan's high altitude city of Thimphu, using cellular automata and Markov chain. Environmental Challenges 2, 100017.
Waring, B., Neumann, M., Prentice, I.C., Adams, M., Smith, P., Siegert, M., 2020. Forests and Decarbonization – Roles of Natural and Planted Forests. Front. For. Glob. Change 3:58. https://doi.org/10.3389/ffgc.2020.00058
Warnatzsch, E.A., Reay, D.S., 2019. Temperature and precipitation change in Malawi: Evaluation of CORDEX-Africa climate simulations for climate change impact assessments and adaptation planning. Science of The Total Environment 654, 378–392. https://doi.org/10.1016/J.SCITOTENV.2018.11.098.
Wassie, S.B., 2020. Natural resource degradation tendencies in Ethiopia: a review. Environmental Systems Research 2020 9:1 9, 1–29.

Wessem, J.M., & Laffin, M.K., 2020. Regional Atmospheric Climate Model 2 (RACMO2), version 2.3p2.

Wolde, Z., Wei, W., Kunpeng, W., Ketema, H., 2020. Local community perceptions toward livelihood and water–energy–food nexus: A perspective on food security. Food Energy Secur 9, e207. https://doi.org/10.1002/FES3.207

Wolde, Z., Wei, W., Likessa, D., Omari, R., Ketema, H., 2021. Understanding the Impact of Land Use and Land Cover Change on Water–Energy–Food Nexus in the Gidabo Watershed, East African Rift Valley. Natural Resources Research 2021 30:3 30, 2687–2702. https://doi.org/10.1007/S11053-021-09819-3.

WoldeYohannes, A., Cotter, M., Kelboro, G., Dessalegn, W., 2018. Land Use and Land Cover Changes and Their Effects on the Landscape of Abaya-Chamo Basin, Southern Ethiopia. Land 2018, Vol. 7, Page 2 7, 2. https://doi.org/10.3390/LAND7010002

Worako, A.W., Haile, A.T., Taye, M.T., 2022. Implication of bias correction on climate change impact projection of surface water resources in the Gidabo sub-basin, Southern Ethiopia. Journal of Water and Climate Change 13. https://doi.org/10.2166/wcc.2022.396

Worku, G., 2014. Land use and land cover change in Ameleke Watershed, South Ethiopia. Journal of Natural Sciences Research 4, 42–47.

Worku, G., Teferi, E., Bantider, A., Dile, Y.T., Taye, M.T., 2018. Evaluation of regional climate models performance in simulating rainfall climatology of Jemma sub-basin, Upper Blue Nile Basin, Ethiopia. Dynamics of Atmospheres and Oceans 83, 53–63.

Worku, T., Tripathi, S.K., 2015. Watershed Management in Highlands of Ethiopia: A Review. OAlib 02, 1–11. https://doi.org/10.4236/OALIB.1101481

World Population Review, 2021. Ethiopia Population. Available online: Ethiopia Population (2021) (Demographics, Maps, Graphs). https://worldpopulationreview.com (accessed 8.15.21).

Wu, M., Nikulin, G., Kjellström, E., Belušić, D., Jones, C., Lindstedt, D., 2020. The impact of regional climate model formulation and resolution on simulated precipitation in Africa. Earth System Dynamics 11, 377–394. https://doi.org/10.5194/ESD-11-377-2020

Xue, Y., Janjic, Z., Dudhia, J., Vasic, R., de Sales, F., 2014. A review on regional dynamical downscaling in intraseasonal to seasonal simulation/prediction and major factors that affect downscaling ability. Atmospheric Research 147–148, 68–85.

Yang, L., Zhao, G., Mu, X., Lan, Z., Jiao, J., An, S., Wu, Y., Miping, P., 2023. Integrated assessments of land degradation on the Qinghai-Tibet plateau. Ecol Indic 147.

Yemiru, T., Roos, A., Campbell, B.M., Bohlin, F., 2010. Forest incomes and poverty alleviation under participatory forest management in the bale highlands, Southern Ethiopia. International Forestry Review 12, 66–77. https://doi.org/10.1505/IFOR.12.1.66

Yesuph, A.Y., Dagnew, A.B., 2019. Soil erosion mapping and severity analysis based on RUSLE model and local perception in the Beshillo Catchment of the Blue Nile Basin, Ethiopia. Environ Syst Res 8, 17 (2019). https://doi.org/10.1186/s40068-019-0145-1

Yirsaw, E., Wu, W., Shi, X., Temesgen, H., Bekele, B., 2017. Land Use/Land Cover Change Modeling and the Prediction of Subsequent Changes in Ecosystem Service Values in a Coastal Area of China, the Su-Xi-Chang Region. Sustainability 2017, Vol. 9, Page 1204 9, 1204. https://doi.org/10.3390/SU9071204.

Zanis, P., Katragkou, E., Ntogras, C., Marougianni, G., Tsikerdekis, A., Feidas, H., Anadranistakis, E., Melas, D., 2015. Transient high-resolution regional climate simulation for Greece over the period 1960-2100: evaluation and future projections. Climate Research 64, 123–140. https://doi.org/10.3354/CR01304.

Zekarias, T., Govindu, V., Kebede, Y., Gelaw, A., 2021. Geospatial Analysis of Wetland Dynamics on Lake Abaya-Chamo, The Main Rift Valley of Ethiopia. Heliyon 7, e07943. https://doi.org/10.1016/J.HELIYON.2021.E07943

Zeleke, T., Giorgi, F., Mengistu Tsidu, G., Diro, G.T., 2013. Spatial and temporal variability of summer rainfall over Ethiopia from observations and a regional climate model experiment. Theoretical and Applied Climatology 111, 665–681.

Zeleke, T.T., Giorgi, F., Diro, G.T., Zaitchik, B.F., 2017. Trend and periodicity of drought over Ethiopia. International Journal of Climatology 37, 4733–4748. https://doi.org/10.1002/JOC.5122.

Zhai, H.J., Hu, B., Luo, X.Y., Qiu, L., Tang, W.J., Jiang, M., 2016. Spatial and temporal changes in runoff and sediment loads of the Lancang River over the last 50 years. Agric Water Manag 174, 74–81. https://doi.org/10.1016/J.AGWAT.2016.03.011.

Zhang, D., Liu, X., Wu, Xiaoyu, Yao, Y., Wu, Xinxin, Chen, Y., 2018. Multiple intra-urban land use simulations and driving factors analysis: a case study in Huicheng, China. 56, 282–308. https://doi.org/10.1080/15481603.2018.1507074.

Zhao, L., Jia, K., Liu, X., Li, J., Xia, M., 2023. Assessment of land degradation in Inner Mongolia between 2000 and 2020 based on remote sensing data. Geography and Sustainability 4. https://doi.org/10.1016/j.geosus.2023.01.003.

Zhu, Z., Qiu, S., Ye, S., 2022. Remote sensing of land change: A multifaceted perspective. Remote Sens Environ 282, 113266. https://doi.org/10.1016/J.RSE.2022.113266

Annex

Table A1. Standard normal homogeneity test result of mean annual rainfall

Station name	T0	p-value	Hypothesis
Dilla	4.76	0.224	H0
Hagereselam	1.291	0.927	H0
Haisawite	1.288	0.925	H0
Yergalem	5.008	0.133	H0
Yergacheffe	2.513	0.518	H0

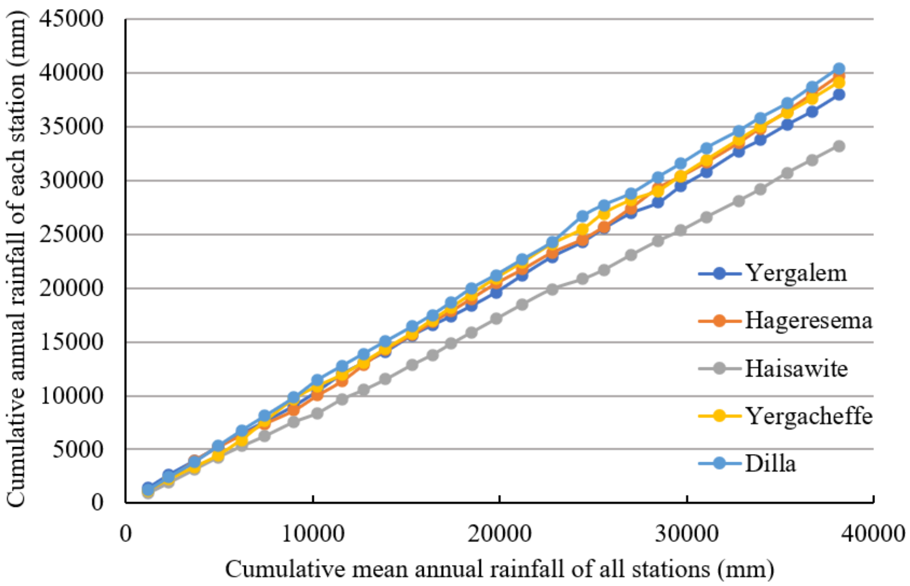

Figure A1. Double mass curve of mean annual rainfall

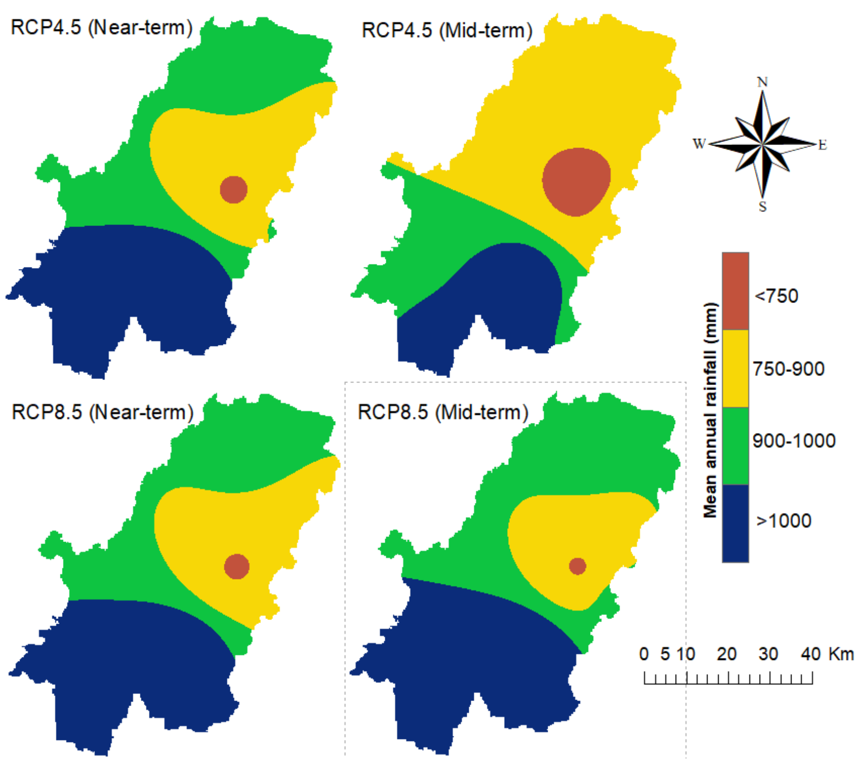

Figure A2. The spatial pattern of projected mean annual rainfall under RCP4.5 and RC8.5

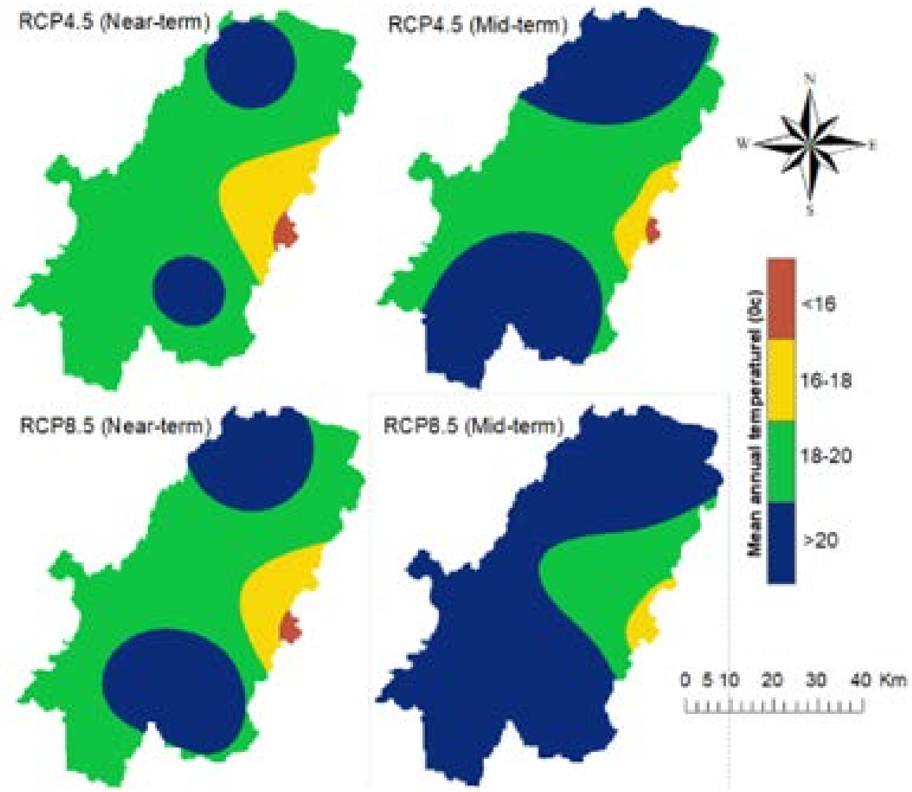

Figure A3. The spatial pattern of projected mean annual temperature under RCP4.5 and RC8.5

Table A2. Summary of land degradation indicators based on SDG 15.3.1

Land degradation indicator	1985-2003		2003-2021	
	Area (sq km)	Percent of land area	Area (sq km)	Percent of land area
LP indicator				
Land area with improved productivity	38.8	1.58%	4.3	0.17%
Land area with stable productivity	2,045.2	83.21%	1,642.3	66.81%
Land area with degraded productivity	359.0	14.61%	796.5	32.40%
Land area with no data for productivity	14.9	0.61%	14.9	0.61%
Total land area	2,458.0	100%	2,458.0	100.00%
LC indicator				
Land area with improved land cover	305.1	12.41%	262.5	10.68%
Land area with stable land cover	1,270.6	51.69%	1,156.3	47.04%
Land area with degraded land cover	882.4	35.90%	1039.2	42.28%
Land area with no data for land cover	0.0	0.00%	0.0	0.00%
Total land area	2,458.0	100.00%	2,458.0	100.00%
SOC indicator				
Land area with improved SOC	306.7	12.5%	291	11.84%
Land area with stable SOC	1290.4	52.5%	1,196.10	48.66%
Land area with degraded SOC	848.6	34.52%	958.6	39.00%
Land area with no data for SOC	12.3	0.50%	12.3	0.50%
Total land area	2458.0	100.00%	2458.0	100.00%
Combined indicators				
Land area improved	336.8	13.70%	305.2	12.42%
Land area stable	1,005.8	40.92%	758.2	30.85%
Land area degraded	1,096.6	44.61%	1,375.80	55.97%
Land area with no data	18.8	0.76%	18.8	0.76%
Total land area	2,458.0	100.00%	2,458.0	100.00%

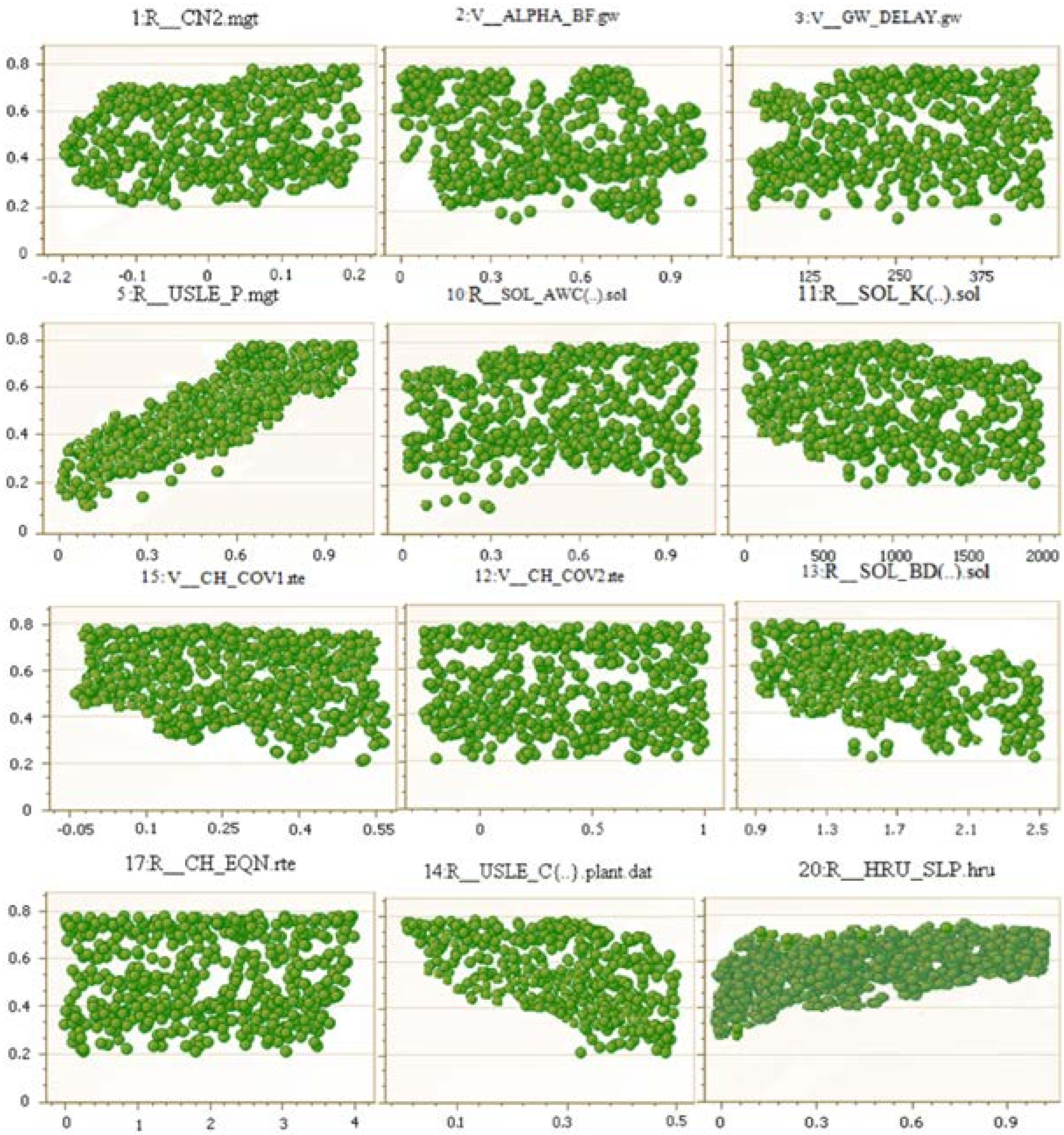

Figure A4. Dotty plots of most sensitive parameters considered for SWAT calibration (Note: For each dotty plot, the X-axis represents the parameter's value for each simulation and the Y-axis represents the corresponding NSE values).